9 March 2012 | $10

Science

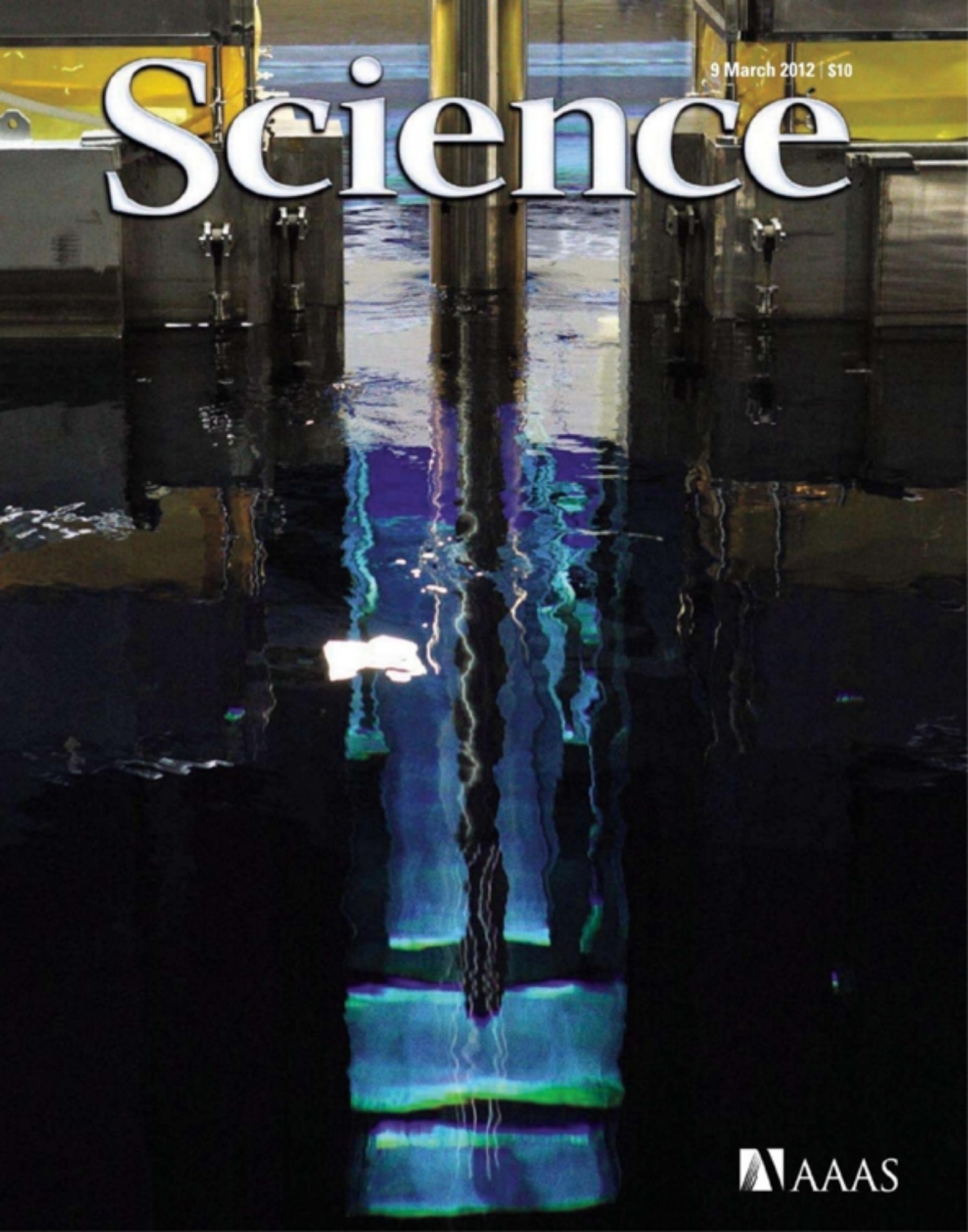

AAAS

EDITORIAL

NEWS OF THE WEEK

NEWS & ANALYSIS

NEWS FOCUS

LETTERS

BOOKS *ET AL.*

POLICY FORUM

PERSPECTIVES

CONTENTS continued >>

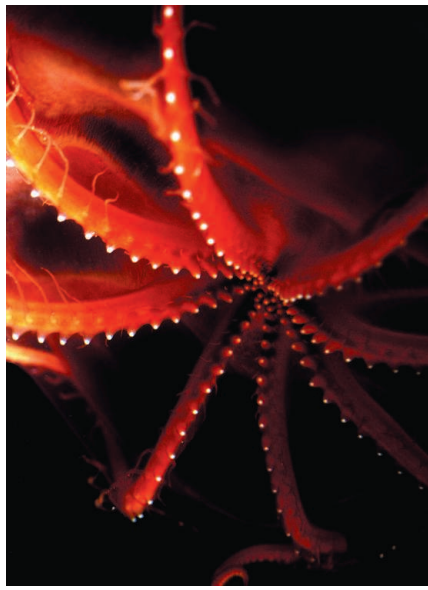

page 1160

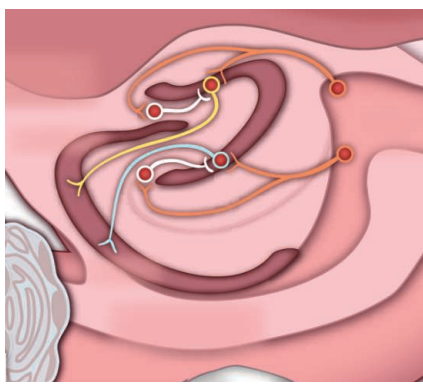

pages 1175 & 1238

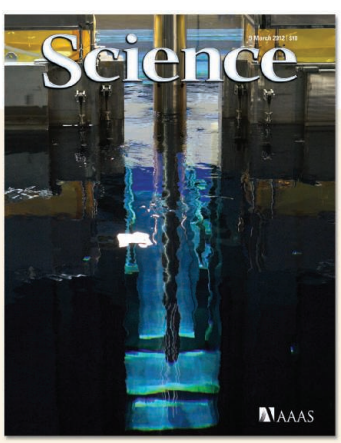

COVER

Cooling pool containing a plutonium-uranium mixed-oxide fuel rod at Fukushima Dai-ichi nuclear power station, Japan, in August 2010. A tsunami on 11 March 2011 damaged three of the station's reactors, prompting reassessment of Japan's reliance on nuclear power and its approach to disaster preparedness. See the Review by Burns *et al.* (page 1184), as well as the related Editorial (page 1147) and News story (page 1164).

Photo: Tomohiro Ohsumi/Bloomberg via Getty Images

DEPARTMENTS

Published by AAAS

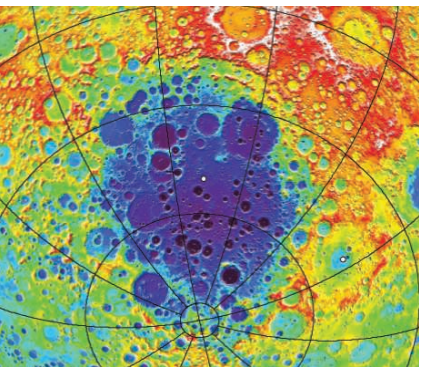

pages 1176 & 1212

page 1222

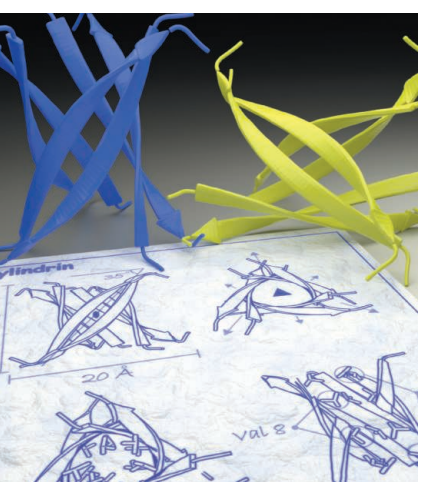

page 1228

REVIEWS

BREVIA

RESEARCH ARTICLE

REPORTS

CREDITS: (MIDDLE) CLAY WILTON; (BOTTOM) COURTESY OF ARTHUR LAGANOWSKY AND DAVID EISENBERG

Published by AAAS

SCIENCEONLINE

SCIENCEXPRESS
www.sciencexpress.org

Extrachromosomal MicroDNAs and Chromosomal Microdeletions in Normal Tissues
Y. Shibata et al.
The formation of circular microDNAs can result in somatic and germline microdeletions in mammalian cells.
10.1126/science.1213307

A Segmentation Clock with Two-Segment Periodicity in Insects
A. F. Sarrazin et al.
Oscillating gene expression, a key feature of vertebrate segmentation, is shown to occur during segmentation in beetles.
10.1126/science.1218256

Mapping the Core of the *Arabidopsis* Circadian Clock Defines the Network Structure of the Oscillator
W. Huang et al.
Morning and evening components of circadian rhythms are coordinated and stabilized by a repressor.
10.1126/science.1219075

Gap Junctions Compensate for Sublinear Dendritic Integration in an Inhibitory Network
K. Vervaeke et al.
Synaptic charge spreads into the dendrites of neighboring interneurons via dendritic gap junctions.
10.1126/science.1215101

A 2D Quantum Walk Simulation of Two-Particle Dynamics
A. Schreiber et al.
An optical approach extends quantum walk methodology from one to two dimensions.
10.1126/science.1218448

TECHNICALCOMMENTS

Comment on "Fossilized Nuclei and Germination Structures Identify Ediacaran 'Animal Embryos' as Encysting Protists"
S. Xiao et al.
Full text at www.sciencemag.org/cgi/content/full/335/6073/1169-c

Response to Comment on "Fossilized Nuclei and Germination Structures Identify Ediacaran 'Animal Embryos' as Encysting Protists"
T. Huldtgren et al.
Full text at www.sciencemag.org/cgi/content/full/335/6073/1169-d

SCIENCENOW
www.sciencenow.org
Highlights From Our Daily News Coverage

Sharing the Blame for the Mammoth's Extinction
A new study attributes the worldwide demise of these big beasts to both climate change and humans.
http://scim.ag/Blame_Extinction

Plants Gone Wild: Antarctica Edition
Tourists and scientists are ferrying seeds of invasive species to the coldest continent.
http://scim.ag/Plants_Antarctica

Proposed Cloaking Device for Water Waves Could Protect Ships at Sea
This scheme works on a principle different from electromagnetic invisibility cloaks.
http://scim.ag/Cloaking-Device

SCIENCESIGNALING
www.sciencesignaling.org
The Signal Transduction Knowledge Environment
6 March issue: http://scim.ag/ss030612

RESEARCH ARTICLE: Akt and ERK Control the Proliferative Response of Mammary Epithelial Cells to the Growth Factors IGF-1 and EGF Through the Cell Cycle Inhibitor $p57^{Kip2}$
D. T. Worster et al.

PODCAST
J. G. Albeck et al.
Signaling from two growth factors converges on the cell cycle inhibitor p57 to regulate proliferation and limit oncogenesis.

RESEARCH ARTICLE: STING Specifies IRF3 Phosphorylation by TBK1 in the Cytosolic DNA Signaling Pathway
Y. Tanaka and Z. J. Chen

PERSPECTIVE: The STING in the Tail for Cytosolic DNA-Dependent Activation of IRF3
A. Bowie
The scaffold STING directs the kinase TBK1 toward its substrate, the transcription factor IRF3, to promote antiviral signaling.

SCIENCETRANSLATIONAL MEDICINE
www.sciencetranslationalmedicine.org
Integrating Medicine and Science
7 March issue: http://scim.ag/stm030712

RESEARCH ARTICLE: Fasting Cycles Retard Growth of Tumors and Sensitize a Range of Cancer Cell Types to Chemotherapy
C. Lee et al.

PERSPECTIVE: Impersonalized Medicine
H. Scrable
Fasting simultaneously enhances normal cell function and potentiates the effects of conventional chemotherapeutic agents on tumor growth, metastasis, and long-term survival.

RESEARCH ARTICLE: Chimerism and Tolerance Without GVHD or Engraftment Syndrome in HLA-Mismatched Combined Kidney and Hematopoietic Stem Cell Transplantation
J. Leventhal et al.

FOCUS: The Quest for Transplantation Tolerance—Have We Finally Sipped from the Cup?
J. F. Markmann and T. Kawai
New advances in achieving hematopoietic chimerism may facilitate immunological tolerance to kidney transplants.

RESEARCH ARTICLE: A Human Stem Cell Model of Early Alzheimer's Disease Pathology in Down Syndrome
Y. Shi et al.
Cultured cerebral cortex neurons generated from human Down syndrome–induced pluripotent stem cells rapidly develop Alzheimer's disease pathologies.

SCIENCECAREERS
www.sciencecareers.org/career_magazine
Free Career Resources for Scientists

Science in the Community
E. Pain
Researchers have much to gain from involving citizens as research partners—provided they are prepared and open-minded.
http://scim.ag/CommunityScience

Your Research, Their Hope
M. Price
Scientists working with patient-advocacy groups need to set legal and ethical guidelines so interactions can be mutually beneficial.
http://scim.ag/Research_Hope

Biotech Training Programs Expand Employment Options
C. Mintz
Trainees who obtain industry-specific training are more likely to find jobs in the life-sciences industry.
http://scim.ag/MintzBiotechTraining

SCIENCEPODCAST
www.sciencemag.org/multimedia/podcast
Free Weekly Show

On the 9 March *Science* Podcast: magnetic anomalies on the Moon, nuclear fuel in a reactor accident, light adaptations in the deep sea, and more.

SCIENCEINSIDER
news.sciencemag.org/scienceinsider
Science Policy News and Analysis

SCIENCE (ISSN 0036-8075) is published weekly on Friday, except the last week in December, by the American Association for the Advancement of Science, 1200 New York Avenue, NW, Washington, DC 20005. Periodicals Mail postage (publication No. 484460) paid at Washington, DC, and additional mailing offices. Domestic individual membership and subscription (51 issues): $149 ($74 allocated to subscription). Domestic institutional subscription (51 issues): $990; Foreign postage extra: Mexico, Caribbean (surface mail) $55; other countries (air assist delivery) $85. First class, airmail, student, and emeritus rates on request. Canadian rates with GST available upon request, GST #1254 88122. Publications Mail Agreement Number 1069624. **Printed in the U.S.A.**

Change of address: Allow 4 weeks, giving old and new addresses and 8-digit account number. **Postmaster:** Send change of address to AAAS, P.O. Box 96178, Washington, DC 20090–6178. **Single-copy sales:** $10.00 current issue, $15.00 back issue prepaid includes surface postage; bulk rates on request. The identification code for *Science* is 0036-8075. *Science* is indexed in the *Reader's Guide to Periodical Literature* and in several specialized indexes.

AAAS
ADVANCING SCIENCE, SERVING SOCIETY

Published by AAAS

Bee Adventurous

Individuals differ in their behavior, sometimes in consistent ways. For example, some people may seek out new experiences, while others prefer to stick with what they know. This is true in bees as well, where some workers take on the dangerous, novelty-seeking task of scouting more often than others. **Liang *et al.*** (p. 1225) found that bees that display such scouting behavior not only tend to scout in multiple contexts (both foraging and searching for nests) but also show differences in gene expression in their brains. Experimental manipulation of gene expression predictably changed scouting behavior. The molecular underpinnings of bee scouting behavior appear to be similar to those associated with novelty-seeking in vertebrate species, including humans.

CREDITS (TOP TO BOTTOM): ZACHARY HUANG/HTTP://BEETOGRAPHY.COM; KIM *ET AL.*

Mechanics of a Meltdown

For all the potential hazards presented by nuclear power plants, there have been very few incidents that have caused human or environmental harm. However, those that have happened have often had disastrous consequences, for example, the accidents at Chernobyl in Ukraine and, just last year, at Fukushima Daiichi in Japan. **Burns *et al.*** (p. 1184; see the cover) review the state of knowledge on the chemical and physical processes following the nuclear reactor accident and how these results may inform decision-making during future events. Because a large portion of prior research has focused on radionuclide transport following leaks from nuclear waste repositories, and not active reactors, experiments at the more extreme conditions experienced in major nuclear core-melt accidents may have more predictive value.

Lessons from SIV

HIV infection in humans is a chronic infection and, if left untreated, the majority of infected individuals will succumb to AIDS. Many species of African nonhuman primates are chronically infected with simian immunodeficiency virus (SIV); however, in the majority of these species, the animals remain healthy despite the presence of high viral loads. **Chahroudi *et al.*** (p. 1188) review the underlying immune mechanisms that help protect natural hosts from progressing to AIDS and how these responses differ from what is observed in HIV-infected humans and SIV-infected nonhuman primate species that develop AIDS.

Smooth Operator

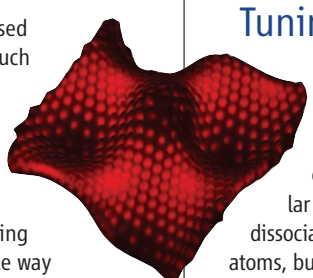

When thin sheets are compressed they can buckle and wrinkle, such as when the edges of a sheet of paper, or two areas of skin, are pushed together. Variations in local thickness and stiffness will alter the buckling patterns, but controlling this in a simple and predictable way is difficult. **Kim *et al.*** (p. 1201; see the Perspective by **Sharon**) used halftone lithography with two photomasks to create highly cross-linked dots embedded in a lightly cross-linked matrix of a swellable polymer. This material could generate "smooth" swelling profiles on thin sheets with arbitrary two-dimensional geometries so that complex three-dimensional structures could be produced.

Making Immune Cells Young Again

Hematopoiesis, the development of the immune system, occurs in distinct waves. The immune system is first populated by cells that arise from fetal hematopoietic stem cells (HSCs) and then later by cells derived from adult HSCs. Furthermore, fetal HSCs give rise to lymphocytes with innate immunelike properties, whereas adult HSCs give rise to classical T and B cells. **Yuan *et al.*** (p. 1195, published online 16 February) now uncover the molecular mechanism behind these distinct waves of hematopoiesis. Expression of the RNA binding proteins Lin28 and Lin28b is enriched in fetal hematopoietic stem/progenitor cells (HSPCs) in mice and humans. Ectopic expression of Lin28 in mouse adult HSPCs was sufficient to induce the differentiation of both classical and innate-like lymphocyte lineages.

A Useful Cover-Up

Many industrial catalysts that consist of metal nanoparticles adsorbed on metal oxide supports undergo deactivation after prolonged use. Organic reactants can decompose and cover the metal with carbon ("coking"), and other processes can push the size distribution to fewer but larger particles that have less overall surface area available for reaction ("sintering"). **Lu *et al.*** (p. 1205) used atomic-layer deposition to apply a uniform overlayer of alumina onto supported palladium nanoparticles. This coating greatly increased the resistance of the nanoparticles to coking and sintering during the oxidative dehydration of ethane to ethylene.

Tuning Hydrogen Adsorption

Heterogeneous metal catalysts for hydrogenating unsaturated organic compounds need to bind molecular hydrogen strongly enough that it dissociates and forms adsorbed hydrogen atoms, but must not bind these atoms too strongly, or the transfer to the organic molecule will be impeded. **Kyriakou *et al.*** (p. 1209) examined surface alloy catalysts created when palladium (Pd) atoms are adsorbed on a copper (Cu) surface using scanning tunneling microscopy and desorption techniques under ultrahigh vacuum conditions. The Pd atoms could bind hydrogen dissociatively—which, under these conditions, the Cu surfaces could not—allowing the Cu surface to take up adsorbed hydrogen atoms. These weakly bound hydrogen atoms were able to selectively hydrogenate styrene and acetylene.

Bringing Magnetic Materials to the Moon

The Apollo missions to the Moon revealed that portions of the lunar crust are strongly magne-

Continued on page 1146

Continued from page 1145

tized. Lunar rocks are poor at recording the magnetic field, thus these magnetic anomalies have been difficult to explain. Based on numerical simulations of large-scale impacts, **Wieczorek *et al.*** (p. 1212; see the Perspective by **Collins**) show that the vast majority of lunar magnetic anomalies can be explained by highly magnetic materials that originated outside the Moon and were delivered by the asteroid that hit the Moon and formed the South Pole–Aitken basin, the largest impact basin in the solar system.

A Price of Civilization

Large expanses of rainforests in parts of Central Africa were abruptly replaced by savannas around 3000 years ago, presumably because of climate change. However, that succession occurred at a time of expansion by Bantu tribes, from near the border of present-day Cameroon and Nigeria to the south and east, in a migration that brought with it agriculture and iron-smelting technologies. **Bayon *et al*.** (p. 1219, published online 9 February; see the Perspective by **Dupont**) analyzed the nearby marine sedimentary record and found that chemical weathering in Central Africa also increased markedly at this time. This increase in weathering could have been caused by forest clearing by the Bantu to create arable land and to fuel their smelters, rather than climate change alone.

Avoiding Infanticide

In male dominated hierarchies, newly dominant males will sometimes kill resident infants. In lab studies in mice conducted in the 1950s, Hilda Bruce showed that females introduced to an unfamiliar male will terminate their pregnancies, a process subsequently referred to as a Bruce Effect. **Roberts *et al*.** (p. 1222, published online 23 February) followed multiple dominance transitions within wild gelada baboons and showed that live birthrate among females previously identified as pregnant within unstable groups was much lower than within stable groups. Furthermore, females that terminated their pregnancies following transitions had a much shorter interbirth interval than those that did not, suggesting a higher overall reproductive success and fitness.

A Time and a Place

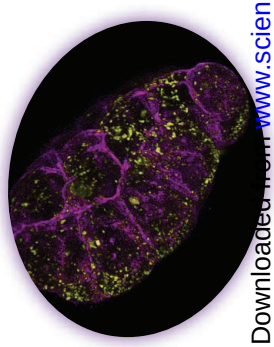

The onset of morphogenetic cell shape changes is thought to be triggered by initiation of actomyosin contractions. **Roh-Johnson *et al.*** (p. 1232, published online 9 February; see the Perspective by **Razzell and Martin**) have now discovered in both *Caenorhabditis elegans* and *Drosophila* embryos that the actomyosin contractions driving morphogenesis run constitutively, only being engaged to trigger cell shape changes at a specific time during development.

Nucleosome Maps and Mutation

Understanding the processes governing the accumulation of mutations impacts many facets of evolutionary biology. Combining data from a mutation accumulation experiment in a DNA repair-deficient yeast strain with genome-wide substitution, **Chen *et al*.** (p. 1235) demonstrate that C/G to T/A changes are more likely to affect regions that are nucleosome-free. Furthermore, a similar pattern was seen when comparative analyses were performed among yeast species and in lines of Medaka fish and nematodes. The results are consistent with a model in which DNA bound by nucleosomes is protected against mutations caused by DNA damage.

Neurogenesis and Pattern Integration

The adult hippocampus continuously produces new neurons that integrate into the dentate gyrus network and contribute to information processing. What features of adult-born neurons are important for information processing in the dentate gyrus? **Marín-Burgin *et al*.** (p. 1238, published online 26 January; see the Perspective by **Kempermann**) labeled newborn neurons and used sophisticated electrophysiological and imaging techniques to show that immature neurons integrated a broader variety of synaptic inputs from different origins compared with mature neurons, which were highly input specific. Thus, immature neurons may represent a population of integrators that are broadly tuned during a transient period and may encode most features of incoming information. After maturation, new granule cells display a high activation threshold and input specificity to become good pattern separators.

CREDIT: CHRIS HIGGINS/UNC CHAPEL HILL AND LIANG GAO/JANELIA FARM

Published by AAAS

Koji Omi is the founder and chairman of the Science and Technology in Society forum and is the former Japanese Minister of Science and Technology Policy and former Japanese Minister of Finance.

Worldwide Lessons from 11 March

IT HAS BEEN 1 YEAR SINCE A DEVASTATING EARTHQUAKE AND TSUNAMI STRUCK THE NORTHEAST coast of Japan, a disaster that continues to be analyzed by many people around the world, from different perspectives. There are important lessons to be learned as Japan faces critical decisions not only about rebuilding but also in planning for the nation's future energy needs—lessons that are also relevant to many other countries.

Japan is no stranger to natural disasters. The Hanshin-Awaji earthquake of January 1995 destroyed much of Kobe and killed more than 6000 people. Most of the fatalities were caused by building collapses. Since that incident, scientists, engineers, and architects have greatly improved the construction of buildings, bridges, and roads using technologies that make human-made structures earthquake-resistant. Because of such efforts, few buildings collapsed in the 11 March 2011 earthquake, demonstrating that the stricter measures applied since 1995 have improved safety. Similarly, lessons should be learned from the Fukushima Daiichi nuclear power station accident to guide future investments.

In the earthquake last year, most of the approximately 19,000 fatalities were caused not by the earthquake but by the tsunami that followed. When the earthquake struck, all 11 nuclear reactors in operation in Japan's northeastern Tohoku district successfully shut down, and their emergency cooling systems worked according to design. At the Fukushima Daiichi complex, the cooling was maintained by emergency diesel power generators, but the tsunami that arrived 40 minutes later destroyed those cooling systems and the external electricity supply line. The result was a core meltdown (the collapse of fuel elements) in three of the nuclear reactors that released large amounts of radiation into the air and sea (see the Review by Burns *et al*., p. 1184). Some areas near the Fukushima Daiichi complex still have such high levels of radiation in the soil that the inhabitants have not been allowed to return home. By the end of 2011, the temperature inside the reactors had dropped to below 100°C, making the situation there manageable.

Public attitudes toward nuclear power are changing, and today there is an understandably greater concern about nuclear safety worldwide. The events of 11 March have created public fear and confusion. But humankind must retain the nuclear power option, given its growing demands for energy. The lessons learned from the Fukushima disaster will guide better and safer decisions regarding nuclear power plant design for this important energy resource. We need to analyze last year's disaster at Fukushima rationally, and the time has come to make decisions using the best science and engineering technologies. The power station was damaged not by the earthquake but by the tsunami, because the height of a possible tsunami had been underestimated and the protection was inadequate. Certainly, it will be crucial to prevent future tsunamis of great magnitude from threatening coastal nuclear power stations throughout Japan.

A statement issued in October 2010 by the Science and Technology in Society forum, of which I am founder and chairman, said that "Any future energy supply should include a wide range of options that adhere to the best standards of safety and environmental and social compatibility and are available at competitive prices. Different countries may choose different paths to an energy-secure future. Nuclear energy will continue to play a significant role for the foreseeable future." Development of alternative renewable energy sources—solar, wind, biomass, and others—should be encouraged, but these should be combined with nuclear power to meet future energy needs. The global energy supply must respond to concerns about global climate change, and from the perspective of environmental preservation, nuclear power makes sense. Two hundred years ago, no one believed that powered flight was possible. About 100 years ago, the Wright brothers successfully flew the first aircraft. Today, flying is safe, ordinary, and indispensable, and few view it as hazardous. This is an example of what science and technology can achieve.

– Koji Omi

10.1126/science.1221277

Published by AAAS

EDITED BY KRISTEN MUELLER AND JAKE YESTON

EVOLUTION

Unraveling the Origin of Cotton

The origin and evolution of *Gossypium hirsutum*, the most widely planted cotton species, is an unsolved puzzle because of its hybrid origin from Old and New World species. To better understand the evolution of cotton, Palmer *et al*. shotgun sequenced 454 2000-year-old archaeological samples of cotton from Africa and South America. On the basis of their results and comparisons with genetic data from extant species, they assigned the African lineage to the species *G. herbaceum* and the South American lineages to the species *G. barbadense*. From these data, the authors show that *G. barbadense* shows overall genome stability with few changes in the placement and number of transposable elements over the past 2000 years. In contrast, *G. herbaceum* showed significant differences in transposable element composition over time. On the basis of these results, the authors postulate that the ancient *G. herbaceum* lineage is more like the ancestral form of one of the original species parents of *G. hirsutum* than that of the extant lineages. Furthermore, they suggest that cotton genome evolution is characterized by bursts of transposable element activity followed by genome stability. — LMZ

Mol. Biol. Evol. **29**, 10.1093/molbev/mss070 (2012).

CLIMATE SCIENCE

Seasonal Subtleties

Much has been made of an alleged lack of global climate warming over the past decade, a condition to which climate change deniers repeatedly have referred in their attempts to argue that global temperatures do not support the consensus view that climate warming is continuing as expected. Have we been looking in the right place for evidence that climate still is getting hotter, though? Cohen *et al.* provide evidence that we have not. Using a combination of observational data and climate modeling for the period between 1988 and 2010, they show that warming has continued apace and that the seeming slowdown in the upward march of global annual average temperatures is a reflection of marked seasonal differences: Only in the winter has it not gotten warmer. Therefore, by looking only at yearly averages, some have missed the warming that never has stopped and have been afforded a chance to argue incorrectly that global warming is a fiction, even though both the observational record and climate models clearly show that pauses in the temperature rise lasting decades are both common and expected for a warming climate. — HJS

Geophys. Res. Lett. **39**, L04705 (2012)

NEUROSCIENCE

Setting the Right Course

Neurons are remarkably asymmetric, with a cell body surrounded by dendrites and a single axon. Such asymmetry requires that the orientation of the neuronal growth axis be defined early in the development of the neuron. Gärtner

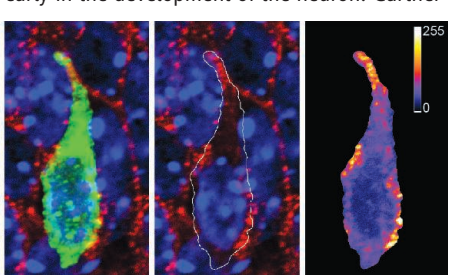

et al. looked at mouse hippocampal embryonic neurons in the first stages of polarization in vitro to determine how this process occurs. They found that the first neurite formed even before the orientation of the Golgi and centrosome, previously believed to be the key orchestrators of polarity. Initiation of the first neurite instead involved the polar concentration of the cell adhesion molecule N-cadherin. Added N-cadherin could be used to artificially specify neurite position, which would then signal the rearrangement of the internal organelles in a cytoskeleton-dependent fashion. Similar early polarization of N-cadherin was observed in embryonic neurons in situ. Furthermore, embryos with defective neuronal N-cadherin failed to properly align their neurons and had defects in neuronal migration. Thus, localized N-cadherin signaling appears to provide a cornerstone for very early events in hippocampal neuron polarization and outgrowth. — SMH

EMBO J. 10.1038/emboj.2012.41 (2012).

PSYCHOLOGY

Collective Power

What percentage of Americans own pets? This question obviously has an answer; just as obviously, any single individual is unlikely to know it or to be able to offer a close estimate. Nevertheless, the average of a number of such guesses may end up quite close indeed. Using questions of this type, covering U.S. commerce, geography, and demography, Minson and Mueller describe a study of how individuals and pairs perform when asked to answer these questions and how ready they are to incorporate input from outsiders. They found that pairs generated estimates that were closer to the true values than individuals working on their own were able

Published by AAAS

to do. On the other hand, when individuals were given a chance to revise their estimates upon hearing of the judgments of others, they did so to a greater extent than the pairs, so that the original accuracy advantage enjoyed by the pairs disappeared. It appears that the justifiably greater confidence exhibited by the pairs in the first stage may have led them to discount the value of the opinions of others. — GJC

Psychol. Sci. **23**, 10.1777/0956797611429132 (2012).

EVOLUTION

The Great Gene Giveaway

The vast majority of genes in eukaryotes are inherited vertically; that is, they are transferred through sexual or asexual reproduction from parent(s) to offspring (i.e., from one generation to the next). Prokaryotes are not quite so obliging. Among bacteria and archea, there is a substantial amount of lateral (or horizontal) gene transfer; that is, genes being exchanged between unrelated organisms independent of reproduction.

Christin *et al.* use comparative studies of DNA sequences (phylogenetics) to provide evidence of repeated lateral gene transfers occurring in plants. Different species of the grass lineage *Alloteropsis* use either the C3 or the more recently evolved C4 photosynthetic pathway to fix carbon from the air. Analysis of two enzymes critical for the C4 pathway reveals that individual C4 *Alloteropsis* species seem to have picked up these nuclear genes from four other genera of grass: *Setaria palmifolia*, found in South Africa; *Themeda quadrivalvis*, in Australia; and a Cenchrinae species; with the first transfer, from Melinidinae, occurring before the species divergence of *Alloteropsis*. Lateral transfer may have occurred because of the close physical proximity of the different plant species, all of which are wind-pollinated, resulting in the transfer of pollen between them. Acquisition of the C4 genes may then have provided a selective advantage, because C4 is more efficient than C3 photosynthesis. — GR

Curr. Biol. 10.1016/j.cub.2012.01.054 (2012).

MATERIALS SCIENCE

A Gentle View of Organics

The electronic properties of devices based on organic small molecules strongly depend on the architecture and organization of the active molecules, which can change over space and time. Thus, effective analytical probes must operate not only with fine temporal and spatial resolution but also over large sample sizes, without altering or damaging the specimens. Altoe *et al.* show that scanning transmission electron microscopy can be applied to the study of thin organic films. Damage to the samples is avoided through a low electron dose administered with scanned parallel beams, with the beam diameter determined by the sensitivity of the particular material. The authors mapped the structure of thin films of pentathiophene butyric acid (5TBA) and two of its derivatives. For Langmuir-Blodgett processed films of 5TBA, they observed islands approximately 1 μm in diameter, each comprising one or two crystalline domains with different lattice orientations. The authors also identified regions with lower diffraction intensity, which they associated with a high defect concentration—a factor of critical importance when troubleshooting poor performance in organic electronic devices. — MSL

Nano Lett. **12**, 10.1021/nl203776n (2012).

TOXICOLOGY

What's Fed to the Fish

Human activities send a dizzying number of organic small molecules into various bodies of water, and the first step in assessing the dangers they may pose is to determine how much of each compound gets sequestered (and possibly transformed) in fish and other aquatic organisms. Direct uptake measurements are time-consuming and challenging, so validated models would be of great use, but thus far studies that compare different models across a broad spectrum of experimental data have been scarce. Stadnicka *et al.* strive to make progress in this vein by measuring correlations of model predictions with literature data on the uptake of 39 organic compounds in two different fish species: rainbow trout and fathead minnow. In particular, they compare the accuracy of one-compartment models treating fish as a single continuous system with that of a physiologically based toxicokinetic model incorporating more fine-grained distinctions between accumulation in fatty tissue and in organs such as liver and kidneys. On the whole, the models fared similarly, matching measured concentrations to within an order of magnitude for 68% of the compounds, though predictions were poor for minnow accumulation of certain polar compounds, such as phenol and its derivatives. — JSY

Environ. Sci. Technol. **46**, 10.1021/es2043728 (2012).

CREDIT: ISTOCKPHOTO.COM

Published by AAAS

AROUND THE WORLD

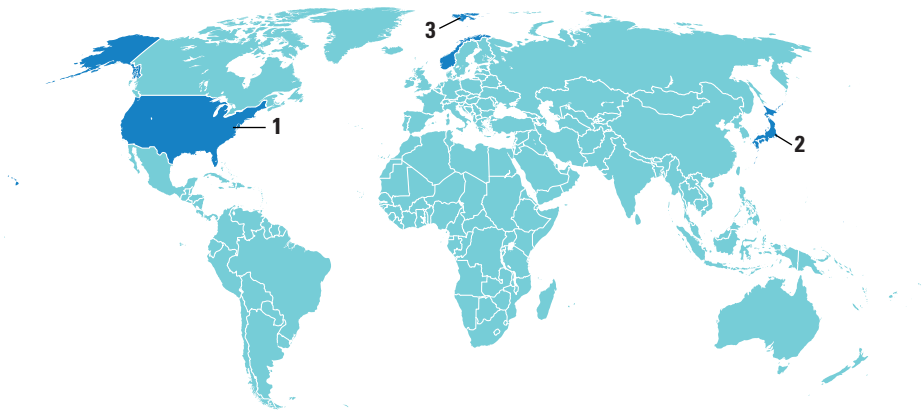

Washington, D.C. **1**

Study of Diesel Lung Cancer Risks Sees Daylight

After a nearly 20-year legal fight over their data, U.S. government scientists have finally published two papers showing that underground miners exposed to high levels of diesel fumes have a threefold increased risk for contracting lung cancer compared with those exposed to low levels. The $11.5 million Diesel Exhaust in Miners Study (DEMS) followed 12,315 miners, controlling for key carcinogens such as cigarette smoke, radon, and asbestos. This allowed scientists to isolate the effects of diesel fumes. U.S. regulators now rate diesel exhaust as a "potential human carcinogen," but new data could prompt a revision of that classification and could also influence an upcoming review of international safety regulations.

An industry coalition had long denounced the study as flawed and took the government to court several times, eventually winning in 2001 the right to review all papers for 90 days before publication. With the case still on appeal, DEMS scientists published immediately after the latest 90-day review expired in early March. The papers appeared online in the 5 March issue of *Journal of the National Cancer Institute*. **http://scim.ag/dieselcancer**

Exhale. After lengthy legal battles, data linking diesel fumes in mines to lung cancer have been published.

Tokyo **2**

Panel Blasts Nuclear Industry's Safety Lapses

"Professional negligence on safety issues" led to the Fukushima Daiichi Nuclear power plant disaster, Koichi Kitazawa, a leading academic, said in Tokyo on 1 March, discussing an investigation into the accident by a private sector group. Believing in "a myth of absolute safety" and convinced "there was no room for improvement," Japan's nuclear industry failed to learn from accidents in other countries, he said.

Kitazawa, a chemist at the University of Tokyo and the Japan Science and Technology Agency, headed the investigation on behalf of the Rebuild Japan Initiative Foundation, a nongovernmental organization established by prominent business people, academics, and diplomats. The group wanted to provide an independent look at what went wrong. The group's report, released on 27 February, has a long list of nuclear safety problems, including having too many reactors at one plant (there are six at Fukushima Daiichi) and storing too much spent fuel on site. It also became obvious that reactor operators are not prepared for accidents.

Given all that could have gone wrong, "We were very lucky," that more radiation was not released, Kitazawa said. The panel is calling for a complete overhaul of the nuclear industry and its legal framework.

Svalbard, Norway **3**

Global Seed Vault Turns 4

In honor of the Svalbard Global Seed Vault's fourth birthday on 26 February, countries from around the world sent 24,948 seed samples to the chilly storage facility, also known as the "Doomsday Seed Vault." The birthday shipment included wheat varieties grown in a range of climates from Armenia and the Pamir Mountains in Tajikistan. The United States contributed barley integral to the Pacific Northwest's microbrew industry, as well as amaranth, a gluten-free alternative to wheat cultivated by the Aztecs. And an international institute based in Colombia sent 1365 samples of forage crops grown to feed livestock. Some of the many samples exhibit evidence of flood, drought, or cold tolerance, making them potentially valuable genetic resources.

Planted. Svalbard's seed vault received thousands of new seed samples including forage seeds (*top*) from tropical plants (*bottom*) from Colombia.

Opened in 2008 on Norway's Svalbard archipelago, the vault acts as a backup depository for the world's crop collections. Countries and institutions send samples of their varieties to Svalbard for safekeeping in case something happens to their primary collections.

CREDITS (TOP TO BOTTOM): © NEIL PALMER/CIAT (2); THORNEY LIEBERMAN/GETTY IMAGES

Published by AAAS

Gorilla Genome Sequenced

For 35-year-old Kamilah, it's just another week at the San Diego Zoo. But not for her genome: After 6 years, the Wellcome Trust Sanger Institute in the United Kingdom has published the DNA sequence of this western lowland gorilla, the last of the four great apes whose genetic blueprint needed deciphering. Comparison with the human, chimp, and orangutan revealed that while the chimp and human are closest kin, 15% of the human genome more closely matches the gorilla's.

Furthermore, about 500 genes show accelerated evolution in chimps, humans, and gorillas, suggesting an important role for those genes, researchers reported this week in *Nature*. Some researchers had thought that accelerated hearing genes were important in the evolution of language in humans, but now gorillas show acceleration in the same genes, notes Sanger's Aylwyn Scally. Based on the genome data and the fossil record, Scally and colleagues propose that the protochimp-human split from gorillas occurred 10 million years ago and humans split from chimps about 6 million years ago. http://scim.ag/gorillagenome

CREDITS (TOP TO BOTTOM): SAN DIEGO GLOBAL; IMAGES COURTESY OF MARCH OF DIMES (2)

NEWSMAKERS

Bioethicist Leaves Texas Stem Cell Bank

Controversial bioethicist **Glenn McGee** resigned last week from a Texas company that banks adult stem cells for use in medical treatments.

McGee drew attention last month for serving as editor-in-chief of the *American Journal of Bioethics* (*AJOB*) while working since December for CellTex Therapeutics in Houston. The company licenses technology from a South Korean company, RNL Bio, that treats people with various medical conditions with adult stem cells processed from the patients' own fat cells. Such treatments have not been approved for routine use by U.S. regulators. Critics suggested that McGee's employment with CellTex posed a conflict of interest with his *AJOB* duties.

Last week, *Nature* reported that CellTex has allegedly been paying a physician in Texas to inject patients with stem cells prepared by CellTex, probably illegally. Later that day, McGee announced his departure from CellTex on Twitter. "Enough," he wrote, adding: "I am preparing timely, lengthy, pointed comments on the whole matter."

THEY SAID IT

"These are probably the two most famous unpublished manuscripts in life science history."

—Michael Osterholm, a member of the U.S. government's National Science Advisory Board for Biosecurity (NSABB), referring to two controversial studies about H5N1 viruses submitted to *Science* and *Nature*. He said it at a 29 February meeting in Washington, D.C., organized by the American Society for Microbiology (see p. 1155).

Skin Stem Cell Scientists Win March of Dimes Prize


Green


Fuchs

Two scientists who study the molecular workings of skin stem cells and have led the way to understanding the basis for many skin disorders have won the March of Dimes Prize in Developmental Biology. Cell biologist **Howard Green** of Harvard Medical School in Boston was the first to succeed in growing skin grafts for burn victims. Cell biologist **Elaine Fuchs** of the Rockefeller University in New York City, who began her career as a postdoctoral researcher under Green, has focused her research on the molecular biology of skin and other epithelial cells, and pioneered the field of reverse genetics.

Fuchs says she is honored to share the award with her former mentor. "It illustrates a thread that began with [Green] developing the very first stem cells that could be maintained and propagated in culture," she says. Green's work, which saved the lives of many burn victims, inspired her own research into how normal stem cells develop into tissues, and later into how cancer cells develop and propagate, work that is leading to the development of new gene therapies to treat skin cancer and other disorders.

The winners, who will receive the prize 30 April, will share an award of $250,000.

FINDINGS

Transplant Procedure Helps Both Sides Get Along

The immune system's job is to keep out foreign invaders—which can also mean attacking transplanted organs. Transplant recipients take immunosuppressive drugs for life so their bodies won't reject the new tissue—risking kidney damage, infections, heart disease, and increased susceptibility to cancer. Still, many transplants are eventually rejected. Adding some of the donor's bone marrow (which manufactures immune cells), can help—but if the donor's immune system takes over, it can >>

Published by AAAS

>>FINDINGS

attack the recipient's tissues, called "graft versus host disease" (GVHD).

A clinical trial held at Northwestern University and described in *Science Translational Medicine* this week shows a way to evade both difficulties. Researchers at the University of Louisville in Kentucky engineered bone-marrow-producing cells from kidney donors to remove the cells likely to cause GVHD, while increasing "facilitating cells" that make the recipient's system more receptive to the transplant.

Of eight recipients who received the treatment the day after the transplant, five were off immunosuppressants, with normal kidney function and no sign of GVHD, within a year. "It's likely that the facilitating cells increase regulatory T cells, which balance immune system activity," says study co-author Suzanne Ildstad. "One patient says he's never felt better than when he was finally off immunosupression."
http://scim.ag/transplantcells

Spreading the Blame for The Mammoth's Extinction

The wooly mammoth of North America, a 3-meter-tall Australian kangaroo, and hundreds of other species of oversized animals around the world may have been the victims of collusion between changing climate and human depredation, according to a new study this week in the *Proceedings of the National Academy of Sciences*.

Zoologists Graham Prescott and David Williams and their colleagues at the University of Cambridge compiled extinction dates over the past few tens of millennia for 110 genera of megafauna across Australia, Eurasia, New Zealand, North America, and South America. They compared the timing of extinctions with the timing of the arrival of humans, of severe climate change, and of both. "It seems likely that both climate and human factors played a role," says Prescott.

The study "makes a clear case for there being an interaction" between humans and climate, says paleoecologist Anthony Barnosky of the University of California, Berkeley. "It shows what happens when two bad things happen at once." However, ecological statistician Andrew Solow of Woods Hole Oceanographic Institution in Massachusetts worries "that too much of the detail was omitted. This is a first step."
http://scim.ag/mammothext

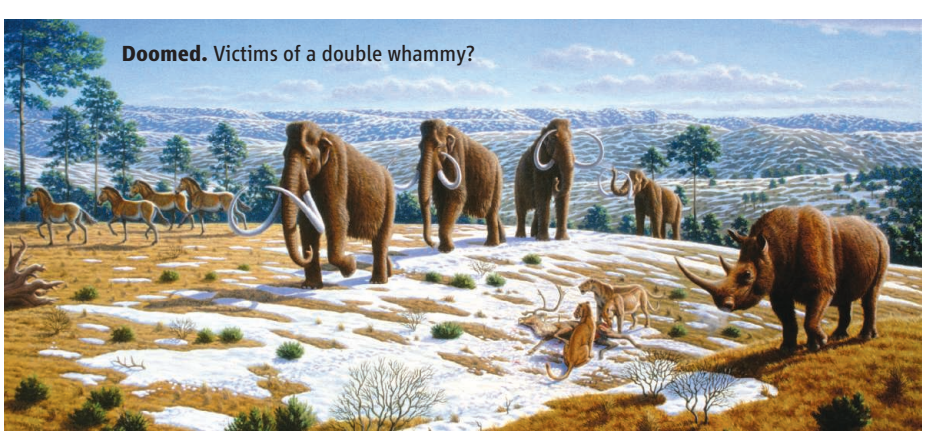

Doomed. Victims of a double whammy?

Random Sample

Archaeologists Protest 'Glamorization' of Looting on TV

In the endless search for fresh material, two cable TV shows highlighting a little-known subculture—amateur treasure-hunters—are debuting within a month of each other. But this is not just a harmless, quirky trend, archaeologists say. Both shows "promote and glorify the looting and destruction of archaeological sites," Society for American Archaeology President William F. Limp wrote in a message posted last week to the SAA listserv.

National Geographic Channel's show *Diggers* debuted 28 February with two episodes: The metal-detector-bearing hosts first poke around an Old West prison and then a former South Carolina plantation. On 20 March, Spike TV's show *American Digger*, hosted by former professional wrestler Randy Savage, will premiere featuring a team of "diggers" scouring "target-rich areas, such as battlefields and historic sites, in hopes of striking it rich by unearthing and selling rare pieces of American history," according to a recent announcement by the station.

What the on-air fortune seekers are doing is not illegal, Spike TV spokesperson Shana Tepper told *Science*: They are not venturing into National Parks or other federal lands. "Our show is shot on private property," she said. "They're getting artifacts that are otherwise rotting in the ground."

But archaeologists remain concerned. Iowa's State archaeologist John Doershuk posted a review of *Diggers* to the American Cultural Resources Association listserv, lamenting that "no effort was made to document where anything came from or discussion of associations—each discovered item was handled piece-meal." In addition to Facebook petitions, professional societies such as SAA have sent letters of condemnation to Spike TV and National Geographic.

"These programs encourage looting," University of Colorado, Boulder, archaeologist Steve Lekson told *Science*. "When treasure hunters loot sites, ripping artifacts out of the ground, we lose any chance of understanding context—what was with what, its date, how it was used, what it can tell us about history—all so somebody can have a trinket on their mantelpiece."
http://scim.ag/diggersTV

Science LIVE

Join us on 15 March at 3 p.m. EST for a live chat with leading experts on a hot topic in science. **http://scim.ag/science-live**

Published by AAAS

AVIAN INFLUENZA

Surprising Twist in Debate Over Lab-Made H5N1

For the past several months, the media, the public, scientific groups, and a key U.S. government advisory panel on biosecurity have wrestled with how to deal with two unpublished studies they thought described the creation of a bird flu virus capable of triggering an influenza pandemic with the potential to kill millions of people. *The New York Times* even billed it as a "doomsday virus." But now, a researcher who created one of the H5N1 mutants and a leading U.S. health official say the threat has been blown out of proportion, offering what they said were clarifications and "new data" to better gauge the risk it presents. Contrary to widespread reports, the researcher, Ron Fouchier of Erasmus MC in Rotterdam, the Netherlands, revealed that the virus made in his lab does not kill ferrets infected by the aerosol route. And it is more difficult to transmit the virus than Fouchier previously described.

Clarifying agents. Ron Fouchier (*left*) and Anthony Fauci urged people to rethink threat posed by engineered bird flu at a recent meeting in Washington, D.C.

CREDIT: MICROBEWORLD.ORG

These revelations promise to influence—although certainly not end—a contentious debate about whether to publish details about this virus and a second, related one that's less virulent. The wild-type H5N1 virus has decimated chicken flocks across Asia but has caused confirmed cases of disease in only about 600 humans, as it rarely spreads from person to person. Publishing the exact mutations the virus needs in order to spread among mammals could guide research on defensive measures and help derail an emerging pandemic, but many fear that the knowledge could help bioterrorists start one. To date, this debate has taken place largely in an information vacuum. Only a select group of people outside the two research groups involved have read drafts of papers describing the work, one of which was submitted to *Science* and the other to *Nature*. On 29 February, Fouchier attempted to partially fill that vacuum by offering glimpses of his group's data at a public meeting held by the American Society for Microbiology (ASM) in Washington, D.C. "There are a lot of misperceptions about what you can and cannot conclude from these studies," Fouchier said at a panel discussion on the topic.

Fouchier sparked the controversy in September 2011 when he revealed at an influenza conference in Malta that his lab had engineered H5N1 to transmit readily in mammals for the first time. Fouchier's group used the popular ferret model, and as reported in the conference newspaper, *The Influenza Times*, a mere five mutations made the virus transmissible. "This is very bad news, indeed," said Fouchier in *The Influenza Times* account of his presentation. "This virus is airborne and as efficiently transmitted as the seasonal virus." He made similar statements to *Science* in November, calling the mutant "probably one of the most dangerous viruses you can make."

In December, the U.S. government's National Science Advisory Board for Biosecurity (NSABB) recommended that the researchers and the journals redact key information from the papers. The diverse panel—which includes scientists from several disciplines, veterinarians, and biosecurity experts—also questioned whether the teams should have used more stringent biocontainment measures to safeguard against these viruses escaping from the lab. An uproar followed. Some said the experiments never should have been performed. Fouchier and the researcher who led the second team, Yoshihiro Kawaoka of the University of Wisconsin, Madison, and the University of Tokyo, criticized the call for redaction and the attempts to control the free flow of scientific communication, as did many other scientists. Kawaoka also stressed in a *Nature* comment in January 2012 that his mutant did not kill ferrets and was no more dangerous than the strain that caused the relatively mild 2009 pandemic.

But the researchers and the journals agreed to follow NSABB's recommendation, and the influenza community called for a voluntary 2-month moratorium on research with such mutant viruses. Then in February, an expert group consisting mainly of influenza researchers met with Fouchier and Kawaoka for 2 days at the World Health Organization (WHO) in Geneva and came to a conclusion that directly contradicted that of NSABB: Redaction did not make sense, they said, for both scientific and practical reasons.

At the ASM meeting, NSABB acting chair Paul Keim of Northern Arizona University in Flagstaff led the discussion with Fouchier; fellow NSABB member Michael Osterholm of the University of Minnesota, Twin Cities; *Science* Editor-in-Chief Bruce Alberts; and Anthony Fauci, who heads the U.S. National Institute of Allergy and Infectious Diseases, which funded both experiments. Fouchier reported that his team swabbed the noses of four ferrets with the mutant virus, which then spread to three of four ferrets in a neighboring cage by the aerosol route. The researchers reisolated the virus from one of these animals, swabbed the noses of two uninfected ferrets, and found that they spread it to two of two animals in a neighboring cage.

Fouchier criticized press accounts that suggested, as he put it, that "this virus would spread like wildfire if it would come out of our facility." Not only did the mutant fail to spread 100% of the time, he said, animals infected

via the aerosol route were not as likely to transmit the virus as ferrets infected with seasonal influenza strains that routinely spread between humans: They made copies of the virus more slowly, and the peak levels of virus were much lower. "We have to conclude that this virus does not spread yet like a pandemic or seasonal influenza virus," Fouchier said, in contrast to what he reportedly said in Malta. He did not respond to *Science*'s request to discuss this discrepancy.

As for lethality, Fouchier presented data from a second set of experiments, which found that only one of eight ferrets infected with the mutant virus through nasal swabs developed severe disease, and none died. He noted that when they put "very, very high doses" into the lungs of six ferrets, "yes, the animals will drop dead." In the aerosolized transmissions of the virus, he stressed, "we actually see no severe disease at all." This is in stark contrast to what Fauci said was the widely held perception that one ferret sneezes and all the ferrets in adjoining cages die; he singled out a report by ABC News on 18 February that said aerosol transmission killed "all 40 of the exposed animals" in neighboring cages. "These viruses do not kill ferrets if they're sneezed on," Fouchier said.

Fouchier further contended that if H5N1 does acquire mutations that make it more transmissible in humans, it likely will not cause severe disease in most people. To date, H5N1 has killed nearly 60% of the confirmed cases, but he said he did not think this fatality rate was accurate, because many cases that do not cause serious illness probably go undetected. He also pointed to an experiment he and his colleagues published in the *Journal of Virology* in March 2011, which showed that ferrets given seasonal flu virus before being exposed to wild-type H5N1 did not develop severe disease. "You all have been infected previously with seasonal flu," Fouchier said. "It would be unlikely that you would have no cross-protection against a virus like H5N1." (Osterholm later told *Science* that "there's absolutely no data to support that [assertion] beyond this animal model, and we have an abundance of data from real life that speak against it.")

In another surprising twist, Fauci said he and other members of the WHO group had recommended that the researchers revise their manuscripts "to include new data and elicit clarifications of old data" and submit them to NSABB, which should reconvene and reconsider the issues. Given the secrecy surrounding the manuscripts and the reluctance of people who have read them to discuss details, it is difficult to determine what actually is new or being clarified. "This was overwhelmingly less about new data than making sure there was a clear understanding of the old data," Fauci told *Science*.

Fauci said he was glad Fouchier had a chance to clarify that aerosol transmission of mutant H5N1 did not kill ferrets and that the virus, as some wilder news reports speculated, would not wipe out half the human population. "Thank goodness we had the opportunity today to clear the air," Fauci said. But there are other fog banks on the horizon.

Science contacted seven of the 23 NSABB members, and although several promised to review revised manuscripts with an open mind, they all said the new information and the clarifications presented at the ASM discussion, at first blush, did not change their views. "The issue is you have a virus generated in laboratory that's now transmissible [in mammals]," says NSABB member Arturo Casadevall, a microbiologist at the Albert Einstein College of Medicine in New York City. "This virus has the capacity to recombine, and we have no idea what will come out."

No date has been set for reconvening NSABB. **–JON COHEN**

With reporting by David Malakoff.

RESEARCH SPENDING

A Bumper Year for Chinese Science

BEIJING—Another year, another chance for scientists here to pop the champagne corks. In a draft budget released on 5 March at the opening session of the annual National People's Congress, China has earmarked 32.45 billion yuan ($5.14 billion) for basic research in 2012—up 26% from last year's appropriation.

Overall, central government spending on science and technology is slated to rise 12.4%, to 228.54 billion yuan ($36.23 billion). Scientists will also benefit from a 24% jump in funding for Project 985 and Project 211, which funnel money to elite universities.

Slowdown strategy. With a slackening economy in sight, Wen Jiabao says China will focus on research that boosts growth.

CREDIT: LI XUEREN/XINHUA/LANDOV

In a 2-hour speech at the Congress, comparable to the U.S. State of the Union address, Premier Wen Jiabao dwelled primarily on China's economic health. Many economists expect growth to slow in China this year, and the central government has set humbler goals. Wen announced that the target for GDP growth in 2012 would be lowered from 8% to 7.5%. Chinese scientists are expected to do their part to fan the embers. Echoing a theme of last year's speech, Wen pledged to "more closely integrate science and technology with the economy."

The cash infusion for basic research will be divided among the National Natural Science Foundation of China, scores of "key" state laboratories, and select institutes. The exact distribution of funds is expected to become clear later this month, after the Congress and the Chinese People's Political Consultative Conference, together called *Liang Hui*, conclude.

With land reform at the top of the political agenda this year, agricultural research got a call out in Wen's speech. A whopping 53% boost in spending on agricultural S&T will mean 10.1 billion yuan ($1.60 billion) for targets such as high-yield crops, controlling animal-borne epidemics, and improving drought management. More delicately, the premier nodded at China's recent food-safety scandals, pledging that the government would strengthen oversight of the food and drug industries.

Wen acknowledged mounting criticism of China's development model, saying, "We will show the world with our actions that China will never seek economic growth at the expense of its ecological environment and public health." The statement drew a rare round of applause from delegates.

On the agenda this session is a proposal to distribute research grants more equitably. If implemented, it could really sweeten the pot for Chinese scientists.

–MARA HVISTENDAHL

SCIENTIFIC MISCONDUCT

Reviewer's Déjà Vu, French Science Sleuthing Uncover Plagiarized Papers

Last August, Patrick Jansen, an ecologist at Wageningen University in the Netherlands, thought a paper he was asked to review for the *International Journal of Biodiversity and Conservation* (*IJBC*) seemed familiar. Suspicious, he ran it through the Turnitin antiplagiarism software often used by instructors to catch students who have copied others' work.

Jansen was startled to find that about 90% of the text was copied from a 2007 paper in *Conservation Biology* that he had coauthored with ecologist Pierre-Michel Forget of France's National Museum of Natural History. The paper submitted to *IJBC* examined how human hunting of small animals negatively affected the dispersal of seeds of the Moabi tree, *Baillonella toxisperma*, in the Republic of the Congo. Jansen and Forget's original paper reported on the crabwood tree, *Carapa procera*, in French Guiana and Surinam. But aside from the different tree and location, the two papers were nearly identical, including the text, figures, tables, and statistical analyses.

After a few insistent e-mails to the journal, Forget and Jansen were given the name of the submitted paper's corresponding author: Serge Valentin Pangou, director of the Study and Research Group on Biological Diversity (GERDIB) in Brazzaville, the Congo's capital. While GERDIB is not well known internationally, it is an important institution in the Congo that often carries out ecological and environmental studies for the government, researchers familiar with it say. And according to foreign scientists who have worked in the Congo, as its director, Pangou serves as a powerful gatekeeper who can grant research permits to them, as well as to Congolese graduate students and junior researchers.

Forget, whose father was a well-known private detective in France, began investigating Pangou's published scientific papers, eventually concluding that at least nine of them, published between 2006 and 2011, were plagiarized in whole or in part. An investigation by *Science* supports Forget's conclusions and also finds that some of Pangou's coauthors were unaware that their names were used. The affair has already led to the retraction of four papers on which Pangou is the corresponding author, as well as the rejection of the paper submitted to *IJBC*.

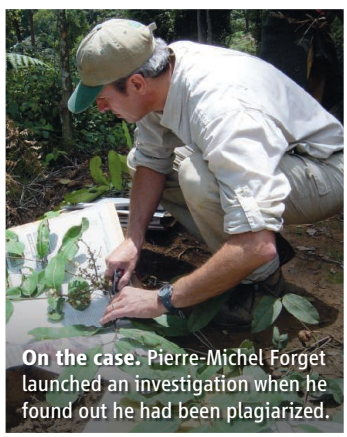

On the case. Pierre-Michel Forget launched an investigation when he found out he had been plagiarized.

Pangou tells *Science* that he accepts "all of the responsibility" for the papers that have already been withdrawn, but he contends that he did not deliberately engage in plagiarism, chalking it up to "the abusive utilization of bibliograph[ies]" which he "regrets sincerely." He did, however, admit to *Science* that he added some authors to papers without their knowledge.

Forget, who has worked for many years in Africa, says he became "obsessed" with the case and persisted even after some colleagues suggested privately that he might be harming African science by exposing the alleged misdeeds of a high-level research official like Pangou. "Plagiarism is an international problem, not an African one," he says.

Forget's investigation also raises questions about how rapidly journals react to such charges. As Forget contacted journals, some acted quickly. The editors of the botany journal *Candollea* immediately retracted a 2009 paper by Pangou and three co-authors that turned out to be largely copied from an earlier paper in the *Journal of Tropical Ecology*. It also included sections from the Ph.D. thesis of one of Forget's colleagues. *Candollea* accompanied the retraction notice with a short editorial denouncing plagiarism.

Others were slower off the mark, Forget says. The editors of *Food Chemistry*, published by Elsevier, took months to act after being informed by an author of a 2011 paper in the journal that his paper had been plagiarized by Pangou just months later in the *International Research Journal of Plant Science* (*IRJPS*). Only after an inquiry by *Science* late last month did Elsevier notify *IRJPS*'s editors about the offending paper and ask for a retraction, which they then quickly did.

Wendy Hurp, Elsevier's publisher for food science journals, says the delay in dealing with the accusation was due to an "oversight" and that Elsevier usually acts quickly to run suspected papers through the CrossCheck antiplagiarism database. In this particular case, Hurp's team found that 59% of Pangou's paper was identical to the earlier one in *Food Chemistry*.

In two of the four cases in which papers have been retracted, Pangou has written on official GERDIB stationery to the editors involved, taking overall responsibility but putting the blame on either "bad usage of biblio-

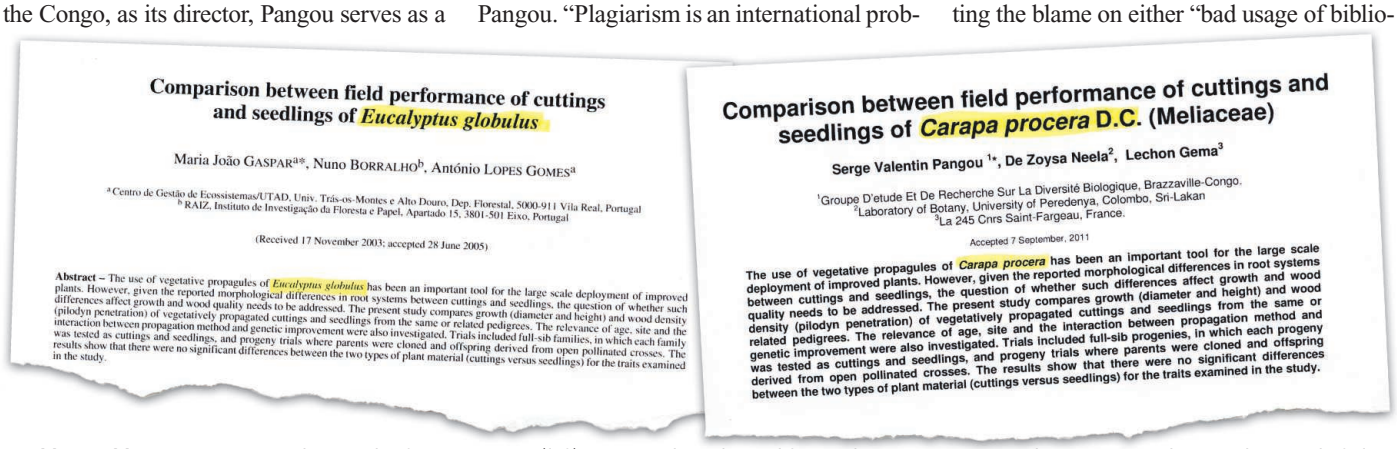

Comparison between field performance of cuttings and seedlings of *Eucalyptus globulus*

Maria João GASPAR[a]*, Nuno BORRALHO[b], António LOPES GOMES[a]

[a] Centro de Gestão de Ecossistemas/UTAD, Univ. Trás-os-Montes e Alto Douro, Dep. Florestal, 5000-911 Vila Real, Portugal
[b] RAIZ, Instituto de Investigação da Floresta e Papel, Apartado 15, 3801-501 Eixo, Portugal

(Received 17 November 2003; accepted 28 June 2005)

Abstract – The use of vegetative propagules of *Eucalyptus globulus* has been an important tool for the large scale deployment of improved plants. However, given the reported morphological differences in root systems between cuttings and seedlings, the question of whether such differences affect growth and wood quality needs to be addressed. The present study compares growth (diameter and height) and wood density (pilodyn penetration) of vegetatively propagated cuttings and seedlings from the same or related pedigrees. The relevance of age, site and the interaction between propagation method and genetic improvement were also investigated. Trials included full-sib families, in which each family was tested as cuttings and seedlings, and progeny trials where parents were cloned and offspring derived from open pollinated crosses. The results show that there were no significant differences between the two types of plant material (cuttings versus seedlings) for the traits examined in the study.

Comparison between field performance of cuttings and seedlings of *Carapa procera* D.C. (Meliaceae)

Serge Valentin Pangou [1]*, De Zoysa Neela[2], Lechon Gema[3]

[1]Groupe D'etude Et De Recherche Sur La Diversité Biologique, Brazzaville-Congo.
[2]Laboratory of Botany, University of Peredenya, Colombo, Sri-Lakan
[3]La 245 Cnrs Saint-Fargeau, France.

Accepted 7 September, 2011

The use of vegetative propagules of *Carapa procera* has been an important tool for the large scale deployment of improved plants. However, given the reported morphological differences in root systems between cuttings and seedlings, the question of whether such differences affect growth and wood quality needs to be addressed. The present study compares growth (diameter and height) and wood density (pilodyn penetration) of vegetatively propagated cuttings and seedlings from the same or related pedigrees. The relevance of age, site and the interaction between propagation method and genetic improvement were also investigated. Trials included full-sib progenies, in which each progeny was tested as cuttings and seedlings, and progeny trials where parents were cloned and offspring derived from open pollinated crosses. The results show that there were no significant differences between the two types of plant material (cuttings versus seedlings) for the traits examined in the study.

PHOTO CREDIT: © PIERRE-MICHEL FORGET

Double trouble. A 2005 paper in the *Annals of Forest Science* (*left*) was copied nearly word for word in a 2011 paper in the *International Research Journal of Plant Science* (*right*) that has since been retracted. Serge Pangou has admitted sole responsibility.

Published by AAAS

graphic review" or on a "junior researcher" co-author. When *Science* asked about that co-author, Pangou said he had lost track of her; attempts by *Science* to find the researcher have so far failed.

Three co-authors contacted by *Science* said Pangou has either not been in touch with them recently or not informed them that they were listed as co-authors on his papers. One, a Sri Lankan researcher named Neela de Zoysa, appears on four of the papers Forget says are plagiarized, and on another one published last year whose originality has not yet been questioned. She is identified in the papers as being at the University of Peradeniya in Sri Lanka, a position she held long ago in the 1980s, but de Zoysa, reached in Massachusetts where she has lived since 1991, says she had no knowledge of the papers and has had no contact with Pangou since 1985. De Zoysa, who has since worked at Harvard and Brandeis universities but is now an independent botanist, says she met Pangou briefly in Paris at a workshop that year. Pangou, when informed of de Zoysa's statements by *Science*, said in an e-mail that he had been telling "half-truths" and "wished to personally address my apologies" to her.

Another co-author on Pangou's papers is Théophile Bouki, a forest engineer who works for the African Network of Model Forests in Yaoundé, Cameroon, and who recently received his doctoral degree in France. Bouki, who spent time in Brazzaville as a student and knows Pangou, is listed as a co-author on four papers Forget has concluded are plagiarized, including the *Candollea* paper. Bouki says Pangou never showed him the papers ahead of time and that in at least one case he was completely unaware of its publication. In a telephone interview, Pangou agreed that Bouki had nothing to do with the alleged plagiarism.

In an earlier e-mail to *Science*, Pangou said that the retractions and accusations had already "demolished my scientific career," adding that he had "learned my lesson" and that "such failings will not happen anymore."

One Western scientist who works in the Congo and knows Pangou, but who asked not to be identified, says that "years of government neglect" of the war-torn country's scientific effort, along with the Congo's "isolation from the international community," has led to a failure to teach ethical standards to researchers, even though there are "a number of well-trained and honest people here who are trying to make a difference."

Indeed, Forget says that his crusade against plagiarism is for the benefit of the younger generation of African scientists. As for Pangou, the son of a detective believes "the case is now closed." **–MICHAEL BALTER**

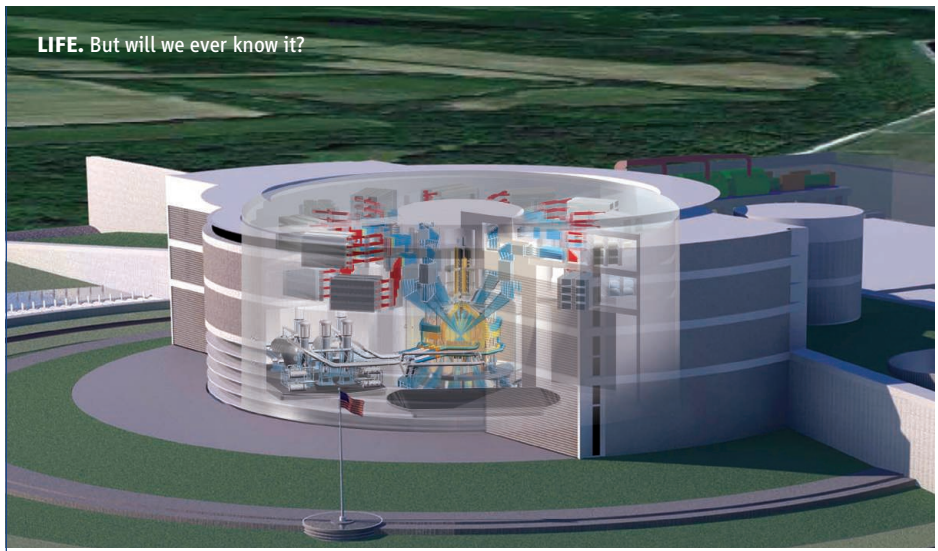

LIFE. But will we ever know it?

CREDIT: LAWRENCE LIVERMORE NATIONAL LABORATORY

ENERGY RESEARCH

Report on Future of Fusion Research Says U.S. Should Hedge Its Bets

The United States should fund a national program of research into inertial fusion energy, but it's too early to pick a winning technology. So says an interim report released this week from a committee that has been surveying research at national laboratories and universities since July 2010 on behalf of the National Research Council (NRC) of the U.S. National Academies. This interim conclusion will come as a relief to many in the field who have been concerned that the National Ignition Facility (NIF) at Lawrence Livermore National Laboratory—the world's largest and most advanced inertial fusion facility—would come to dominate the U.S. research effort (*Science*, 28 October 2011, p. 445).

Most fusion research focuses on magnetic confinement, using powerful electromagnets to contain a thin plasma of hydrogen isotopes and heat it until the nuclei fuse. Inertial confinement is an alternative method in which small capsules of hydrogen-isotope fuel are crushed to produce the intense temperature and pressure needed for fusion to occur.

Although researchers have been working on inertial confinement fusion for more than 50 years, no device has yet achieved "ignition," a self-sustaining fusion reaction that generates at least as much energy as it consumes. NIF, which was completed in 2009, is aiming to achieve ignition before the end of September this year. With this prospect in view, the Department of Energy asked NRC to carry out this review and formulate a road map for research toward a power-producing demonstration reactor. In the past, the United States has taken a scattershot approach toward inertial confinement fusion research, supporting different techniques through a variety of funding channels.

In its interim statement—released on 7 March to help with federal budget planning—the committee concluded that "many of the technologies needed … are still at an early stage of technological maturity." Those technologies include the "driver" used to crush the fuel capsule, such as lasers, heavy ion beams, or powerful pulses of electric current. The driver can also be trained either directly onto the fuel capsule or indirectly onto a heavy metal container, which then heats the capsule inside by bathing it in x-rays. Other issues for a power reactor will be developing a reaction chamber that can withstand intense neutron bombardment for years on end and discovering a way to produce the fuel capsules quickly and cheaply. (A reactor may consume a million or more capsules every day.)

The interim report notes that while "there have been impressive R&D efforts to develop a wide range of driver technologies, … very little effort has been spent on developing the technology of the reactor chambers or on addressing materials problems peculiar to inertial fusion."

The most thorough forward look at a future inertial fusion plant was carried out by staff at NIF. It resulted in a conceptual design dubbed the Laser Inertial Fusion Energy

Published by AAAS

(LIFE) plant. By sticking as closely as possible to the technology of NIF and using only components that are commercially available now, the NIF researchers estimate that they could build a demonstration plant in 12 years. Other researchers are skeptical that the technology is that far advanced. "The extreme optimism of some advocates of LIFE is unsupportable," says Robert McCrory, director of the Laboratory for Laser Energetics at the University of Rochester in New York, who is not a member of the committee.

The NRC committee came down firmly on the side of a diverse program of research. "There's a fairly long and challenging technical road ahead for all these techniques, including LIFE," says Ronald Davidson of Princeton Plasma Physics Laboratory, co-chair of the committee. The interim report concluded that, "based on the presentations and materials provided, … it would be premature to down-select among driver options at the present time."

The committee is due to complete its final report midyear. Given the tough financial straits that fusion research currently finds itself in (*Science*, 24 February, p. 901), how the report is received may depend on whether NIF achieves its ignition goal. "Until we see some evidence that fusion is going to work, it would be premature to invest large amounts in technology," McCrory says. **–DANIEL CLERY**

PARTICLE PHYSICS

Last Hurrah: Final Tevatron Data Show Hints of Higgs Boson

The hunt for the Higgs boson, the most sought-after particle in physics and the key to physicists' explanation of how all particles get their mass, is heating to a boil. This week, scientists working with an atom smasher in the United States called the Tevatron, which shut down in September 2011, reported that, having analyzed all the data they'll ever get, they see hints of the Higgs. The signs are not strong enough to clinch a discovery, but they jibe nicely with hints reported last year by researchers working with Europe's higher-energy Large Hadron Collider (LHC).

The result "doesn't make me more convinced [that the Higgs is there], because I'm already convinced," says Gordon Kane, a theorist at the University of Michigan, Ann Arbor. "But I hope it makes a larger fraction of the audience out there convinced."

Located at the Fermi National Accelerator Laboratory (Fermilab) in Batavia, Illinois, the Tevatron smashed protons into antiprotons to blast into fleeting existence subatomic particles not ordinarily seen in nature. Those collisions occurred within two massive particle detectors, known as CDF and D0, which strived to identify new particles as they quickly decayed into combinations of more familiar ones. In their final data sets, the CDF and D0 teams see more candidate Higgs decays than one would expect from random background processes, scientists reported 7 March at the conference *Rencontres de Moriond* in La Thuile, Italy.

The excesses are in line with Higgs hints reported in December 2011 by researchers working with the LHC at the European particle physics laboratory, CERN, near Geneva, Switzerland (*Science*, 16 December 2011, p. 1482). The LHC smashes protons into protons within two even bigger detectors that are hunting the Higgs, called ATLAS and CMS. The ATLAS and CMS teams both see excesses of candidate Higgses with a mass of about 125 giga–electron volts (GeV), or 133 times the mass of the proton. The CDF and D0 teams see candidates with roughly the same mass although with poorer mass resolution. "If you look at what ATLAS sees, at what CMS sees, and at what CDF and D0 see, it starts to look like a consistent picture," says Fermilab's Rob Roser, co-spokesperson for CDF.

Key differences between the Tevatron and the LHC also suggest that researchers with both machines are seeing Higgs bosons with the properties predicted by physicists' standard model. For example, a Higgs would emerge from a proton-antiproton collision at the Tevatron slightly differently from the way one would spring from a proton-proton collision at the LHC. Also, the CDF and D0 teams search for Higgses decaying into a different combination of particles from the ones sought by the ATLAS and CMS teams. Still, the results from Tevatron and the LHC roughly agree with each other and with standard model predictions.

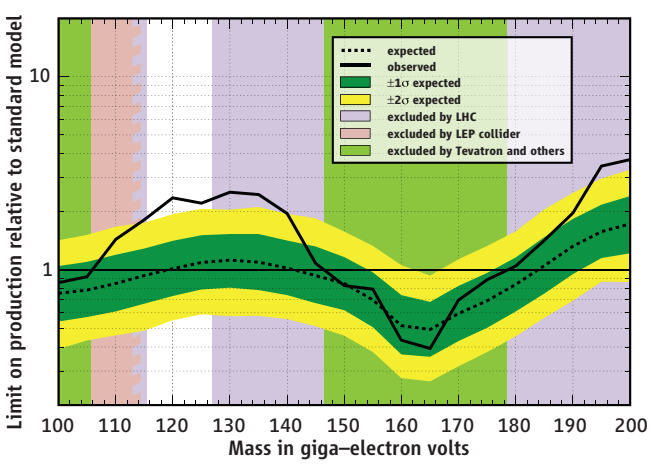

The plot. The dashed line shows the limit on Higgs production physicists expected to set. The solid line reveals the observed excess.

The Tevatron signal isn't overwhelming. Physicists measure the strength of a signal in multiples of the uncertainty in it, denoted sigma. A higher multiple implies a lower chance that background decays could mimic the signal and signifies a more robust result. Together, CDF and D0 see a 2.2-sigma excess. That combined result is as strong as either the ATLAS or CMS result alone, says Fermilab's Dmitri Denisov, co-spokesperson for D0. But, he says, it falls short of the 5-sigma standard for discovery or even the 3-sigma standard for "evidence" of the Higgs.

All hints will be put to the test by the end of the year, as the LHC collects more data. And if a 125-GeV Higgs does emerge, will Tevatron researchers deserve some of the glory? "I think people would have to mention us in the same sentence" as the LHC teams, Roser says. But, Denisov notes, "whoever passes 5 sigma will make the discovery, and the Tevatron cannot do that."

For now, some urge caution. "It's exciting," says Howard Gordon of Brookhaven National Laboratory in Upton, New York. But "we should wait until the end of the year to say anything more definitive."

As for what might have been, Denisov says physicists presented the result to Fermilab Director Pier Oddone a week earlier. "At the end, we said, 'Look, Pier, we want to run the Tevatron again,' " Denisov says. In response to the joke, he says, Oddone smiled. **–ADRIAN CHO**

CREDIT: FERMILAB

Published by AAAS

Light in the DEEP

From fish to squid, marine creatures have evolved sophisticated ways to make, use, and perceive light, inspiring researchers interested in optics and animal ecology and behavior

Green sight. Light striking the lens of the fish *Chlorophthalmus agassizi* triggers fluorescence at green wavelengths to which its retina is particularly sensitive.

WHEN ALISON SWEENEY WAS COLLECTING squid from the Gulf of California in 2006, a peculiar fish came up in the trawl net. Ten centimeters long, it had upward-pointing eyes that seemed to have a green tint. Sweeney, now a postdoc at the University of California, Santa Barbara, shone purple light on the fish's lens and was shocked to see that the lens converted the light to fluorescent green and formed green images. She didn't quite know what to make of this transformation, so she took a photograph, filed it away, and didn't give it much thought.

Five years later, more green-eyed fish showed up in Sweeney's nets during another cruise. This time, Sweeney, along with Yakir Gagnon, a postdoc at Duke University in Durham, North Carolina, took a closer look. In tests onboard and back in the lab, they confirmed that the light produced by the lens was transmitted to the back of the eye, where the photoreceptors are. "That should not be possible based on normal optics," because fluorescence typically goes out in all directions, says Gagnon's adviser, Sönke Johnsen. Sweeney, Gagnon, and Johnsen think the fish transforms and directs the light to see better: "The lens is emitting light that is matched to the light the retina can [best] absorb," Gagnon reported in January at the Society for Integrative and Comparative Biology (SICB) meeting in Charleston, South Carolina.

The green-eyed fish (*Chlorophthalmus agassizi*) lives where most of the light comes from bioluminescent organisms that emit bluish flashes. By converting all that incoming light to one green wavelength, the fish can make its retina more sensitive than if it had to have photoreceptors devoted to a range of wavelengths. "The fluorescence may be used by the animal to enhance its visual sensitivity," says Edith Widder, a marine biologist and head of the Ocean Research and Conservation Association in Fort Pierce, Florida. "It's a very intriguing idea."

Chlorophthalmus isn't the only undersea creature playing with light. Indeed, the sea is full of creatures with unusual eyes and innovative ways to manipulate light, traits that evolved out of necessity in a world where there's no place to hide and food and mates can be hard to find. A bottom-dwelling sea pen, when touched, sends a green glow shooting up its stem and out of its plume, but the glow turns from green to blue at the tips of the plume. One octopus has turned its suckers into light organs that emit bioluminescence. The tube-shouldered fish startles would-be attackers by discharging bioluminescent cells from its shoulder-mounted tube. To avoid being seen, organisms often play optical tricks. In some cases, they become transparent; in others they use illumination to distract potential predators or enlist help from predators of their attackers. "In the ocean, almost every animal you pull out is doing something clever with light," Johnsen says.

Lighting up. In this octopus, *Stauroteuthis syrtensis*, suckers have evolved into light organs, possibly used to lure in prey.

These twinkling organisms have fascinated humans for millennia, but only in the past decade have the instruments to understand optical systems become commonplace. With them, researchers have learned what light is where, what organisms are seeing, and what they are doing. They have documented visual arms races between predator and prey that have resulted in the evolution of visual systems very different and much more sophisticated than our own. Even though there's often not much of it in the deep, "light is very key," Johnsen says.

Seeing what's down there

The visual world beneath the waves is remarkably different from the one terrestrial organisms experience. The deeper you go, the bluer the light becomes, and in open ocean, it dims 10-fold every 75 meters, seeming to fade out completely by 1000 meters. This low light has prompted the evolution of

CREDITS: EDITH WIDDER (3)

specialized bodies and eyes, and organisms often generate their own light to communicate and find food.

Just as a darkening night sky reveals twinkling stars, a descent to the deep reveals a panoply of flashing bioluminescent organisms. They include most types of marine life, from bacteria to fish, with comb jellies having the highest proportion of glowing species. Above 1000 meters, an estimated 70% to 90% of the organisms are bioluminescent; below that, about 50% are. Flashes can be quick blinks, just tens of milliseconds long, or stretched out for several seconds or more. They can be intermittent or regular; up to 160 per minute have been recorded. And the fact that so many deep-sea organisms have eyes despite the total lack of sunlight attests to the importance of these points of pulsing light.

Light shapes the world of marine creatures. From 150 to 650 meters deep, fish tend to be silvery with dark backs and light organs on their bellies to counter the effect of being backlit from above and, therefore, visible to predators below. Lower down, red and black are the colors of choice for both fish and crustaceans. Red light doesn't penetrate that deep and self-generated spotlights by fish are bluish, so those body colors render individuals virtually invisible.

Researchers didn't begin to appreciate the extent of the lit world undersea until the 1950s, when they lowered a photomultiplier, which converts light energy into electrical current, into the depths. "It was shocking when they realized how much light was down there," Widder says.

The U.S. Navy became concerned that bursts of bioluminescence might reveal submarine locations and funded the development of tools to measure and observe it. Widder and her colleagues eventually used those tools to compile a dictionary of flash patterns that can be used to identify different plankton emitters and map plankton distribution. "There's a whole language of light down there, and we are barely beginning to understand it," she says.

Online

sciencemag.org

Podcast interview (http://scim.ag/pod_6073) with author Elizabeth Pennisi.

Worried that submersibles, with their bright lights and loud noises, were scaring off animals she wanted to study, Widder and her colleagues came up with an ultrasensitive camera system that uses far-red light for illumination. As "bait," they built an electronic jellyfish with LEDs that flash in the pattern of the burglar alarm jelly, which seems to use bioluminescence when attacked to call in predators of its attackers. Her team is now analyzing data from one of these "Eye-in-the-Sea" systems they installed on the bottom of Monterey Bay for a year.

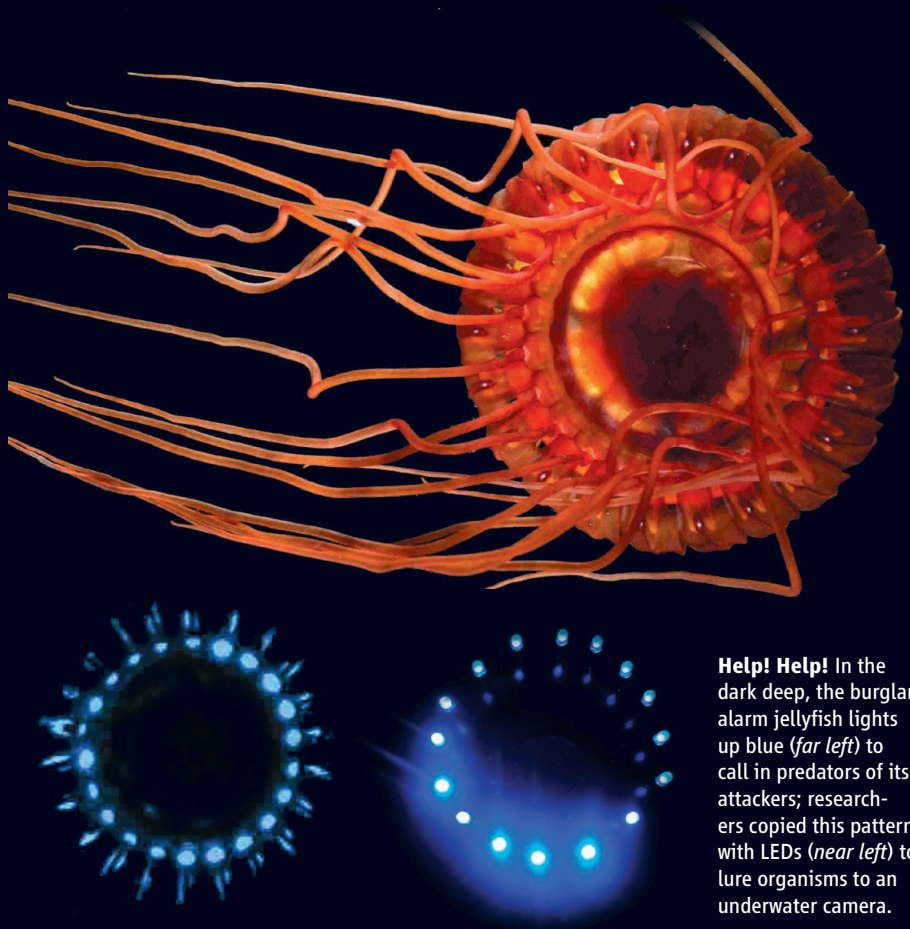

Help! Help! In the dark deep, the burglar alarm jellyfish lights up blue (*far left*) to call in predators of its attackers; researchers copied this pattern with LEDs (*near left*) to lure organisms to an underwater camera.

Shipboard instruments have also become far more sophisticated. When Duke's Johnsen came to study with Widder in 1997, their typical onboard equipment consisted of an $80,000 spectrometer the size of a small refrigerator with a liquid nitrogen tank to cool its components and a computer and monitor, all of which took up precious lab space. It was difficult to characterize the optical properties and do detailed physiological studies on live or even freshly dead specimens.

Now a credit card–sized spectrometer costing just a few thousand dollars, more sensitive cameras, and portable, robust light sources make the research much easier. Researchers are also better at measuring underwater light. Jules Jaffe of the University of California, San Diego, has even built a glass sphere that contains six cameras, each facing a different direction, to capture what a squid experiences visually. "Having small, reliable optical equipment means we can do things that we could only dream of 10 years ago," Johnsen says.

Tracking the light fantastic

Johnsen and others are using these instruments to piece together how light is used and perceived. On a cruise in 2009, Tamara Frank was at first puzzled to find that some cells in the eyes of crustaceans were sensitive to ultraviolet light, even though UV in sunlight doesn't reach the depths where the animals live. Frank, a biological oceanographer at Nova Southeastern University in Fort Lauderdale, Florida, and Johnsen surmise that the UV receptors help the animals discriminate between the bioluminescence of corals, sea pens, and echinoderms living

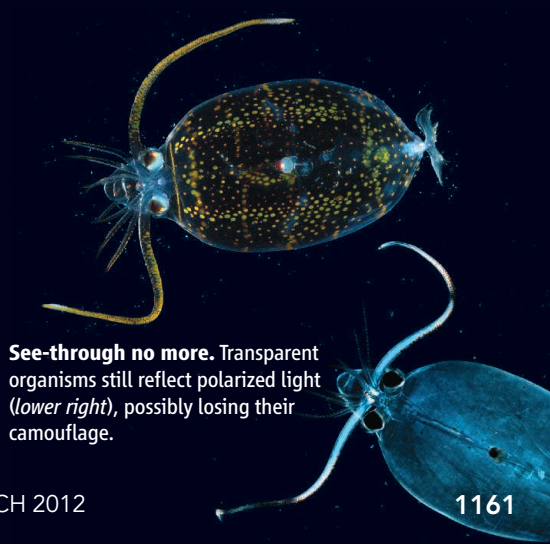

See-through no more. Transparent organisms still reflect polarized light (*lower right*), possibly losing their camouflage.

CREDITS: EDITH WIDDER (5)

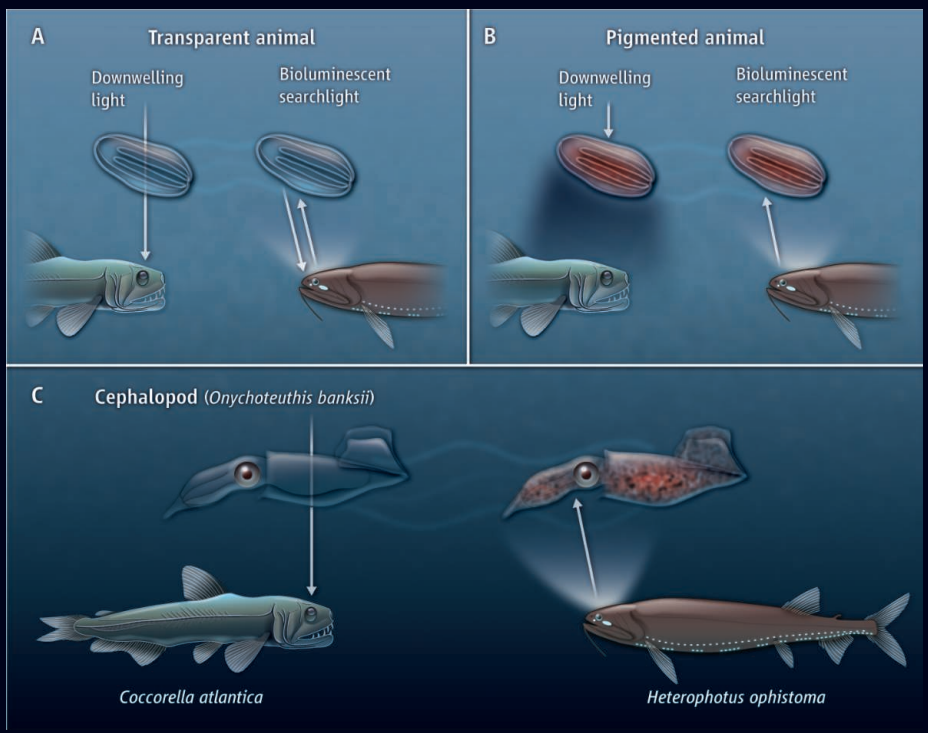

Master of disguise. Transparent organisms are invisible in downwelling light but can be seen by fish with bioluminescent searchlights; red-pigmented animals have the reverse problem. But a transparent squid and octopus (*above*, *far right*) turn red rapidly when hit with a searchlight, remaining invisible.

on the sea floor and that of more palatable waterborne creatures. They knew from previous studies that benthic organisms give off a greener glow. The crustaceans "may be sorting out food from poison," Johnsen says.

As these researchers have delved into the details of other optical structures, they are finding out how organisms work their magic with light. Because cells can control the spacing and sizing of optical components on a scale that approximates the wavelength of light, "they can make structures with remarkably cool optical properties that make the optics and telecommunication industries drool," Johnsen says.

Consider the problem of trying to disappear in midocean. Many fish have silvery sides that reflect incoming light in such a way that predators don't see them. But the polarization of the reflected light is different from that of the incoming light, so predators with polarized vision should be able to spot their prey. Yet when Justin Marshall, a visual ecologist at the University of Queensland in Brisbane, Australia, and Johnsen filmed dozens of fish in the Great Barrier Reef with a camera with a filter for seeing polarized light, they found some species, such as herring, to be much less conspicuous than expected.

They turned to computer modeling to understand why. Under their scales, fish have stacks of guanine crystal plates. Because the plates vary in thickness and spacing, with some parallel and others tilted, they create a biological mirror. Using equations microscope designers depend on to optimize reflective coatings for lenses, the two researchers found that the thickness of the stacks affects the polarization of light reflected from the scales. When 50 plates were stacked up together, the polarization of the reflected light was virtually the same as that of the incoming light, preserving the camouflage, Johnsen reported at the SICB meeting in January.

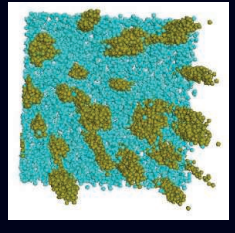

Clam care. Computer simulations (*above*) show that the iridescent cells (blue) that make giant clams colorful form a layer that transmits light to columns of algae (green) deeper down.

Some squid and octopi go to even greater lengths to hide from predators, alternating between transparent and opaque depending on the lighting conditions, Johnsen and a colleague reported in the 22 November 2011 issue of *Current Biology*. Organisms that live between 600 and 1000 meters tend to be transparent if they usually dwell in the upper part of that range or red and black if they hang out farther down. But deep-sea fish with spotlights can detect a transparent creature because the transparency is imperfect and will reflect that spotlight; and a red or black silhouette will stand out in any downwelling light (see diagram upper left). Johnsen and his postdoc Sarah Zylinski found that the transparent *Japetella heathi*, an 80-millimeter-long octopus, will expand red-pigmented cells when subjected to blue light such as the spotlight of a predatory fish. The blue light is not reflected by the red pigments, so the predator doesn't see its would-be prey. The octopus did not respond to a red light and remained transparent. *Onychoteuthis banksii*, a 140-millimeter-long squid, uses a similar camouflage tactic, turning red in blue light. "It's a moving game between the hiders and the seekers," Johnsen says.

Not all innovations with respect to light are motivated by the need to hide. Sweeney has been studying the biophotonics of giant clams, which are iridescent because they have pigmented cells called iridocytes in their mantles. The function of iridocytes has been a mystery, but they tend to be colocated with brown algae that live in the clam. As with corals, clams get carbon from the algae in return for providing nitrogen. Sweeney wondered whether the iridocytes might be serving the algae somehow.

Extraordinary Eyes

"Stomatopods have the most remarkable visual systems of any animal on the planet." So says Justin Marshall, a visual ecologist at the University of Queensland in Brisbane, Australia. Known as a mantis shrimp because of a superficial resemblance—but no real relationship—to shrimp, and claws that look and indeed work like the front legs of a praying mantis, these 30-centimeter-long furtive crustaceans live in burrows in reefs, rubble, or sediment. Their compound eyes, which are on stalks, constantly scan back and forth, taking in the scene and building up an image line by line.

Human eyes have four types of visual pigments: three for color vision and one for seeing in dim light. Stomatopods have 16, eight that span the visible spectrum, with others for ultraviolet wavelengths. Whereas we have to wear sunglasses to see polarized light, Marshall and his colleagues have found that stomatopods have built-in receptors that distinguish not just polarized from nonpolarized light, but also linear from circular polarized light, as well as right and left circular polarized light. (Polarized light energy typically vibrates along a plane, but when it passes through certain filters, it may change course and move in clockwise or counterclockwise loops. Oncologists use this type of light to detect skin cancers.)

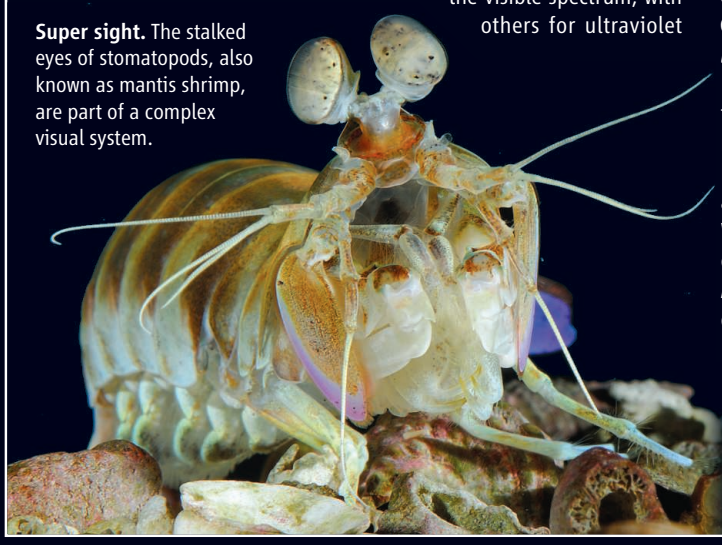

Super sight. The stalked eyes of stomatopods, also known as mantis shrimp, are part of a complex visual system.

In the same way that birds use color to recognize potential mates and rivals, stomatopods seem to depend on polarized signatures, says Thomas Cronin, a visual ecologist at the University of Maryland, Baltimore County, who has worked with Marshall for decades. With Tsyr-Huei Chiou, now based at National Cheng Kung University in Tainan, Taiwan, Cronin and Marshall have discovered how the stomatopod *Odontodactylus scyllarus* creates these signatures.

Chiou knew that light reflected by paddlelike structures located at the base of the stomatopod's antennae is polarized. But he could find no evidence that the paddles physically manipulate the light. Instead, he found a red carotenoid pigment known as astaxanthin, which absorbs and retransmits light that matches the tissue's polarization signature. When Chiou removed this pigment, polarization disappeared, he and his colleagues report in an upcoming issue of *The Journal of Experimental Biology*. "This is the first demonstration of the use of a carotenoid to produce a polarizing signal," Chiou says.

He and his colleagues think that by combining different proteins, different stomatopod species come up with telltale polarization patterns. These patterns come in handy because unlike colors, which change depending on the nature of the incoming light, they are the same under the great variety of lighting conditions encountered at different depths. **–E.P.**

Electron micrographs revealed that the iridocytes form a layer along the outer edge of the clam tissue, and the algae grew in pillars embedded in the iridocyte layer. Sweeney measured light reflection and transmission from the iridocytes and with postdoc Amanda Holt and other colleagues developed a computer model to assess the effect of the iridocytes on incoming light and how that light might affect the algae. (The model took advantage of algorithms designed to predict light scattering by dust particles in Saturn's rings.) They found that the arrangement of the iridocytes protects the algae from intense, potentially harmful light, but transmits lower energy light down to the lower part of the algal pillars, enabling those algae to thrive in limited sunlight, she reported at the SICB meeting. "The distribution and makeup of iridocytes is a precisely optimized optical solution," she said.

Eyeing applications

The study of light in marine organisms is turning out to have potential practical applications. Most notable is green fluorescent protein, whose discovery in jellyfish in the 1960s and subsequent development as a tag to follow cellular processes garnered the 2008 Nobel Prize in chemistry. Today, researchers are scouting out other novel light-emitting chemistries—for example, the yellow bioluminescence of a polychaete worm called *Tomopteris*, for new tag technology.

The tools developed to understand transparency in zooplankton are proving useful in shedding light on human cataracts, Johnsen says. With M. Joseph Costello of the University of North Carolina School of Medicine in Chapel Hill, he has found that some unexpected age-related changes are involved in clouding the lens. "This could change the way we treat and prevent [cataracts]," Johnsen notes.

Widder is using bioluminescent bacteria as a biomarker for pollution. She collects sediment samples, mixes in the bacteria, and notes by the fading glow how toxic the samples are. The test is a good, cheap way to tell where in an estuary pollution has built up.

Queensland's Marshall is working with electronic and optical engineers to redesign cameras. One project, called "Prawns in Space," aims to make satellite sensors work more along the lines of a mantis shrimp eye (see sidebar).

Even the green-eyed fish, with its directed fluorescence, may lead to better optics.

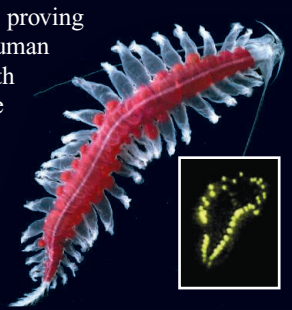

Latest in GFP? Researchers hope one day to tap the unique yellow bioluminescence of this polychaete for cell-labeling studies.

Sweeney has found that when she and her colleagues grind up the lens and suspend it in water, the aqueous solution still retains the light-altering and transmitting properties of the intact lens, suggesting that a molecule rather than a higher order structure may be responsible for directed fluorescence. To track down that molecule, Sweeney needs to net more green-eyed fish on her next cruise. And who knows what other surprises will come up in her trawl nets. **–ELIZABETH PENNISI**

CREDITS (TOP TO BOTTOM): ROY CALDWELL/UNIVERSITY OF CALIFORNIA, BERKELEY; EDITH WIDDER (2)

Obliterated. Rikuzentakata must rebuild from scratch.

JAPAN DISASTER

One Year After the Devastation, Tohoku Designs Its Renewal

Taking stock of the 11 March 2011 earthquake and tsunami, experts are planning communities that should be more resilient the next time disaster strikes

RIKUZENTAKATA, JAPAN—Under a newly fallen snow are the remnants of a lost world: Jumbled concrete foundations, wooden debris piled neatly, hollow shells of shattered buildings. The only clue to the town center is the train station's GPS location; there is nothing left of the structure. Rikuzentakata and many of its 20,000 inhabitants were erased on 11 March 2011.

In the year since the magnitude-9 Tohoku earthquake and subsequent tsunami, Japan's leading experts in engineering, seismology, urban planning, emergency response, and economics have been laying the groundwork for the rebirth of Rikuzentakata and dozens of other obliterated villages. By studying the patterns of destruction, conducting simulations, and probing how well evacuation plans worked, they hope to make communities along Japan's northeast coast better able to withstand and recover from the next megatsunami.

But as planners try to turn idealized visions of a safe city into plans for reconstruction, nature—and human nature—is forcing compromises. Experts concur that building towering seawalls to resist a once-in-a-millennium tsunami, like the one that struck here last March, "is not pragmatic," says Fumihiko Imamura, a tsunami engineer at Tohoku University in Sendai. And rearranging cities to make them safer—by moving houses to higher ground, for example—runs into logistical and political problems. "People agree on the concepts," Tatsuo Hirano, Japan's minister for reconstruction, said at a recent press conference in Tokyo. "But for the specifics, where and what kind of city to rebuild, it is very difficult to come to an agreement."

The sheer scale of the task ahead complicates matters. Shaking from the enormous earthquake last March inflicted minor structural damage for the most part, because the epicenter was quite far—80 kilometers—off the coast. The ensuing tsunami, which pummeled more than 1300 kilometers of coastline, took a dreadful toll: 15,852 dead, 3287 missing, $210 billion in damage to buildings and infrastructure, and more than 300,000 left homeless. Over the next 10 years, the government expects to spend $285 billion on reconstruction of the devastated Tohoku region. As each day passes, fewer displaced residents plan to return—and restoring economic vitality grows that much harder.

Lonesome pine. The tsunami wiped out all but one of 60,000 pine trees that formed a buffer between Rikuzentakata and the sea.

Extra protection

In the wake of the disaster, the first priority across Tohoku was to provide temporary housing and shops for evacuees. Crews also began gathering up an estimated 22 million tons' worth of wrecked houses and other structures for eventual disposal. Cars and appliances are being recycled. Concrete will be reused in new seawalls built to withstand more modest—and more frequent—tsunamis. According to Hirano, getting rid of debris will take 2 to 3 years.

The inevitable delay in reconstruction has given expert committees time to mull options and tailor proposed measures to local conditions. The starting point is coastal defenses. Of the region's 300 kilometers of seawalls, 180 kilometers were washed away. Tsunami erosion, earthquake-related subsidence, and the loss of seawalls means that many areas along the coast are now submerged, especially at high tide. Massive sandbag dikes erected since last March protect coastal highways and other critical infrastructure.

In some areas, tsunami barriers fended off the big one. In Fudai, a village 190 kilometers north of the quake's epicenter, 15-meter-tall floodgates stretch 200 meters across a narrow river valley; a concrete-topped embankment spans a neighboring valley. Before the Tohoku quake, critics derided the

CREDITS (TOP TO BOTTOM): ISSEI KATO/REUTERS/NEWSCOM; D. NORMILE/*SCIENCE*

Published by AAAS

$44 million structures as a waste of money. But they protected the heart of Fudai from the full brunt of the tsunami last March. Although 20-meter-high waves topped the barriers, the village tallied just one death among the 3000 residents and little damage.

Replicating that approach all along the coast would be far too costly, Imamura says. For one thing, Fudai's topography gave it an advantage. Its floodgates were built at a point between the shore and the town where mountains pinch the valley to a narrow neck, providing an obvious and cost-effective location for a barrier. The tsunami there was half the 40-meter height recorded in other areas. Another issue, Imamura says, is that concrete structures in marine environments must be rebuilt every 50 to 100 years.

A national committee on tsunami countermeasures has recommended rebuilding coastal walls or levees up to 12 meters tall—several meters taller than the old barriers. Their height would be designed to withstand the second or third biggest tsunamis to have hit a particular location, based on simulations and analyses of historical records. The committee also called for an important modification. Last year, water pouring over walls and embankments in some spots washed away supporting soil on the landward side, toppling the structures and leaving communities more exposed to the sea. To avoid such scouring, the committee recommended erosion-resistant foundations and sloping embankments on the landward side.

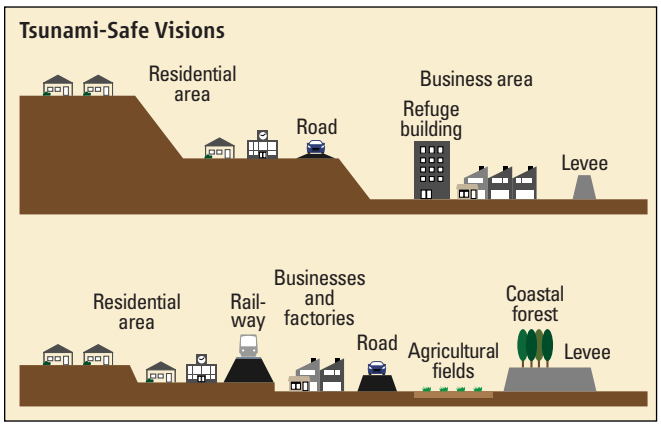

Common sense. Moving homes, schools, and hospitals to higher ground (*top*) or behind a series of barriers (*bottom*) will make cities more tsunami-resistant.

The need to rebuild scores of kilometers of barriers offers an opportunity for a more ecological approach. "Typically, these walls have been built as close as possible to the waterline," says Yukihiro Shimatani, a watershed management expert at Kyushu University in Fukuoka. He headed a government committee that suggested moving the walls inland so that beaches could be more natural. Undisturbed shorelines typically have a beach with an intertidal zone backed by dunes, then often marshes with brackish water and a transition zone to the inland ecosystem. The committee's report notes that the interplay of waves, sand, wind, and vegetation creates a niche habitat for shore birds, insects, and marine life. Seawalls at the water's edge divide the shore ecosystem. Rebuilding barriers at the landward side of the transition zone would not only protect precious coastal habitat but also reduce the force from storm surges, Shimatani says.

Aiming high

Experts are also debating approaches to building behind the barriers, and a consensus is emerging. For starters, they agree that residential areas and critical facilities such as schools and hospitals should be moved inland and uphill wherever possible. Where that is impractical—if high ground is too distant, for instance—a sufficient number of new buildings should be tall and sturdy enough to serve as tsunami shelters. (In Rikuzentakata, waves reached the roof of the four-story city hall.) Low-lying land near the shore should be reserved for parks, forests, and fields. Ideally, a second ring of embankments supporting roads and railways would protect business districts from waves that top shoreline barriers. Many Tohoku coastal communities rely on marine products; tsunami refuges will have to be built for workers at processing plants near the sea.

If much of that sounds like age-old common sense, it is. After last year's disaster, numerous news reports told of discoveries of ancient stone markers on hillsides warning future generations not to build nearer to the sea. "Before World War II, residential construction was not allowed in many areas in recognition of the tsunami danger," Hirano explained. "But during the postwar period of high economic growth, there was tremendous demand for housing, and those restrictions were relaxed."

To some extent, Rikuzentakata's picturesque layout—on a plain facing Hirota Bay ringed by coastal mountains—embodied the old wisdom. Along the shore was a beach fringed by a dense pine forest and, inland from the trees, a 5.5-meter-tall embankment. Behind the barrier, a sliver of natural marsh buffered agricultural fields. The business district was farther inland, in the middle of the petite plain, and surrounded by residential areas. The Kesen River valley was protected by tsunami gates. But the 18-meter tsunami overwhelmed these defenses, submerging the entire plain. Rikuzentakata's planners got many things right but still failed to protect their town.

Rikuzentakata is a prime example of the conundrum facing experts planning Tohoku's reconstruction. Survivors in this

GRAPHIC SOURCE: ADAPTED FROM MIYAGI PREFECTURE REPORT; PHOTO CREDIT: ISSEI KATO/AFP/GETTY IMAGES

Radioactive Limbo. While the tsunami-ravaged Tohoku region plans its recovery (see main text), contaminated areas around the Fukushima Daiichi power plant are a no-man's land that may remain deserted for decades.

Last December, plant operator Tokyo Electric Power Co. and the government announced that they had achieved a cold shutdown, meaning the nuclear fuel is stably maintained by reliable cooling at temperatures below 100°C. The company also reports that there is little or no radiation leaking from the plant. Next comes decommissioning and cleanup, a process that the government says could take 40 years.

No timetable has been set for resolving issues surrounding the evacuation zone. The government lifted evacuation advisories for some areas but has kept a 20-kilometer band around the reactors strictly off-limits, leaving about 80,000 people unable to return to their homes. Because some areas have high levels of contamination from cesium-134 and cesium-137, experts expect that the government will designate a broad swath of land around the plant as a permanent exclusion zone, similar to the one that has encircled Chernobyl since the disaster there more than 25 years ago. **–D.N.**

Published by AAAS

Nuclear Ambivalence No More?

TOKYO—The crisis at Fukushima Daiichi nuclear power plant that riveted the world last spring has had a potent effect on the industry's future. With one exception, it simultaneously strengthened opposition in nations already wary of nuclear power and made those committed to building—and exporting—nuclear reactors all the more determined to continue their programs.

The exception, of course, is Japan, which has had a major change of heart. Japan's energy plans called for nine new reactors, which would raise its total to 63 by 2020. Critics had long questioned industry claims that nuclear power is the cheapest energy option. After Fukushima, politicians and even some industry insiders joined the chorus. "The costs of dealing with spent fuel and decommissioning plants were taken out" of official numbers provided by utilities, says Tatsuo Masuda, an energy markets expert at Nagoya University of Commerce and Business. The government has promised to use a more accurate accounting of nuclear power costs in a new energy policy due this summer. In the meantime, the Cabinet has indicated that the nation needs to reduce dependence on nuclear power. In another bleak sign for the industry's future in Japan, the long-hobbled Monju experimental fast breeder reactor could be terminated, local press report. Tokyo Electric Power Co., hit by huge losses at Fukushima, will likely scale back its support for nuclear research in academia.

No thanks! Public opposition could kill the experimental Monju reactor.

Sentiment against the industry has hardened in Germany, which announced last May that it would shut down all 17 of its nuclear reactors by 2022. Last June, Italian voters opted for a nonnuclear future, passing a referendum that overturns 2009 legislation calling for new nuclear power plants. Italy shuttered its last nuclear power plants in 1990.

The European Union has been supporting a $400-million-a-year international effort to develop safer and more advanced Generation IV reactors. But with two of the largest E.U. members losing interest in nuclear power, a cloud hangs over related research. "Work on Generation IV reactors [in Germany] has almost totally stopped because the interest of the industry, and thus its financial support, has diminished significantly," says Peter Fritz, a vice president at Karlsruhe Institute of Technology in Germany. Europe's nuclear research focus, he says, is shifting toward waste disposal.

On the other side of the world, South Korea announced plans last November to become a nuclear export powerhouse, with a goal of capturing 20% of the global market by 2030. South Korea has 23 operating nuclear reactors and aims to have 40 by 2030. South Korean companies are preparing to build four reactors in the United Arab Emirates. Its plan includes support for R&D on next-generation reactors. China, meanwhile, suspended approvals for new reactor construction days after the disaster. It has 14 operating reactors and 27 under construction, and plans to increase the percentage of its electricity produced by nuclear power from the current 1% of the total to 6% by 2020. The status of these plans is unclear. "China is sending mixed signals" on its nuclear policy, says Jan Vande Putte, a nuclear energy specialist with Greenpeace International in Amsterdam.

This year, at least five countries—Vietnam, Bangladesh, United Arab Emirates, Turkey, and Belarus—plan to start building their first nuclear power plants. Most surprising may be Belarus, which absorbed about 80% of the radioactive fallout from the 1986 Chernobyl disaster. More than 25 years after the accident, Belarus is spending $1 million per day on rehabilitating the region, screening foodstuffs for safety, performing medical exams for those exposed, and implementing other ongoing countermeasures, Vladimir Chernikov, chair of the Chernobyl Consequences Mitigation Agency in Minsk, said at a recent press conference in Tokyo. Despite that burden, Belarus decided in January 2011 to build its first nuclear power plant; the decision was not revisited after Fukushima. "The Belarus people understand there is no [economical] alternative at the moment," Chernikov said.

The United States may be on the cusp of a renaissance. Last month, the U.S. Nuclear Regulatory Commission granted the first construction permits for new nuclear reactors since 1978, the year before the Three Mile Island accident in Pennsylvania. Back then, it cost about $2 billion in today's dollars to build a reactor. The price tag has since risen to as much as $9.4 billion. Without generous subsidies, that construction cost may end up pricing nuclear power out of the market. **–D.N.**

With reporting by Gretchen Vogel.

and other coastal communities initially wanted walls that would stand up to a rare tsunami like the one that ran ashore last March, says Setsuo Hirai, a civil engineer who is deputy director of Iwate Prefecture's reconstruction office. But building and maintaining such a huge structure "would be unreasonable," he says, adding that officials quickly brought citizens around to that view. Instead, a new 12-meter-tall embankment will be built. Preliminary plans also envision a memorial park along the shore, with a museum that will double as a tsunami refuge. The main north-south highway and the rail line will be built atop new embankments to limit flooding and divert water that tops the coastal levee into fields and parks. The business district will be raised by 5 meters.

New housing is a thornier problem. Because the displaced population is large and the terrain mountainous, "it's not possible to move everyone who was living [in Rikuzentakata] to high ground," Hirai says. Tracts will be carved out of surrounding mountains, and some former residential areas near the town center will be rebuilt 5 meters higher. Many details must be worked out. Hirai says it is not clear if they will replant the coastal pine forest, a hallmark of Rikuzentakata. And leaving space for ecological beaches in front of the seawalls may be desirable, "but there is a question of [sufficient] land," says Masaaki Minami, a disaster management specialist at Iwate University in Morioka.

Such compromises must be made all along the coast, not just in bigger towns. There are innumerable coves that are home to just a few households. Property and livelihoods—typically fishing and seaweed cultivation—have been handed down for generations. "There are very strong ties to the land and the sea," Minami says. Although many younger people have moved away, elders want to restore the life they knew, he says.

Notwithstanding all the efforts to make the built environment safer, the most important aspect of protecting lives is what Minami calls "soft countermeasures": raising awareness, developing evacuation plans and drills, and improving tsunami warning systems. Last March, many people delayed evacuating or ignored warnings because over the years too many tsunami alerts were never followed by actual waves. "We need research into making the warnings more reliable," Minami says. Not just in Tohoku; massive tsunamis can strike anywhere along Japan's coasts, and much of the rest of the country is even less prepared. Another national committee is probing the issue. But implementing countermeasures in areas untouched by Tohoku may be even more difficult than in Rikuzentakata, which is starting with a clean slate.

–DENNIS NORMILE

CREDIT: WIKIMEDIA COMMONS

Published by AAAS

SCIENCE FUNDING

The Next Big(ger) Thing

Physicists, chemists, and materials scientists are looking to build on the success of nanoscale science by unraveling the mysteries at the mesoscale

Photo copy. Photosynthesis is one of many natural mesoscale processes researchers would love to imitate.

CREDIT: FOTOSEARCH

BOSTON—The U.S. Department of Energy (DOE) is exploring plans to launch a major new research initiative in mesoscale science, where the quantum world of single atoms and small atomic clusters meets the bulk scale of classical physics. The mesoscale is a step up in size and complexity from the nanoscale, which has been the focus of more than $18 billion in U.S. research since the National Nanotechnology Initiative (NNI) took shape in 2001.

It's in this no-man's land between quantum and classical physics that a wide array of "emergent" phenomena reveal themselves. For example, superconductivity, in which electrons flow without resistance, arises only in large collections of atoms. Properties such as magnetism, rigidity, and melting are other collective behaviors that cannot be understood at the atomic level, says Robert Laughlin, a physicist at Stanford University in Palo Alto, California. Even life itself is considered an emergent phenomenon. "I know molecules and reactions are not alive. But I also know that collections of reacting molecules are alive. How does that happen? We have no clue," says George Whitesides, a chemist at Harvard University.

This summer, members of DOE's Basic Energy Sciences Advisory Committee (BESAC) expect to release a report on mesoscale science that's likely to serve on Capitol Hill as justification for research funding. Last week, BESAC members sought advice on the possible new research agenda from scientists gathered here at the American Physical Society (APS) meeting and were met largely with enthusiastic support.

"I'm a big admirer of work in this area," Whitesides says. "Progress in science often comes from looking at questions in new ways." Other researchers agree. "I think it's a great thing to be doing," says Yet-Ming Chiang, a materials scientist at the Massachusetts Institute of Technology in Cambridge and founder of A123 Systems, a company that manufactures advanced lithium ion batteries. Batteries and other energy-related devices such as solar cells, fuel cells, and supercapacitors are seen as quintessential mesoscale challenges. Although a battery's ability to store electricity is due to the nanoscale structure of individual components such as the anode, cathode, and electrolyte, the device's real-world performance depends on how all the components work together at the mesoscale.

The mesoscale is a challenge to define because it isn't an exact size range. "We all have a good understanding of the nanoscale because we are familiar with the nanometer [1 billionth of a meter]," says Kate Kirby, a physicist at the Harvard-Smithsonian Center for Astrophysics and current APS executive officer. "But we don't have a 'mesometer.' "

Whatever this mid-range length scale is, the mesoscale turns out to be one of the hardest areas to work in. Engineers have long had tools for modeling and probing bulk materials in structures such as bridges and buildings. And physicists now have good tools for characterizing materials at the atomic level. But bridging that gap isn't easy. "The complexity of going from one to the other is vast," says Arun Majumdar, who heads DOE's Advanced Research Projects Agency–Energy effort.

Supporters say the potential payoff is worth the effort. A mesoscale initiative could lead to progress on a host of challenges, such as gaining control of how to assemble collections of nanoscale devices into functional materials and understanding just how materials fail, all the way from the level of the deformation of atoms in a crystal lattice to the propagation of cracks and ultimately the fracturing of a bulk material, says George Crabtree, a physicist at Argonne National Laboratory in Illinois and co-leader of the upcoming BESAC mesoscale report. To gain such understanding across wide ranges of length and energy, researchers will need to develop new suites of tools capable of monitoring several electronic and optical properties of a material simultaneously and tracking how those properties change together over time, Crabtree adds.

As part of NNI, DOE and other funding agencies sponsored a network of nanoscience centers to make new tools for synthesizing and characterizing materials widely available to researchers. It's too early to know whether funding agencies will push for dedicated mesoscale science centers, says Harriet Kung, who directs the Basic Energy Sciences (BES) office within DOE's Office of Science. Current plans are more modest. This year, DOE has set aside $12 million in funding for mesoscale work it's calling "materials by design." The Obama Administration requested another $20 million in next year's budget to continue the effort within BES.

For now, any would-be mesoscale initiative will be limited to DOE. However, because the challenges and opportunities at the mesoscale are common to many scientific arenas, including biomedicine and engineering, a mesoscale initiative may eventually spread to other federal funding agencies as well. Says Crabtree: "We hope to see it bloom." **–ROBERT F. SERVICE**

Published by AAAS

LETTERS

edited by Jennifer Sills

Asian Medicine: Exploitation of Wildlife

TRADITIONAL ASIAN MEDICINE'S EFFECTS ON WILDLIFE CONSERVATION cannot be ignored. The endangered musk deer (*Moschus* spp.) provides a typical example.

The adult male musk deer secretes musk, which is one of the world's most expensive natural medical resources (1 gram is worth US$250). Musk is used broadly in traditional Asian medicine. There are at least 884 traditional Chinese medicine prescriptions and 347 products that use musk in China (*1*). Nearly 1000 kg of musk are consumed per year in traditional Chinese medicine alone (*2*).

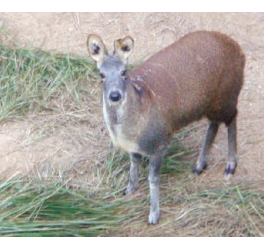

Because the musk deer has been deemed endangered by the Convention on International Trade in Endangered Species of Wild Fauna and Flora (CITES) (*3*), musk extraction from wild musk deer has been forbidden since the 1980s in China. In response, musk deer farming was initiated in the 1950s in China, as well as India, Nepal, and Russia (*4*). Today, more than 95% of the world's population of captive musk deer (about 6000 deer) is kept in about 30 musk deer farms in China (*5*). Sustainable musk extraction has been achieved in these farms, but only 20 kg of musk can be produced from musk deer farming per year (*6*), falling far short of the demand in China, not to mention the even greater demand in global traditional Asian medicine.

Given that even sustainable musk deer farms cannot produce enough musk to meet global demand, we should scientifically assess whether the musk used in traditional Asian medicine is effective. If not, musk deer farming should be phased out, and the captive musk deer should be reintegrated into natural habitats according to a scientifically supported plan. If the musk is shown to be medically effective, we should develop a synthetic alternative to natural musk that can both replace natural musk in traditional Asian medicine and protect natural populations of musk deer.

XIUXIANG MENG,[1]* DEGUANG LIU,[2] JINCHAO FENG,[1] ZHIBIN MENG[3]

[1]College of Life and Environmental Sciences, Minzu University of China, Beijing, 100081, China. [2]College of Plant Protection, Northwest A & F University, Yangling, Shaanxi, 712100, China. [3]Institute of Zoology, Chinese Academy of Sciences, Beijing, 100101, China.

*To whom correspondence should be addressed. E-mail: mengxiuxiang@muc.edu.cn

References

1. Z. Jiang, in *Advances in Biodiversity Conservation and Research in China VI*, Biodiversity Committee of the Chinese Academy of Sciences, Ed. (China Meteorological Press, Beijing, 2005), pp. 329–348 [in Chinese].
2. R. Parry-Jones, J. Wu, *Musk Deer Farming as a Conservation Tool in China* (TRAFFIC East Asia, Hong Kong, 2001).
3. Y. Zhou *et al.*, *Folia Zool*. **53**, 129 (2004).
4. V. Homes, *On the Scent: Conserving Musk Deer—The Uses of Musk and Europe's Role in Its Trade* (TRAFFIC Europe, Brussels, 1999).
5. X. Meng *et al.*, *Asian-Aust. J. Anim. Sci*. **24**, 1474 (2011).
6. X. Meng *et al.*, *Anim. Sci*. **82**, 5 (2006).

Asian Medicine: Exploitation of Plants

AS THE MARKET DEMAND FOR WILD CHINESE herbs has grown, the production scale of the Chinese herb industry has expanded dramatically. However, concealed by the prosperity of the Chinese medicinal herb industry is a huge ecological problem. In recent years, intensive and unrestrained exploitation of wild Chinese herbs has damaged natural resources. An estimated 2000 wild Chinese herbs are at risk of extinction (*1*).

Severe ecological deterioration and soil erosion seriously threaten the habitats of many wild Chinese herbs, especially in fragile ecological environments such as high-altitude areas or arid regions. For example, a recent media report (*2*) suggested that intensive and unrestrained gathering of the edible cyanobacterium *Nostoc commune var. flagelliforme* has led to the degradation of almost 150,000 km^2 of grassland in Inner Mongolia (about 18% of the total grassland in the region) (*1*, *3*).

If China continues its current pattern of natural resource exploitation, the biodiversity losses and environmental deterioration will severely jeopardize China's road to sustainability. Moreover, many wild Chinese herbs and other species that share their habitat are likely to be lost, as has happened to the Southern Chinese Tiger (*Panthera tigris amoyensis*) (*3*). Many of these species have not yet been adequately studied, so their true benefits to mankind and the environment are not yet known.

To improve governance and the ability to meet both socioeconomic and environmental goals, governments at all levels must understand the problem created by the competition between socioeconomic and environmental goals. Solving this requires stronger coordination between national policies and local needs, which will lead to production and conservation efforts based on approaches that encourage sustainability by balancing economic growth with environmental needs.

SHIXIONG CAO[1]* AND QI FENG[2]

[1]College of Economics and Management, Beijing Forestry University, No. 35, Qinhuadong Road, Haidian District, Beijing, 100083, China. [2]Cold and Arid Regions Environmental Engineering Research Institute, Chinese Academy of Sciences, Lanzhou, Gansu 730000, China.

*To whom correspondence should be addressed. E-mail: shixiongcao@126.com

CREDIT: XIUXIANG MENG

Explaining political behaviors
1177

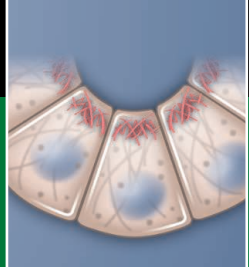

A clutch for constriction
1181

References

1. The Decline of Chinese Herbal Medicines, "Chinese medicinal plants die: The truth of an industry resource" (http://news.163.com/special/00013A7D/zcy.html) [in Chinese].
2. China Statistics Bureau, *Statistical Yearbook of China* (China Statistics Press, Beijing, 2010) [in Chinese].
3. "Why we can't stop the illegal exploitation of *Nostoc commune var. flagelliforme* despite many laws passed," *Legal System Daily* (13 April 2006); http://news.sina.com.cn/o/2006-04-13/08188684001s.shtml [in Chinese].

Business Journals Combat Coercive Citation

A. W. WILHITE AND E. A. FONG ("COERCIVE citation in academic publishing," Policy Forum, 3 February, p. 542) perform a valuable service in exposing the practice by some journal editors to increase their journals' impact factors by coercing authors to add frivolous citations to recent works in their journals. Wilhite and Fong point to a handful of business journals as being among the worst offenders. They name names in table S12.

As a former head of the Policy Board of the Journal of Consumer Research, I can attest that business journal editors have a strong self-interest in stamping out coercive citation, and they have taken concrete steps to do so over the past 2 years. In August 2010, 15 marketing journal editors met specifically to discuss and root out the practice. On 15 November 2010, 26 editors of some of the most prestigious journals in business wrote a letter to more than 600 business school deans decrying coercive citation (*1*). They argued that journal editors would have little incentive to engage in coercive citation if deans and business school faculties judged articles on their own merits rather than based on impact factors of the journals in which they were published. The 26 editors recommended vigilance in identifying spikes in the ratio of citations coming from their own journals relative to others, which might signal editorial manipulation by a new editorial team.

Those efforts have borne fruit; the journals in my own field have taken the pledge. I hope that Wilhite and Fong's Policy Forum will produce a much broader impact across the sciences.

JOHN G. LYNCH

Leeds School of Business, University of Colorado–Boulder, Boulder, CO 80309–0419, USA. E-mail: john.g.lynch@colorado.edu

Reference

1. J. G. Lynch, Frivolous Journal Self-Citation (2010); http://ama-academics.communityzero.com/elmar?go=2371115.

Letters to the Editor

Letters (~300 words) discuss material published in *Science* in the past 3 months or matters of general interest. Letters are not acknowledged upon receipt. Whether published in full or in part, Letters are subject to editing for clarity and space. Letters submitted, published, or posted elsewhere, in print or online, will be disqualified. To submit a Letter, go to www.submit2science.org.

Chimp Research Policy: Think Global

IN THEIR POLICY FORUM "GUIDING LIMITED use of chimpanzees in research" (6 January, p. 41), B. M. Altevogt *et al*. note that breeding existing U.S. chimpanzee captives would likely be too slow to meet the demands of "a public health emergency." This is true, but echoes the peculiar (although administratively understandable) approach of the Institute of Medicine's report, which considers only chimpanzees currently captive in the United States. There are more than 800 chimpanzees held in sanctuaries in Africa, mostly young victims of the bushmeat trade (*1*). When possible, these orphans are returned to the wild, but between individuals who cannot be reintroduced and the arrival of new orphans, the supply seems likely to remain high indefinitely.

Investment in African sanctuaries would ensure the well-being of these chimpanzees, as well as the availability of chimpanzees in case of a genuine global public health emergency. This suggestion is predicated on an agreement as to what constitutes an "emergency"; the litmus test would be an international acceptance of the need to transport and use sanctuary individuals. Such transport is currently excluded by the Pan African Sanctuary Alliance policy, and chimpanzees are regulated by the Convention on International Trade in Endangered Species of Wild Fauna and Flora (CITES), so the bar would be very high but presumably not insurmountable. If global chimpanzees are taken into account, there is no need to continue captive breeding for purposes of maintaining a large subject pool. Much research in comparative genomics and behavior can be conducted at African sanctuaries as well as at U.S. research centers. In fact, migration of such projects to Africa would not only help build academic infrastructure there but save money; maintenance costs are less than 1/10th of the $44 per day per individual cited for U.S. facilities (*2*).

Neither health nor chimpanzees are exclusively North American issues, and our approach to both should be global, not local.

JIM MOORE

Associate Professor Emeritus, University of California, San Diego, La Jolla, CA 92093, USA. E-mail: jjmoore@ucsd.edu

References

1. Pan African Sanctuary Alliance (http://pasaprimates.org/).
2. Duke University Evolutionary Anthropology, Why Sanctuaries? (http://evolutionaryanthropology.duke.edu/research/3chimps/why-sanctuaries-).

TECHNICAL COMMENT ABSTRACTS

Comment on "Fossilized Nuclei and Germination Structures Identify Ediacaran 'Animal Embryos' as Encysting Protists"

Shuhai Xiao, Andrew H. Knoll, James D. Schiffbauer, Chuanming Zhou, Xunlai Yuan

On the basis of putative nuclei and endospores, Huldtgren *et al*. (Reports, 23 December 2011, p. 1696) propose that embryo-like Doushantuo microfossils are nonmetazoan holozoans akin to mesomycetozoeans. However, both size and preservation preclude interpretation of internal structures as nuclei. Moreover, the authors may have conflated two different populations; some specimens display a pseudoparenchymatous organization incompatible with a mesomycetozoean comparison.

Full text at www.sciencemag.org/cgi/content/full/335/6073/ 1169-c

Response to Comment on "Fossilized Nuclei and Germination Structures Identify Ediacaran 'Animal Embryos' as Encysting Protists"

Therese Huldtgren, John A. Cunningham, Chongyu Yin, Marco Stampanoni, Federica Marone, Philip C. J. Donoghue, Stefan Bengtson

The objections of Xiao *et al*. to our reinterpretation are based on incorrect assumptions. The lack of nanocrystals lining the nuclear membrane is consistent with membrane fossilization, and nucleus volume through development is correlated to cytoplasm volume and fully consistent with sizes of eukaryote nuclei. Identical envelope structure unites the developmental stages of the fossils, and 2^n cleavage and Y-shaped junctions are holozoan symplesiomorphies.

Full text at www.sciencemag.org/cgi/content/full/335/6073/1169-d

Response to Comment on "Fossilized Nuclei and Germination Structures Identify Ediacaran 'Animal Embryos' as Encysting Protists"

Therese Huldtgren,[1,2] John A. Cunningham,[3] Chongyu Yin,[4] Marco Stampanoni,[5,6] Federica Marone,[5] Philip C. J. Donoghue,[3]* Stefan Bengtson[1,7]*

The objections of Xiao *et al*. to our reinterpretation are based on incorrect assumptions. The lack of nanocrystals lining the nuclear membrane is consistent with membrane fossilization, and nucleus volume through development is correlated to cytoplasm volume and fully consistent with sizes of eukaryote nuclei. Identical envelope structure unites the developmental stages of the fossils, and 2^n cleavage and Y-shaped junctions are holozoan symplesiomorphies.

Xiao *et al*. (*1*) claim that our reassessment (*2*) of previously interpreted "animal embryos" (*3*) rests on two flawed interpretations: The structures we identify as nuclei are not nuclei, and the proposed life cycle conflates two distinct organisms. Both claims are flawed.

We identified the nuclei based on a number of morphological features involving recurrence, position within cells, shape, volumetric relationship between nuclei and cells, and evidence of mitotic division. In all these features, the structures conform to typical cell nuclei. We interpreted the taphonomic history to involve shrinkage of nucleoplasm, leaving a major part of the original nucleus volume molded by diagenetic void-filling apatite and the nucleoplasm forming a smaller globular body. Xiao *et al*. do not question our observations or our taphonomic analysis. A recent study (*4*) by two of the co-authors of Xiao *et al*. (*1*) even states that the nucleus-like bodies "may... topologically represent nuclei or other organelles" and that their presence falsifies the hypothesis that the Doushantuo fossils are giant bacteria (*5*, *6*). Yet, in their comment on our paper, they conclude the opposite.

The first of their two arguments against the nucleus interpretation concerns crystal structure. Based on their previous taphonomic analyses of Doushantuo fossils (*7*) they claim that cell walls and membranes "commonly" incorporate membrane-molding nanocrystals and that nuclear membranes should do so, too. However, that study concluded that membrane-adpressed nanocrystals "exclusively occur in algal and acritarch fossils, but not in phosphatized animal embryo cells or embryonic envelopes" (i.e., the very fossils under discussion here). Walls and membranes of the latter are instead said to be "typically characterized by botryoidal and isopachous cements" [i.e., the fabric of void-filling apatite that also characterizes the molds of nuclei (*2*, *4*)].

Minor differences in the crystallographic nature of the boundaries are in any case irrelevant in the context. Some factor must have created the parting surfaces that shaped the molds into their spitting images of nuclei. The original presence of a nuclear membrane, now only preserved as the surface of a mold, is so far the only reasonable hypothesis.

The other argument against the nucleus interpretation concerns size. The structures in the cleaving cells are said to be too large to be nuclei and the spores at release stage too small to host the full set of genetic material. Because eukaryotic nuclei in extreme cases may be up to 5 mm long (*8*) and our nondividing fossil nuclei are 44 to 106 μm in maximum diameter, the first objection is void. The second one seems to be based on a misconception that the size of the nuclei reflects the size of the genome. Nucleus size is mainly a function of cell size, however, and the karyoplasmic ratio (i.e., the volumetric ratio of nucleus versus cell) is remarkably stable in eukaryotic cells (*9*). Differences in cell (and therefore nucleus) size between taxa may indeed be related to genome size (*10*), but the karyoplasmic ratio is maintained nonetheless. Most important, the ratio is stable also in growing cells (*11*, *12*); thus, the same genome will be incorporated into nuclei of widely different sizes.

We interpreted the large cell size in the early cleavage stages of the Doushantuo fossils as the result of hypertrophic growth of the mother cell preceding encystment and palintomic cleavage; the large nucleus size is then a predictable result of hypertrophy. A modern analog (a parasitic dinoflagellate) shows hypertrophic growth with constant karyoplasmic ratio followed by palintomic cleavage resulting in spores an order of magnitude smaller than the nuclei of the late hypertrophic stages [figure 28 in (*13*)]. Xiao *et al*.'s conclusion that "either the nucleus interpretation or the ontogenetic connection must be incorrect" is therefore wrong.

Xiao *et al*.'s assertion that the inner cells of the "peanuts" are vegetative (i.e., not potentially gamete-forming) is both unsubstantiated and unfalsifiable. In most of our specimens, such as the one in figure 3, H to J, in (*2*), there is a clear diagenetic gradient where the innermost cells are not infilled and have their walls thickened by diagenetic cement. What we observed and claimed is that the peripheral cells are detached and form isolated structures that are consistent with a function as propagules. Xiao *et al*. dismiss these structures as taphonomic artifacts on the grounds that their appearance does not fully match that of the endospores of two modern mesomycetozoean taxa. This reflects their misconception that we based our reconstruction of the fossil life cycle on comparisons with those two modern taxa. Rather, our interpretation of the fossil life cycle was based on the intrinsic features of the fossils, where the identical envelope structure (*2*, *14*–*16*) was a central piece of evidence that the fossils belong to the same organism; in fact, Xiao and colleagues have previously used this same criterion to assemble stages in the development of these same Doushantuo fossils (*17*, *18*). We compared our observations with the very similar life cycles in modern protists, including both alveolates and mesomycetozoeans; however, we did not claim that the fossils are alveolates or mesomycetozoeans, but we noted that in both modern groups, as in the fossils, palintomic cleavage produces propagules, not multicellular bodies. In general appearance, the fossils may be most similar to modern mesomycetozoeans, but there are no synapomorphies that warrant a placement within that clade. Indeed, we concluded only that the fossils did not represent prokaryotes, crown metazoans, or multicellular stem-metazoans; we did not preclude a unicellular stem-metazoan affinity, but there is no evidence to substantiate such a placement.

Xiao *et al*. (*1*) seem to agree with us that at least some of the features used in support of animal affinity are holozoan symplesiomorphies. They insist, however, on invoking regular 2^n cleavage and Y-shaped junctions between cleavage cells as animal characters, erroneously claiming that these do not occur in mesomycetozoeans

[1]Department of Palaeozoology, Swedish Museum of Natural History, 10405 Stockholm, Sweden. [2]Department of Geological Sciences, Stockholm University, 10691 Stockholm, Sweden. [3]School of Earth Sciences, University of Bristol, Bristol BS8 1RJ, UK. [4]Institute of Geology, Chinese Academy of Geological Sciences, Beijing 100037, China. [5]Swiss Light Source, Paul Scherrer Institute, CH-5232 Villigen, Switzerland. [6]Institute for Biomedical Engineering, University and Eidgenössische Technische Hochschule Zürich, CH-8092 Zürich, Switzerland. [7]Nordic Center for Earth Evolution, Swedish Museum of Natural History, 10405 Stockholm, Sweden.

*To whom correspondence should be addressed. E-mail: stefan.bengtson@nrm.se (S.B.); phil.donoghue@bristol.ac.uk (P.C.J.D.)

and most other protists. Indeed, both these characters are known from, e.g., mononucleate mesomycetozoeans (*19*). Early-branching holozoans have an animal-like genome that includes key elements of the genetic repertoire required for animal-grade multicellularity (*20*, *21*). Evidently, the molecular machinery required for the formation of the Y-shaped cell junctions seen in the Doushantuo fossils evolved outside the metazoan total-group, indeed outside of opisthokonts, but was lost in Fungi and choanoflagellates (*20*). Similarly, the structure of the envelope is not a metazoan synapomorphy either, as we previously discussed (*2*).

Despite our differences, Xiao and colleagues are in close agreement with our general conclusions. This contrasts with common interpretations of the Doushantuo fossils as advanced metazoans [e.g., (*16*, *22*–*24*)].

References

1. S. Xiao, A. H. Knoll, J. D. Schiffbauer, C. Zhou, X. Yuan, *Science* **335**, 1169 (2012); www.sciencemag.org/cgi/content/full/335/6073/1169-c.
2. T. Huldtgren *et al*., *Science* **334**, 1696 (2011).
3. S. Xiao, Y. Zhang, A. Knoll, *Nature* **391**, 553 (1998).
4. J. D. Schiffbauer, S. Xiao, K. S. Sharma, G. Wang, *Geology* **40**, 223, 10.1130/G32546.1 (2012).
5. J. V. Bailey, S. B. Joye, K. M. Kalanetra, B. E. Flood, F. A. Corsetti, *Nature* **445**, 198 (2007).
6. J. V. Bailey, S. B. Joye, K. M. Kalanetra, B. E. Flood, F. A. Corsetti, *Nature* **446**, E10 (2007) reply.
7. S. Xiao, J. D. Schiffbauer, in *From Fossils to Astrobiology,* J. Seckbach, M. Walsh, Eds. (Springer-Verlag, New York, 2008), pp. 89–117.
8. E. S. Robinson, *J. Parasitol.* **59**, 678 (1973).
9. M. D. Huber, L. Gerace, *J. Cell Biol.* **179**, 583 (2007).
10. T. Cavalier-Smith, *Ann. Bot.* **95**, 147 (2005).
11. P. Jorgensen *et al*., *Mol. Biol. Cell* **18**, 3523 (2007).
12. F. R. Neumann, P. Nurse, *J. Cell Biol.* **179**, 593 (2007).
13. D. W. Coats, T. R. Bachvaroff, C. F. Delwiche, *J. Eukaryot. Microbiol.* **59**, 1 (2012).
14. P. Liu, C. Yin, F. Tang, *Prog. Nat. Sci.* **16**, 1079 (2006).
15. P.-j. Liu, C.-y. Yin, S.-m. Chen, F. Tang, L.-z. Gao, *Acta Geosci. Sin.* **30**, 457 (2009).
16. Z. Yin *et al*., *Precambrian Res.* 10.1016/j.precamres.2011.08.011 (2011).
17. S. Xiao, J. W. Hagadorn, C. Zhou, X. Yuan, *Geology* **35**, 115 (2007).
18. S. Xiao, C. Zhou, X. Yuan, *Nature* **446**, E9; discussion, E10 (2007).
19. S. Raghu-Kumar, *Bot. Mar.* **30**, 83 (1987).
20. A. Sebé-Pedrós, A. J. Roger, F. B. Lang, N. King, I. Ruiz-Trillo, *Proc. Natl. Acad. Sci. U.S.A.* **107**, 10142 (2010).
21. A. Sebé-Pedrós, A. de Mendoza, B. F. Lang, B. M. Degnan, I. Ruiz-Trillo, *Mol. Biol. Evol.* **28**, 1241 (2011).
22. J.-Y. Chen *et al*., *Proc. Natl. Acad. Sci. U.S.A.* **106**, 19056 (2009).
23. J.-Y. Chen *et al*., *Precambrian Res.* **173**, 191 (2009).
24. Z.-j. Yin, M.-y. Zhu, *Acta Palaeontol. Sin.* **49**, 325 (2010).

25 January 2012; accepted 31 January 2012
10.1126/science.1219076

Comment on "Fossilized Nuclei and Germination Structures Identify Ediacaran 'Animal Embryos' as Encysting Protists"

Shuhai Xiao,[1]* Andrew H. Knoll,[2] James D. Schiffbauer,[1,3] Chuanming Zhou,[4] Xunlai Yuan[4]

On the basis of putative nuclei and endospores, Huldtgren *et al*. (Reports, 23 December 2011, p. 1696) propose that embryo-like Doushantuo microfossils are nonmetazoan holozoans akin to mesomycetozoeans. However, both size and preservation preclude interpretation of internal structures as nuclei. Moreover, the authors may have conflated two different populations; some specimens display a pseudoparenchymatous organization incompatible with a mesomycetozoean comparison.

We welcome Huldtgren *et al*.'s (*1*) demonstration that Ediacaran microfossils commonly interpreted as animal embryos display characters that may be holozoan symplesiomorphies. This finding is fully consistent with, and perhaps a predictable consequence of, their earlier interpretation as stem group metazoans (*2*). Huldtgren *et al*.'s claim that these fossils are nonmetazoan holozoans analogous to mesomycetozoeans, however, rests on two flawed interpretations.

First, Huldtgren *et al*. interpret tomographically discrete nucleus-like structures in the embryo-like fossils as true nuclei, arguing that the cells divided via closed mitosis (nuclear membrane remaining intact during cytokinesis) rather than the open mitosis (nuclear membrane disintegrated during cytokinesis) observed in living metazoans. By itself, this interpretation would not falsify the stem-group animal hypothesis because open mitosis, a feature that evolved independently in multiple clades, could have evolved after the fossils diverged from the main line of metazoan evolution. Two observations, however, convince us that the structures in question cannot be preserved nuclei. First, petrographic and scanning electron microscopy studies show that the structures are preserved as late diagenetic, void-filling, botryoidal cements (*1*, *3*). The late diagenetic origin of the structures means that they cannot be molds of nuclei, because phosphatic molding on a nuclear membrane template would necessarily have occurred during very early diagenesis. Internal molds of cells with crystallites nucleated on or adpressed against membranes or walls, for example, commonly incorporate nanocrystals (*4*) distinct from the void-filling, botryoidal microcrystals that replicate the nucleus-like structures (*3*). These botryoidal microcrystals are secondary overgrowths on a preexisting phosphatic substrate, similar to late diagenetic structures in other Doushantuo microfossils such as *Vernanimalcula* (*5*, *6*). Thus, the behavior of the nuclear membrane during cytokinesis cannot be inferred from these late diagenetic structures. Moreover, the sheer size (up to 200 μm) of these microstructures precludes their interpretation as germline nuclei. Only certain ciliates are known to have macronuclei approaching the size of nucleus-like structures in Doushantuo fossils (*7*), but as Huldtgren *et al*. were not arguing for a ciliate interpretation, the large size of the fossil microstructures requires another explanation. The purported nuclei, which according to Huldtgren *et al*. [figure S6 in (*1*)] maintain a constant size through successive cell divisions, are volumetrically ~10^4 times larger than cells interpreted as reproductive spores formed by repeated cell divisions; these spores are supposed to (but physically could not) have hosted the putative nuclei with a full set of genetic material. Thus, either the nucleus interpretation or the ontogenetic connection must be incorrect.

The second problem with Huldtgren *et al*.'s interpretation involves the multicellular structures viewed as part of the life cycle of the embryo-like populations. Peanut-shaped individuals are interpreted as germination structures, based on comparisons to the extant mesomycetozoeans *Ichthyophonus* and *Rhinosporidium seeberi*. *Ichthyophonus* does indeed form peanut-like structures entirely filled with endospores, but at least the interior cells in structures illustrated by Huldtgren *et al*. [figure 3, E to J, in (*1*)] are not spores; they are vegetative cells with distinct cell walls that form a pseudoparenchymatous thallus that developed through apical cell division. Exterior cell clusters appear to be detached, but this is a taphonomic artifact, as movies kindly provided to us by Huldtgren *et al*. show that the purported endospores are attached

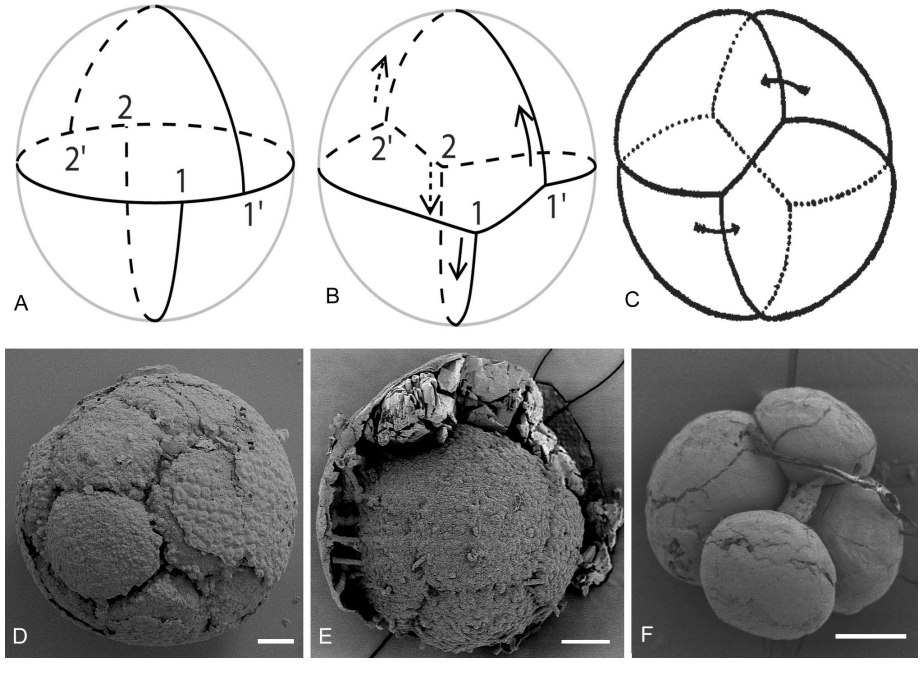

Fig. 1. Cell cleavage and taphonomic degradation of *Parapandorina*-stage fossils. (**A** to **C**) The formation of a Y-shaped cell junction requires cell membrane flexibility and cell-cell adhesion. The sketch illustrates the second round of cell division (*14*). (**D**) Well-preserved specimen with nearly intact cell size and shape. Note the Y-shaped cell junctions. (**E**) Degraded and shrunken cells within a partially preserved envelope. Note the Y-shaped cell junctions. (**F**) Degraded and rounded cells. The cell in front became spherical and began separation from other cells, whereas the cell in back still maintained a polyhedral shape. Scale bars, 100 μm.

[1]Department of Geosciences, Virginia Polytechnic Institute and State University, Blacksburg, VA 24061, USA. [2]Department of Organismic and Evolutionary Biology, Harvard University, Cambridge, MA 02138, USA. [3]Nanoscale Characterization and Fabrication Laboratory, Institute for Critical Technology and Applied Science, Virginia Polytechnic Institute and State University, Blacksburg, VA 24061, USA. [4]State Key Laboratory of Paleobiology and Stratigraphy, Nanjing Institute of Geology and Paleontology, Chinese Academy of Sciences, Nanjing 210008, China.

*To whom correspondence should be addressed. E-mail: xiao@vt.edu

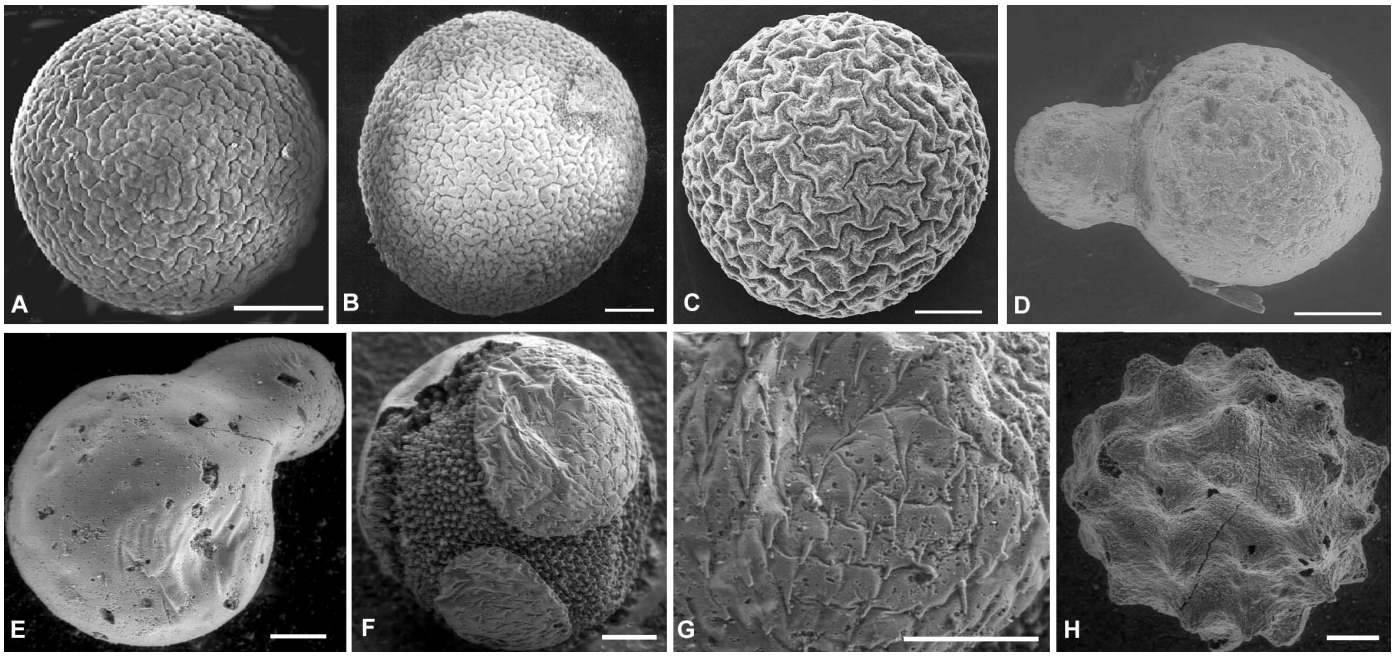

Fig. 2. Comparison between (A) modern animal cysts, (B) Doushantuo microfossils, and (C to H) Cambrian fossils in association with the animal embryo fossils *Olivooides*, *Pseudooides*, or *Markuelia* from South China. (**A** to **C**) Similar ornamentation on modern animal cyst (A), Doushantuo fossil *Tianzhushania ornata* (B), and Cambrian microfossil (C). (**D** and **E**) Forms similar to lobate Doushantuo fossils. (**F**) Two spiny acritarchs (similar to the Doushantuo form *Cavaspina acuminata*) on an *Olivooides* animal embryo. (**G**) Enlarged view of (F) to show detail of processes. (**H**) Form similar to the Doushantuo form *Asterocapsoides sinensis*. Scale bars, 100 μm. [(A) from Belk *et al*. (*26*); (B) from Xiao and Knoll (*10*); (C) from Dong (*25*); (D) to (H) courtesy of X.-P. Dong]

to the thallus through cellular filaments and are indeed surrounded by faintly preserved thallus cells. The result is inconsistent with any life cycle known for *Ichthyophonus* and is distinct from the zonal maturation of spores in *Rhinosporidium seeberi* (*8*). Moreover, the proposed ontogenetic connection between *Megaclonophycus*-stage fossils (~10^3 cells) and peanut-shaped fossils (~10^6 cells) leaves a large developmental gap that cannot be bridged by a common envelope because no such feature is preserved in the anatomical illustrations provided. Doushantuo fossil assemblages do include distinctly lobate, cellularly differentiated, pseudoparenchymatous thalli, but these have been interpreted as red algae (*9*). Thus, we believe that Huldtgren *et al*. have conflated two distinct organisms in their interpretation.

Stripped of the two invalid attributions, the Doushantuo embryo-like fossils can be accommodated by the stem-group metazoan interpretation but are inconsistent with a mesomycetozoean analog. Their ornamented envelopes can be compared with those of modern animal eggs (*10*) but are entirely different from sporangium walls of modern mesomycetozoeans (*11*, *12*). Also, their cells form an obligate multicellular organization with stable and reproducible Y-shaped cell junctions (Fig. 1), distinct from facultative cell aggregation in clonal protists. Considering that partial degradation of modern embryos (*13*) and *Parapandorina* fossils results in cell volume reduction, rounding, and separation (Fig. 1E–F), it is remarkable that the Y-shaped junction is maintained even in shrunken cells (Fig. 1E). This indicates that this configuration is biologically stable and not an artifact of the physical confinement of cells within a rigid envelope. The biological formation of Y-shaped cell junctions requires flexible cell membranes and cell-cell adhesion (*14*), an important step toward complex multicellularity (*15*). Third, cell cleavage in *Parapandorina* (as in modern animals) follows a 2^n sequence, whereas cytokinesis in most protists, including mesomycetozoeans, does not follow a 2^n sequence because it commonly involves multinucleate stages (*16*–*18*).

We agree with Huldtgren *et al*. that some of the features used in support of the animal embryo interpretation (*10*) may be holozoan symplesiomorphies and that the Doushantuo fossils do not show all the features that collectively define crown-group Metazoa. However, we would expect a stem-group animal to have holozoan symplesiomorphies, lack some or most crown-group synapomorphies (*19*), and evolve autapomorphies and homoplasies. Indeed, it has been proposed that early animal evolution may have involved a synzoospore stage without embryogenesis (*20*). Given the problems regarding the nuclear and life cycle arguments advanced by Huldtgren *et al*., we believe that the obligate, stable, and reproducible multicellular organization of the *Megasphaera-Parapandorina-Megaclonophycus* complex places them on the animal branch of the holozoan tree, because animals are the only holozoans that have evolved this degree of multicellularity. Another possibility is that at least some of the microfossils attributed to embryo-like populations represent the distinctive reproductive propagules produced by the early branching animals such as *Trichoplax* (*15*, *21*). This would be consistent with recent interpretations of some Ediacaran macrofossils as little more than upper and lower epithelia that lined a fluid-filled or mesogloea-like interior and fed by absorption or phagocytosis (*15*, *22*, *23*). As a final note, we draw attention to similar microfossils (Fig. 2) found in association with undisputed Cambrian animal embryos (*24*, *25*). The presence of similar forms in association with Cambrian (and living) animal embryos does not prove that the Doushantuo microfossils are animal, but it does offer another avenue to further test the mesomycetozoean comparison.

References

1. T. Huldtgren *et al*., *Science* **334**, 1696 (2011).
2. J. W. Hagadorn *et al*., *Science* **314**, 291 (2006).
3. J. D. Schiffbauer, S. Xiao, K. S. Sharma, G. Wang, *Geology* **40**, 223, 10.1130/G32546.1 (2012).
4. S. Xiao, J. D. Schiffbauer, in *From Fossils to Astrobiology*, J. Seckbach, M. Walsh, Eds. (Springer-Verlag, New York, 2008), pp. 89–117.
5. S. Xiao, X. Yuan, A. H. Knoll, *Proc. Natl. Acad. Sci. U.S.A.* **97**, 13684 (2000).
6. V. A. Petryshyn, D. J. Bottjer, J.-y. Chen, F. Gao, *Precambrian Res.* 10.1016/j.precamres.2011.08.003 (2012).
7. X. Fan, X. Chen, W. Song, K. A. S. Al-Rasheid, A. Warren, *Int. J. Syst. Evol. Microbiol.* **61**, 1476 (2011).
8. L. Mendoza, R. A. Herr, S. N. Arseculeratne, L. Ajello, *Mycopathologia* **148**, 9 (1999).
9. S. Xiao, A. H. Knoll, X. Yuan, C. M. Pueschel, *Am. J. Bot.* **91**, 214 (2004).
10. S. Xiao, A. H. Knoll, *J. Paleontol.* **74**, 767 (2000).
11. P. A. Cohen, A. H. Knoll, R. B. Kodner, *Proc. Natl. Acad. Sci. U.S.A.* **106**, 6519 (2009).
12. V. N. Sergeev, A. H. Knoll, N. G. Vorob'Eva, *J. Paleontol.* **85**, 987 (2011).
13. E. C. Raff, J. T. Villinski, F. R. Turner, P. C. J. Donoghue, R. A. Raff, *Proc. Natl. Acad. Sci. U.S.A.* **103**, 5846 (2006).

14. S. Xiao, *Paleobiology* **28**, 244 (2002).
15. A. H. Knoll, *Annu. Rev. Earth Planet. Sci.* **39**, 217 (2011).
16. L. Mendoza, J. W. Taylor, L. Ajello, *Annu. Rev. Microbiol.* **56**, 315 (2002).
17. W. L. Marshall, M. L. Berbee, *Mol. Biol. Evol.* **27**, 2014 (2010).
18. J. N. Lohr, C. Laforsch, H. Koerner, J. Wolinska, *J. Eukaryot. Microbiol.* **57**, 328 (2010).
19. C. R. Marshall, J. W. Valentine, *Evolution* **64**, 1189 (2010).
20. K. V. Mikhailov *et al.*, *Bioessays* **31**, 758 (2009).
21. M. Eitel, L. Guidi, H. Hadrys, M. Balsamo, B. Schierwater, *PLoS ONE* **6**, e19639 (2011).
22. M. Laflamme, S. Xiao, M. Kowalewski, *Proc. Natl. Acad. Sci. U.S.A.* **106**, 14438 (2009).
23. E. A. Sperling, J. Vinther, *Evol. Dev.* **12**, 201 (2010).
24. X.-P. Dong, *Acta Palaeontol. Sin.* **48**, 390 (2009).
25. X.-P. Dong, *Acta Geol. Sin.* **83**, 429 (2009).
26. D. Belk, G. Mura, S. C. Weeks, *J. Crustac. Biol.* **18**, 147 (1998).

6 January 2012; accepted 31 January 2012
10.1126/science.1218814

SCIENCE POLICY

The Economic Logic of U.S. Science

Maryann Feldman

Increasingly science is about money. Publish or perish has been replaced by fund or famish. Scientific results and publications, while born of diligence and dedication and inspired by creative insights, simply do not get off the ground without resources. Scientists compete for scarce societal resources. With this funding come expectations of accountability and measurable outcomes, intensified by research assessment exercises and performance metrics. Moreover, at a time when the research system is evolving in response to precarious government funding, scientists should question whether the prevailing incentives and expectations are appropriate to move science in the most productive direction.

How Economics Shapes Science should be required reading for all scientists and students of science, who are increasingly called upon to adopt the language and logic of economics and engage in policy discussions. Paula Stephan (an economist at Georgia State University) makes her case in simple, easy-to-follow language, using timely examples. Each chapter provides a review of the topic, consideration of policy implications, and suggestions for future research.

The book starts by summarizing the case that private industry alone will not invest in the socially optimal level of research, which will ultimately decrease the rate of innovation and lower economic growth. The logic is worth repeating at a time when there are calls for limiting government support for research and researchers face pressures to engage in lower-risk projects. Stephan convincingly argues that monetary incentives increasingly determine the behavior of researchers at the expense of scientists' desire to participate in the joy of solving problems, receive recognition, and obtain a good reputation.

Stephan debunks the idea that science is a winner-take-all endeavor and argues for a tournament model that rewards different levels of skills and accomplishment. The current system often exacerbates relatively minor initial differences in the skill level of scientists, leading to resource inequality and disparities in achievement and income. Cohorts who enter a tight labor market are likely to find themselves at institutions of lower reputation, with fewer resources, higher teaching loads, and less distinguished colleagues. The consequences of these effects are difficult to overcome and endure over a researcher's career. Stephan documents how salaries in science have lost ground compared with other professions. This is indeed ironic at a time when science is considered fundamental for economic growth and international competitiveness—a case that Stephan reviews in the book's penultimate chapter (a useful summary of the logic behind current policy).

How Economics Shapes Science

by Paula Stephan

Harvard University Press, Cambridge, MA, 2012. 383 pp. $45, £33.95, €40.50. ISBN 9780674049710.

Stephan is specifically concerned with the disadvantages for younger scientists, who currently have a more difficult time establishing primacy within their chosen field. Research demands collaboration of a team of experts spanning multiple disciplines who are organized into hierarchy according to rank. Scientists starting their careers face additional difficulties because all sources of research support are subject to cyclical fluctuations. Whereas there are perennial warnings of a shortage of scientists and engineers, Stephan documents the surpluses in academic labor markets that can prompt universities to adapt their staffing structures, including increased reliance on non–tenure-track faculty and postdocs and offering tenure without a commitment to fund a scientist's salary. Stephan asks why people keep going to graduate school in the sciences if career results are so disappointing. She suggests the availability of stipends, overconfidence, and recruitment by faculty create incentives for an unsustainable system. She concludes that the system does not serve individual scientists well.

The final chapter offers a critical assessment of the university research system in the United States. Stephan asks whether we efficiently apportion costs and incentives or the system could be better. She argues that universities have adopted the management practices of real estate shopping malls, allocating space to the highest bidder with little concern for the totality of the scientific enterprise, the balance between disciplines, or the integrity of inquiry. Research with uncertain outcomes is discouraged when researchers rely on grants for their salary; collaboration is less likely when scientists are in constant competition. The current research paradigm discourages research that disproves theories, which risks loss of funding. Researchers are awarded for incrementally continuing a line of research, even when that research is no longer practical. This concluding chapter could also serve as the opening of another book, one that critically evaluates alternative approaches that might improve the efficiency of the scientific enterprise as well as the distribution of its rewards among individual scientists.

The science of science policy is coming of age. Stephan's 1996 article, "The economics of science" (*1*), was instrumental in defining the field, and this book will have similar impact. The National Science Foundation now runs a grants program, the Science of Science Innovation and Policy, aimed at understanding how science shapes innovation and technological progress. There is also an important interagency effort (STAR metrics) to collect and analyze data on the impact of federal spending on research and innovation outcomes. *How Economics Shapes Science* provides a comprehensive overview and introduction for scientists who would like to understand these developments. Indeed, the science of science policy will be enhanced when scientists, who have traditionally eschewed policy and politics, actively engage and contribute to the discussion.

References

1. P. E. Stephan, *J. Econ. Lit.* **34**, 1199 (1996).

10.1126/science.1217823

The reviewer is at the Department of Public Policy, Campus Box 3435, University of North Carolina, Chapel Hill, NC 27599, USA. E-mail: feldmanm@email.unc.edu

Published by AAAS

HISTORY OF SCIENCE

Pictures of Remembering

Elizabeth Johnston

The history of the memory sciences resembles in some respects the claims about memory made by one particular psychologist—Bartlett, whose mantra was that the fate, significance, and meaning of all psychic material was in the hands of future users.

With *Memory: Fragments of a Modern History*, historian Alison Winter has written a riveting account of the past century of work on the science of memory that has a distinctly Bartlettian flair. Frederic Bartlett emphasized the power of his participants' preexisting interests, experience, and knowledge to inform their construction of a coherent narrative from an initially disjointed and confusing tale (*1*). In a similar vein, Winter's historical expertise and prior interests guide her transformation of the checkered, messy tale of a diverse set of memory investigations into a coherent narrative about shifts in conceptions of memory within psychology, medicine, and neuroscience. We also learn about the cultural traction such representations of memory gained in the world beyond the laboratory and the clinic. Winter achieves this feat through detailed examination of several cases, selecting some telling examples (what Bartlett would call outstanding detail) to illustrate her wide-ranging account.

Memory
Fragments of a Modern History
by Alison Winter
University of Chicago Press, Chicago, 2011. 329 pp. $30, £19.95. ISBN 9780226902586.

Some of Winter's examples are well-traveled routes in the history of memory research that she enlivens by providing more social and historical context than is usual within the scientific literature. Her observations about the widespread use of new photographic technologies to capture family memories in the middle of the 20th century help to make sense of the popular appeal of experiments like Wilder Penfield's brain stimulation studies and "flashbulb" memories. Penfield explained his remarkable and perplexing demonstration that past experiences could sometimes be evoked by stimulating his epileptic patients' temporal lobes by likening memory to motion picture film that could be replayed. Roger Brown and James Kulik's introduction of a special flashbulb memory mechanism to account for the apparent richness of emotional memories similarly resonated with the reinvention of memory as akin to the photographic technologies being widely used to document family life.

Photographic memories. 1920s advertisement.

Other case studies will be less familiar to contemporary memory researchers. For example, the invention of a "truth serum" in the early 20th century by Texas obstetrician Robert House. Paradoxically, House initially used the drug scopolamine to induce amnesia for the pain of childbirth. House was inspired to reframe it as a truth serum after a supposedly unconscious patient gave him precise instructions for finding the scales he needed to weigh her newborn. Scopalamine was the first of a series of drugs (including Sodium Pentothal) that were thought to provide direct access to memories despite people's desire to conceal the truth. It is a prime example of the recurring view that memories locked into the unconscious can be extracted wholesale by special means. Those techniques could be pharmacological (as with truth serum), electrical stimulation (as in Penfield's brain studies), hypnosis (another of Winter's case studies), or the right therapeutic technique or memory cue.

Winter follows the peregrinations of the memory-unlocking theme throughout the 20th century into its bitter contention in the false or recovered memories of the childhood-abuse wars of the 1990s. Her historical methods, including archival research and interviews, bring forth a compelling account of the False Memory Syndrome Foundation's (FMSF) promotion of an opposing view of memory as unstable and unreliable. Winter notes the irony inherent in the extent of the social and political advocacy work required for FMSF to gain widespread acceptance of a view of memory that it presented as unvarnished scientific fact.

Throughout the book, Winter explores the role of media, especially film, in forming popular ideas about memory. During World War II, the truth serum drugs of the 1930s (particularly Sodium Pentothal) became the basis of psychiatrists' "narcoanalytic" treatment of traumatic memories. The narcoanalytic method was promoted through U.S. Army films such as *Combat Exhaustion* (1945), which demonstrated the use of pentothal to recover memories of war trauma. Winter points out the importance of visually showing the memory flashback, rather than just having the soldier describe his memory, in creating the representation of returning memories as filmlike. In Winter's concluding chapter on contemporary work, the film metaphor of memory takes a new turn in a neural recording study. In 2008, researchers recorded from single electrodes in the brains of preoperative epileptic patients while they viewed short film clips, such as a Tom Cruise interview on the Oprah Winfrey Show (*2*). They found that when their participants later brought clips to mind, the same neurons were activated as during the initial viewing. This is the most recent exemplar of the many studies that Winter identifies as satisfying our "craving for neurophysiological 'high fidelity'" that yields faithful recordings of past events.

The notion that "secreted within us are perfect records of past experiences" was the very theory that Bartlett vigorously opposed—the "trace theory" of memory. Winter does a masterful job of explicating Bartlett's perspective, despite its odd placement late in the book between recovered memories and the FMSF. Regardless of this quibble, her rich account of the development of Bartlett's work, from his early fellowship dissertation studies of conventionalization to his dynamic model of memory schema, shows that it is more than an argument for the falsity of memory. Bartlett's adaptive and motivated account of remembering is consonant with the possibility of a new era of remembering that Winter floats in the concluding paragraph of her stimulating text.

The reviewer is at the Department of Psychology, Sarah Lawrence College, 1 Mead Way, Bronxville, NY 10708, USA. E-mail: ebj@slc.edu

References
1. F. C. Bartlett, *Remembering: A Study in Experimental and Social Psychology* (Cambridge Univ. Press, Cambridge, 1932).
2. H. Gelbard-Sagiv, R. Mukamel, M. Harel, R. Malach, I. Fried, *Science* **322**, 96 (2008).

10.1126/science.1218655

PUBLIC HEALTH

Surveillance of Animal Influenza for Pandemic Preparedness

How might we prepare to cope better with future pandemics, particularly ones with greater severity?

J. S. M. Peiris,* L. L. M. Poon, Y. Guan

The 2009 H1N1 pandemic was not as severe as initially feared. This has led to complacency in some quarters that future pandemics will be of comparable impact and as readily dealt with. However, by September 2009, just 5 months after the recognition of the novel pandemic H1N1 virus, almost 50% of children in Hong Kong were already infected (*1*), which reflects the speed of spread of the virus to and within international travel hubs. In most parts of the world, vaccines were not available in time to substantially affect the first wave of disease. A more virulent virus, such as one comparable to the 1918 H1N1 virus or the H5N1 "bird flu," spreading with such speed would be a global catastrophe.

The 2009 pandemic virus was circulating in humans in Mexico for about 4 months before it was recognized (*2*). The first known cases of severe acute respiratory syndrome (SARS) occurred in Foshan City, Guangdong, China, in mid-November 2002, and triggered initial investigations by the Guangdong Health Bureau in mid-January 2003; the etiological agent was identified in mid-March 2003 (*3*). Earlier detection of novel pandemic viruses once they have emerged in humans would provide longer lead times for vaccine development and is crucially important. Pandemic influenza viruses arise, in part or whole, from influenza viruses of other animals. Precursors of the 1957 and 1968 pandemics circulated in animals for some years before emerging in humans (*4*). What is the role of influenza virus surveillance in animals for pandemic preparedness?

Some criteria that can be used to assess the risk of animal influenza viruses include the high prevalence of animal influenza viruses in species found in close proximity to humans (e.g., domestic livestock); those undergoing rapid genetic change or reassortment; viruses with a predilection for binding to α 2,6-linked sialic acid (the influenza receptors found on human upper respiratory epithelia) (*5*–*7*); efficient infection of ex vivo organ cultures of the human upper respiratory tract (nasopharynx and bronchus) (*8*, *9*); and transmission by airborne droplets in ferrets, the best available animal model for human transmission (*10*, *11*). Evidence of repeated zoonotic transmission to humans and lack of cross-reactive "herd-immunity" in the human population are also important. The severity of disease associated with zoonotic human infection should also be considered, not because severity alone makes a virus more likely to be pandemic but because preemptive preparations are more rationally targeted at viruses with potential to cause exceptionally severe pandemics.

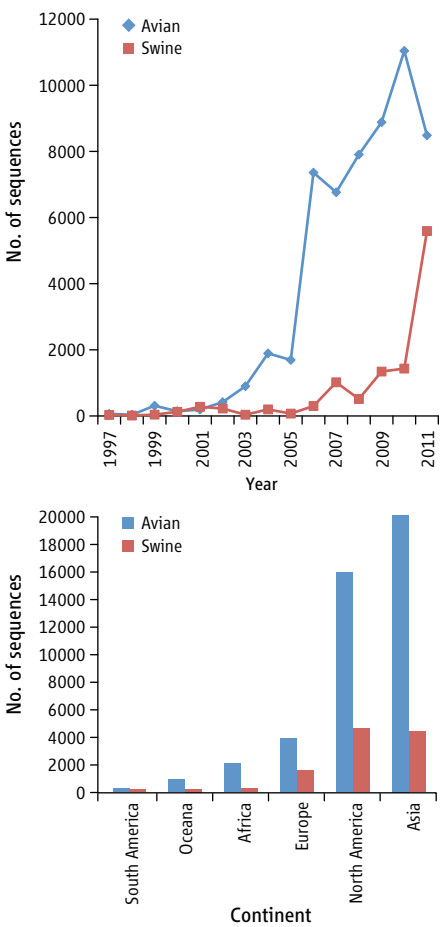

Avian and swine influenza virus statistics. (Top) The number of avian and swine influenza viral genome sequences (by year of deposit) available in the Influenza Viral Sequence Database (*29*). Only nonidentical viral nucleotide sequences were counted. (**Bottom**) Cumulative sequence data by continent in which sampling was done.

Identification of molecular signatures associated with transmissibility of animal viruses to humans and between humans will be an important additional parameter. Attempts to define molecular markers associated with host adaptation and transmission have been under way for many years but have gathered speed with development and integrated application of virus reverse genetics, glycan arrays, studies in ferrets, and the use of ex vivo organ cultures of the human respiratory tract. Recent studies have tried to elucidate the molecular changes that allowed the 1918 H1N1, 1957 H2N2, and 2009 swine-origin pandemic H1N1 viruses to become transmissible in humans (*7*, *8*, *12*–*14*). Investigations of changes that confer mammalian transmissibility to avian H9N2 (*11*), H7 (*6*), and H5N1 viruses (*10*, *15*) have begun to provide insights. Future studies will try to identify common mechanisms across avian influenza virus subtypes that confer increased mammalian transmissibility.

Before 2009, the application of ecological, virological, host-immunity, and molecular criteria led to the identification of virus subtypes H2, H7, H5N1, and H9N2 as potential pandemic threats (*16*). These criteria would also have led to identification of the precursors of the 2009 pandemic, which were undergoing rapid genetic reassortment (*17*), with receptor binding to α 2,6-linked sialic acids and with evidence of repeated human transmission (*18*). The reason why they were not high on the list of pandemic candidates was the (mistaken) belief that a pandemic could not arise from viruses with hemagglutinin subtypes already endemic in humans.

Virological and molecular surveillance of influenza viruses in animals is ongoing (see the graphs). In practice, there are a number of constraints. Reports of outbreaks may lead to culling of farm animals and to restrictions in international trade, which could lead to economic losses to the farmer and the country. Furthermore, whereas veterinarians focus on viruses with economic impact on livestock, viruses of pandemic risk may not necessarily cause illness in the animal reservoir. Indeed, this was probably the case

School of Public Health, Li Ka Shing Faculty of Medicine, Sassoon Road, Pokfulam, Hong Kong Special Administrative Region (SAR), P.R. China.

*Author for correspondence. E-mail: malik@hku.hk

Published by AAAS

with the precursors of the 1957, 1968, and 2009 pandemics. Thus, surveillance needs to be targeted at healthy as well as ill animals, an effort that is unlikely to be of high priority for animal health. Detecting influenza viruses in apparently healthy domestic livestock may make them unmarketable, which explains the reluctance in the swine industry of developed, as well as developing, countries to permit surveillance of their swine herds for influenza viruses.

However, appropriate choice of strategy can help address some of these concerns. For example, the systematic surveillance in live poultry markets in Hong Kong and China (*19*) provided advance warning (unfortunately not widely heeded) of the impending emergence of highly pathogenic avian influenza (HPAI) H5N1 that caused outbreaks in poultry and disease in humans in many Asian countries in 2004. These warnings prompted Hong Kong to introduce evidence-based interventions in the poultry industry, minimizing the impact of H5N1 within Hong Kong (*20*). Surveillance of pigs in an abattoir in Hong Kong (anonymized and unlinked to supplying farms) allowed systematic and long-term surveillance to be carried out on swine influenza in southern China (*21*).

The 2009 pandemic virus, which very likely emerged from swine, spread worldwide in the human population and transmitted from humans back to swine in many parts of the world. Pandemic H1N1 infection in swine has readily reassorted with other swine influenza viruses, to give rise to a range of reassortants (*22*, *23*), some of which have infected humans (*24*). The 2009 pandemic H1N1 virus is changing more rapidly in swine than in humans (*22*–*24*), which makes it particularly important to have global surveillance of influenza in swine. However, we still have little or no data on influenza viruses circulating in swine in Mexico, the putative birthplace of the pandemic virus of 2009, or from swine in South and Central America, Africa, and South Asia.

Although current data on influenza viruses in animals are patchy and far from satisfactory, the situation has improved over the last decade (see the graphs). Concern about the spread of HPAI H5N1 has mobilized resources and the "One Flu for One Health" paradigm, which views human, animal, and wild-life health issues in a holistic manner (*25*), may have also increased awareness. OFFLU is a collaboration among the laboratories of the animal health sector [Food and Agricultural Organization of the United Nations (FAO), and World Organization for Animal Health (OIE)] to improve understanding of the ecology and evolution of animal influenza viruses for assessment of human health risk (*26*). Capacity-building efforts of FAO, OIE, World Health Organization (WHO), and U.S. Centers for Disease Control and Prevention (CDC); research networks such as those of the Centers of Excellence for Influenza Research and Surveillance (CEIRS) funded by the National Institute of Allergy and Infectious Diseases [NIAID, U.S. National Institutes of Health (NIH)]; and others have contributed to new data. Using H5N1 as an example, virus isolation and sequence data from human and avian isolates are available from many affected countries (supporting online table), through concerted efforts within countries, sometimes assisted by WHO or OIE reference laboratories or through other collaborative arrangements. Although concerns about sharing viruses and benefits associated with surveillance have surfaced in some instances, recent WHO Pandemic Influenza Preparedness (PIP) initiatives have aimed at equity (*27*). The biannual WHO influenza vaccine strain selection meetings of the Global Influenza Surveillance and Response System, although primarily focused on selection of the most appropriate influenza virus strains for seasonal vaccines, also reports on antigenic and genetic characteristics of zoonotic influenza viruses for pandemic preparedness. Recent reports include data in "real-time" on contemporary virus genetic sequence and antigenic data from many countries (e.g., Vietnam, Egypt, Bangladesh, India, China, and Cambodia) (*28*).

As we continue to urge more data collection, we should not ignore the progress that has been made and the data that are already available. If molecular signatures for transmissibility of animal influenza viruses in humans are better defined, identifying such mutations in viruses isolated during surveillance in animals (and from zoonotic transmission events in humans) might be possible and would be a further incentive to enhance animal surveillance.

The research questions pertinent to influenza are also relevant to the broader challenges posed by other emerging infections (e.g., SARS and Nipah virus). There is no guarantee of short-term success. However, understanding the viral and host determinants that permit animal influenza and other emerging viruses to transmit to and between humans is arguably one of the most important research questions today. Discussions have started (and need to continue) on how the various types of data may be used for risk assessment and pandemic preparedness and on what concrete actions may follow. Even though a specific pandemic precursor may or may not be identified in time to allow preemptive intervention, prioritizing influenza virus subtypes and antigenic variants for vaccine preparation will be a major step forward. The long-term benefits of such research, which are less readily communicated to the lay public than fears, should not be ignored. Nature remains the most efficient bioterrorist of all!

References and Notes

1. J. T. Wu *et al.*, *Clin. Infect. Dis.* **51**, 1184 (2010).
2. G. J. Smith *et al.*, *Nature* **459**, 1122 (2009).
3. WHO Regional Office for the Western Pacific, *SARS: How a Global Epidemic Was Stopped* (WHO, Manila, Philippines, 2006), chap. 1, p. 3.
4. G. J. Smith *et al.*, *Proc. Natl. Acad. Sci. U.S.A.* **106**, 11709 (2009).
5. L. M. Chen *et al.*, *Virology* **422**, 105 (2012).
6. J. A. Belser *et al.*, *Proc. Natl. Acad. Sci. U.S.A.* **105**, 7558 (2008).
7. C. Pappas *et al.*, *PLoS ONE* **5**, e11158 (2010).
8. R. W. Chan *et al.*, *J. Virol.* **85**, 11581 (2011).
9. N. van Doremalen *et al.*, *PLoS ONE* **6**, e25755 (2011).
10. T. R. Maines *et al.*, *Virology* **413**, 139 (2011).
11. E. M. Sorrell, H. Wan, Y. Araya, H. Song, D. R. Perez, *Proc. Natl. Acad. Sci. U.S.A.* **106**, 7565 (2009).
12. N. Van Hoeven *et al.*, *Proc. Natl. Acad. Sci. U.S.A.* **106**, 3366 (2009).
13. S. S. Lakdawala *et al.*, *PLoS Pathog.* **7**, e1002443 (2011).
14. H. L. Yen *et al.*, *Proc. Natl. Acad. Sci. U.S.A.* **108**, 14264 (2011).
15. M. Enserink, D. Malakoff, *Science* **335**, 20 (2012).
16. R. J. Webby, R. G. Webster, *Science* **302**, 1519 (2003).
17. R. J. Webby, K. Rossow, G. Erickson, Y. Sims, R. Webster, *Virus Res.* **103**, 67 (2004).
18. V. Shinde *et al.*, *N. Engl. J. Med.* **360**, 2616 (2009).
19. Y. Guan *et al.*, *Proc. Natl. Acad. Sci. U.S.A.* **99**, 8950 (2002).
20. E. H. Lau *et al.*, *Emerg. Infect. Dis.* **13**, 1340 (2007).
21. D. Vijaykrishna *et al.*, *Nature* **473**, 519 (2011).
22. D. Vijaykrishna *et al.*, *Science* **328**, 1529 (2010).
23. M. F. Ducatez *et al.*, *Emerg. Infect. Dis.* **17**, 1624 (2011).
24. K. Nulluswami *et al.*, *Morb. Mortal. Wkly. Rep.* **60**, 1 (2011); www.cdc.gov/mmwr/preview/mmwrhtml/mm6035a6.htm.
25. I. Capua, G. Cattoli, *Emerg. Infect. Dis.* **16**, 719 (2010).
26. OFFLU, www.offlu.net/.
27. PIP Framework, www.who.int/influenza/pip/en/.
28. Antigenic and genetic characteristics of influenza A(H5N1) and influenza A(H9N2) viruses and candidate vaccine viruses developed for potential use in human vaccines (WHO, Geneva, September 2011); www.who.int/influenza/resources/documents/characteristics_virus_vaccines/en/index.html.
29. National Center for Biotechnology Information (NIH) Influenza Virus Resource, www.ncbi.nlm.nih.gov/genomes/FLU/.

30. We thank H. Yen for critical comments on the manuscript. Supported by the Area of Excellence Scheme of the University Grants Committee (AoE/M-12/06), Hong Kong SAR, and contract HHSN266200700005C from NIAID, NIH, USA.

Supporting Online Material

www.sciencemag.org/cgi/content/full/335/6073/1173/DC1

10.1126/science.1219936

NEUROSCIENCE

Youth Culture in the Adult Brain

Differences in information processing between older and newly born neurons are observed in the mammalian hippocampus.

Gerd Kempermann

In the adult mammalian hippocampus, the brain region responsible for learning and memory, local precursor cells continually produce new neurons, but how these immature cells contribute to information processing has not been clear. On page 1238 of this issue, Marín-Burgin *et al*. (*1*) show that immature neurons born in the adult mouse hippocampus are more likely to respond to incoming information—quite in contrast to the older neurons in the vicinity that are much harder to impress and show much greater specificity in their response.

The hippocampus has a prominent entrance portal called the dentate gyrus, where incoming information undergoes processing steps that are critical to higher cognitive function. The dentate gyrus consists of a relatively homogeneous population of granule cells, which are excitatory neurons that send their axons through the mossy fiber tract to area CA3 in the hippocampus. Whereas the mossy fiber connection is a structure of extensive plasticity (*2*, *3*), the dentate gyrus is a site of the most unusual type of plasticity—adult neurogenesis (*4*–*6*). Local stem and progenitor cells generate new granule cells and, hence, new mossy fibers, albeit at very low numbers. So few cells can make such a difference because the dentate gyrus presides over a structural bottleneck in the network. The new neurons optimize the mossy fiber connection to just the strength that is needed to meet the functional challenges, while keeping the connection as lean and efficient as possible (*7*).

Physical activity as a generic signal, indicating the increased likelihood of impending cognitive challenges, promotes precursor cell proliferation in the dentate gyrus. Learning and the experience of complexity promote the survival of newborn cells. New neurons preferentially respond in such situations (*8*, *9*), but the physiological basis for this has been unclear. During their maturation period (~2 months in a mouse), new cells transiently show increased synaptic plasticity (*10*–*12*). Their threshold to induce long-term potentiation (long-lasting signal transmission with other neurons) is reduced, indicating that new cells learn more easily than older granule cells. Long-term potentiation in the adult dentate gyrus is almost entirely contributed by new cells, because the preexisting network is massively inhibited from being activated; that is, adult cells have relatively fixed patterns of responsiveness to specific stimuli (*13*, *14*). Adult neurogenesis was thought to be only an investment for the future, because the challenge that triggered the neurogenic response would have long passed once the new neurons matured enough to participate in a network activity. The current idea is that adult neurogenesis maintains a pool of highly plastic immature cells that satisfy particular computational needs. Greater overall levels of activity keep the network responsive by maintaining a greater potential for new cells to be recruited into acute activity and presumably to facilitate lasting changes to the network.

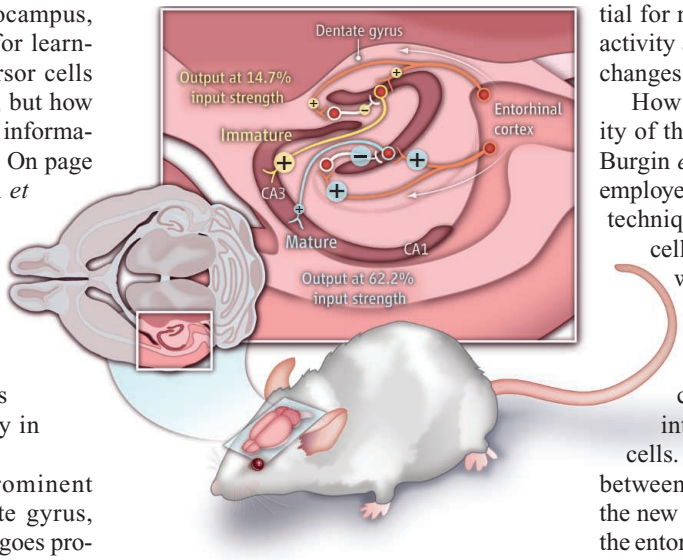

Age-dependent difference. Granule cells in the mouse dentate gyrus receive both excitatory input (+) and (via local interneurons) inhibitory input (–) from the entorhinal cortex. Mature granule cells receive much more input, but their ratio of excitation to inhibition favors inhibition. Immature granule cells, by contrast, have relatively fewer inhibitory inputs. This altered balance (*1*) biases activity in the dentate gyrus toward the young cells, which respond at much lower input strength than the older cells, but are less specific.

How does this particular functionality of the young cells come about? Marín-Burgin *et al*. labeled newborn neurons and employed electrophysiological and imaging techniques to show that immature granule cells go through a critical period during which they are more, rather than less, responsive to excitatory input. An incoming stimulus from the entorhinal cortex excites the granule cells but at the same time, activates interneurons that inhibit the granule cells. The authors show that this balance between excitation and inhibition renders the new cells more sensitive to stimuli from the entorhinal cortex than older granule cells (see the figure). The new neurons are not only more plastic than older granule cells, but are also more likely to generate action potentials (information in the form of electrical impulses) in response to an incoming stimulus. This implies that the young cells respond to a broad variety of synaptic input, whereas old cells respond to more specific input. The young cells also show signs of functional maturity much earlier than previously assumed. They perform mature functions but with youthful vigor.

The impression that young granule cells are particularly responsive to synaptic input led to speculation that the older granule cells might become superfluous and "retire" (*15*). Marín-Burgin *et al*. caution against such a notion. As in other aging communities, the contribution of experienced older members might still be relevant. Experience acquired at a younger age will lastingly affect the abilities of the network as a whole. Marín-Burgin *et al*. speculate that the mix of young and old cells imparts a particular functionality to the dentate gyrus. Young neurons are good integrators and tuned to a broad variety of inputs, whereas old cells display high input specificity and hence are better separators. Both attributes might be needed for the dentate gyrus to perform its functional roles: to allow pattern separation and prevent catastrophic interference, provide contextual and affective annotations, and contribute to cognitive flexibility in situations where novel information has to be integrated into previously formed

Center for Regenerative Therapies Dresden (CRTD) and German Center for Neurodegenerative Diseases (DZNE) Dresden, 01307 Dresden, Germany. E-mail: gerd.kempermann@crt-dresden.de

Published by AAAS

representations. This does not ultimately settle the question of what neurogenesis in the adult dentate gyrus is good for, but suggests that new neurons are critical for hippocampal function.The functional relevance of adult-born neurons is network-specific, and adult hippocampal neurogenesis is thus distinct from the only other neurogenic region of the adult brain, the olfactory bulb. The healthy dentate gyrus turns out to be a house for many generations of cells under one roof and the site of an intriguing collaboration between the young and the older.

References

1. A. Marín-Burgin, L. A. Mongiat, M. Belén, A. F. Schinder, *Science* **335**, 1238 (2012); 10.1126/science.1214956.
2. H. Schwegler, W. E. Crusio, I. Brust, *Neuroscience* **34**, 293 (1990).
3. H. Schwegler, H. P. Lipp, H. Van der Loos, W. Buselmaier, *Science* **214**, 817 (1981).
4. J. B. Aimone, W. Deng, F. H. Gage, *Trends Cogn. Sci.* **14**, 325 (2010).
5. G. Kempermann, in *Adult Neurogenesis 2–Stem Cells and Neuronal Development in the Adult Brain*, G. Kempermann, Ed. (Oxford Univ. Press, New York, 2011).
6. L. A. Mongiat, A. F. Schinder, *Eur. J. Neurosci.* **33**, 1055 (2011).
7. G. Kempermann, *J. Neurosci.* **22**, 635 (2002).
8. N. Kee, C. M. Teixeira, A. H. Wang, P. W. Frankland, *Nat. Neurosci.* **10**, 355 (2007).
9. A. Tashiro, V. M. Sandler, N. Toni, C. Zhao, F. H. Gage, *Nature* **442**, 929 (2006).
10. C. Schmidt-Hieber, P. Jonas, J. Bischofberger, *Nature* **429**, 184 (2004).
11. J. S. Snyder, N. Kee, J. M. Wojtowicz, *J. Neurophysiol.* **85**, 2423 (2001).
12. S. Ge, C. H. Yang, K. S. Hsu, G. L. Ming, H. Song, *Neuron* **54**, 559 (2007).
13. M. D. Saxe *et al*., *Proc. Natl. Acad. Sci. U.S.A.* **103**, 17501 (2006).
14. A. Garthe, J. Behr, G. Kempermann, *PLoS ONE* **4**, e5464 (2009).
15. C. B. Alme *et al*., *Hippocampus* **20**, 1109 (2010).

10.1126/science.1219304

GEOCHEMISTRY

Moonstruck Magnetism

Do magnetic anomalies on the Moon indicate the remains of a giant asteroid impact?

Gareth S. Collins

A surprising result of the Apollo missions was the discovery of strong, localized magnetic fields emanating from the lunar crust (*1*). One reason these fields are so enigmatic is that endogenous lunar rocks contain a low abundance of metallic iron, making them very weakly magnetic (*2*–*4*). How, then, did the Moon record such strong magnetic signatures? On page 1212 of this issue, Wieczorek *et al*. (*5*) propose that many of the Moon's magnetic anomalies originate from highly magnetic deposits of a giant asteroid that collided with the Moon early in its history. These readily magnetized, extralunar deposits subsequently recorded magnetic fields that may have been generated by an ancient lunar core dynamo and/or transient impact-generated fields.

The generation of a magnetic anomaly requires two things—a magnetic field and a magnetic mineral that will record it. On Earth, the principal magnetic minerals are iron oxides and sulfides produced in the oxidizing terrestrial environment. By contrast, in the reducing lunar environment, metallic iron-nickel alloys are the main carriers of remanent magnetization. Meteoritic materials can contain magnetic minerals of both types. Whereas magnetic minerals are generally abundant in meteoritic material, they are extremely rare in the Moon's crust and upper mantle because of the nature of the Moon's formation and its thermal evolution. As a result, endogenous lunar materials are very poor at recording magnetic fields, whereas meteoritic material can be orders of magnitude more magnetic. Wieczorek *et al*. use this observation to show that the strength of the lunar magnetic anomalies would require unrealistically thick deposits of unidirectionally magnetized lunar crustal materials, but can be explained by relatively thin deposits of meteoritic material.

On the basis of the observation that the spatial distribution of many of the anomalies corresponds to the northern "rim" of the mammoth South Pole–Aitken (SPA) impact basin on the far side of the Moon, ~2500 km in diameter (*6*), Wieczorek *et al*. go on to propose that deposits from the SPA impactor are the source materials for the lunar magnetic anomalies. According to their hypothesis, the SPA impactor was ~200 km in diameter, approached the Moon from the south, and collided at an oblique angle to form an elongated crater. In the process, impactor debris was sprayed downrange to the north and deposited near the northern basin rim. Computer simulations of SPA-scale impacts performed to test this hypothesis predict final impactor deposits that can explain the observed strength and distribution of many of the Moon's magnetic anomalies.

Wieczorek *et al*.'s innovation explains where the Moon's main magnetic field recorders came from, but what was the source of the ancient magnetic fields? Evidence for an iron core in the Moon that is currently at least partially molten (*7*) suggests that one possibility is an ancient lunar dynamo. Support for this

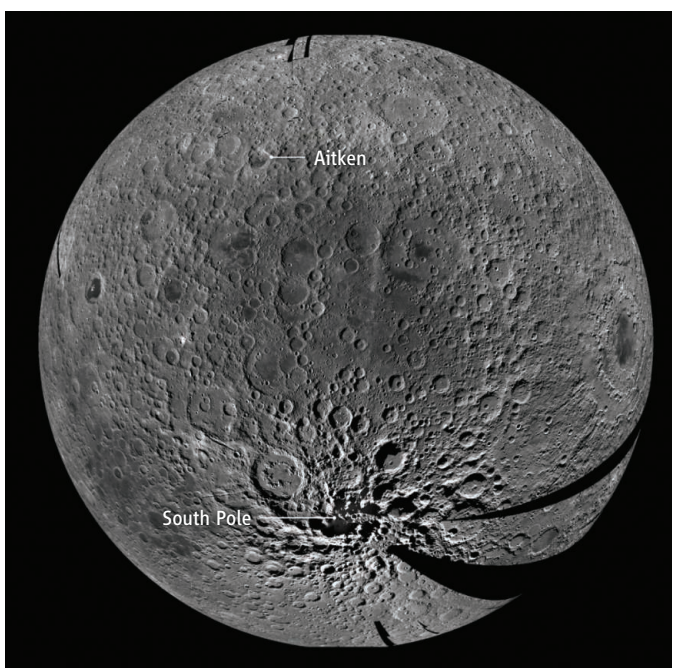

Making an impact. The South Pole–Aitken basin on the far side of the Moon, the largest and oldest definitive impact crater in the solar system, spans more than one-quarter of the Moon's circumference from Aitken crater in the north to the lunar South Pole. This image is a mosaic from the Lunar Reconnaissance Orbiter Camera (LROC) Wide Angle Camera (WAC).

CREDIT: NASA/GSFC/ARIZONA STATE UNIVERSITY

Department of Earth Science and Engineering, Imperial College London, London SW7 2AZ, UK. E-mail: g.collins@imperial.ac.uk

idea comes from paleomagnetic analyses of lunar samples (*8*–*10*), which suggest that an ancient lunar magnetic field, comparable in intensity to Earth's present field, persisted for several hundred million years. This long duration is difficult to explain by an Earth-like dynamo driven by thermal or chemical convection (*11*), but recent work has revived the idea, suggesting that an ancient lunar dynamo could have been powered by differential rotation between the Moon's core and mantle, either continuously over several hundred million years (*12*) or for short periods after giant impacts (*13*). Broad magnetic anomalies over several Nectarian-aged (from 3.92 to 3.85 billion years ago) impact basins, recorded by slow cooling over long time periods, are also evidence for an early lunar core dynamo (*14*). However, it is also possible that the highly magnetic impactor remnants were magnetized by transient impact-generated fields (*6*) long after they were deposited. As these ephemeral fields are strongest at the impact antipode, this idea explains the intriguing correlation between some of the largest magnetic anomalies and the antipodes of the four largest young impact basins on the Moon (*15*).

As the largest and oldest impact crater in the solar system, the SPA basin is of immense importance and is a strong candidate location for future sample-return missions. Although the detailed geologic record of Earth's formative past was erased long ago, the Moon preserves materials in its crust and mantle that date from before continents grew and life began to stir on Earth. The huge SPA impact brought deep lunar materials to the surface, and sampling these otherwise inaccessible rocks could hold the key to understanding how the Earth-Moon system formed and evolved. Moreover, an accurate absolute age for the basin would provide a vital anchor for interpreting the violent bombardment history of the Earth and Moon and its influence on the evolution of life on Earth. If Wieczorek *et al*.'s hypothesis is correct, a sample-return mission to SPA's northern rim may also uncover ancient meteoritic material from the giant asteroid that formed the basin itself. And if this highly magnetic material is accessible, it could prove an invaluable resource for human colonization of the Moon.

References

1. P. Dyal, C. W. Parkin, C. P. Sonett, *Science* **169**, 762 (1970).
2. M. Fuller, S. M. Cisowski, *Geomagnetism* **2**, 307 (1987).
3. K. Lawrence, C. Johnson, L. Tauxe, J. Gee, *Phys. Earth Planet. Inter.* **168**, 71 (2008).
4. P. Rochette, J. Gattacceca, A. V. Ivanov, M. A. Nazarov, N. S. Bezaeva, *Earth Planet. Sci. Lett.* **292**, 383 (2010).
5. M. A. Wieczorek, B. P. Weiss, S. T. Stewart, *Science* **335**, 1212 (2012).
6. L. L. Hood, N. A. Artemieva, *Icarus* **193**, 485 (2008).
7. R. C. Weber, P.-Y. Lin, E. J. Garnero, Q. Williams, P. Lognonné, *Science* **331**, 309 (2011).
8. I. Garrick-Bethell, B. P. Weiss, D. L. Shuster, J. Buz, *Science* **323**, 356 (2009).
9. S. M. Cisowski, D. W. Collinson, S. K. Runcorn, A. Stephenson, M. Fuller, *J. Geophys. Res.* **88**, A691 (1983).
10. E. K. Shea *et al*., *Science* **335**, 453 (2012).
11. D. R. Stegman, A. M. Jellinek, S. A. Zatman, J. R. Baumgardner, M. A. Richards, *Nature* **421**, 143 (2003).
12. C. A. Dwyer, D. J. Stevenson, F. Nimmo, *Nature* **479**, 212 (2011).
13. M. Le Bars, M. A. Wieczorek, O. Karatekin, D. Cébron, M. Laneuville, *Nature* **479**, 215 (2011).
14. L. L. Hood, *Icarus* **211**, 1109 (2011).
15. R. P. Lin, K. A. Anderson, L. L. Hood, *Icarus* **74**, 529 (1988).

10.1126/science.1217681

SOCIAL SCIENCE

Experimenting with Politics

Social scientists are turning increasingly to experiments to explain important political behaviors.

James N. Druckman[1] and Arthur Lupia[2]

In his 1909 presidential address to the American Political Science Association, A. Lawrence Lowell (*1*) advised the then-fledgling discipline against following the natural scientists into greater use of experimental designs. This attitude toward experiments was still dominant at the end of the World War II, when political scientists were using increasingly intricate statistical methods to characterize relationships, but still ran few experiments. The tide began to turn in the 1980s, when scholars started to integrate the accumulated knowledge of traditional political science with the theoretical approaches of psychology and economics. This trend generated more acute causal predictions, which, along with technological developments, led political scientists to increasingly turn to experiments. Today, experiments are often the preferred method to explain the causes and consequences of political behaviors (*2*).

Political scientists commonly use three different experimental methods. Laboratory experiments place subjects in situations that show how people reach decisions as voters, jurors, or legislators. Political scientists also embed experiments in large, and often nationally representative, surveys. These experiments elucidate how variations in the descriptions or presentations of political phenomena affect the perceptions and feelings of diverse citizen populations. Finally, in field experiments, researchers integrate random assignment into real political campaigns or attempts to implement policy. These experiments can clarify the relative effectiveness of various tactics and strategies.

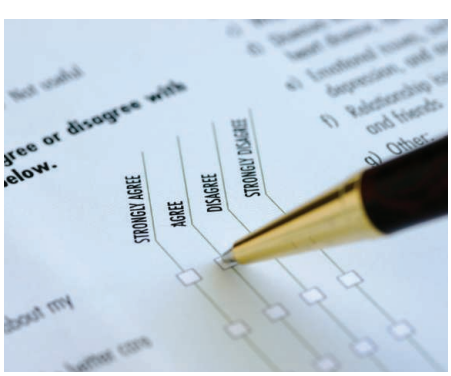

Your opinion counts. In survey experiments, political scientists explore how the attitudes, perceptions, and emotions of citizens affect their responses in opinion surveys.

Laboratory experiments can, for example, inform the design and effectiveness of governmental institutions. In a classic laboratory experiment by Ostrom *et al*. (*3*), each subject decided how much to withdraw from a group fund that mimicked a scarce environmental resource. If the subjects overwithdrew, then the group as a whole earned less. Allowing group members to shame those who overwithdrew, or to shame and fine, yielded greater collective benefits than did fines alone. The results challenged the long-standing presumption that a group's ability to produce high-value public goods—such as good air quality for all, despite individual incentives to pollute—requires an external author-

[1]Department of Political Science and Institute for Policy Research, Northwestern University, Evanston, IL 60208, USA. [2]Department of Political Science and Institute for Social Research, University of Michigan, Ann Arbor, MI 48104, USA. E-mail: druckman@northwestern.edu; lupia@isr.umich.edu

ity to impose punishments for noncompliance. The work stimulated a large body of research into when and how common political factors, such as ethnic heterogeneity in politically salient groups, affect the possibility of effective self-governance in the absence of external coercion (*4*).

Survey experiments (see the first figure) are particularly valuable for clarifying voter behavior. For example, Kuklinski *et al*. (*5*) used a "list experiment" to elicit the extent to which citizens are willing to admit racial anxiety or animus. Subjects were presented with a list of items and asked, "How many of them upset you?" Some received a three-item list; others received a four-item list where the added item was "a black family moving in next door." Among white survey respondents in the American South, the four-item group reported an average 2.37 items that made them upset, compared to 1.95 items in the three-item group. Given that the groups are otherwise identical, the implication is that 42% of southern respondents [(2.37 – 1.95) × 100] were upset by the thought of a black neighbor. This finding contrasts with non-southerners who reported that a similar number of items made them upset regardless of whether they chose from the list of three or four items. It also is telling that just 19% of southern respondents admitted that a black neighbor would upset them when asked the question directly.

Survey experiments can also provide a window into how people will think if policies are described in different ways. Schuldt *et al*. provide a compelling example in their study of one of the most debated issues of our time: climate change (*6*). The authors randomly assigned some survey respondents to answer a question about whether "global warming" has been happening. Other respondents were asked a version of the question that replaced the words "global warming" with "climate change." The authors examined how the wording differences affected response patterns among politically relevant subpopulations. For example, 60% of Republican respondents believed climate change to be occurring, whereas only 44% of them believed global warming was taking place. Collectively, such experiments give users of surveys the means to more accurately interpret existing survey responses, and also provide unique data on the extent to which stated attitudes are robust to situational variations.

For decades, traditional opinion surveys have shown that many citizens cannot recall seemingly basic political facts, such as which political party controls a majority of seats in the U.S. Congress. Academics and members of the press, in turn, drew broad claims about voter incompetence from such data (*7*). Experimental research has produced a different view (*8*). For example, Lodge *et al*. (*9*) studied how citizens' memories of specific candidate attributes affect their subsequent preferences. After asking respondents to report their opinions on a set of issues, the researchers gave them a fact sheet describing the issue positions of two candidates. After a randomly determined delay of between 1 and 31 days, 80% of respondents failed to recall candidate issue positions. Yet, most respondents expressed strong preferences for the candidate who most closely shared their positions. Common "political fact tests" may thus reveal very little about how voters think.

Political power. Political field experiments have provided insight into effective voter mobilization strategies.

In a more recent related study, Prior and Lupia (*10*) asked 1200 selected members of a national survey to answer a set of fact-based political questions. They randomly assigned some respondents to a control group that mimicked traditional surveys. In a second group, respondents were paid 1 dollar for every correct answer. Relative to the control group, payment produced a 32% increase in correct answers for respondents who reported following politics "some of the time" (rather than "most of the time" or "not at all"). Thus, opinion surveys may underestimate what voters know because they offer little motivation for respondents to think about the questions during the interview.

In recent years, field experiments have gained greater visibility, particularly in the context of voter mobilization (see the second figure). A leading example is that of Gerber and Green (*11*), who randomly distributed messages—for example, through personal contact, by phone, or by mail—to potential voters during an election campaign. Compared to voters who received no reminder or a mail or phone reminder, a personal visit boosted turnout. More recently, Gerber *et al*. (*12*) performed a study in which some subjects received a message that their neighbors would be informed about whether they turned out to vote. These subjects were much more likely to vote in the election than were subjects who received no message.

Findings from these voter mobilization experiments have affected the manner in which political parties conduct campaigns (*13*) and have been used as a model for inquiries about the effectiveness of voter mobilizations strategies. For example, researchers in China showed that during a regional election in 2003, door-to-door canvassing to encourage people to vote increased turnout by over 10% (*14*). In another study, researchers randomly assigned 49 Indonesian villages to one of two methods for choosing an economic development program. In roughly half of the villages, chosen citizen representatives made the decision. In the other villages, all eligible villagers could vote directly on which program to pursue. The experimental treatment had small effects on the villages' chosen projects, but villagers who were given the opportunity to vote viewed the chosen projects as more valuable and were far more satisfied with the outcome (*15*). Collectively, these efforts reveal effective routes to increasing electoral participation in ways that lend legitimacy to electoral outcomes.

The studies described above and others like them have transformed political science into a discipline in which experiments are increasingly seen as a preferred method of discovery and inference. Yet, important challenges persist in expanding the domain of experimental political science. One such challenge is that typical experimental subjects often lack the experience needed to act "as if" they were professional legislators; yet, legislators themselves are often reluctant to participate in experiments as subjects. Another challenge is that politics entails not just debates about the empirical consequences of choosing one policy over another, but also disagreements over basic values. Experiments have less power to settle such questions. Nevertheless, many aspects of modern politics follow a logic that can be evaluated scientifically. Political science experiments are increasingly helping researchers and citizens around the world to better understand how humans organize themselves.

Published by AAAS

References

1. A. L. Lowell, *Am. Polit. Sci. Rev.* **4**, 1 (1910).
2. J. N. Druckman, D. P. Green, J. H. Kuklinski, A. Lupia, Eds., *Cambridge Handbook of Experimental Political Science* (Cambridge Univ. Press, New York, 2011).
3. E. Ostrom, J. Walker, R. Gardner, *Am. Polit. Sci. Rev.* **86**, 404 (1992).
4. E. Coleman, E. Ostrom, in *Cambridge Handbook of Experimental Political Science*, J. N. Druckman, D. P. Green, J. H. Kuklinski, A. Lupia, Eds. (Cambridge Univ. Press, New York, 2011), pp. 339–352.
5. J. H. Kuklinski *et al.*, *Am. J. Pol. Sci.* **41**, 402 (1997).
6. J. P. Schuldt, S. H. Konrath, N. Schwarz, *Public Opin. Q.* **75**, 115 (2011).
7. M. X. Delli Carpini, S. Keeter, *What Americans Know About Politics and Why It Matters* (Yale Univ. Press, New Haven, CT, 1996).
8. P. M. Sniderman, R. A. Brody, P. E. Tetlock, *Reasoning and Choice: Explorations in Political Psychology* (Cambridge Univ. Press, New York, 1991).
9. M. Lodge, M. R. Steenbergen, S. Brau, *Am. Polit. Sci. Rev.* **89**, 309 (1995).
10. M. Prior, A. Lupia, *Am. J. Pol. Sci.* **52**, 169 (2008).
11. A. S. Gerber, D. P. Green, *Am. Polit. Sci. Rev.* **94**, 653 (2000).
12. A. S. Gerber *et al.*, *Am. Polit. Sci. Rev.* **102**, 33 (2008).
13. D. P. Green, A. S. Gerber, *Get Out the Vote: How to Increase Voter Turnout* (Brookings Institution, Washington, DC, ed. 2, 2008).
14. M. Guan, D. P. Green, *Comp. Polit. Stud.* **39**, 1175 (2006).
15. B. A. Olken, *Am. Polit. Sci. Rev.* **104**, 243 (2010).

10.1126/science.1207808

MATERIALS SCIENCE

Swell Approaches for Changing Polymer Shapes

Patterning of cross-linked regions in polymer gel sheets with ultraviolet light creates unequal stresses and drives their buckling into complex three-dimensional shapes.

Eran Sharon

Most machines work by moving rigid elements or frameworks. In some cases, flexible elements, such as membranes, are attached to the framework and are passively deformed by its motion. In contrast, octopuses, hearts, caterpillars, and growing mushrooms are examples of natural structures made of soft tissue that move or change configurations through a completely different mechanism. Each element of the tissue—cells or compartments—undergoes some sort of active deformation, such as swelling, that creates stresses within the structure. The entire structure changes shape to relieve these internal stresses. Such control of shape and motion by active deformation has not yet been implemented into engineering design technique because of theoretical and experimental difficulties. On page 1201 of this issue, Kim *et al*. (*1*) present a technique for the production of gel sheets that are patterned into regions that can swell to different extents and actively deform into three-dimensional (3D) shapes.

A body that undergoes nonuniform growth or swelling is likely to contain residual stresses; the swelled components no longer fit together. Because the elements are "glued" together, they will be locally deformed (for example, if just one side of a sheet swells, it will bend into a U shape). For more complex structures, it is not easy to predict the final swelled shape (global configuration) of the body or to design a distribution of swelled elements to create a desired global configuration.

How can one construct soft material to undergo the desired, nonuniform swelling? During the past decade, there has been progress in both theoretical modeling and experimental realization of shaping by active swelling. The research was focused mainly on the study of thin elastic sheets. In particular, non-Euclidean plates (NEPs) (*2*) are thin sheets that undergo some lateral growth or swelling that is uniform across the thickness of the plate but varies with location within the plate. If we consider a network of points in the sheet and the edges connecting them, the set of edges in the swollen state undergo unequal distortions (defining new "reference states") and will no longer lie in a flat plane but will buckle into a 3D configuration. The theory of NEPs uses the framework of differential geometry to express the reference lengths and the energy of such sheets, allowing the calculation of equilibrium configurations of NEPs.

Kim *et al*. constructed NEPs from gel sheets made of *N*-isopropylacrylamide (NIPAm), a hydrogel that reduces its volume when heated above 33°C (*3*). Ultraviolet (UV)–induced cross-linking of selected regions of the gel led to differences in local swelling: Swelling or shrink-

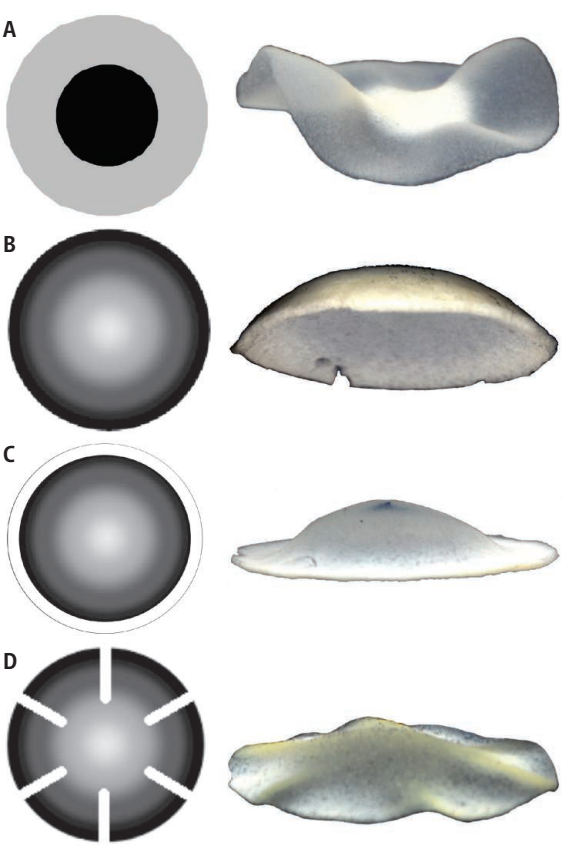

Shape-shifting sheets. Examples of masks (left) and the resultant buckled NIPAm gel sheets (right) are shown. In these macroscopic-scale examples (5 cm in diameter) the local "gray level" of the mask determines the amount of UV irradiation onto different regions of the sheet. Illuminated regions have greater cross-linking density, which decreases their shrinkage ratio. The presence of regions that undergo different amounts of shrinkage creates a 3D shape once the plates are activated in a hot bath. (**A**) A dark center region leads to an enhanced shrinkage in the center and the formation of a wavy disc. (**B**) A continuous gradient of gray scale can be tuned to construct a spherical dome shape. Small changes of the mask in (B) in the form of a clear ring along the margins (**C**), or six radial clear lines (**D**) leads to different modulations of the spherical dome. Samples were made by I. Levine at The Hebrew University of Jerusalem.

The Racah Institute of Physics, The Hebrew University of Jerusalem, Jerusalem, Israel. E-mail: erans@vms.huji.ac.il

age of a highly cross-linked gel was minor, but the weakly cross-linked gel underwent large volume changes when the temperature was varied. The UV light exposure was performed with a patterned mask of micrometer-sized opaque dots with varying diameter. This process "printed" regions on the sheets that shrank a lot (opaque dots, weakly cross-linked regions) or a little (UV-exposed, highly cross-linked regions). Regions containing large dots tended to shrink more than those with small dots, and as long as the sheet was not too thin, this discrete "print" was converted into sheets that underwent smooth, nonuniform swelling.

Several preprogrammed geometrical shapes were created this way, and the authors performed the nontrivial tasks of calculating swelling profiles, producing the NEPs, and measuring the shapes of gel discs a few hundred micrometers in diameter. Even on such a small scale, the authors showed impressive quantitative agreement between experiments and theoretical predictions. In this sense, shaping by active deformation can be regarded as an existing design technique on the submillimeter scale.

Shaping of NEPs has some distinctive characteristics. First, a 2D printed "picture" is converted into a 3D shape; the figure shows centimeter-scale NEP discs made of selectively cross-linked NIPAm gel, along with the masks that were used for their production. The conversion of mask's local gray levels into swelling ratios and finally into 3D shapes shows how the connection between the "picture" and the "shape" of a sheet is often surprising. Some very simple masks create complex 3D shapes. In addition, this method only sets lateral reference lengths, which may correspond to several different surfaces and hence shapes. A configuration of a NEP is selected from many possible ones that have relatively small energetic differences. As a result, NEPs show extraordinary responsiveness; they easily undergo shape changes between very different configurations as a result of small changes in parameters. This property might be desired in biomechanics and industrial design.

In principle, NEPs can be constructed from other materials, such as nematic elastomers and electroactive polymers. The underlying geometrical principles that govern shaping by active deformation are possibly relevant on a nanometer scale for use with self-assembled supramolecular structures. This broad relevance is likely to motivate the development of software packages that will allow convenient study and design of shape-transforming sheets. Finally, the physics of shaping by active deformation allows for a better understanding of naturally occurring systems, such as invertebrate's motion and morphogenesis during growth (*4*).

References

1. J. Kim, J. A. Hanna, M. Byun, C. D. Santangelo, R. C. Hayward, *Science* **335**, 1201 (2012).
2. E. Efrati, E. Sharon, R. Kupferman, *J. Mech. Phys. Solids* **57**, 762 (2009).
3. T. Tanaka, *Phys. Rev. Lett.* **40**, 820 (1978).
4. U. Nath, B. C. Crawford, R. Carpenter, E. Coen, *Science* **299**, 1404 (2003).

10.1126/science.1219020

ECOLOGY

The Human Factor

Marine sediments suggest that climate was not the sole driver of the African rainforest crisis 3000 years ago.

Lydie Dupont

How did early farming cultures affect the surrounding vegetation? Did their activities disturb the forest beyond their fields, or was their land use compatible with natural developments? On page 1219 of this issue, Bayon *et al*. (*1*) report an important step toward answering this question by showing that climatic changes alone cannot explain the vegetation changes that occurred in West Central Africa between 2000 and 3000 years ago.

Linguistic analyses of Bantu languages suggest that Bantu-speaking peoples expanded from their homelands in eastern Nigeria southward and eastward during the first millennium B.C.E. (*2*). Although there are not many relevant archaeological sites, evidence from Cameroon, Gabon, and Congo supports the interpretation that this expansion involved agriculturists who brought iron-smelting technologies with them. For instance, the earliest pottery of the Congo basin, dated ~400 B.C.E., is found in its western part along tributaries of the Congo River (see the figure). This pottery style is associated with those of Iron Age cultures in Cameroon. Analysis of the pottery style development indicates migration and expansion along the larger tributaries of the Congo River during the following centuries (*3*). The impact of these people and their expansion on the surrounding vegetation is difficult to discern, because pollen records do not provide unambiguous indicators of human versus climatic effects on the forest.

During the first millennium B.C.E., extensive changes took place in the rainforest of West Central Africa. Numerous pollen records suggest that the mature rainforest was replaced by a lighter type of forest with more pioneer trees, a forest adapted to a drier or longer dry season, or savannah vegetation (see the figure) (*4*). This "rainforest crisis" has been widely attributed to climate change alone, laying the blame for the forest changes on decreased precipitation and a longer dry season (*5*–*7*).

In northern Africa, a trend to drier conditions started roughly 5000 years ago (*8*); over the course of the next ~2000 years, this drier climate extended south into Central Africa (*9*). However, 3000 to 2000 years ago, the mature rainforest declined even more than during the period of the Last Glacial Maximum between 17,000 and 24,000 years ago, when climatic conditions around the world were drastically different from those seen in the past 10,000 years (*10*). The extensive rainforest changes between 2000 and 3000 years ago are difficult to reconcile with moderate changes in climate in West Central Africa at this time, as indicated by biogeochemical proxies of continental temperature and precipitation (*11*).

Bayon *et al*. show that the rainforest crisis involved more than aridification and increased seasonality. Using marine sediments deposited in front of the mouth of the Congo River, they measured two proxies for the weathering of rocks for the time period from 20,000 to 2000 years ago.

First, they determined the ratio between aluminum (Al) and potassium (K). This ratio depends on both the lithology of the source rock and the degree of chemical weathering. Chemical weathering is high under warm, wet conditions. Hence, Al/K ratios are higher in clays from rivers draining warm tropical areas than in those from colder and/or drier environments. Al/K ratios in marine sediments off the Congo River normally covary

MARUM–Center for Marine Environmental Sciences, University of Bremen, P.O. Box 330440, 28334 Bremen, Germany. E-mail: dupont@uni-bremen.de

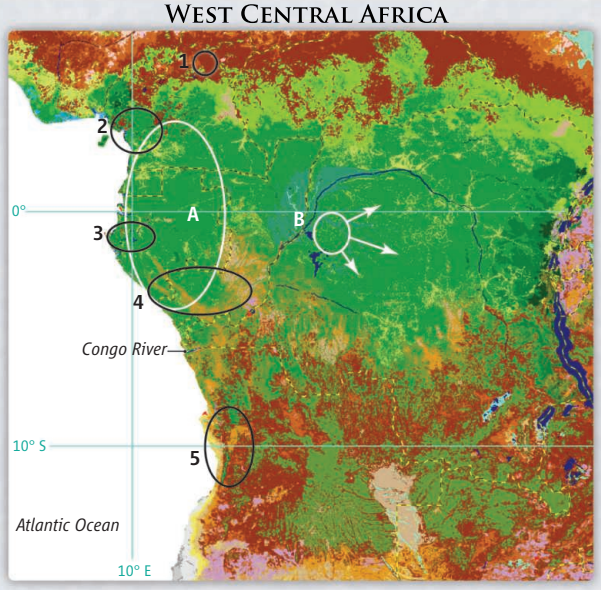

1 ~3000 years ago: submontane semideciduous forest changes to savannah
2 2500 to 2700 years ago: disturbed rainforest, pioneer trees, patches of savannah
3 2500 to 2400 years ago: mature rainforest replaced by secondary forest
4 3000 to 2500 years ago: grasslands extend at swampy and forested sites
5 3700 to 2000 years ago: two-step decrease of forest, extension of savannah

A time of change. Pottery styles from late Neolithic and iron-age cultures nearer the coast (area A) may have been a precursor of the earliest pottery, dated 2500 to 2100 years ago, found in the inner Congo Basin (area B) (*3*). Results reported by Bayon *et al*. suggest that this expansion of agriculturists may have been partly responsible for extensive changes in the rainforest between ~3700 and 2500 years ago (numbers 1 to 5) (*5*–*7*). Satellite-derived vegetation map of Central Africa from (*12*). Forest in green, forest-savannah mosaic in light green, woodland in brown, grassland in yellow, agriculture in pink.

with other proxies for continental temperature and precipitation.

Second, they measured hafnium (Hf) and neodymium (Nd) isotopes. Both the Nd and the Hf isotopic composition of rocks are determined by magmatic processes in the upper continental crust and depend on the rock source, but Hf isotopes are additionally changed by weathering of silicates. By comparing the isotopic composition of these trace elements in marine sediments, changes in silicate weathering can be deduced. Bayon *et al*. find that the Hf isotopic composition was relatively low during the Last Glacial Maximum (~20,000 years ago) and increased during deglaciation, whereas the Nd isotopic composition remained constant.

The results from both weathering proxies can be explained by changing climate, except for the period between 3000 and 2000 years ago. During the African rainforest crisis of the first millennium B.C.E., both proxies show that weathering increased despite reduced precipitation and constant temperatures.

Hence, although climate played a role in the rainforest crisis, it cannot have been the only factor. The explanation may lie with human activities, which may have had a strong impact on the forest through slash-and-burn agriculture and/or cutting trees for iron smelting (*1*). If so, then the next task will be to differentiate the relative impacts of human land-use effects and climatic influences.

The results of Bayon *et al*. also caution against using the tropical forest development of past millennia as a direct indicator of the West African monsoon. The climatic interpretation of the rainforest crisis invokes a shift in the yearly migration pattern of the Intertropical Convergence Zone to explain aridity and seasonality in West Central Africa (*5*–*7*). However, if only part of the forest change is climatically induced, any inferences using this forest decline will overestimate the aridification and increased seasonality of the past 3000 years.

References

1. G. Bayon *et al*., *Science* **335**, 1219 (2012); 10.1126/science.1215400.
2. K. Bostoen, *J. Afr. Hist.* **48**, 173 (2007).
3. H.-P. Wotzka, *Studien zur Archäologie des Zentralafrikanischen Regenwaldes, Africa Praehistorica 6* (Heinrich-Barth-Institut, Cologne, Germany, 1995).
4. C. Assi-Kaudjhis *et al*., *Geo-Eco-Trop* **34**, 1 (2010).
5. A. Vincens, G. Buchet, M. Servant, ECOFIT Mbalang Collaborators, *Clim. Past* **6**, 281 (2010).
6. A. Vincens *et al*., *J. Biogeogr.* **26**, 879 (1999).
7. A. Ngomanda *et al*., *Quat. Res.* **71**, 307 (2009).
8. A.-M. Lézine, *Quat. Res.* **32**, 317 (1989).
9. P. Hoelzmann *et al*., in *Past Climate Variability Through Europe and Africa*, R. W. Battarbee *et al*., Eds. (Springer, Dordrecht, Netherlands, 2004), pp. 219–256.
10. J. Lebamba, A. Vincens, J. Maley, *Clim. Past* **8**, 59 (2012).
11. J. W. H. Weijers *et al*., *Science* **315**, 1701 (2007).
12. A Land Cover Map of Africa. European Commission, Joint Research Centre, 2003. See http://bioval.jrc.ec.europa.eu/products/glc2000/glc2000.php.

10.1126/science.1219903

CELL BIOLOGY

Embryonic Clutch Control

A molecular clutch couples actin-based contractions to changes in cell shape that drive morphogenesis.

William Razzell[1] and Paul Martin[1,2]

All embryos, from worms to humans, are shaped during development by morphogenetic steps that tug, bend, fold, and sculpt epithelial sheets into forms that resemble, or are the precursors of, the final adult structure (*1*). Most of these changes are the consequence of constrictions of the apical surfaces of epithelial cells that are powered by pulsatile contracting cytoskeletal (actomyosin) networks. On page 1232 of this issue, Roh-Johnson *et al*. (*2*) show that, just as in a car where the power of the engine is linked to forward movement by means of a clutch, clutch control is also the rate-limiting step for contracting cells in tissues.

One of the best-studied examples of apical constriction driving morphogenetic episodes is gastrulation in the fly *Drosophila melanogaster*, in which a strip of approximately 1200 epithelial cells buckles inward and invaginates to internalize the presumptive mesoderm of the embryo (*3*). Variations of this process drive gastrulation in all organisms, as well as other morphogenetic events such as neural tube formation in vertebrates (*4*), which gives rise to the brain and spinal cord, and to formation of the optic and otic vesicles, which develop into the human eye and inner ear, respectively (see the figure). Concerted apical constrictions of cells are generated by the assembly and contractility of actomyosin networks composed of myosin II molecules that tug on actin filaments (*5*). These networks are linked to the plasma membrane by adherens junctions, protein complexes that also weld one cell to its neighbor (*6*). Live imag-

[1]School of Biochemistry, Faculty of Medical and Veterinary Sciences, University of Bristol, Bristol BS8 1TD, UK. [2]School of Physiology and Pharmacology, Faculty of Medical and Veterinary Sciences, University of Bristol, Bristol BS8 1TD, UK. E-mail: william.razzell@bristol.ac.uk; paul.martin@bristol.ac.uk

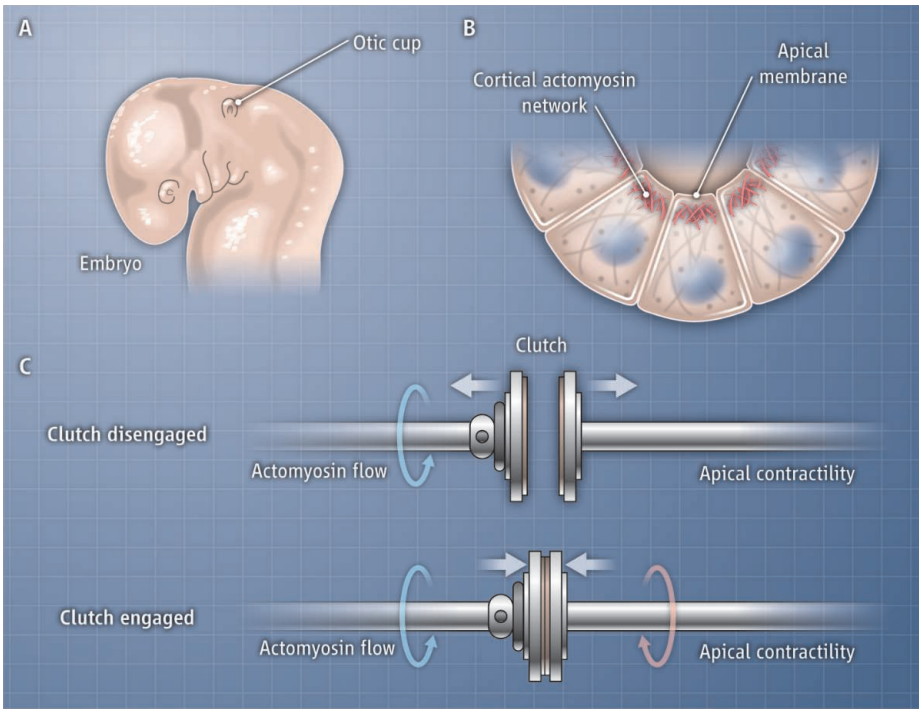

Cell apical constrictions during embryonic morphogenesis. (**A**) Concerted apical constrictions in epithelial sheets drive invaginations to form structures such as the otic cup from which the human inner ear derives. (**B**) Constricting cells become wedge-like to drive many morphological movements. (**C**) As in a car, the engine (actomyosin flow) during gastrulation can run without output. Only when the clutch is engaged and the motor is directly linked to the effector (apical plasma membrane) can there be movement of the apical membrane.

ing of the fly embryo has revealed the pulsatile and ratchet-like nature of cell contractions during gastrulation and other morphogenetic processes, with periods of shrinkage and resting before another round of contraction (*5*, *7*). This contractile machinery is exquisitely responsive to mechanical cues from neighboring cells and tissue; gentle probing with a needle can trigger actomyosin assembly and drive epithelial invagination (*8*); similarly, disrupting adherens junctions, which changes tissue tensions, can alter the polarity of apical constrictions (*9*). The presumption has been that the regulatory step for apical constrictions is determined by when and where cells assemble and contract their actomyosin networks.

Roh-Johnson *et al*. challenge and extend this idea through a series of elegant studies in the worm *Caenorhabitis elegans*. In this model organism, two neighboring endodermal precursor cells (Ea and Ep) constrict their apical surfaces and ingress beneath the surface during gastrulation. The authors followed actomyosin network dynamics in these cells by tracking fluorescently tagged myosin II and, concomitantly, measured changes in the shape of the apical membrane. They observed that myosin moves centripetally toward the center of the cell at a constant pace, whereas the apical cell surface initially shrinks slowly, or not at all. At early stages, actomyosin flow (the engine) runs for several minutes before any cell constriction actually happens. Only later does myosin movement occur in unison with the movement of "contact zones" (adherens junctions). After a transitional period of "slippage," the flow of actomyosin is only later efficiently coupled to constriction of the apical cell surface. The authors observed very similar mechanisms operating during *Drosophila* gastrulation, and it might now be feasible to live image and observe whether the same is true for vertebrate embryos, too (*10*).

What explains the initial lack of linkage between actomyosin flow and cell shrinkage? Roh-Johnson *et al*. suggest that a "molecular clutch" engages the myosin II engine with the apical membrane so that actomyosin contractility can drive shrinkage of the apical cell surface. Because cortical tension generated within the apical actomyosin network increased only a little after clutch engagement, constriction of the apical plasma membrane must reflect a change in efficiency of the link between actomyosin and contact zones.

Clutch control of myosin flow is not an entirely novel concept. In the migrating neural growth cone, the actomyosin engine is continually running, but only when positive guidance cues are received does a region of lamellae engage the clutch and extend forward (*11*). What are the benefits to having a clutch during morphogenesis? It may be easier to synchronize the start of a morphogenic event if the engines of all the participating cells are already running and clutch engagement is the rate-limiting step. Indeed, Roh-Johnson *et al*. observed that cells "rev" their actomyosin engines at least once or twice before the first sign of cell contraction is seen. It might also be easier to subtly respond to local cues (for example, the faltering contraction by a neighboring cell) by slightly altering the degree of engagement of the clutch—as one might when starting a car on hills of different inclines—than by crudely switching the engine on or off.

What is the molecular basis of this clutch and how is it regulated? Roh-Johnson *et al*. show that disruption of the small GTP-binding protein Rac, or of various components of adherens junctions (cadherin and the catenins), disengages actomyosin flow from cell contractions in the worm embryo. Further clues may come from observing the altered linkage between actomyosin contractions and the generation of tissue tension in fly embryos that harbor mutations in either of two key transcription factors, snail and twist (*9*). Or, possibly clutch machinery is regulated by a factor called folded gastrulation, a diffusible signal that synchronizes cell constrictions during fly gastrulation (*12*). Perhaps the ezrin-radixin-moesin family of proteins, which both transduces signals in the cell as well as links actomyosin with the plasma membrane (*13*), is a potential candidate for clutch proteins. We can now shift attention slightly away from the engine and unravel how the clutch works although, as those who drive manual transmission cars can attest, clutches are not always the easiest of gadgets to get to grips with.

References

1. J. M. Sawyer *et al*., *Dev. Biol.* **341**, 5 (2010).
2. M. Roh-Johnson *et al*., *Science* **335**, 1232 (2012); 10.1126/science.1217869.
3. M. Leptin, *Dev. Cell* **8**, 305 (2005).
4. S. L. Haigo, J. D. Hildebrand, R. M. Harland, J. B. Wallingford, *Curr. Biol.* **13**, 2125 (2003).
5. A. C. Martin, M. Kaschube, E. F. Wieschaus, *Nature* **457**, 495 (2009).
6. V. Koelsch *et al*, *Science* **315**, 384 (2007).
7. J. Solon, A. Kaya-Copur, J. Colombelli, D. Brunner, *Cell* **137**, 1331 (2009).
8. P.-A. Pouille, P. Ahmadi, A.-C. Brunet, E. Farge, *Sci. Signal.* **2**, ra16 (2009).
9. A. C. Martin, M. Gelbart, R. Fernandez-Gonzalez, M. Kaschube, E. F. Wieschaus, *J. Cell Biol.* **188**, 735 (2010).
10. Y. Yamaguchi *et al*., *J. Cell Biol.* **195**, 1047 (2011).
11. L. Bard *et al*., *J. Neurosci.* **28**, 5879 (2008).
12. R. E. Dawes-Hoang *et al*, *Development* **132**, 4165 (2005).
13. A. L. Neisch, R. G. Fehon, *Curr. Opin. Cell Biol.* **23**, 377 (2011).

10.1126/science.1220388

CREDIT: C. BICKEL/*SCIENCE*

RETROSPECTIVE

Roy J. Britten (1919–2012)

Eric H. Davidson

A molecular biologist founded fundamental concepts in DNA sequence organization and gene expression that underlie modern genomics and genome evolution.

Roy John Britten died on 21 January at the age of 92 in Corona del Mar, California. Born in Washington, DC, in 1919, his academic career took him to both coasts of the United States, where his fundamental discoveries in DNA sequence organization and gene expression influenced the fields of evolutionary and developmental biology and heralded the era of modern genomics.

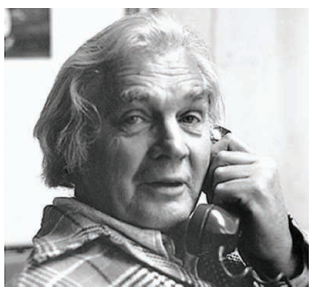

Roy and I were scientific partners for a quarter of a century, beginning about the time we started work on the gene regulation model for animal cells that we published in 1969 in these same pages. I can still recall my immediate conviction, the first time I read about Roy's work, that his was the way to get at the fundamental questions about genes, genomes, and gene regulation that I was passionately set on solving. In those days, the mid-1960s, the work of Roy and his colleagues was published mainly for cognoscenti, who knew to look in the Annual Report of the Director of the Department of Terrestrial Magnetism (DTM) of the Carnegie Institution. From the pages of this slight, paper-covered journal, there emerged for several important years in a row a very powerful intellectual breeze. Its force was due not only to what Roy's group at DTM was discovering but also to their means of discovery, the sophisticated quantitative experimental approaches by which the secrets of the animal genome were being unraveled.

Roy had studied physics as an undergraduate at the University of Virginia; during World War II, he was a participant in a Manhattan Project technological study (which, as he always said, fortunately failed completely); and his subsequent graduate degree from Princeton (in 1951) was also in physics. But after that, he went to the biophysics group at DTM and soon switched to the study of macromolecular processes and then to the nature of the animal genome per se. In this transition, Roy brought with him from physics a suite of potent scientific tools and levers, ways of thought not then common in biology. Later, in Roy's next transition at the California Institute of Technology (Caltech) in 1971, when together we tried to focus on the grand problems of gene expression systems, developmental regulatory control, and mechanisms of evolutionary change therein, this same suite of scientific approaches stood out even more sharply from those then current in these fields. Mental attitudes in venerable, knowledge-rich fields, such as developmental biology, change more slowly than does knowledge of the mechanisms that emerge continuously from leading-edge experimental science. This continues to be true and also explains why striking advances often come from new immigrants into old fields.

In retrospect, conceptual analyses of kinetic experimentation were among the most potent and fruitful of the explanatory pathways that characterized Roy's thought. This began in the early days when Roy worked on radioisotopic flux in bacterial RNAs (1961 to 1963) and used this to distinguish messenger RNA (mRNA) from ribosomal RNA synthesis. In the 1964–1965 DTM Annual Report appeared the opening chapter of Roy's classic and brilliant experimental use of DNA renaturation kinetics, which revealed the quantitative, predictable relationships between renaturation rate and genome size from bacteria to vertebrates, and the existence in animal genomes of both repetitive and single-copy DNA. In one fell swoop, this work (published in *Science* in 1968 with D. E. Kohne) ultimately put to rest all manner of fantastic interpretations of the animal genome (although it took some years for this to occur). Mechanistic kinetic thought in biological processes has two corollaries: It implies mathematical analyses using differential calculus to formulate what is going on in the test tube or in the cell, and it involves system-level conceptualization. In Roy's work, both later turned out to be preadapted to solving problems in many areas beyond analysis of renaturation kinetics. Roy's efforts in renaturation kinetics per se came to an almost sudden halt long ago, as we both moved into other matters, although in my lab there occasionally surfaces from an odd drawer a type of water-jacketed chromatography column that was our 1970's renaturation workhorse.

Beginning in the years Roy and I worked together at Caltech, quantitative kinetic analysis provided the crucial tools that showed how repetitive sequences are spatially distributed in the genome and revealed the absolute rates of synthesis and turnover of populations of mRNA and nuclear RNA, as well as transcript population dynamics and structure. Beyond this, no image of Roy's conceptual scientific persona can omit his focal fascination with the properties of large sets of DNA molecules: first the populations of sheared molecules in renaturation reactions, then populations of repeated sequences in diverse organisms. The evolutionary importance of populations of diverse transposable genomic sequence elements became the major fascination of the final phase of Roy's scientific life, which lasted right up to his death. Roy was interested in genomes more than in particular genes and in DNA more than in particular nucleotide sequences. Underlying all this—again beginning in his time at DTM when he and his colleagues carried out some of the first interspecific comparisons of genomes by hybridization (1963)—was an abiding interest in physical clues that would explain evolution of the genome.

Throughout the long years of Roy Britten's scientific life, whatever specific problem he was engaged with, he approached it by more or less the same set of scientific pathways, always with great intellectual force. We have in more recent time seen a great many physicists transit into biology, but not so many whose intellectual tastes led them directly into mainline problems where insights gained provide the foundations for new fields that flower decades hence. Roy's giant contribution to knowledge of genome organization, size, complexity, and sequence content provided a standard of evidence and a factual springboard for many recent de novo genome projects. Such was Roy's accomplishment in the science underlying large areas of modern genomics and genome evolution as well.

10.1126/science.1220828

California Institute of Technology, Pasadena, CA 91125, USA. E-mail: davidson@caltech.edu

CREDIT: COURTESY OF R. BRITTEN/CALIFORNIA INSTITUTE OF TECHNOLOGY

Nuclear Fuel in a Reactor Accident

Peter C. Burns,[1]* Rodney C. Ewing,[2] Alexandra Navrotsky[3]

Nuclear accidents that lead to melting of a reactor core create heterogeneous materials containing hundreds of radionuclides, many with short half-lives. The long-lived fission products and transuranium elements within damaged fuel remain a concern for millennia. Currently, accurate fundamental models for the prediction of release rates of radionuclides from fuel, especially in contact with water, after an accident remain limited. Relatively little is known about fuel corrosion and radionuclide release under the extreme chemical, radiation, and thermal conditions during and subsequent to a nuclear accident. We review the current understanding of nuclear fuel interactions with the environment, including studies over the relatively narrow range of geochemical, hydrological, and radiation environments relevant to geological repository performance, and discuss priorities for research needed to develop future predictive models.

Nuclear fuels are designed to perform under the extreme but well-defined conditions of a nuclear reactor operating normally. UO_2, used in most commercial power plants, is a suitable fuel in part because of its high melting point (2865°C) and high thermal conductivity. Fresh (unirradiated) UO_2 fuel is modestly radioactive and chemically pure, whereas irradiated (used) fuel is chemically complex and extremely radioactive. During reactor operation, the composition of the fuel gradually changes as ^{235}U is fissioned and transuranium elements (Np, Pu, and higher actinides) form through neutron capture by ^{238}U and subsequent β-decay. The UO_2 fuel retains many of the generated transuranium elements and some fission products within its structure, whereas other radionuclides form new oxide phases, are trapped as gases in bubbles, or segregate as metallic inclusions. Due to the long-term risks associated with transportation, storage, and disposal of used fuel, studies have examined the interaction of irradiated UO_2 fuels with the geochemical and hydrologic environments of potential geological repositories. Such interactions will occur over tens to hundreds of thousands of years, during which time the thermal and radiation fields diminish substantially (*1*–*3*). However, much less attention has focused on irradiated fuel and its interaction with the environment during and after an accident at an operating nuclear reactor. Conditions in such events are often unanticipated, and a substantial amount of potentially harmful radioactive material can be released just at the time when the thermal output and level of radioactivity are highest. Furthermore, explosions and melting of fuel and of reactor structural and containment materials slow the accident response, and the movement and redistribution of fuel and moderators create the added concern of continued or sporadic criticality. Months to years may pass before remotely controlled instruments can reveal the final condition and configuration of the fuel. An understanding of how damaged fuel will interact with local, rapidly changing conditions is essential to reduce the potential release of radionuclides.

What Happens During a Nuclear Core-Melt Accident?

A core-melt accident occurs when cooling capacity is lost in an operating or recently shutdown nuclear reactor and melting of the reactor core, including nuclear fuels, ensues. Even after stopping fission of uranium in a fuel by insertion of neutron-absorbing control rods, tremendous amounts of heat generated by radioactive decay must be removed to prevent the core from melting. Such core-melt events have not been particularly rare. The first occurred in the early 1950s, with about 20 having occurred worldwide in military and commercial reactors. Some of these had negligible environmental impact, but little information is available concerning some of the events that took place in the former Soviet Union and/or on their nuclear-powered submarines. The most recent and dramatic incidents occurred at operating commercial nuclear power plants: Three Mile Island, USA (1979); Chernobyl, USSR (1986); and Fukushima, Japan (2011) (Fig. 1). Each was very different in its scale and the conditions experienced by the fuel during and after the accident.

At Three Mile Island, a single pressurized water reactor core was partially melted after interruption of cooling. Approximately half of the core was damaged or melted; some 20 metric tons of melted fuel and structural materials flowed to the bottom of the pressure vessel (*4*). The remaining fuel was damaged by the failure of about 90% of the fuel cladding. Radioactive fission product gases were released from primary containment by venting, but there was no dispersion of particulates of the fuel, and most fission products and transuranium elements were contained within the facility (*4*).

In contrast to the containment of radioactivity at Three Mile Island, the accident at Chernobyl resulted in the explosive release of radioactive material (*5*). Steam explosions and burning graphite destroyed the graphite-moderated reactor. Fission gases (e.g., Kr and Xe) and volatile fission products (e.g., I and Cs) were released. Explosions caused the dispersal of about 6 tons of fuel as air-borne particles. Most of the core, about 190 tons, was damaged or melted. The formation of "lava" consisting of melted fuel assemblies, structural materials such as concrete and steel, and sand, lead, and boric acid, added to control criticality and reduce the release of radionuclides, is a remarkable feature of the Chernobyl event. The "lava" moved to the lower levels of the reactor, forming "flows" with an estimated mass of tens of metric tons. Unusual actinide phases, such as a high-uranium zircon ($U_xZr_{1-x}SiO_4$), formed in this solidified melt (*6*).

The accident at Fukushima Daiichi in Japan, following the magnitude 9.0 Tohoku-oki earthquake and subsequent tsunami on 11 March 2011, occurred while only three (units 1, 2, and 3) of six boiling water reactors were in operation. Most

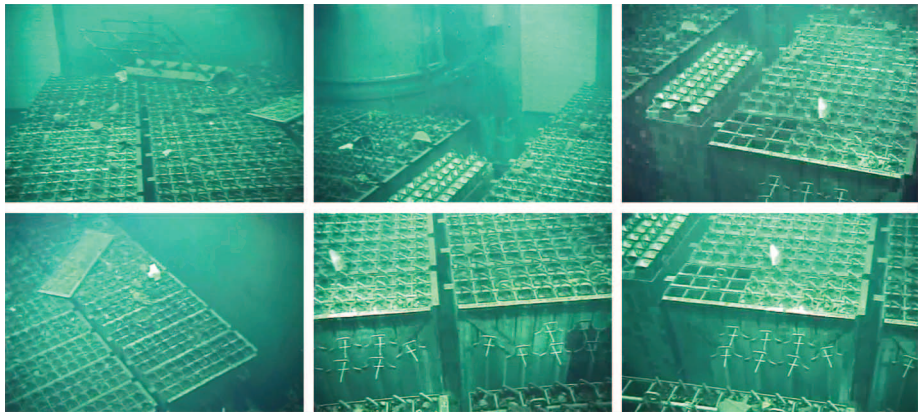

Fig. 1. Images extracted from a video posted 8 May 2011 by TEPCO entitled "Status of the spent fuel pool of unit 4 of Fukushima Daiichi nuclear power station." These images, obtained by an underwater robotic camera, show used fuel assemblies and debris in the pool.

[1]Department of Civil Engineering and Geological Sciences, and Department of Chemistry and Biochemistry, University of Notre Dame, 156 Fitzpatrick Hall, Notre Dame, IN 46556, USA. [2]Department of Earth and Environmental Sciences, and Department of Nuclear Engineering and Radiological Sciences, University of Michigan, Ann Arbor, MI 48109, USA. [3]Peter A. Rock Thermochemistry Laboratory, University of California, Davis, One Shields Avenue, Davis, CA 95616, USA.

*To whom correspondence should be addressed. E-mail: pburns@nd.edu

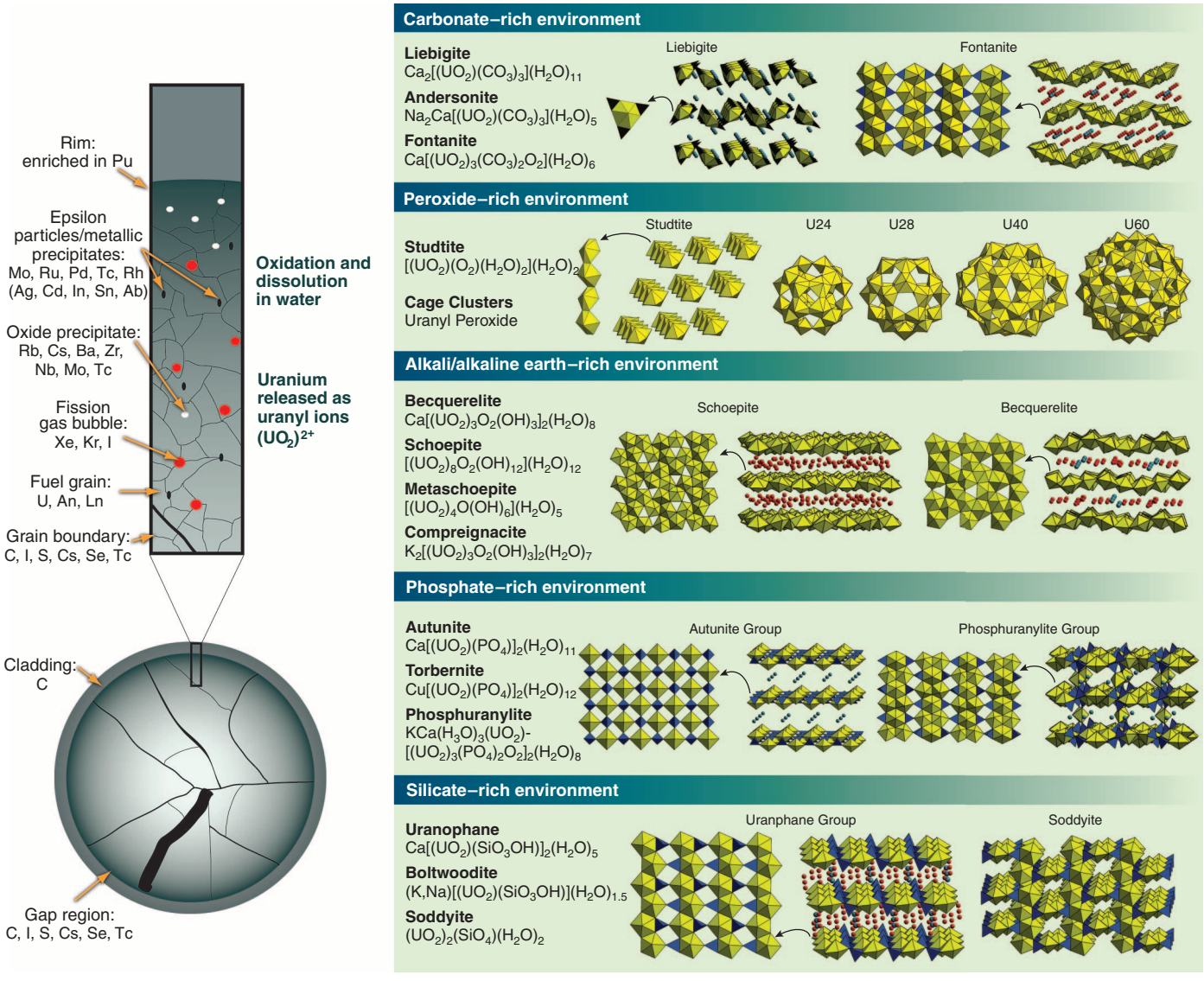

Fig. 2. A schematic representation of irradiated UO_2 fuel [left, adapted from (*2*)] and the structures of various uranyl minerals and nanoscale clusters (right). A cross-section of the 10-mm-wide fuel element and its zirconium alloy cladding is shown, where heat-induced cracks are evident. An expanded view of the fuel and cladding near its edge illustrates that fission products concentrate at grain boundaries, in epsilon phase metallic precipitates, and in gaseous bubbles. Actinides and lanthanides are in the UO_2 structure. For the structure representations (*35*, *39*), uranyl polyhedra are shown in yellow, and O atoms are illustrated as red balls.

of the fuel in these reactors was UO_2, although there were also 32 mixed-oxide fuel assemblies containing ~6% Pu in unit 3, corresponding to ~4% of the core loading. The operating units shut down promptly in response to the earthquake; however, when the tsunami inundated the site about 40 min later, electrical power was lost, followed by the loss of on-site backup power, resulting in a station blackout and a loss of reactor coolant. A partial core-melt event ensued in units 1, 2, and 3. In a preliminary analysis, the Japanese operator TEPCO has surmised that there was a nearly immediate loss of core cooling in unit 1 and almost all of the fuel assemblies melted and accumulated in the bottom of the pressure vessel. Partial melting of the cores in units 2 and 3, damaging approximately one-third of the fuel assemblies in each, occurred over the following days. Reaction of the zirconium alloy (Zircaloy) fuel cladding with water at high temperatures generated hydrogen gas that accumulated and exploded in four of the units. Seawater was injected into the three active reactors and sprayed onto fuel storage pools (e.g., near unit 4) to cool them (Fig. 1). With boiling and evaporation of seawater, large amounts of salt may have deposited in the reactor cores. The release of radioactivity other than gaseous and volatile fission products at Fukushima Daiichi, unlike at Chernobyl, was dominated by the many metric tons of seawater used to cool the cores and storage pools. An unknown fraction of this water was released to the environment, together with accumulation in the basements and trenches of the reactors. Direct discharge of contaminated water to the ocean and groundwater occurred through approximately 8 April 2011 (*7*). Estimates of the amount of radioactivity released differ by a factor of about 20, with one of the higher estimates indicating that 27,000 terabecquerels of ^{137}Cs was discharged to the ocean (*8*).

What Types of Radioactive Materials Are Released from Damaged Nuclear Fuel?

Fresh (unirradiated) light water reactor fuel typically consists of UO_2 with 1 to 5 atomic percent fissile ^{235}U. When such fuel is removed from a reactor, its radioactivity is 10^{17} becquerel/metric ton, about a factor of a million higher than that of fresh fuel. A year later, the dose rate 1 m from a fuel assembly is about 1 million millisieverts (mSv) per hour (natural background ≈ 3 mSv/year), which will give a lethal dose to a human in less than a minute. The bulk of the penetrating β and γ ionizing radiation arises from short-lived fission products (e.g., ^{131}I, ^{137}Cs, ^{90}Sr) and activation products of components of the fuel assemblies

(e.g., Co, Ni, Nb). Alpha radiation is mostly from the transuranium elements (e.g., ^{239}Pu, ^{237}Np, ^{241}Am), some of which are long-lived (e.g., ^{239}Pu and ^{237}Np with half-lives of 24,100 and 2.1 million years, respectively). After about 10,000 years, the total activity of fuel is less than 0.01% of the activity a year after removal from the reactor (*9*). Tremendous heat is generated by radioactive decay initially, about 2 MW per ton immediately after removal from the reactor, declining to about 20,000 W per ton after a year (*10*).

Irradiated UO_2 fuels, the details of which are important for reactor operation and potential disposal in a geological repository (*11*, *12*), consist of more than 95% UO_2. The complex mixture of other components within the fuel assembly depends on the conditions of reactor operation (Fig. 2) (*13*). Gaseous fission products (e.g., Xe and Kr) are present as finely dispersed bubbles within fuel grains (*14*). Metallic fission products (e.g., Mo, Tc, Ru, Rh, Pd) are dispersed in the fuel as micrometer- or nanometer-sized immiscible particles (*14*). Other fission products occur as oxide precipitates (e.g., Rb, Cs, Ba, Zr) or in solid solution within the UO_2 fuel matrix (e.g., Sr, Zr, Nb, and lanthanides) (*14*). Transuranium elements are in solid solution within the UO_2 matrix (e.g., Np, Pu, Am) (*14*). The steep thermal gradient present in a single fuel pellet during reactor operation, from 400°C at the rim to 1700°C in the center, causes grain coarsening and microfracturing and ensures that the distribution of radionuclides is heterogeneous (*14*). Volatile elements (e.g., Cs, I) migrate into grain boundaries and fractures within the fuel, as well as into the "gap" between the edges of the fuel pellet and the surrounding metal cladding (*14*). Nonuniform burn-up in a fuel pellet gives higher concentrations of ^{239}Pu near the pellet edge, an increase in porosity, polygonization of the UO_2 grains, and a reduction in the size of individual grains (~0.15 to 0.3 μm) (*13*).

Several experiments in the United States, France, Canada, and Japan give considerable insight into the progression of core-melt incidents and release of fission products from damaged fuel (*14*–*17*). Stages occur as temperature increases (*17*): melting of the Ag-In-Cd absorber alloy at 800°C; deformation and bursting of fuel cladding at 750° to 1100°C; steam oxidation of structural and fuel rod materials beginning at 1200°C; eutectic interactions of cladding with stainless steel beginning at 1300°C; melting of stainless steel by 1450°C and interactions of cladding with UO_2 fuel by 1500°C; melting of cladding at 1760°C; partial reduction of UO_2 due to interactions with cladding and partial dissolution of the fuel and formation of a Zr-U-O melt above 1760°C; and melting of ZrO_2 at 2690°C and UO_2 at 2850°C. Studies of irradiated fuel to temperatures as high as 2530°C indicate release fractions of ~90% for cesium, iodine, and noble gas fission products; up to 50% for molybdenum; less than 1% for strontium; and very low release of actinides (*14*). Release of volatile fission products to the atmosphere can occur as soon as the fuel assembly is damaged. These contribute greatly to the shorter-term environmental impact because of the penetrating ionizing radiation they produce and their mobility in air and water. After the initial release of gaseous and volatile radionuclides from damaged fuel assemblies, and in the absence of subsequent explosions that disperse radioactive material such as at Chernobyl, the major potential pathway for continued release of radionuclides is through flowing water.

How Does Water Interact with Irradiated Fuel?

Many radionuclides form aqueous complexes that are soluble in water. Furthermore, water promotes dissolution of the rod/fuel matrix, which releases radionuclides trapped within the matrix (*3*, *10*, *18*, *19*). Some of these radionuclides have long half-lives (10^3 to 10^6 years) and pose a much longer environmental hazard than the short-lived gaseous and volatile fission products with half-lives of minutes to a few years. Several of the longer-lived radionuclides of concern are redox active (e.g., isotopes of Tc, Se, Np, Pu), and their concentration in water depends strongly on oxidation state, with solid phases with higher oxidation state typically having higher solubility. Exposure to air is sufficient to oxidize some of these cations, albeit slowly under ambient conditions. The radiolytic breakdown of water creates oxidants (e.g., hydrogen peroxide) that can accelerate the oxidative corrosion of fuel (*19*–*23*).

Under oxidizing conditions, UO_2 fuel dissolves in aqueous solution by oxidation to uranyl $(UO_2)^{2+}$ ions (*10*). The uranyl cation is readily complexed by inorganic and organic species (*10*). The concentration of uranyl in aqueous systems is strongly influenced by complexing species, such as peroxide, carbonate, or nitrate, which greatly enhance solubility, or phosphate, silica, or vanadate, which reduce solubility (*24*). Complexation effects can be pH dependent. Uranyl peroxide species that are insoluble under acidic conditions are highly soluble in alkaline solutions, and carbonate complexes the uranyl ion only under alkaline conditions (*25*). The mobility of dissolved uranyl cations can be diminished by adsorption of uranium onto mineral surfaces (*26*) and by reduction to less soluble U(IV) by microbial activity (*27*).

Secondary solid uranyl alteration phases that can form subsequent to water contacting irradiated fuel depend on the amount of water present, the flow rate, the intensity of the radiation field, the availability of species in the water that can complex metals, and redox reactions. On cooled Chernobyl "lava" exposed to water, two secondary phases have been identified: $Na_4(UO_2)(CO_3)_3$ and studtite $[(UO_2)(O_2)(H_2O)_2(H_2O)_2]$ (*28*). Studtite incorporates peroxide from the radiolytic decomposition of water and suggests local highly oxidizing conditions. Studtite has been reported as a major alteration phase of fuel-element claddings underwater in a cooling pond (*29*). Studtite also forms on spent fuel in deionized water under laboratory conditions (*19*) and on UO_2 doped with alpha emitters or irradiated by an external source in water (*21*–*23*).

Interaction of irradiated fuel with groundwater can lead to the formation of secondary uranyl minerals (Fig. 2) (*3*, *10*, *18*). In general, the long-term fate of uranium released to the environment from dissolving fuel is dispersal or formation of mineral phases that are generally similar to those from which the uranium was initially mined. Combining water and irradiated UO_2 can result in uranyl oxyhydrate minerals, such as schoepite and studtite (Fig. 2). If silica, vanadate, or phosphate are in solution, uranyl minerals such as autunite, carnotite, or uranophane may form. The specific uranyl compounds that precipitate are heavily influenced by the cations and anions available in the aqueous solution—for example, Na and K in the case of seawater (*30*).

Uranyl minerals can reduce the mobility of key radionuclides, analogous to the role of the original UO_2 fuel in retaining radionuclides within its matrix. Uranyl minerals can incorporate radionuclides into their structures as major constituents (Cs, Sr) or by substitution at the U sites (Pu, Np) (*31*, *32*), and the details of their struc-

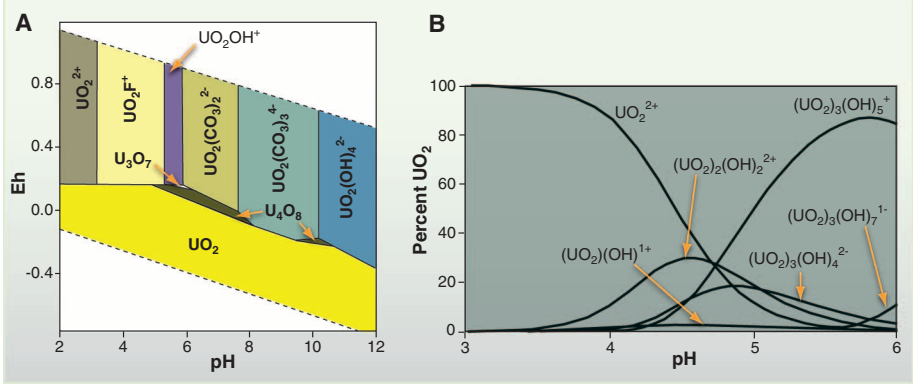

Fig. 3. Examples of stability diagrams for uranium systems. (**A**) Speciation of uranium in a hypothetical groundwater at 25°C [adapted from (*8*)]. (**B**) Speciation of U(VI) versus pH in NaCl solution at 25°C, concentration of UO_2 = 0.001 M, I = 0.5 M [adapted from (*40*)].

tures dictate the extent of incorporation. The solubility and stability of uranyl minerals with incorporated radionuclides are important factors in determining the long-term environmental impact of fuel dissolution. There has been substantial improvement in the thermodynamic database for such minerals over the past decade (*33*), so it is, in principle, possible to calculate the equilibrium phase diagrams for aqueous uranyl systems as a function of pH and the concentrations of various cations and anions (Fig. 3). Much of the remaining uncertainty in such calculations arises from poorly known activity coefficients of uranium species in aqueous solution, especially above room temperature. This uncertainty increases with increasing concentrations of other species in the aqueous phase. Most studies have focused on the reactions of nuclear fuel in groundwater, which is very dilute compared to the seawater to which the Fukushima Daiichi fuel was exposed. The uncertainty also increases with rising temperature because of large uncertainties in the thermodynamic properties of aqueous species at elevated temperatures.

Peroxide produced by radiolysis of water increases the dissolution rate of fuel by oxidizing U(IV) to U(VI) (*19*–*23*). If the aqueous system is acidic to neutral and contains low concentrations of complexing agents other than peroxide, studtite will precipitate once peroxide levels are high enough, as seen in laboratory experiments (*19*) and on stored fuel elements (*29*). Thermochemical measurements have shown that, although studtite is not stable in the absence of peroxide, it is stabilized by the low concentrations of peroxide produced by radiolysis even in natural uranium deposits, and its formation at the fuel-water interface is thermodynamically reasonable (*34*). If the water is alkaline, soluble nanoscale uranyl peroxo cage clusters are likely to form and persist in solution (*35*). Recent studies have identified a large variety of such clusters containing uranyl ions and peroxide groups (Fig. 2). These cage clusters, as well as simpler uranyl peroxo-complexes, form in peroxide-bearing solutions and can crystallize with appropriate charge-balancing alkali ions, including sodium, or remain in aqueous solution for several months or more (*36*). Calorimetric studies suggest that such alkali uranyl peroxide cluster compounds are energetic intermediates between uranyl species in solution and alkali uranyl minerals when peroxide and alkali ions are present (*36*). It is unknown whether such alkali uranyl peroxide cluster compounds form under the high-salinity conditions encountered at Fukushima Daiichi, or whether they offer another mechanism for corrosion of fuel and transport and/or precipitation of uranium when seawater is encountered, but this possibility must be considered.

Rates of dissolution of UO_2 in water have been studied under conditions relevant to geological repositories (*1*, *10*, *37*), where the aqueous phase is groundwater. Most of these tests followed set protocols that were not optimized to provide fundamental kinetic data that could be modeled and extrapolated to other conditions, such as a reactor accident. There is controversy over whether microbial action substantially increases dissolution rates under certain conditions (*38*). Thus, at present there is no reliable way of predicting dissolution rates of damaged fuel in water under the conditions of a nuclear accident, especially one like Fukushima Daiichi in which fuel is exposed to hot or boiling seawater for periods of weeks to months. Fukushima Daiichi itself would provide a very instructive experiment if and when it becomes possible to retrieve and study the fuel.

Outlook

Nuclear reactor core-melt accidents are inherently complex and difficult to model, a situation that can be greatly exacerbated by the addition of large quantities of seawater or other materials during and subsequent to the event. Yet, an understanding of the factors that determine radionuclide release is central to taking appropriate and timely action in order to minimize impacts on the environment and human health. Release of volatile and gaseous fission products during a core-melt event is effectively instantaneous, and this contributes dramatically to the near-term environmental impact due to their atmospheric dispersion. Water that interacts with damaged fuel will transport radionuclides that present both short-term and longer-term environmental risk, beginning with the core-melt event and potentially continuing for many years if the damaged fuel is not adequately isolated from the environment. The events at Fukushima Daiichi have demonstrated the importance of water-borne radionuclide transport after a core-melt event, with as much as 27,000 terabecquerels of ^{137}Cs being released to the ocean (*8*).

At present, there is not an adequate, quantitative understanding of water interactions with damaged fuel, including reaction mechanisms and rates, radionuclide release and transport, and exposure pathways. Resolidified fuel from a core-melt accident is very heterogeneous and has a much more complex phase chemistry than undamaged fuel. Past repository-focused studies of the release of radionuclides from undamaged fuel generally cannot be extrapolated to the extreme conditions of temperature and radiation field that occur during and subsequent to a core-melt event. Central to gaining a predictive understanding is the characterization of resolidified fuel derived from a core-melt event in terms of the distribution and reactivity of radionuclides, the basic phase chemistry, and the resulting microstructure. Some of this information can be obtained by investigating simulated core-melt events with fuel analogs that contain nonradioactive isotopes of the fission products distributed in UO_2. The need to understand the behavior of actinides, for which there are no nonradioactive isotopes, and the effects induced by intense radiation fields require studies using radioactive materials. The role of complexation in mobilizing radionuclides in water at high temperatures, as well as that of nanoscale actinide materials in promoting the dissolution of fuel, must be better understood. Studies outlined here are both difficult and expensive, but are essential to reduce the risk associated with an increasing reliance on nuclear energy. The resulting understanding may also help in the future design of fuel assemblies and reactors that are better able to withstand potential accidents.

References and Notes

1. D. W. Shoesmith, *J. Nucl. Mater.* **282**, 1 (2000).
2. E. C. Buck, B. D. Hanson, B. K. McNamara, in *Energy, Waste, and the Environment: A Geochemical Perspective*, R. Gieré, P. Stille, Eds. (Geological Society of London, Special Publications, London, 2004), vol. 236, pp. 65–88.
3. P. A. Finn, J. C. Hoh, S. F. Wolf, S. A. Slater, J. K. Bates, *Radiochim. Acta* **74**, 65 (1996).
4. M. Rogovin, G. T. Frampton, "Three Mile Island: A report to the commissioners and to the public" (Nuclear Regulatory Commission, Washington, DC, 1980).
5. E. B. Anderson, B. E. Burakov, E. M. Pazukhin, *Soviet Radiochem.* **34**, 632 (1992).
6. E. B. Anderson, B. E. Burakov, E. M. Pazukhin, *Radiochim. Acta* **60**, 149 (1993).
7. K. Buesseler, M. Aoyama, M. Fukasawa, *Environ. Sci. Technol.* **45**, 9931 (2011).
8. "Synthèse actualisée des connaissances relatives à l'impact sur le milieu marin des rejets radioactifs du site nucléaire accidenté de Fukushima Dai-ichi" (Institut de Radioprotection et de Sûreté Nucléaire, 2011).
9. A. Hedin, *Spent Nuclear Fuel—How Dangerous Is It?* (Swedish Nuclear Fuel and Waste Management, Stockholm, 1997).
10. J. Bruno, R. C. Ewing, *Elements* **2**, 343 (2006).
11. L. H. Johnson, D. W. Shoesmith, in *Radioactive Waste Forms for the Future,* W. Lutze, R. C. Ewing, Eds. (North-Holland, Amsterdam, 1988), pp. 635–698.
12. V. M. Oversby, in *Materials Science and Technology*, R. W. Cahn, P. Haasen, E. J. Kramer, Eds. (VCH Verlagsgessellschaft mbH, Germany, 1994), vol. 10B, chap. 12, pp. 391–442.
13. H. Kleykamp, *J. Nucl. Mater.* **131**, 221 (1985).
14. B. J. Lewis, W. T. Thompson, F. C. Iglesias, in *Comprehensive Nuclear Materials*, R. J. M. Konings, Ed. (Elsevier, Amsterdam, 2012), vol. 2, pp. 515–546.
15. T. Fuketa, H. Sasajima, Y. Mori, K. Ishijima, *J. Nucl. Mater.* **248**, 249 (1997).
16. P. Hofmann, *J. Nucl. Mater.* **270**, 194 (1999).
17. B. J. Lewis, R. Dickson, F. C. Iglesias, G. Ducros, T. Kudo, *J. Nucl. Mater.* **380**, 126 (2008).
18. R. J. Finch, E. C. Buck, P. A. Finn, J. K. Bates, in *Scientific Basis for Nuclear Waste Management XXII*, D. J. Wronkiewicz, J. H. Lee, Eds. (Materials Research Society, Warrendale, PA, 1999), vol. 556, pp. 431–438.
19. B. Hanson *et al.*, *Radiochim. Acta* **93**, 159 (2005).
20. D. Y. Chung *et al.*, *J. Radioanal. Nucl. Chem.* **284**, 123 (2010).
21. F. Clarens *et al.*, *Environ. Sci. Technol.* **38**, 6656 (2004).
22. C. Corbel *et al.*, *J. Nucl. Mater.* **348**, 1 (2006).
23. G. Sattonnay *et al.*, *J. Nucl. Mater.* **288**, 11 (2001).
24. D. Gorman-Lewis, P. C. Burns, J. B. Fein, *J. Chem. Thermodyn.* **40**, 335 (2008).
25. D. L. Clark, D. E. Hobart, M. P. Neu, *Chem. Rev.* **95**, 25 (1995).
26. T. D. Waite, J. A. Davis, T. E. Payne, G. A. Waychunas, N. Xu, *Geochim. Cosmochim. Acta* **58**, 5465 (1994).
27. Y. Suzuki, S. D. Kelly, K. M. Kemner, J. F. Banfield, *Nature* **419**, 134 (2002).
28. B. E. Burakov, E. E. Strykanova, E. B. Anderson, in *Scientific Basis for Nuclear Waste Management XX*, W. J. Gray, I. R. Triay, Eds. (1997), vol. 465, pp. 1309–1311.
29. J. Abrefah, S. Marschmann, E. D. Jenson, "Examination of the surface coatings removed from K-East Basin fuel elements" (PNNL-11806, Pacific Northwest National Laboratory, Richland, WA, 1998).
30. R. J. Finch, R. C. Ewing, *J. Nucl. Mater.* **190**, 133 (1992).

31. P. C. Burns, P. C. Ewing, M. L. Miller, *J. Nucl. Mater.* **245**, 1 (1997).
32. M. Douglas *et al.*, *Environ. Sci. Technol.* **39**, 4117 (2005).
33. T. Y. Shvareva *et al.*, *Geochim. Cosmochim. Acta* **75**, 5269 (2011).
34. K. A. H. Kubatko, K. B. Helean, A. Navrotsky, P. C. Burns, *Science* **302**, 1191 (2003).
35. P. C. Burns, *Min. Mag. (London)* **75**, 1 (2011).
36. F. A. Armstrong, J. Hirst, *Proc. Natl. Acad. Sci. U.S.A.* **108**, 14049 (2011).
37. D. W. Shoesmith, S. Sunder, *J. Nucl. Mater.* **190**, 20 (1992).
38. A. Johnsson, A. Odegaard-Jensen, G. Skarnemark, K. Pedersen, *J. Radioanal. Nucl. Chem.* **279**, 619 (2009).
39. P. C. Burns, *Can. Mineral.* **43**, 1839 (2005).
40. A. Gianguzza, D. Milea, F. J. Millero, S. Sammartano, *Mar. Chem.* **85**, 103 (2004).

Acknowledgments: This material is based on work supported as part of the Materials Science of Actinides Center, an Energy Frontier Research Center funded by the U.S. Department of Energy, Office of Science, Office of Basic Energy Sciences under Award Number DE-SC0001089.

10.1126/science.1211285

Natural SIV Hosts: Showing AIDS the Door

Ann Chahroudi,[1,3] Steven E. Bosinger,[3] Thomas H. Vanderford,[3] Mirko Paiardini,[2,3]* Guido Silvestri[2,3]*

Many species of African nonhuman primates are naturally infected with simian immunodeficiency viruses (SIVs) in the wild and in captivity. In contrast to HIV-infected humans, these natural SIV hosts typically do not develop AIDS, despite chronic infection with a highly replicating virus. In this Review, we discuss the most recent advances on the mechanisms of protection from disease progression in natural SIV hosts, with emphasis on how they differ from pathogenic HIV/SIV infections of humans and rhesus macaques. These mechanisms include: (i) resolution of immune activation after acute infection, (ii) restricted pattern of target cell infection, and (iii) protection from mother-to-infant transmission. We highlight the areas that should be pursued in future studies, focusing on potential applications for the treatment and prevention of HIV infection.

Over thousands of years, species-specific strains of simian immunodeficiency virus (SIV) have endemically infected more than 40 species of African nonhuman primates (*1*, *2*) that we will refer to as "natural SIV hosts" or simply, "natural hosts" (Box 1). Multiple cross-species transmissions of SIV_{cpz} from chimpanzees and SIV_{smm} from sooty mangabeys (SMs) to humans have resulted in the current epidemics of HIV-1 and HIV-2, respectively (*3*). SIV_{smm} is also the origin of the SIV_{mac} strains that are used to experimentally infect various species of Asian macaques, resulting in a disease called simian AIDS (*4*). In marked contrast to pathogenic HIV infection of humans and SIV_{mac} infection of rhesus macaques (RMs), SIV infections of natural hosts are typically nonpathogenic, despite high levels of virus replication (*5*–*9*). The only exception is the SIV_{cpz} infection of chimpanzees that is associated with a significant increase in mortality, although not to the levels seen in HIV-1 or SIV_{mac} infections (*10*). Importantly, the benign infection of natural hosts is distinct from the nonprogressive HIV/SIV infections of a rare subset of humans and RMs, called elite controllers, in which the absence of AIDS is at least partly related to the ability of the immune system to suppress virus replication (*11*, *12*). Understanding the mechanisms responsible for the AIDS resistance of natural SIV hosts is considered a key priority in contemporary AIDS research, with major implications for HIV prevention and therapy.

What Is the Phenotype of SIV Infection in Natural Hosts?

Two species of natural SIV hosts that have been intensively studied as captive animals, SMs and the African green monkeys (AGMs), are housed in primate centers in the United States and Europe. Limited information is available about other species such as mandrills, drills, suntailed monkeys, and a few others. In this Review, we mainly discuss data generated from SMs and AGMs because relatively little is known about the phenotype of SIV infection in other natural SIV host species. Given the many similarities of these two models, we discuss them together unless otherwise noted in specific instances. Table 1 shows the main virological and immunological aspects of pathogenic and nonpathogenic primate lentivirus infections.

In summary, key similarities between SIV infection of natural hosts and pathogenic HIV/SIV infections of humans and RMs include: (i) high viremia (*5*–*9*), (ii) short in vivo life span of productively infected cells (*13*, *14*), (iii) significant loss of mucosal $CD4^+$ T cells during acute infection (*15*, *16*), (iv) high levels of innate and adaptive immune activation during acute infection (*17*–*21*), and (v) the inability of the host cellular and humoral immune system to control virus replication (*22*–*24*). This last observation is of great theoretical and practical importance, because it shows that the AIDS resistance of natural SIV hosts is independent of adaptive antiviral immune responses that suppress virus replication. This feature of natural SIV infection highlights the tremendous challenge of artificially inducing, with an AIDS vaccine, a type of protective immunity that has not been selected for in many thousands of years of evolutionary pressure posed by lentiviruses on the nonhuman primate immune system.

Key features of SIV infection that appear to be specific to natural hosts include: (i) preservation of healthy levels of peripheral $CD4^+$ T cells (*5*); (ii) preservation of mucosal immunity and absence of microbial translocation (*16*, *25*–*27*); (iii) normal lymph node architecture and function (*5*); (iv) preservation of T cell regeneration (*28*); (v) preferential sparing of central memory $CD4^+$ T cells (Tcm) from direct virus infection (*29*, *30*); and (vi) lack of chronic immune activation (*5*, *6*, *31*–*33*). The viral and host factors that contribute to the lack of chronic immune activation and their impact on the benign phenotype of natural SIV infection are depicted in Fig. 1. Another fascinating characteristic of natural SIV infections is the rarity of mother-to-infant-transmission (MTIT) as compared with pathogenic HIV/SIV

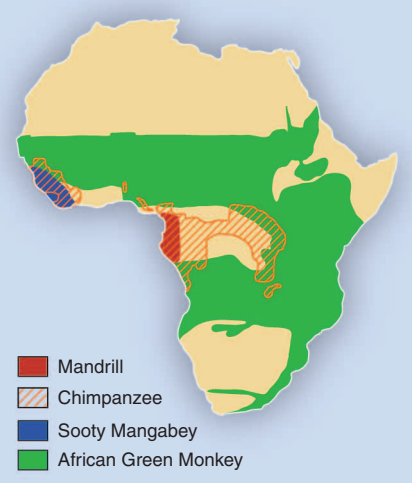

Box 1. More than 40 species of African monkeys are endemically infected with a species-specific strain of SIV. Multiple cross-species transmissions of SIV from chimpanzees to humans during the preparation of bush meat, aided by the rise of urbanization in early 20th century Africa, has resulted in the HIV-1 epidemic and all of its subtypes. High rates of mutation, replication, and recombination have fueled the success of these and other zoonotic events, resulting in the generation of the pathogenic lentiviruses, HIV-1, HIV-2, and SIV_{mac} in their respective hosts. The geographic range of selected natural hosts is shown. [Map adapted from (*69*)]

[1]Departments of Pediatrics, Emory University School of Medicine, Atlanta, GA, USA. [2]Department of Pathology and Laboratory Medicine, Emory University School of Medicine, Atlanta, GA, USA. [3]Yerkes National Primate Research Center (YNPRC), Emory University, Atlanta, GA, USA.

*To whom correspondence should be addressed. E-mail: gsilves@emory.edu (G.S.); mirko.paiardini@emory.edu (M.P.)

infections (*34*–*36*). In this Review, we discuss three key aspects of natural nonhuman primate lentiviral infections that have recently emerged as important correlates and likely determinants of the benign nature of the epidemics in these monkey species: (i) the rapid resolution of acute immune activation, (ii) the restricted pattern of target cells, and (iii) the protection from MTIT. These and other proposed mechanisms of nonpathogenic infection of natural SIV hosts are shown in Table 2.

How Does Acute Immune Activation Resolve in Nonpathogenic SIV Infection?

The early events of SIV infection in natural hosts have been studied by experimentally infecting SMs and AGMs with their species-specific virus, thus allowing detailed virological, immunological, and molecular analyses of the acute phase of SIV infection in these animals. Similar to pathogenic HIV/SIV infections, primary SIV infection of natural hosts is associated with a peak of virus replication occurring 10 to 15 days after virus inoculation, followed by a postpeak decline that is coincident with the emergence of cellular immune responses to SIV (*37*). Experimentally SIV-infected SMs and AGMs exhibit a modest but transient decline of peripheral $CD4^+$ T cell counts and a more severe loss of mucosal $CD4^+$ T cells in both the gastrointestinal tract and lung (*15*, *16*). In contrast to pathogenic infections where mucosal $CD4^+$ T cells become progressively depleted during chronic infection, natural SIV hosts stabilize (SMs) or even recover (AGMs) their levels of mucosal $CD4^+$ T cells (*15*, *16*). Both SMs and AGMs mount initial strong innate and adaptive immune responses to the virus, which are characterized by the production of type I interferons (IFNs) by plasmacytoid dendritic cells, up-regulation of type I IFN response genes, activation and proliferation of T cells, and production of proinflammatory cytokines (*17*–*21*). However, the innate immune response to the virus resolves within 4 to 8 weeks postinfection, despite continuous virus replication (*17*, *19*, *21*). This resolution distinguishes SIV infection of natural hosts from pathogenic HIV/SIV infections, where the type I IFN response persists throughout the chronic phase of infection (*38*, *39*).

The chronic phase of SIV infection in natural hosts is also characterized by low levels of adaptive immune activation (as measured by lymphocyte proliferation and apoptosis), preserved T cell regeneration (as measured by thymic and bone marrow function), and normal lymph node function and architecture (*5*, *40*). The consequences of pathogenic HIV/SIV infections on lymph node function and architecture include continuous B cell activation and germinal center reaction, hypocellularity of the paracortex (where T cells reside), and the disruption of the fibroblastic reticular cell network that is associated with substantial collagen deposition (*41*–*43*). These features are all conspicuously absent during the chronic phase of SIV infection in SMs and AGMs (*5*, *40*). The presence of chronic immune activation and related immunopathology and impaired T cell renewal is clearly associated with disease progression during pathogenic HIV/SIV infections (*44*, *45*). In fact, the level of residual immune activation in patients in which HIV replication has been successfully suppressed by antiretroviral therapy is the strongest predictor of ineffective immune recovery (*46*). Thus, the rapid resolution of immune activation in natural SIV infections may be a crucial factor that enables these animals to avoid AIDS.

The mechanisms underlying the resolution of immune activation in the postacute phase of SIV infection in SMs and AGMs have been intensively investigated. Due to limited space, our discussion of these studies will focus on the mechanisms that are consistent with the bulk of the available experimental data. The first hypothesis is that natural SIV hosts actively down-regulate the innate and adaptive immune responses to the virus. This hypothesis is supported by longitudinal analysis of the transcriptome in acutely SIV-infected SMs revealing an initial immune response to the virus that is similar to that observed in pathogenic HIV/SIV infections, but that returns to a preinfection profile within a few weeks (*17*–*21*). Molecular and histological studies have suggested that specific immune regulatory pathways, such as those involving programmed cell death–1 and adenosine deaminase acting on RNA-1, may be activated during the rapid resolution of immune activation in natural SIV hosts. Studies are currently being carried out in several laboratories, including ours, to better define these immune regulatory pathways and ultimately identify targets for immune-based interventions aimed at reducing the HIV-associated chronic immune activation.

A second hypothesized mechanism to explain the resolution of immune activation in natural hosts is that infected $CD4^+$ T cells become resistant to activation after down-modulation of the cell surface CD3–T cell receptor (TCR) complex by the Nef protein of SIV_{smm} and SIV_{agm} (*47*). Infected $CD4^+$ T cells with low surface levels of CD3-TCR may be refractory to further antigenic stimulation and thus contribute to an overall less activated immunological environment. This hypothesis is supported by the finding that the Nef protein of HIV-1 and SIV_{cpz}, strains that cause pathogenic infections with high levels of chronic immune activation, has lost the ability to down-modulate CD3-TCR (*47*). Whereas the chronic immune activation and pathogenic outcome of SIV_{mac} infection of RMs cannot be explained solely by this mechanism (as SIV_{mac} Nef can down-modulate CD3-TCR) (*47*), it should be noted that the very high viral loads observed in this model of infection may favor chronic immune activation despite the specific effects of Nef. Currently, experiments are being conducted in which AGMs are infected with SIV_{agm}

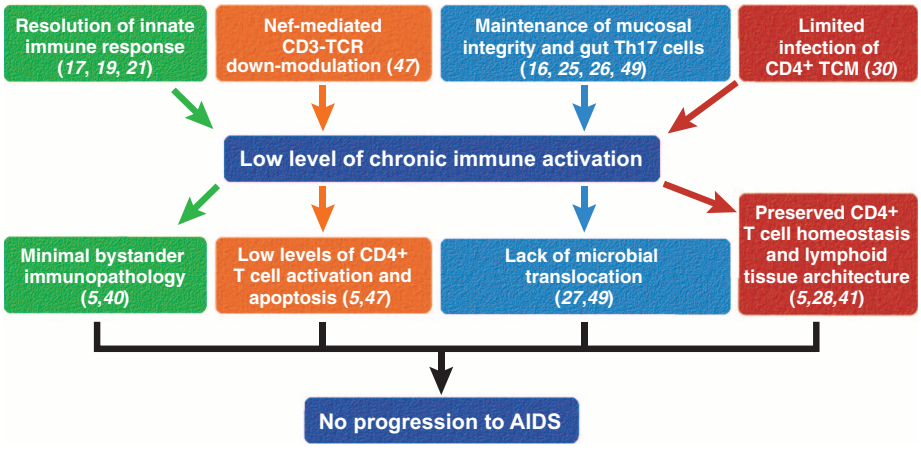

Fig. 1. Mechanisms responsible for the low immune activation and lack of disease progression in SIV-infected natural hosts. The main immunological and virological features contributing to the lack of chronic immune activation and their key consequences resulting in protection from AIDS in natural SIV hosts are depicted.

Table 1. Main features of SIV infection of natural hosts versus nonnatural hosts.

Natural host (SMs, AGMs)	Phenotype	Nonnatural host (RMs, humans)
No	AIDS	Yes
Healthy	Level of peripheral $CD4^+$ T cells	Low
High	Viral load	High
Yes	Virus cytopathicity	Yes
Ineffective	Host immune control	Ineffective
Yes, stable	Depletion of mucosal $CD4^+$ T cells	Yes, progressive
No	Mucosal immune dysfunction/microbial translocation	Yes
No	Chronic immune activation	Yes
Tem > Tcm	Pattern of infected cells	Tcm > Tem
Rare	Vertical transmission	Frequent

containing an "HIV-1–like" Nef to better define the in vivo role of this viral protein.

The third hypothesized mechanism for the resolution of immune activation in natural hosts is that preservation of mucosal immunity prevents translocation of microbial products from the intestinal lumen to the systemic circulation. Microbial translocation is thought to cause chronic immune activation and disease progression during pathogenic HIV/SIV infections (*27*), although controversy exists in the literature (*48*). In natural hosts, consistent data show that the significant depletion of mucosal $CD4^+$ T cells (~50 to 90% from baseline levels) observed during acute SIV infection of SMs and AGMs is not progressive (*15*, *16*), does not result in the selective loss of interleukin-17–producing T helper cells (T_H17) (*25*, *26*), and is not associated with focal loss of intestinal epithelial integrity (*49*), suggesting preservation of the mucosal barrier. Interestingly, increased immune activation was induced in SIV-infected AGMs by mimicking the effect of microbial translocation through systemic injections of bacterial lipopolysaccharide (*50*), consistent with the hypothesis that preserved mucosal immune function protects natural SIV hosts from chronic immune activation and disease progression.

Finally, a fourth hypothesis to explain the resolution of immune activation is the low levels of virus replication in lymph nodes and other organized lymphoid tissues observed in chronic SIV infection of AGMs and SMs (*37*, *51*). This limited viral replication in lymphoid tissues is probably related to lower levels of infection of central memory $CD4^+$ Tcm (see next section for details) (*30*). According to this hypothesis, reduced virus replication in the main anatomic sites in which immune responses are initiated allows a more effective resolution of the early virus-induced immune activation as compared with pathogenic HIV/SIV infections in which virus production in lymph nodes remains higher. Although the relative contribution of each of these four mechanisms and any as-yet undescribed factors to the low immune activation observed during chronic SIV infections of natural hosts remains unknown, all available experimental data confirm that immune quiescence is a typical feature of nonpathogenic infections and is likely a key determinant of their benign nature.

What Is the Role of Target Cell Restriction in Natural SIV Hosts?

In recent years, the observation that SIV infection of SMs is characterized by a specific pattern of infected cells in vivo—in which $CD4^+$ Tcm are relatively spared, whereas $CD4^+$ effector memory T cells (Tem) are the main viral targets (*30*)—has led to a model of AIDS pathogenesis that proposes that the subset of cells infected is more important than the total number of infected cells or the level of plasma viremia in causing the immune deficiency (Fig. 2). $CD4^+$ Tcm reside in

Table 2. Proposed mechanisms for the nonpathogenic phenotype of SIV infection of natural hosts.

Hypothesis	Evidence	Discussion	Conclusion
SIV strains infecting natural hosts are incapable of causing AIDS due to attenuation of cytopathicity.	(i) Direct inoculation of RMs with SM plasma or tissues can result in progression to AIDS (*2*). (ii) Life span of infected cells is similar in natural and nonnatural hosts (*13*, *14*).	Nonpathogenicity of natural host infection is not due to viral attenuation.	Hypothesis not supported
Specific properties of SIV accessory proteins result in reduced pathogenesis in natural hosts.	(i) The Nef gene of natural host SIVs has the ability to down-modulate CD3-TCR from the surface of infected $CD4^+$ T cells, but this function was lost in SIVs infecting chimpanzees and humans (*41*). (ii) SIV's ability to antagonize Tetherin becomes mediated by different virus gene products during cross-species transmission (*59*).	Coevolution of SIVs and their natural hosts has resulted in viral phenotypes that limit immune activation-mediated pathogenesis.	Hypothesis supported
Long-lived central memory $CD4^+$ T cells are relatively resistant to SIV infection, resulting in preserved $CD4^+$ T cell homeostasis and protection from SIV-induced immunopathology.	(i) SM central memory $CD4^+$ T cells exhibit low levels of SIV co-receptor expression and are less infected in vivo and in vitro (compared with SM effector memory $CD4^+$ T cells and RM central memory $CD4^+$ T cells) (*30*). (ii) SIV replication in lymph nodes is decreased in SMs and AGMs relative to RMs (*37*, *44*).	Restriction of infection to expendable T cell subsets at peripheral sites via modulation of SIV receptor/co-receptor expression reduces pathogenicity by preserving long-lived cells in primary lymphoid tissues.	Hypothesis supported
An effective adaptive immune response suppresses viral replication in natural hosts.	(i) Natural hosts have high viral loads similar to those seen in pathogenic SIV infection of RMs and HIV infection of humans (*5*–*9*). (ii) SIV-specific T cell responses in SMs are not superior to those of pathogenic infections in terms of magnitude, breadth, and polyfunctionality (*22*, *24*). (iii) Neutralizing antibody titers against autologous SIV are low in SMs (*23*).	The lack of pathogenicity in natural hosts is not associated with successful immune control of virus replication to levels similar to those of HIV-infected elite controllers.	Hypothesis not supported
Natural hosts avoid progression to AIDS by limiting chronic immune activation and bystander immunopathology.	(i) Immune activation mediated pathology is nearly absent in natural hosts despite high levels of virus replication (*5*, *18*). (ii) Innate and adaptive immune responses return to baseline after acute infection of SMs and AGMs but remain high in humans and RMs (*17*–*21*).	Avoidance of chronic immune activation in natural hosts helps to preserve T cell homeostasis and prevent bystander immunopathology and dysregulation of critical immune cell subsets and tissues.	Hypothesis supported
Natural hosts maintain the integrity of the gut mucosal barrier through preservation of the mucosal immune environment.	(i) Microbial products and related markers are found at low levels in the blood and tissues of natural hosts (*27*, *42*). (ii) $CD4^+$ T_H17 cells are not preferentially depleted during SIV infection of natural hosts (*25*, *26*).	Maintenance of the gut mucosal immune system in natural hosts prevents the translocation of microbial products from the intestinal lumen to the systemic circulation where they can induce chronic immune activation.	Hypothesis supported

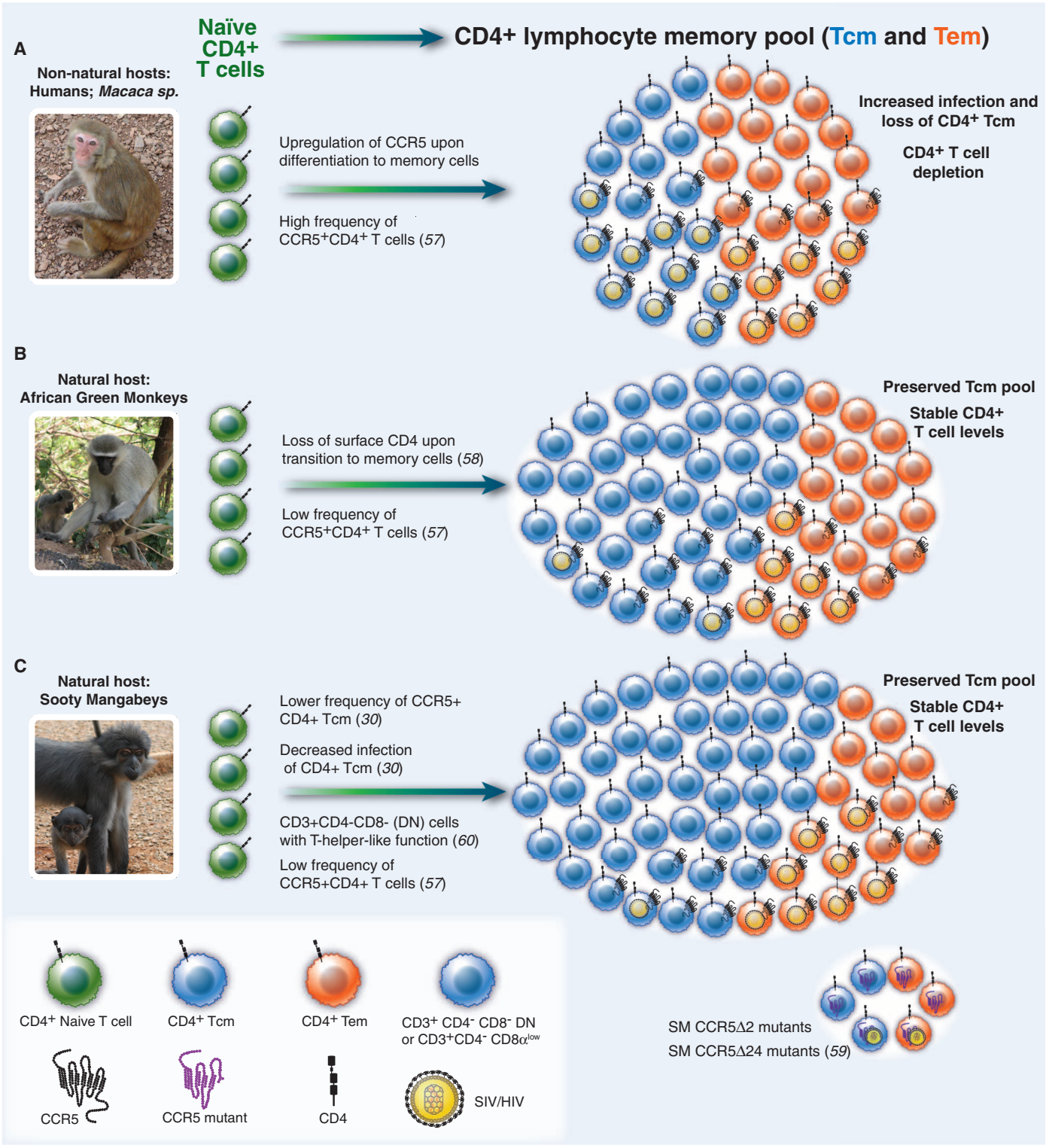

Fig. 2. Proposed mechanisms of target cell restriction in natural host species. (**A**) In pathogenic hosts such as RMs, activation of $CD4^+$ T cells typically leads to robust surface expression of the HIV/SIV co-receptor CCR5, providing targets for infection and viral replication. Infection is distributed within both Tem and Tcm. Infection and disruption of the Tcm pool has been proven to disrupt $CD4^+$ T cell homeostasis in vivo (53). (**B**) Upon transition from naïve $CD4^+$ T cells to memory cells, AGMs lower the surface expression of the CD4 molecule on a subset of $CD3^+CD4\text{-}CD8\alpha^{low}$ lymphocytes that exhibit $CD4^+$ T cell function and are infected by SIV at a lower frequency than naïve or memory $CD4^+$ cells (58). AGMs also exhibit lower levels of CCR5 expression on $CD4^+$ T cells than nonnatural hosts (57). (**C**) Multiple, non–mutually exclusive mechanisms modulating SIV tropism have been described in SMs: (i) Upon activation, SM $CD4^+$ Tcm maintain low levels of CCR5 relative to $CD4^+$ Tem, resulting in significantly decreased levels of SIV infection (30); (ii) SMs have high levels of $CD3^+CD4^-CD8^-$ DN lymphocytes that exhibit T helper function, providing a potential surrogate for $CD4^+$ T cells that is resistant to infection (60); and (iii) ~7% of captive SMs are homozygous for CCR5 mutations that abrogate surface expression, although these animals can be infected with SIV (59). [Photo credit: S.E.B. and K. D. Mir]

lymph nodes and other inductive lymphoid tissues and show strong proliferation in response to antigenic restimulation with limited effector function (such as production of cytokines); in contrast, $CD4^+$ Tem reside in nonlymphoid tissues (i.e., mucosae) and show high effector function but limited proliferation upon restimulation (*52*). Given the central role played by $CD4^+$ Tcm in maintaining the overall homeostasis of the $CD4^+$ T cell pool, direct infection of these cells by HIV/SIV is hypothesized to have a greater potential to damage the immune system than does infection of the likely more expendable $CD4^+$ Tem. This idea is consistent with studies conducted in SIV-infected RMs indicating that progressive depletion of $CD4^+$ Tcm is the key factor dictating the tempo of progression to AIDS, both in the natural history of infection and in the context of vaccination (*53*, *54*). Whereas the mechanisms causing the loss of $CD4^+$ Tcm in SIV-infected RMs are probably complex and multifactorial and include bystander cell death, proliferative senescence, and loss of anatomic niche, it is undisputed that direct virus infection is a key determinant of $CD4^+$ Tcm depletion during pathogenic HIV/SIV infections (*55*). Importantly, in HIV-infected humans, the levels of in vivo infection of $CD4^+$ Tcm are at least as high, if not higher, than those of other memory $CD4^+$ T cell subsets, and $CD4^+$ Tcm represent the largest reservoir of infected $CD4^+$ T cells (*56*).

In SMs, the protection of $CD4^+$ Tcm from SIV infection has been observed both in vivo and in vitro. Ex vivo sorted $CD4^+$ Tcm of naturally SIV-infected SMs have significantly fewer copies of cell-associated SIV-DNA compared with $CD4^+$ Tcm of SIV-infected RMs, and sorted $CD4^+$ Tcm of SIV-uninfected SMs show significantly lower levels of virus production upon experimental in vitro SIV infection when compared with sorted $CD4^+$ Tcm of healthy, uninfected RMs (*30*). The relative resistance to SIV infection by SM $CD4^+$ Tcm as compared with SM $CD4^+$ Tem or $CD4^+$ Tcm of RMs suggests that SMs may have adapted to protect their $CD4^+$ Tcm from virus infection and that this preferential sparing of $CD4^+$ Tcm is a key determinant of the benign nature of SIV infection in these animals. Interestingly, $CD4^+$ Tcm of SMs express lower levels of the main virus coreceptor, the chemokine receptor CCR5, both ex vivo and, even more dramatically, after in vitro activation with various stimuli (*30*, *57*), thus leading to the hypothesis that lower levels of CCR5 represent a mechanism of intrinsic resistance of SM $CD4^+$ Tcm to virus infection that acts at the entry level. Somewhat analogously, $CD4^+$ T cells of AGMs have been shown to down-modulate the expression of the CD4 molecule, the virus receptor, from their surface during the transition from naive to memory cells, thus acquiring resistance to SIV infection (*58*). Notably, a recent genetic study revealed that ~7% of SMs are homozygous for a mutant CCR5 allele (consisting of a two–base pair deletion in the region corresponding to the fourth transmembrane domain of CCR5) that abrogates surface expression of CCR5 (*59*). When infected with SIV, these CCR5Δ2 SMs also remain healthy despite robust virus replication (albeit ~0.5 log lower than CCR5 wild-type animals), indicating that selective CCR5 down-modulation is not the only mechanism protecting $CD4^+$ Tcm from direct virus infection. The discovery of CCR5Δ2 SMs also suggests that the expression of alternative virus co-receptors (i.e., CXCR6, GPR1, etc.) is an additional determinant of the different patterns of target cells observed in SIV-infected natural hosts and RMs.

The role of virus co-receptor tropism in the pathophysiology of SIV infection in SMs was emphasized in a series of elegant studies conducted by Sodora and colleagues, in which development of CXCR4-tropic variants of SIV_{smm} was found to be associated with a rare phenotype characterized by generalized depletion of $CD4^+$ T cells (*60*, *61*). These "CD4-low" SIV-infected SMs maintain a population of $CD3^+CD4^-CD8^-$ [i.e., double-negative (DN)] T cells that exhibit phenotypic and functional features of Tcm and mediate a strong helper T cell effect in vivo when animals are exposed to neoantigens (*60*). Another key feature of these CD4-low SIV-infected SMs is the reduced viremia (~2 logs lower than the "CD4-high" SMs), which may help explain why immune activation remains low in these animals.

This association between low $CD4^+$ T cell counts and low virus replication in SMs was recreated experimentally by monoclonal antibody-mediated in vivo $CD4^+$ lymphocyte depletion in SIV-infected SMs (*29*). When a similar experimental $CD4^+$ lymphocyte depletion was conducted before SIV_{mac} infection of RMs, the subsequent levels of virus replication were remarkably high (~10^8 to 10^9 copies/ml of plasma), with the majority of virus-producing cells in both lymph nodes and mucosal tissues belonging to the macrophage lineage (*62*). The reason(s) why $CD4^+$ lymphocyte depletion is associated with massive virus replication in macrophages in RMs but not in SMs are currently under investigation and may involve both entry and postentry mechanisms that restrict virus infection and/or replication in these cells in natural hosts. The SIV_{smm} and SIV_{mac} (and SIV_{agm} and HIV-2, but not SIV_{mnd-1} and HIV-1) viruses express Vpx that antagonizes the newly described SAMHD1 host restriction factor in myeloid cells (*63*, *64*), and further exploration of the impact of this virus-host interaction, as well as other such interactions, in particular that of BST-2/tetherin with several viral gene products (*65*), is the subject of ongoing research. Collectively, these studies delineate a model in which, in the majority of SIV-infected SMs, $CD4^+$ Tcms are protected from direct virus infection, thus favoring the preservation of $CD4^+$ T cell homeostasis (Fig. 2). In the relatively rare case of infection with a CXCR4-tropic, $CD4^+$ T cell–depleting virus, a combination of "off-shoring" of T helper function to DN T cells and a reduction of virus replication due to the inability to infect macrophages appears sufficient to avoid AIDS.

The resolution of immune activation and target cell restriction that we have thus far described may protect natural SIV hosts from disease progression, and it is likely that these two phenomena favor each other in a virtuous cycle whose establishment is crucial to avoid the immune deficiency that follows HIV/SIV infections of humans and RMs. On the one hand, low levels of infected $CD4^+$ Tcms may limit immune activation by decreasing virus replication and, thus, antigenic burden in the tissues where innate and adaptive immune responses are primed (lymph nodes, spleen, Peyer's patches). On the other hand, low chronic immune activation may promote $CD4^+$ Tcm preservation by reducing direct virus infection (that is enhanced by cell activation), minimizing bystander cell death of uninfected $CD4^+$ Tcms and maintaining the anatomic niche of these cells, which is replaced by tissue fibrosis during pathogenic SIV infection of RMs (*41*). We propose that low immune activation and reduced infection of $CD4^+$ Tcm are the evolutionary result of a mutually beneficial coadaptation between primate lentiviruses and their natural hosts that took place over the many thousands of years in which these viruses have infected African monkey species.

How Are Natural Hosts Protected from Mother-to-Infant SIV Transmission?

A marked feature of SIV infection in natural hosts is the rarity of MTIT (*34*–*36*). In HIV-1–infected humans, mother-to-child transmission can occur in utero, during labor and delivery, and as a consequence of breastfeeding, with a total HIV-1 transmission rate of 35 to 40% in absence of antiretroviral therapy or other preventative measures. In stark contrast, MTIT of SIV in SMs occurs at a rate of <7% and appears to be even less frequent in AGMs and mandrills (*34*–*36*). Interestingly, when infant SMs or AGMs do become infected, either as a consequence of MTIT or through experimental inoculation, the levels of virus replication are significantly lower than those observed in adult animals (*34*, *66*). The mechanisms responsible for the low rate of MTIT in natural SIV hosts remain poorly understood; however, strong preliminary evidence implicates low levels of target cells (and particularly activated $CD4^+CCR5^+$ T cells) (*36*) as a factor involved in both restricted transmission and low viral loads in infants of natural SIV host species. As such, an emerging theory is that there exists a convergence of the immunological mechanisms protecting from disease progression in adult animals and MTIT in offspring. We are not surprised by this relationship. The evolutionary pressure selecting for the benign nature of current SIV infections in natural host species would almost certainly have encompassed more than a disease course similar to that seen in HIV-infected individuals (~10 years from infection to death) in animals infected as adults and with an average life span of only 15 to 20 years. Most likely, the original epidemics of SIV infection with ancestral, putatively pathogenic viruses were characterized by high levels of transmission from mother to offspring, particularly if one considers the obvious deleterious effect of moving the "clock" of infection back 4 to 5 years to infancy, along with the

observation that pathogenic HIV/SIV infections appear to be more severe in children compared with adults. In this view, the genetic features of natural SIV hosts that underlie two key mechanisms of AIDS resistance (i.e., low immune activation and target cell restriction) may at least partially reflect evolutionary selection to protect from MTIT. Further studies are needed to better elucidate the mechanisms restricting MTIT in natural hosts and to understand the relation between these mechanisms and those that protect SIV-infected animals from disease progression.

Future Studies and Implications for Human Health

Although major progress has been made in understanding the pathophysiology of natural SIV infections, several important questions remain unanswered, and further studies are clearly warranted to fully delineate the mechanisms by which natural SIV hosts avoid AIDS. Key areas of investigation that should be prioritized include: (i) the mechanisms responsible for the resolution of immune activation, (ii) the factors restricting virus replication in $CD4^+$ Tcms and macrophages, (iii) the ways in which specific viral gene products (Nef, Vpu, Vpx) interact with the species-specific host immune system to reduce pathogenicity, (iv) the immunological events involved in the preservation of gut mucosal immunity and integrity, and (v) the mechanisms responsible for protection from MTIT. More detailed studies in SMs and AGMs—the two species of natural SIV hosts available for research in the United States and Europe—would certainly benefit from more aggressive use of high throughput genetic, genomic, and proteomic techniques. These studies should be conducted in parallel in humans and RMs and could include the establishment of a basic transcriptome and proteome resource for the key immunological cell types in these different species. In addition, it would be very useful if more species of natural SIV hosts become accessible to researchers in the field. In particular, an increased understanding of lentiviral pathogenesis may be obtained by collecting basic information on the outcome of infection in certain nonhuman primate species (i.e., greater spot nosed monkey, mustached guenons, and monas) that are hosts of SIVs that include *vpu* and whose Nef protein is unable to down-modulate the CD3-TCR complex (*47*). Examination of a broader range of natural hosts will probably reveal additional mechanisms that prevent SIV infections from progressing to AIDS in these animals.

It is clear that rigorous investigations of the mechanisms by which African nonhuman primate natural hosts and their lentiviruses have coevolved to reach a pacific coexistence in nature will continue to provide critical insights into human HIV/AIDS pathogenesis. The direct relevance of studies of natural SIV infection to human health has been emphasized by the recent observation that rare HIV-infected humans exhibit a natural host-like phenotype: stable $CD4^+$ T cell counts despite high viremia, with a transcriptional profile similar to that of SIV-infected SMs (*67*). Ultimately, these insights will translate into successful interventions to prevent and treat HIV infection in humans. In a previous article, we discussed how studies of natural SIV infections inform the development of an AIDS vaccine (*68*), and here we will focus more on the potential impact on HIV therapy. A better understanding of the mechanisms responsible for the resolution of immune activation in natural hosts will guide the development of new agents to treat the chronic immune activation associated with HIV infection that is a key determinant of disease progression. In particular, these studies could identify molecular pathways of immune regulation that are active in natural SIV hosts and that could be targeted to reduce or eliminate the residual immune activation and inflammation that is associated with increased morbidity and end-organ disease during long-term antiretroviral treatment of HIV-infected individuals. In addition, uncovering the mechanisms of T_H17 preservation during natural SIV infection could identify therapeutic targets to improve T_H17 cell homeostasis in HIV-infected individuals, thereby promoting the immunologic restoration of the intestinal mucosal barrier. Furthermore, the observation that the pattern of infected cells may be critical in dictating the progression to AIDS in HIV/SIV infections should prompt more investigations aimed at defining the determinants of $CD4^+$ Tcm infection in HIV-infected humans and whether the level of $CD4^+$ Tcm infection correlates with disease progression and/or residual morbidity in treated individuals. Another area to pursue is the role of $CD4^+$ Tcm infection in establishing the reservoirs of latently infected cells, and, given the long life span of these cells, in causing HIV persistence during antiretroviral therapy. It is hoped that therapeutic interventions will be developed that may more aggressively protect $CD4^+$ Tcm from infection. Finally, a more complete understanding of the block to vertical transmission in natural hosts could majorly affect current treatment of HIV-infected pregnant women and their infants and possibly reduce the number of perinatal HIV infections worldwide.

In the title of this Review, we expressed the hope that natural SIV hosts will tell us how to "show AIDS the door." Indeed, if we are to reach this aim, it would be foolish to ignore the lessons of this experiment conducted by nature over thousands of years. After all, natural SIV hosts are the door through which HIV came to humans, and we believe they will give us the tools to finally close the door on AIDS, just as they did long ago.

References and Notes

1. M. Worobey *et al.*, *Science* **329**, 1487 (2010).
2. S. VandeWoude, C. Apetrei, *Clin. Microbiol. Rev.* **19**, 728 (2006).
3. B. H. Hahn, G. M. Shaw, K. M. De Cock, P. M. Sharp, *Science* **287**, 607 (2000).
4. N. L. Letvin *et al.*, *Science* **230**, 71 (1985).
5. G. Silvestri *et al.*, *Immunity* **18**, 441 (2003).
6. C. Apetrei *et al.*, *J. Virol.* **85**, 13077 (2011).
7. S. Goldstein *et al.*, *J. Virol.* **80**, 4868 (2006).
8. I. Pandrea *et al.*, *J. Med. Primatol.* **35**, 194 (2006).
9. M. A. Rey-Cuillé *et al.*, *J. Virol.* **72**, 3872 (1998).
10. B. F. Keele *et al.*, *Nature* **460**, 515 (2009).
11. S. G. Deeks, B. D. Walker, *Immunity* **27**, 406 (2007).
12. J. T. Loffredo *et al.*, *J. Virol.* **81**, 8827 (2007).
13. S. N. Gordon *et al.*, *J. Virol.* **82**, 3725 (2008).
14. I. Pandrea *et al.*, *J. Virol.* **82**, 3713 (2008).
15. S. N. Gordon *et al.*, *J. Immunol.* **179**, 3026 (2007).
16. I. V. Pandrea *et al.*, *J. Immunol.* **179**, 3035 (2007).
17. S. E. Bosinger *et al.*, *J. Clin. Invest.* **119**, 3556 (2009).
18. J. D. Estes *et al.*, *J. Immunol.* **180**, 6798 (2008).
19. B. Jacquelin *et al.*, *J. Clin. Invest.* **119**, 3544 (2009).
20. L. D. Harris *et al.*, *J. Virol.* **84**, 7886 (2010).
21. S. Lederer *et al.*, *PLoS Pathog.* **5**, e1000296 (2009).
22. R. Dunham *et al.*, *Blood* **108**, 209 (2006).
23. B. Li *et al.*, *J. Virol.* **84**, 6248 (2010).
24. Z. Wang, B. Metcalf, R. M. Ribeiro, H. McClure, A. Kaur, *J. Virol.* **80**, 2771 (2006).
25. J. M. Brenchley *et al.*, *Blood* **112**, 2826 (2008).
26. D. Favre *et al.*, *PLoS Pathog.* **5**, e1000295 (2009).
27. J. M. Brenchley *et al.*, *Nat. Med.* **12**, 1365 (2006).
28. M. Paiardini *et al.*, *Blood* **113**, 612 (2009).
29. N. R. Klatt *et al.*, *J. Clin. Invest.* **118**, 2039 (2008).
30. M. Paiardini *et al.*, *Nat. Med.* **17**, 830 (2011).
31. L. A. Chakrabarti *et al.*, *J. Virol.* **74**, 1209 (2000).
32. I. Pandrea *et al.*, *J. Virol.* **80**, 4858 (2006).
33. B. Sumpter *et al.*, *J. Immunol.* **178**, 1680 (2007).
34. A. Chahroudi *et al.*, *J. Virol.* **85**, 5757 (2011).
35. M. G. Otsyula *et al.*, *Ann. Trop. Med. Parasitol.* **89**, 573 (1995).
36. I. Pandrea *et al.*, *J. Virol.* **82**, 5501 (2008).
37. M. Meythaler *et al.*, *J. Immunol.* **186**, 5151 (2011).
38. A. R. Sedaghat *et al.*, *J. Virol.* **82**, 1870 (2008).
39. M. D. Hyrcza *et al.*, *J. Virol.* **81**, 3477 (2007).
40. S. R. Broussard *et al.*, *J. Virol.* **75**, 2262 (2001).
41. M. Zeng *et al.*, *J. Clin. Invest.* **121**, 998 (2011).
42. G. Pantaleo *et al.*, *Nature* **362**, 355 (1993).
43. T. W. Schacker *et al.*, *J. Clin. Invest.* **110**, 1133 (2002).
44. J. L. Heeney, *Immunol. Today* **16**, 515 (1995).
45. D. L. Sodora, G. Silvestri, *AIDS* **22**, 439 (2008).
46. P. W. Hunt *et al.*, *J. Infect. Dis.* **187**, 1534 (2003).
47. M. Schindler *et al.*, *Cell* **125**, 1055 (2006).
48. A. D. Redd *et al.*, *Proc. Natl. Acad. Sci. U.S.A.* **106**, 6718 (2009).
49. J. D. Estes *et al.*, *PLoS Pathog.* **6**, e1001052 (2010).
50. I. Pandrea *et al.*, *J. Immunol.* **181**, 6687 (2008).
51. O. M. Diop *et al.*, *J. Virol.* **74**, 7538 (2000).
52. M. Pepper, M. K. Jenkins, *Nat. Immunol.* **12**, 467 (2011).
53. A. Okoye *et al.*, *J. Exp. Med.* **204**, 2171 (2007).
54. N. L. Letvin *et al.*, *Science* **312**, 1530 (2006).
55. J. M. Brenchley, G. Silvestri, D. C. Douek, *Immunity* **32**, 737 (2010).
56. J. M. Brenchley *et al.*, *J. Virol.* **78**, 1160 (2004).
57. I. Pandrea *et al.*, *Blood* **109**, 1069 (2007).
58. C. M. Beaumier *et al.*, *Nat. Med.* **15**, 879 (2009).
59. N. E. Riddick *et al.*, *PLoS Pathog.* **6**, e1001064 (2010).
60. J. M. Milush *et al.*, *J. Clin. Invest.* **121**, 1102 (2011).
61. J. M. Milush *et al.*, *J. Immunol.* **179**, 3047 (2007).
62. A. M. Ortiz *et al.*, *J. Clin. Invest.* **121**, 4433 (2011).
63. N. Laguette *et al.*, *Nature* **474**, 654 (2011).
64. K. Hrecka *et al.*, *Nature* **474**, 658 (2011).
65. D. Sauter *et al.*, *Cell Host Microbe* **6**, 409 (2009).
66. B. Beer *et al.*, *J. Acquir. Immune Defic. Syndr.* **18**, 210 (1998).
67. M. Rotger *et al.*, *J. Clin. Invest.* **121**, 2391 (2011).
68. D. L. Sodora *et al.*, *Nat. Med.* **15**, 861 (2009).
69. B. Jacquelin *et al.*, in *Models of Protection Against HIV/SIV: Avoiding AIDS in Humans and Monkeys*, G. Pancino, G. Silvestri, K. Fowke, Eds. (Academic Press, London, 2011), pp. 47–49.

Acknowledgments: We gratefully thank the following individuals, whose unparalleled scientific insight and dedication have contributed substantially to our understanding of the natural SIV hosts: J. Allan, R. Amara, A. Ansari, C. Apetrei, J. Brenchley, L. Chakrabarti, R. Collman, M. Davenport, C. Derdeyn, D. Douek, J. Else, J. Estes, M. Feinberg, R. Grant, A. Haase, B. Hahn, V. Hirsch, A. Kaur, F. Kirchhoff, M. Lederman, P. Marx, M. Muller-Trutwin, I. Pandrea, L. Picker, D. Sodora, J. Schmitz, S. Staprans, R. Veazey, and F. Villinger. We apologize that, due to space constraints, we were only able to cite selected works from these and other authors. We also thank C. Dieffenbach, S. Plaeger, J. Young, A. Embry, and D. Finzi at the Division of AIDS of the National Institute of Allergy and Infectious Diseases, NIH for their continuous intellectual and logistical support of this work. This work was supported by NIH grants R01-AI066998 to G.S. and P51-RR00165 to YNPRC.

10.1126/science.1217550

Fluorescence Imaging of Cellular Metabolites with RNA

Jeremy S. Paige, Thinh Nguyen-Duc, Wenjiao Song, Samie R. Jaffrey*

Imaging small molecules in real time in living cells is usually accomplished with genetically encoded sensors, which are typically fluorescent proteins flanking a ligand-binding domain. Ligand binding induces conformational changes that reorient the fluorescent proteins, which is detected by changes in Förster resonance energy transfer (FRET). However, sensor development is difficult because proteins that undergo conformational changes upon binding a desired target molecule are usually not available. Here, we describe fluorescence imaging of small molecules using RNA. These RNA-based sensors comprise a ligand-binding RNA aptamer and Spinach, an aptamer that binds and switches on the fluorescence of a small-molecule fluorophore. We describe sensors that detect a variety of small molecules in vitro and allow imaging of the dynamic changes and cell-to-cell variation in the intracellular levels of adenosine 5′-diphosphate (ADP) and *S*-adenosylmethionine (SAM) in *Escherichia coli*.

Recently we described RNAs that bind and switch on the fluorescence of molecules that resemble the fluorophore of green fluorescent protein (*1*). These fluorophores do not exhibit nonspecific fluorescence in cells or cytotoxicity (*1*). The brightest RNA-fluorophore complex is an RNA termed Spinach and the fluorophore 3,5-difluoro-4-hydroxybenzylidene imidazolinone (DFHBI). Trafficking of Spinach-tagged RNAs can be imaged in cells (*1*). Because RNA aptamers that selectively bind to essentially any small molecule can be rapidly generated by using in vitro selection (*2*), we sought to develop RNA sensors that comprise small molecule–binding aptamers linked to Spinach so that ligand binding induces binding of Spinach to DFHBI, leading to fluorescence.

Spinach contains three stem loops encircling a central loop (fig. S1, A and B) (*1*). Mutagenesis revealed that one stem loop has an essential structural role in Spinach fluorescence (fig. S1, C and D). We therefore used this stem loop as an entry point for the insertion of small molecule–binding aptamers. Many aptamers are unstructured until they bind their targets (*3*). If a small molecule–binding aptamer and Spinach share the critical stem required for Spinach fluorescence, small-molecule binding can fold the aptamer and stabilize the stem, resulting in fluorescence (Fig. 1A).

We fused aptamers that bind adenosine, ADP, SAM, guanine, or guanosine 5′-triphosphate (GTP) (table S1) to Spinach via a stem sequence that functioned as a "transducer" (fig. S1, E and F). We designed transducers so that stem hybridization is thermodynamically unfavorable because the stem (i) is short, (ii) is composed of "weak" base pairs, such as A-U or G-U, or (iii) contains mismatched base pairs. We tested sensors containing different transducers and assayed for ligand-induced fluorescence (fig. S2 and table S1). The optimal adenosine, ADP, SAM, guanine, and GTP sensors exhibited 20-, 20-, 25-, 32-, and 15-fold increases in fluorescence, respectively, upon binding their cognate ligand (Fig. 1B and fig. S3, A to D). The fluorescence increases were linear in physiological concentration ranges (fig. S3, E to I). Most sensors detected the intended target, but not related metabolites, and exhibited rapid fluorescence activation and deactivation kinetics (fig. S3, J to R). Notably, there are no obvious approaches for designing FRET-based sensors for these metabolites.

We next used these RNAs to monitor metabolite dynamics in live cells. DFHBI-treated *E. coli* expressing the SAM sensor exhibited minimal fluorescence when deprived of methionine, the SAM precursor (Fig. 1C). Providing methionine increased fluorescence ~sixfold over 3 hours (fig. S4, C and D), matching increases measured biochemically. SAM levels exhibited cell-to-cell variability after methionine treatment, with most cells exhibiting continuous increases but others briefly increasing and then decreasing or rapidly increasing their SAM levels (figs. S4 and S5 and movie S1). SAM is regenerated by recycling the SAM by-product *S*-adenosyl-homocysteine (SAH) through the SAH hydrolase or nucleosidase pathways (*4*). Selective inhibition of SAH hydrolase markedly reduced the intercell variability after adding methionine to cells, indicating a role for this pathway in SAM metabolic variability in *E. coli* (figs. S5 and S6).

Similarly, dynamic changes in ADP levels in *E. coli* could be detected by using the ADP sensor (fig. S7), demonstrating the versatility of these RNA-based sensors. These sensors produce ~20-fold increases in fluorescence upon metabolite binding, unlike FRET sensors, which typically exhibit 30 to 100% increases (*5*). Because RNA aptamers can be readily generated against any biomolecule (*2*), the strategies described here should enable the design of sensors to image essentially any molecule.

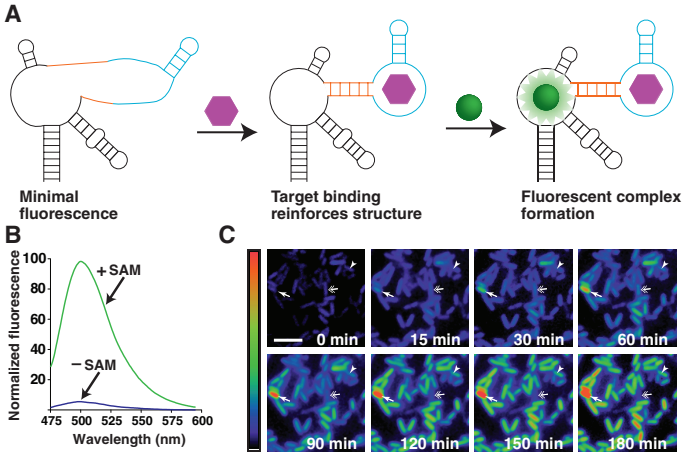

Fig. 1. Imaging SAM in living cells with RNA. (**A**) The sensor RNA comprises Spinach (black), a transducer (orange), and a target-binding aptamer (blue). Target binding to the aptamer promotes stabilization of the transducer stem, enabling Spinach to fold and activate DFHBI fluorescence. (**B**) Emission spectra of the SAM sensor in the presence or absence of SAM. (**C**) Distinct patterns of SAM accumulation after adding methionine to *E. coli* expressing the SAM sensor RNA. Some cells exhibited higher than average (arrow) or slow increases (arrowhead) in SAM. A cell that first increases and then decreases its SAM levels is indicated by a double arrow. Images are pseudocolored to show the fold increase in fluorescence at each time point relative to 0 min (0- to 11.2-fold). Scale bar, 5 μm.

References and Notes

1. J. S. Paige, K. Y. Wu, S. R. Jaffrey, *Science* **333**, 642 (2011).
2. E. J. Cho, J.-W. Lee, A. D. Ellington, *Annu. Rev. Anal. Chem.* **2**, 241 (2009).
3. T. Hermann, D. J. Patel, *Science* **287**, 820 (2000).
4. S. C. Lu, *Int. J. Biochem. Cell Biol.* **32**, 391 (2000).
5. E. A. Lemke, C. Schultz, *Nat. Chem. Biol.* **7**, 480 (2011).

Acknowledgments: We thank V. Schramm for inhibitors and M. Cohen, A. Deglincerti, W. Ping, and S. Blanchard for suggestions. Supported by the McKnight Foundation and NIH grants EB010249 and T32CA062948.

Supporting Online Material

www.sciencemag.org/cgi/content/full/335/6073/1194/DC1
Materials and Methods
SOM Text
Figs. S1 to S8
Table S1
References (*6*–*47*)
Movie S1

22 December 2011; accepted 30 January 2012
10.1126/science.1218298

Department of Pharmacology, Weill Medical College, Cornell University, New York, NY 10065, USA.

*To whom correspondence should be addressed. E-mail: srj2003@med.cornell.edu

Lin28b Reprograms Adult Bone Marrow Hematopoietic Progenitors to Mediate Fetal-Like Lymphopoiesis

Joan Yuan, Cuong K. Nguyen, Xiuhuai Liu, Chrysi Kanellopoulou, Stefan A. Muljo*

The immune system develops in waves during ontogeny; it is initially populated by cells generated from fetal hematopoietic stem cells (HSCs) and later by cells derived from adult HSCs. Remarkably, the genetic programs that control these two distinct stem cell fates remain poorly understood. We report that *Lin28b* is specifically expressed in mouse and human fetal liver and thymus, but not in adult bone marrow or thymus. We demonstrate that ectopic expression of Lin28 reprograms hematopoietic stem/progenitor cells (HSPCs) from adult bone marrow, which endows them with the ability to mediate multilineage reconstitution that resembles fetal lymphopoiesis, including increased development of B-1a, marginal zone B, gamma/delta (γδ) T cells, and natural killer T (NKT) cells.

Hematopoietic stem cells (HSCs) give rise to all the erythroid, myeloid, and lymphoid lineages and are used clinically in transplants to treat patients with a wide variety of blood and immune system disorders that include immunodeficiencies and malignancies. In mice, the major site of hematopoiesis transitions from the fetal liver (FL) to the fetal spleen (FS) and bone marrow (BM) during late embryogenesis. FL HSCs differ phenotypically and functionally from adult BM HSCs, and a developmental switch is thought to occur within the first weeks of postnatal life (*1*–*3*). Adoptive transfer and fetal thymic organ culture studies established that FL HSPCs, unlike adult BM HSPCs, preferentially give rise to lymphocyte subsets that can be collectively referred to as innatelike lymphocytes. For example, $CD5^+$ B cells, referred to as the B-1a subset, and certain γδ-T cell subsets develop almost exclusively in the fetus and/or neonate (*4*–*7*). More recently, a fetal source of HSPCs was found to preferentially give rise to the B-1a and marginal zone (MZ) B cell lineages (*8*). In contrast, adult BM HSPCs are more efficient at reconstituting conventional B and T lymphocyte pools as opposed to the B-1a and fetal γδ-T cell subsets. Although the development of these innatelike lymphocyte subsets requires recombination activating gene (RAG)–mediated V(D)J recombination at the T or B cell antigen receptor loci, their repertoire has been described as semi-invariant or oligoclonal (*9*). Similarly to cells of the innate immune system, they are often strategically localized in the body to respond rapidly to a limited set of conserved antigens. Despite their roles as potent mediators of host defense, the molecular basis for their preference to develop in the fetus or neonate largely remains a mystery. The ability to generate B-1a B cells and $V\gamma3^+$ γδ-T cells [see (*10*) for nomenclature used] is intrinsically programmed in the FL HSCs (*5*, *10*, *11*). Sox17 was identified as a transcription factor that is specifically expressed in and required for the maintenance of fetal but not adult HSCs (*12*). Thus, transcriptional control can distinguish the fetal from adult HSC fate. In this study, we show that a layer of posttranscriptional control involving Lin28b and let-7 microRNAs (miRNAs) contributes to the distinct differentiation potential of these two stem cell types.

***Lin28b* and the let-7 family of miRNAs are differentially expressed in lymphoid progenitors originating from fetal and adult HSCs.** To identify the molecular differences between fetal and adult lymphoid progenitors, we performed global miRNA-expression profiling of FL and adult BM progenitor B (pro-B) cells [$B220^+CD19^+CD24^+CD43^+$ lacking immunoglobulin M (IgM^-)]. This population was chosen because we could readily sort sufficient numbers of these progenitors to high purity, and this choice led to the observation that expression of the let-7 family of miRNAs was largely absent in FL pro-B cells. In the mouse genome, there are 12 let-7 paralogs that result in the expression of nine distinguishable mature miRNA isoforms (isomiRs) (fig. S1). The let-7 miRNAs are broadly and highly expressed in the hematopoietic system (*13*). To our surprise, the eight let-7 isomiRs that were detectable in adult BM pro-B cells were either significantly reduced in expression or undetectable in FL pro-B cells (Fig. 1A). From the same fluorescence-activated cell sorting (FACS), we had isolated the $B220^+CD19^-CD24^-CD43^+IgM^-$ precursors to the pro-B cells (pre-pro-B cells). We determined that mature let-7g and let-7c isomiRs were abundantly expressed in pre-pro-B cells from adult BM but not from FL using quantitative reverse transcription polymerase chain reaction (QRT-PCR) (Fig. 1B). Next, we examined whether the observed global repression of let-7 miRNAs in fetal B cell progenitors was mediated by endogenous Lin28 or Lin28b, encoded by two evolutionarily conserved paralogs, known to specifically block the biogenesis of let-7 miRNAs posttranscriptionally by binding to the terminal loop region of the let-7 primary or precursor miRNAs (pri- or pre-miRNAs) (*14*–*17*). We determined in FACS-sorted populations that *Lin28b* mRNA was abundant in all stages of FL B cell development (Fig. 1C) and also in FL lineage $(Lin)^-Sca\text{-}1^+c\text{-}Kit^+$ (LSK) HSCs and $Lin^-Sca\text{-}1^{int}c\text{-}Kit^{int}$ interleukin-7 receptor α chain–positive ($IL7R\alpha^+$) common lymphoid progenitors (CLPs) (Fig. 1D) but absent in the corresponding populations in adult BM. In contrast, *Lin28* mRNA was not detectable in fetal HSPCs (fig. S2A). These findings indicate that *Lin28b* expression is limited to HSPCs of fetal origin and could account for the observed reduction in mature let-7 expression.

Classic fetal thymus (FT) graft studies suggest that fetal HSPCs seed the thymus between 10 and 13 days of gestation, whereas cells derived from adult HSPCs begin to substantially dilute the first-generation thymocytes at day 7 after birth and have largely replaced them by 2 weeks of age (*18*). To test whether *Lin28b* mRNA expression in the thymus correlates with the presence of fetal HSC-derived cells, we performed QRT-PCR on various FACS-sorted thymocyte populations ranging from the double-negative (DN)2 and DN3 ($CD4^-CD8^-CD25^+CD44^{int}$) cells to the $CD4^+CD8^-$ single-positive (CD4SP) stage from 1-day-old, 1-week-old, and 4-week-old mice. We observed abundant *Lin28b* transcripts in all the tested thymocyte subsets from 1-day-old thymi, with the greatest amount observed in the γδ-T cell receptor–positive ($\gamma\delta\text{-}TCR^+$) thymocytes (Fig. 1E). The abundance of endogenous *Lin28b* mRNA expression was dramatically decreased in thymocytes by 7 days after birth and was undetectable by 4 weeks of age. Declining *Lin28b* expression coincided with rising levels of mature let-7g (fig. S2B). These data demonstrate that endogenous *Lin28b* mRNA expression declines in concordance with the decrease in the proportion of thymocyte progenitors of fetal origin in the postnatal mouse. It is noteworthy that *Lin28b* expression was not maintained in the thymus or peripheral lymphoid populations in sublethally irradiated adult $Rag1^{-/-}$ mice reconstituted with FL HSPCs (fig. S2C). These findings suggest that *Lin28b* expression is turned on during fetal hematopoiesis but not sustained during ontogeny.

To determine whether these observed fetal signatures in mouse HSPCs are conserved in humans, we compared *Lin28b* and let-7g expression in human FL, FT, FS, and $CD34^+$ umbilical

Laboratory of Immunology, National Institute of Allergy and Infectious Diseases (NIAID), National Institutes of Health, Bethesda, MD 20892, USA.

*To whom correspondence should be addressed. E-mail: stefan.muljo@nih.gov

cord blood (CB) cells with that in adult BM, lymph node, and thymus. As in mice, *Lin28b* mRNA expression was exclusively detected in fetal human hematopoietic tissues (Fig. 1F), whereas mature let-7g was more abundant in the adult (fig. S2D). Taken together, these expression analyses reveal a previously unknown molecular difference between HSPCs of fetal and adult origin that is conserved between human and mice and prompted us to identify a heterochronic role of the Lin28b–let-7 axis in regulating hematopoiesis during mammalian ontogeny.

Ectopic Lin28 expression in adult BM HSPCs represses the let-7 family of miRNAs and allows multilineage reconstitution. To test whether ectopic expression of Lin28 can confer characteristics of fetal lymphopoiesis in adult mice, we used a retrogenic BM chimera system. Lin28 was chosen because an excellent antibody was available to confirm its expression. HSPCs from lineage-depleted adult BM of wild-type C57BL/6 mice were transduced with a Lin28-encoding retrovirus and transplanted into sublethally irradiated *Rag1*$^{-/-}$ recipients. Full-length mouse *Lin28* cDNA was cloned into a mouse stem cell virus–based vector upstream of an internal ribosomal entry site followed by green fluorescent protein (GFP) (Lin28-RV) (*19*). Lineage-depleted C57BL/6 bone marrow cells from adult mice were transduced with Lin28-RV or control GFP-RV ex vivo and injected intravenously into sublethally irradiated *Rag1*$^{-/-}$ recipients (fig. S3A). The initial transduction efficiency varied between 20 and 60%, as determined by the frequency of GFP$^+$ cells 24 hours postinfection (Fig. 2A). HSPCs transduced with Lin28-RV mediated multilineage reconstitution with grossly normal proportions of T, B, and myeloid cells in the peripheral lymphoid organs 6 to 8 weeks after transplantation in recipient mice hereafter referred to as Lin28-RV BM chimeras (Fig. 2B and fig. S3). Ectopic Lin28 protein expression was confirmed by Western blot in thymocytes of Lin28-RV BM chimeras (Fig. 2C). To assess the effect of ectopic Lin28 protein on miRNA expression, we performed global miRNA profiling of sorted GFP$^+$ and GFP$^-$ preselection double-positive (DP) thymocytes (CD3^{lo}CD4$^+$CD8$^+$) (fig. S4A). Our results demonstrate that the impact of Lin28-RV on miRNA expression is dramatic and highly specific to the let-7 family members (Fig. 2D). Diminished expression of mature let-7a and let-7g was further validated by QRT-PCR (Fig. 2E). To assess the impact on the transcriptome, we performed deep sequencing of cDNA generated from poly(A)$^+$ RNA (RNA-Seq), comparing sorted GFP$^+$ and GFP$^-$ preselection DP thymocytes in Lin28-RV BM chimeras (fig. S4). Statistical analysis using the Sylamer software demonstrated enrichment only of the complementary let-7 family heptameric seed sequence TACCTCA in 3′ untranslated regions (3′UTRs) of genes up-regulated in GFP$^+$ DP thymocytes (fig. S5) and not the 969 other heptameric seed sequences that were also tested. Out of the 175 up-regulated genes containing this seed motif and passing Bonferroni-corrected E-value threshold of 0.01 identified using Sylamer, we observed a higher-than-expected overlap of 47 and 67 genes with let-7 target genes phylogenetically predicted by PicTar and TargetScan, respectively (tables S1 and S2) (*20*, *21*). Thus, Lin28-RV mediated a dramatic decrease in steady-state levels of mature let-7 miRNAs in our retrogenic system with minimal effects on other miRNAs and resulted in the specific global derepression of putative let-7 target mRNAs. These data reveal that, despite abundant let-7 expression throughout the adult hematopoietic system, we can readily

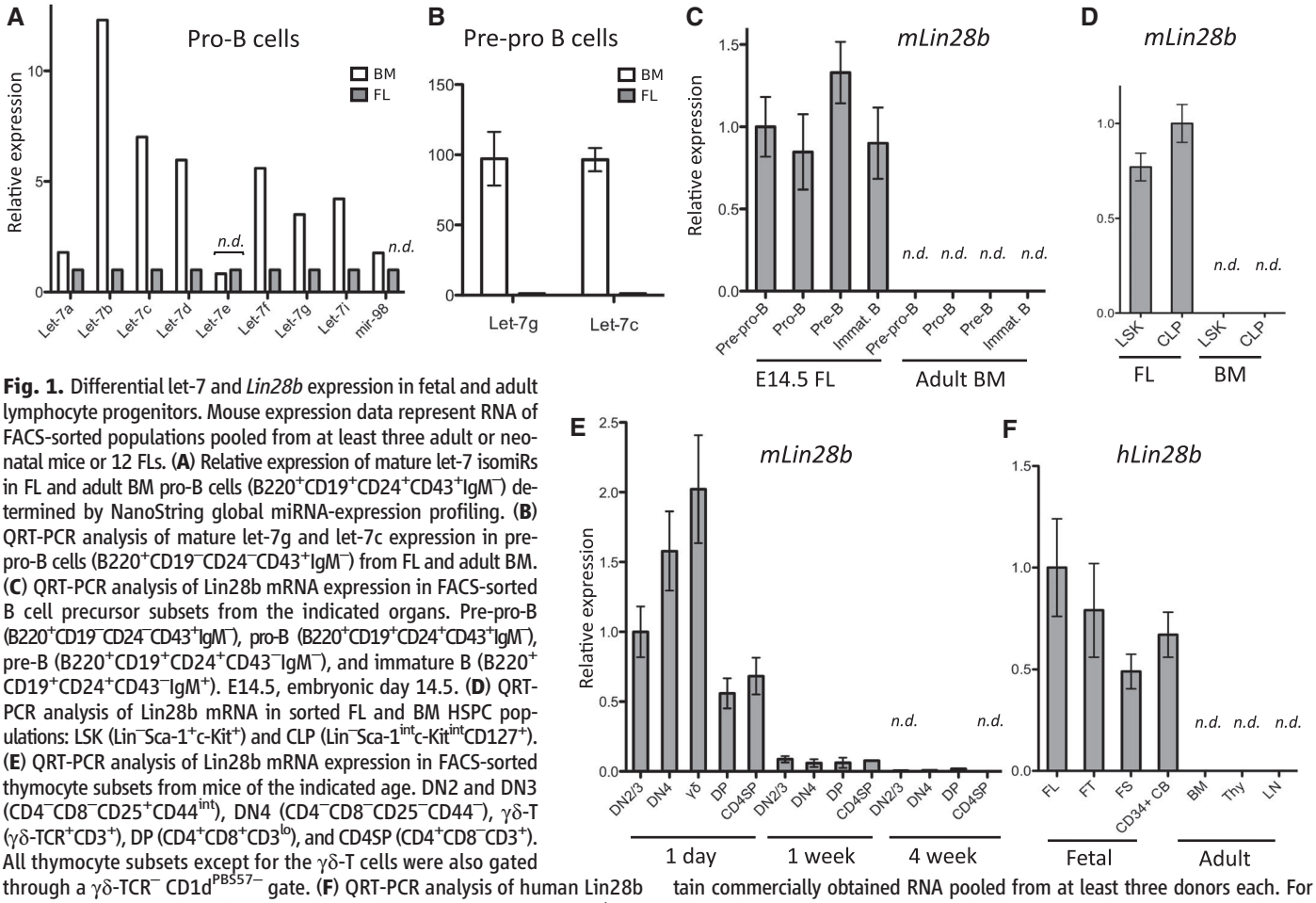

Fig. 1. Differential let-7 and *Lin28b* expression in fetal and adult lymphocyte progenitors. Mouse expression data represent RNA of FACS-sorted populations pooled from at least three adult or neonatal mice or 12 FLs. (**A**) Relative expression of mature let-7 isomiRs in FL and adult BM pro-B cells (B220$^+$CD19$^+$CD24$^+$CD43$^+$IgM$^-$) determined by NanoString global miRNA-expression profiling. (**B**) QRT-PCR analysis of mature let-7g and let-7c expression in pre-pro-B cells (B220$^+$CD19$^-$CD24$^-$CD43$^+$IgM$^-$) from FL and adult BM. (**C**) QRT-PCR analysis of Lin28b mRNA expression in FACS-sorted B cell precursor subsets from the indicated organs. Pre-pro-B (B220$^+$CD19$^-$CD24$^-$CD43$^+$IgM$^-$), pro-B (B220$^+$CD19$^+$CD24$^+$CD43$^+$IgM$^-$), pre-B (B220$^+$CD19$^+$CD24$^+$CD43$^-$IgM$^-$), and immature B (B220$^+$CD19$^+$CD24$^+$CD43$^-$IgM$^+$). E14.5, embryonic day 14.5. (**D**) QRT-PCR analysis of Lin28b mRNA in sorted FL and BM HSPC populations: LSK (Lin$^-$Sca-1$^+$c-Kit$^+$) and CLP (Lin$^-$Sca-1^{int}c-Kit^{int}CD127$^+$). (**E**) QRT-PCR analysis of Lin28b mRNA expression in FACS-sorted thymocyte subsets from mice of the indicated age. DN2 and DN3 (CD4$^-$CD8$^-$CD25$^+$CD44^{int}), DN4 (CD4$^-$CD8$^-$CD25$^-$CD44$^-$), γδ-T (γδ-TCR$^+$CD3$^+$), DP (CD4$^+$CD8$^+$CD3^{lo}), and CD4SP (CD4$^+$CD8$^-$CD3$^+$). All thymocyte subsets except for the γδ-T cells were also gated through a γδ-TCR$^-$ CD1d^{PBS57-} gate. (**F**) QRT-PCR analysis of human Lin28b mRNA expression in the indicated fetal and adult organs: FL, FT, FS, CD34$^+$ CB, BM, thymus (Thy), lymph nodes (LN), and spleen (SPL). Human samples contain commercially obtained RNA pooled from at least three donors each. For all panels, error bars represent standard error of triplicate experimental replicates. n.d. indicates not detectable or below background signal level.

knock down their expression by Lin28-RV transduction without grossly inhibiting multilineage reconstitution.

Lin28 reprograms adult BM HSPCs to undergo fetal-like B lymphopoiesis. It has been reported that FL HSPCs preferentially differentiate into B-1a cells compared with adult HSPCs (*6*, *7*). To test for the effect of Lin28-RV transduction on the development of B-1a cells in adult mice, the peritoneal cavities of Lin28 retrogenic BM chimeras were analyzed 6 to 8 weeks posttransplant for donor-derived B cells. Remarkably, Lin28-RV–transduced adult HSPCs efficiently generated the B-1a subset, whereas untransduced and GFP-RV–transduced adult HSPC controls were biased toward the generation of conventional B-2 cells (Fig. 3, A and B, and fig. S6). In addition to the B-1a subset, growing evidence suggests that a substantial component of the MZ B cell compartment is also of fetal origin (*8*, *22*, *23*). Consistent with this notion, Lin28-RV–transduced HSPCs reproducibly gave rise to an increased percentage of $B220^+CD1d^+CD23^-$ splenic MZ B cells compared with their untransduced (GFP^-) or GFP-RV–transduced controls (Fig. 3, C and D). Similar results were obtained from human Lin28b-RV BM chimeras (fig. S7, A and B). These data indicate that the Lin28b–let-7 axis may account for the long-known differences between fetal and adult fate bias in B cell development and that ectopic Lin28 or Lin28b expression in HSPCs is sufficient to confer fetal-like B lymphopoiesis.

Signaling through IL7Rα has been reported to be required for adult B cell development but dispensable for fetal B lymphopoiesis (*1*). To further examine the notion that ectopic Lin28 expression reprograms adult BM HSPCs to acquire fetal-like B cell development, we investigated whether Lin28-RV could restore B cell potential in adult *Il7rα*$^{-/-}$ BM HSPCs. Recipients reconstituted with *Il7rα*$^{-/-}$ HSPCs transduced with Lin28-RV were analyzed 7 weeks posttransplant for the presence of B cells in the peritoneal cavity and the spleen. In accordance with previous reports, control GFP^- IL7Rα-deficient donor cells failed to give rise to any detectable population of mature $CD19^+B220^+$ B cells. In contrast, sizable populations of GFP^+ Lin28-induced B cells were detected in peritoneal cavities and spleens of Lin28-RV BM chimeras (Fig. 3E). Reminiscent of fetal lymphopoiesis, we observed an overrepresentation of the B-1a and MZ B cell lineages. These results demonstrate that Lin28 acts as a potent reprogramming factor in adult HSPCs to confer fetal-like aspects of B cell development that include independence from IL7Rα-mediated signaling.

Ectopic Lin28 expression favors the development of innatelike T cells. Adult thymocytes mainly differentiate into αβ-T cells but also Vγ2-, Vγ1.1-, and Vγ5-expressing γδ-T cell subsets, whereas fetal thymocytes preferentially rearrange the Vγ3 and Vγ4 TCR gene segments (*24*). In addition, one subpopulation of $V\gamma1.1^+$ T cells is the $CD4^+V\gamma1.1^+V\delta6.3^+$ innatelike T cell subset and has been described to develop perinatally, originating primarily from late embryonic precursors (*25*). We observed a >15-fold increase in the percentage of total $\gamma\delta\text{-TCR}^+$ $CD3^+$ cells among GFP^+ thymocytes in Lin28-RV BM chimeras compared with either the GFP^- thymocytes in the same mouse or GFP^+ thymocytes in the GFP-RV BM chimeras (Fig. 4, A and B). The Lin28-induced γδ-T cells are primarily CD4SP (Fig. 4C), which contributes to an expansion of the overall CD4SP thymocyte compartment (fig. S8A), and do not express the adult-specific Vγ2-TCR chain or the fetal-specific Vγ3-TCR chain. The latter is expected, as the development of $V\gamma3^+$ T cells is known to require both fetal HSCs and a fetal thymus microenvironment (*5*). Remarkably, we identified Lin28-induced γδ-T cells as almost exclusively carrying the $V\gamma1.1^+V\delta6.3^+$ γδ-TCR that normally develops perinatally (Fig. 4D). Both the innatelike $CD4^+V\gamma1.1^+V\delta6.3^+$ and $V\alpha14^+J\alpha18^+$ invariant NKT (iNKT) cells are known to express the promyelocytic leukemia zinc finger protein (PLZF) transcription factor, and the development of $PLZF^+$ CD4 T cells is a physiological process in humans during fetal and perinatal stages of ontogeny (*26*). Indeed, we were able to demonstrate an increased representation of $PLZF^+$ $\gamma\delta\text{-TCR}^+CD3^+$ thymocytes in Lin28-RV BM chimeras (fig. S8B). The ability of Lin28 to induce γδ-T cell development correlates with the finding that $\gamma\delta\text{-TCR}^+$

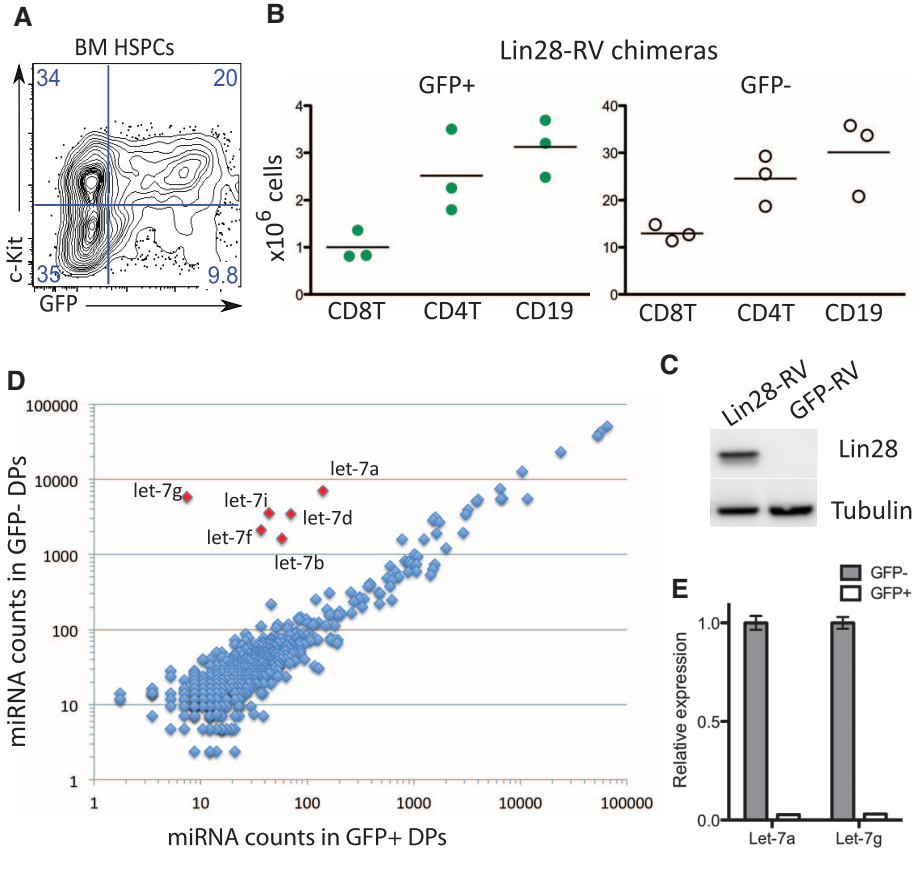

Fig. 2. Lin28-mediated depletion of let-7 and multilineage reconstitution in Lin28-RV BM chimeras. (**A**) FACS plot shows representative frequency of GFP^+ cells among lineage-depleted adult BM cells enriched in HSPCs 24 hours posttransduction with Lin28-RV. (**B**) Absolute numbers of GFP^+ (green) and GFP^- (white) $CD19^+$ B- and $CD4^+$ and $CD8^+$ T-lymphocyte subsets in lymph nodes of three Lin28-RV BM chimeras 6 to 8 weeks after adoptive transfer are plotted. Data are representative of >5 independent reconstitution experiments. (**C**) (Top) Lin28 Western blot of total thymocyte lysate from GFP-RV and Lin28-RV BM chimeras. (Bottom) Tubulin Western blot as a loading control. (**D**) NanoString global miRNA-expression profiling analysis of FACS-sorted GFP^+ and GFP^- DP thymocytes ($CD4^+CD8^+CD3^{lo}$). Normalized counts of individual mature miRNAs in each population are plotted on *x* and *y* axis, respectively (log scale). RNA was pooled from FACS-sorted populations of three individual Lin28-RV BM chimeras. (**E**) QRT-PCR validation of mature let-7a and let-7g expression levels in GFP^- and GFP^+ DP thymocytes from Lin28-RV BM chimera. Error bars indicate standard error of triplicate experimental replicates.

thymocytes naturally express the highest levels of *Lin28b* in neonatal mice (Fig. 1E). In line with our findings regarding B cell development, these data support the ability of Lin28 to confer fetal-like lymphopoiesis in the γδ-T cell lineage.

Although the iNKT cell lineage has not been directly demonstrated to preferentially arise from fetal precursors, several groups have described a

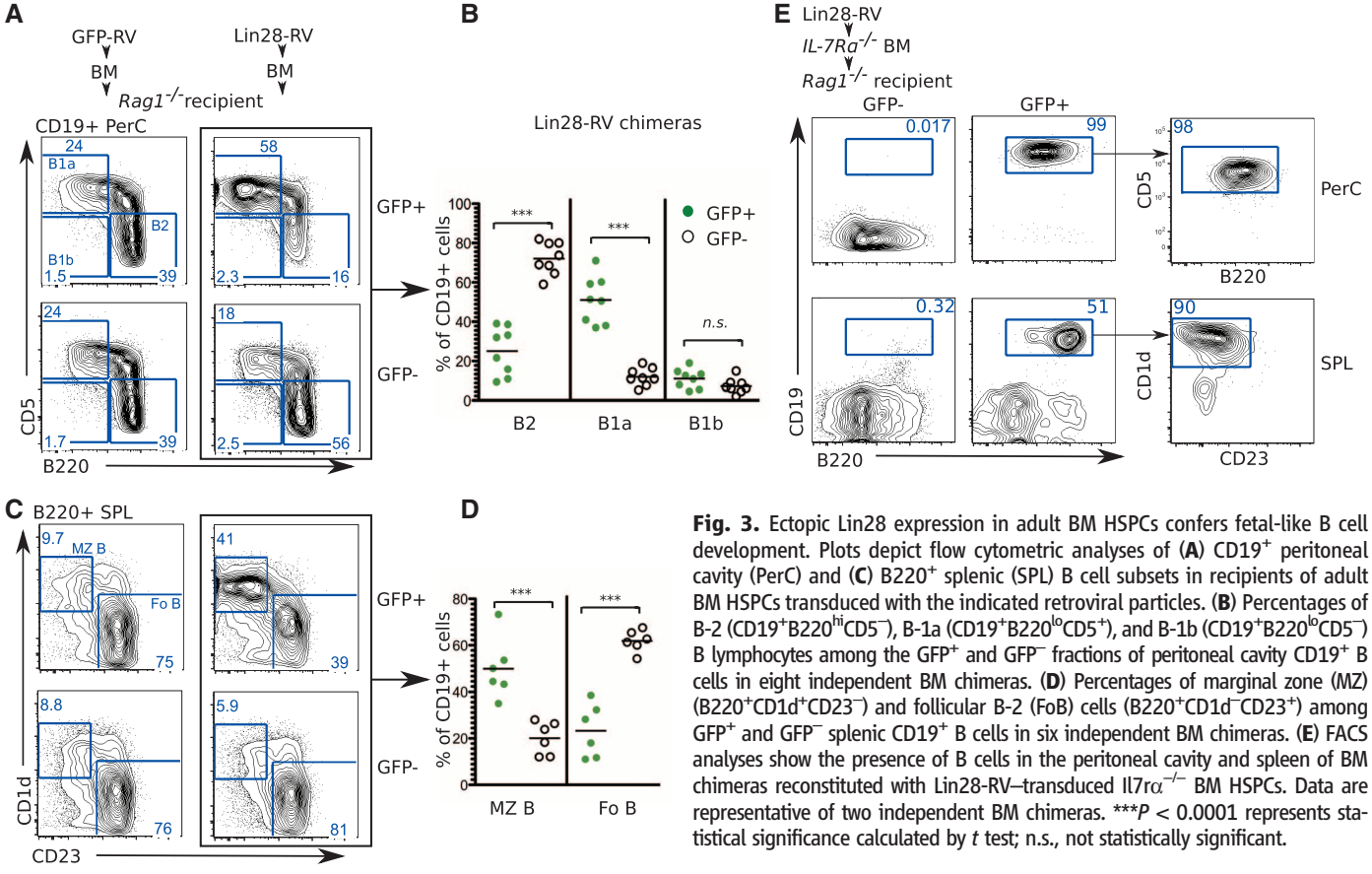

Fig. 3. Ectopic Lin28 expression in adult BM HSPCs confers fetal-like B cell development. Plots depict flow cytometric analyses of (**A**) $CD19^+$ peritoneal cavity (PerC) and (**C**) $B220^+$ splenic (SPL) B cell subsets in recipients of adult BM HSPCs transduced with the indicated retroviral particles. (**B**) Percentages of B-2 ($CD19^+B220^{hi}CD5^-$), B-1a ($CD19^+B220^{lo}CD5^+$), and B-1b ($CD19^+B220^{lo}CD5^-$) B lymphocytes among the GFP^+ and GFP^- fractions of peritoneal cavity $CD19^+$ B cells in eight independent BM chimeras. (**D**) Percentages of marginal zone (MZ) ($B220^+CD1d^+CD23^-$) and follicular B-2 (FoB) cells ($B220^+CD1d^-CD23^+$) among GFP^+ and GFP^- splenic $CD19^+$ B cells in six independent BM chimeras. (**E**) FACS analyses show the presence of B cells in the peritoneal cavity and spleen of BM chimeras reconstituted with Lin28-RV–transduced $Il7r\alpha^{-/-}$ BM HSPCs. Data are representative of two independent BM chimeras. ***$P < 0.0001$ represents statistical significance calculated by *t* test; n.s., not statistically significant.

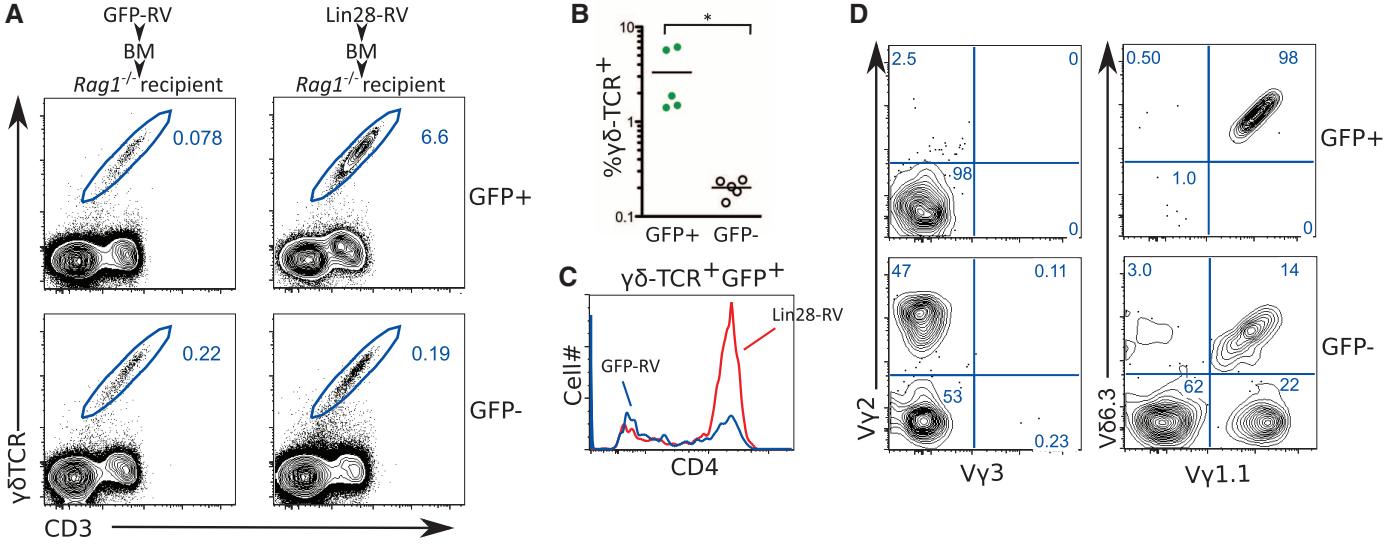

Fig. 4. Ectopic Lin28 expression in adult BM HSPCs promotes the development of $V\gamma1.1^+V\delta6.3^+$ T cells. (**A**) Flow cytometric analysis to enumerate γδ-TCR^+ $CD3^+$ cells in thymi of GFP-RV and Lin28-RV BM chimeras. (**B**) Percentages of γδ-TCR^+ $CD3^+$ thymocytes among GFP^+ and GFP^- cells in the thymi of five independent Lin28-RV BM chimeras. *$P < 0.05$ represents statistical significance calculated by *t* test. (**C**) Flow cytometric analysis shows distribution of surface CD4 expression among GFP^+ γδ-TCR^+ $CD3^+$ thymocytes in the Lin28-RV (red line) and GFP-RV BM (blue line) chimeras. (**D**) Flow cytometric clonotype analysis of γδ-TCR^+ $CD3^+$ thymocytes in the GFP^+ and GFP^- fractions of the Lin28-RV BM chimeras.

transient burst of rapidly proliferating iNKT cell precursors around day 12 after birth (*27*, *28*), consistent with a biased ontogenic window of development. Our discovery of an increased PLZF$^+$ thymocyte population in thymi of Lin28-RV BM chimeras prompted us to further evaluate the effect of Lin28 on iNKT cell development. We observed a 100-fold increase in the percentage of iNKT (CD1d^{PBS57+}CD3$^+$) cells among GFP$^+$ thymocytes in the Lin28-RV BM chimeras compared with the GFP$^-$ thymocytes within the same mouse or a 30-fold increase compared with the GFP$^+$ thymocytes in the GFP-RV BM chimeras (Fig. 5, A and B). This dramatic increase in thymic iNKT cells contributes to a Lin28-induced expansion of the overall CD4SP and DN thymocyte compartments (fig. S8A), as well as the PLZF$^+$ thymocyte pool (fig. S8B). A dramatic increase in the frequency of GFP$^+$ iNKT cells was also observed in the spleen, lymph node, and liver of Lin28-RV BM chimeras (Fig. 5B), translating to higher-than-expected iNKT cell absolute numbers in the spleen (fig. S8C). Positive selection of iNKT cells relies on thymocyte-thymocyte interactions mediated by CD1d (*29*). To determine whether CD1d is required for the development of Lin28-induced iNKT cells, we reconstituted *Rag1*$^{-/-}$ recipients with *Cd1d*$^{-/-}$ HSPCs transduced with Lin28-RV. No iNKT cells were detectable in these recipients, which was consistent with the notion that their positive selection requires CD1d (fig. S9).

Because it is not clear whether iNKT cells develop early during ontogeny, we performed flow cytometric analysis to resolve the proposed developmental stages of the iNKT cell lineage subsequent to the DP thymocyte stage: stage 1 (CD44$^-$NK1.1$^-$), stage 2 (CD44$^+$NK1.1$^-$), and stage 3 (CD44$^+$NK1.1$^+$) (*27*). The composition of the Lin28-induced thymic CD3$^+$CD1d^{PBS57+} population resembled that of a 2-week-old thymus, characterized by a marked increase in the percentage of immature stage 1 iNKT cells (Fig. 5, C and D). Because DP thymocytes are precursors of stage 1 iNKT cells, we quantified the efficiency with which DP thymocytes in wild-type C57BL/6 mice of varying ages give rise to stage 1 iNKT by calculating the ratio of stage 1 iNKT cells to DP thymocytes. Consistent with previous reports, our results indicate a peak in iNKT cell potential between 2 and 4 weeks of age, followed by a sharp decline (Fig. 5, D and E). Thus, our data point toward a higher iNKT cell potential in DP thymocytes of embryonic or neonatal HSPC origin.

Increased numbers of thymic PLZF$^+$ innatelike T cells can produce large amounts of IL-4 and thereby promote thymic development of Eomesodermin (Eomes)$^+$ memory-like CD8$^+$ T cells, characterized by high surface expression of CD44 and low surface expression of CD24 (*30*–*32*). This phenomenon is not normally detectable in adult wild-type C57BL/6 mice because of the infrequency of PLZF$^+$ thymocytes in this strain (*31*, *33*). However, we observed a significant increase in memory-like CD8$^+$ T cells among both GFP$^+$ and GFP$^-$ thymocytes in Lin28-RV BM chimeras but not in the GFP-RV control chimeras (fig. S10). This result demonstrates the ability of Lin28-induced PLZF$^+$ innatelike T cells to support the differentiation of memory-like CD8$^+$ T cells within the thymus and is consistent with the well-characterized IL4-mediated bystander effect that is not cell intrinsic (*34*).

Ectopic Lin28 confers fetal-like signatures to adult LSK HSPCs. It has been reported that the potential to develop into innatelike lymphocytes is intrinsically programmed in HSCs (*5*, *11*). Therefore, we performed cell cycle and gene expression analyses to look for Lin28-induced fetal characteristics in the BM HSCs of Lin28-RV chimeras. Cell cycle analysis of Lin28-RV–transduced BM HSPCs in culture compared with controls did not reveal any significant differences (fig. S11B). However, this is an artificial system that is highly mitogenic for HSPCs. Furthermore, a number of surface markers, including CD34, CD93 (AA4.1), and CD11b, are preferentially expressed on FL HSCs, likely because of their heightened proliferative state (*35*–*40*). We did not detect any Lin28-induced changes in the expression of these markers, nor that of endothelial cell-selective adhesion molecule (ESAM), CD48, and Tie-2 within the LSK HSC compartment in Lin28-RV chimeras (fig. S12A). Taken together, our results suggest that ectopic Lin28 does not grossly affect the cell intrinsic proliferative capacity or the overall composition of the adult LSK HSC compartment

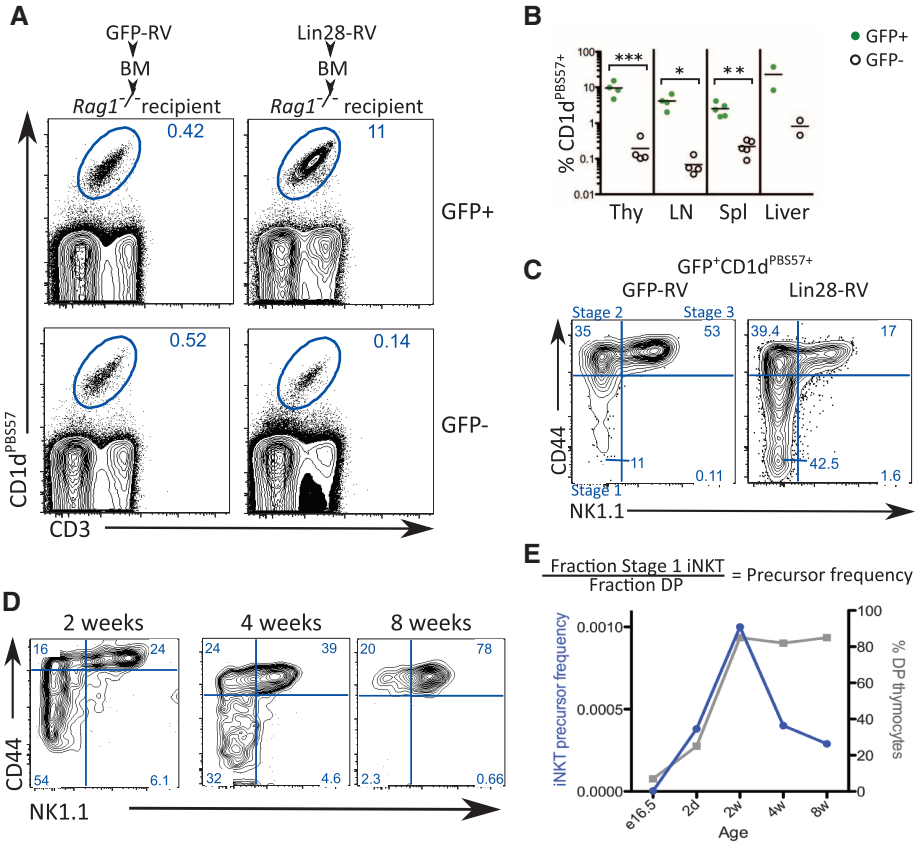

Fig. 5. Ectopic Lin28 expression in adult BM HSPCs promotes the development of iNKT cells. (**A**) Plots depict flow cytometric analysis of thymic iNKT cells defined by double staining of CD1d tetramer loaded with PBS57 (CD1d^{PBS57+}) and antibody against CD3 in GFP-RV and Lin28-RV BM chimeras. (**B**) Percentages of iNKT cells among the GFP$^+$ and GFP$^-$ cells in the indicated organs from Lin28-RV BM chimeras. *P < 0.05; **P < 0.01; ***P < 0.005. Indicated P values represent statistical significance calculated by t test. (**C**) Plots depict flow cytometric analysis of developmental stages 1 to 3 within the iNKT cell compartment among GFP$^+$CD1d^{PBS57+}CD3$^+$ thymocytes in GFP-RV (left) and Lin28-RV BM chimeras (right). Stage 1 (CD44$^-$NK1.1$^-$), 2 (CD44$^+$NK1.1$^-$), and 3 (CD44$^+$NK1.1$^+$). (**D**) Plots depict flow cytometric analysis of developmental stages 1 to 3 iNKT cells in the thymi of intact wild-type C57BL/6 mice of the indicated age. (**E**) Precursor frequency analysis shows iNKT cell potential as a function of age. Left y axis (blue line) indicates the ratio of stage 1 to DP thymocytes in intact C57BL/6 mice of the indicated age (equation shown above graph). Right y axis (gray line) indicates the percentage of DP thymocytes.

and that increased proliferation alone cannot account for the fetal-like developmental potential of HSPCs.

To characterize the effect of ectopic Lin28 on the long-term competence of HSCs, we performed FACS and QRT-PCR analysis of known long-term reconstituting (LT) HSC markers on GFP^+ and GFP^- LSK HSCs from aged Lin28-RV and GFP-RV BM chimeras 10 months after transplantation. CD150 surface expression marks LT HSCs (*41*), and *Mecom* (Evi1) and *Tal1* encode for transcription factors critical in regulating HSC quiescence and long-term competence (*42*, *43*). The presence of GFP^+ Lin28-RV–transduced LSK HSCs 10 months after adoptive transfer, along with comparable expression of surface CD150 protein and *Evi1* and *Tal1* mRNA between Lin28-RV and control LSK HSCs, suggests that ectopic Lin28 does not interfere with LT HSCs (fig. S12).

Hmga2 and *Igf2* have been reported to be targets of the Lin28–let-7 axis (*44*–*46*). Consistent with the finding that Lin28b is critical in conferring fetal HSPC identity, both *Hmga2* and *Igf2* are highly expressed in fetal but not adult HSCs (*47*). To assess whether ectopic Lin28 confers a fetal-like gene expression profile in adult BM HSCs, we performed QRT-PCR of FACS-sorted LSK HSCs and detected marked enhancement in the expression of both genes in the GFP^+ fraction from Lin28-RV BM chimeras (fig. S12B). Collectively, these results demonstrate the ability of ectopic Lin28 expression to confer fetal-like gene expression signatures in LSK HSCs.

In summary, these results identify *Lin28b* expression as a key molecular feature distinguishing fetal from adult BM HSPCs in mice and humans, which sheds new understanding on a long-standing question in the field of lymphocyte development (fig. S13). We demonstrate that ectopic expression of Lin28 in adult murine BM HSPCs dramatically skews the lymphocyte repertoire toward the production of innatelike lymphocyte subsets. Thus, we propose that *Lin28b* is a master regulator gene for fetal HSPC identity that is capable of reprogramming adult BM HSPCs to acquire fetal-like characteristics in a cell autonomous manner. As a result, *Lin28b* is a switch that turns on the development of major subsets of innatelike lymphocytes. Together, these findings highlight how posttranscriptional regulation of gene expression can be pivotal in determining cell-fate decisions.

Our findings have potential clinical implications for improving the reconstitution of innatelike lymphocyte populations on adult BM transplantation. Most HSC transplants utilize adult BM, and it is not known whether B-1 and MZ B cells develop after hematopoietic reconstitution. Because of the scarcity and ethical limitations of human fetal HSCs, they have not been seriously considered for clinical use. Umbilical cord blood is used clinically, but typically contains too few HSCs to reconstitute an adult (*48*). In the mouse, innatelike B-1 cell subsets play a role in T-independent host defense against pathogens such as *Streptococcus pneumoniae* (*49*); protective innate response activator B cells that produce granulocyte-macrophage colony-stimulating factor differentiate from B-1a cells during sepsis (*50*); $V\delta6.3^+$ γδ-T cells provide critical protection against *Listeria monocytogenes* (*51*). Furthermore, the ability of iNKT cells to produce large amounts of cytokines, including interferon-γ, IL-4, and tumor necrosis factor, allows them to modulate a broad spectrum of diseases, including cancer, graft rejection, autoimmunity, and infectious diseases (*52*). Thus, given the growing awareness of the ability of innatelike lymphocytes to influence immunity, it is of clinical interest to determine whether fetal-like HSCs can more effectively achieve reconstitution of the full continuum of the innate and adaptive immune system.

References and Notes

1. K. Kikuchi, M. Kondo, *Proc. Natl. Acad. Sci. U.S.A.* **103**, 17852 (2006).
2. M. B. Bowie *et al.*, *Proc. Natl. Acad. Sci. U.S.A.* **104**, 5878 (2007).
3. L. A. Herzenberg, L. A. Herzenberg, *Cell* **59**, 953 (1989).
4. K. Ikuta, I. L. Weissman, *J. Exp. Med.* **174**, 1279 (1991).
5. K. Ikuta *et al.*, *Cell* **62**, 863 (1990).
6. R. R. Hardy, K. Hayakawa, *Proc. Natl. Acad. Sci. U.S.A.* **88**, 11550 (1991).
7. A. B. Kantor, A. M. Stall, S. Adams, L. A. Herzenberg, L. A. Herzenberg, *Proc. Natl. Acad. Sci. U.S.A.* **89**, 3320 (1992).
8. M. Yoshimoto *et al.*, *Proc. Natl. Acad. Sci. U.S.A.* **108**, 1468 (2011).
9. A. Bendelac, M. Bonneville, J. F. Kearney, *Nat. Rev. Immunol.* **1**, 177 (2001).
10. R. D. Garman, P. J. Doherty, D. H. Raulet, *Cell* **45**, 733 (1986).
11. C. L. Barber, E. Montecino-Rodriguez, K. Dorshkind, *Proc. Natl. Acad. Sci. U.S.A.* **108**, 13700 (2011).
12. I. Kim, T. L. Saunders, S. J. Morrison, *Cell* **130**, 470 (2007).
13. S. Kuchen *et al.*, *Immunity* **32**, 828 (2010).
14. I. Heo *et al.*, *Cell* **138**, 696 (2009).
15. S. R. Viswanathan, G. Q. Daley, R. I. Gregory, *Science* **320**, 97 (2008).
16. E. Piskounova *et al.*, *J. Biol. Chem.* **283**, 21310 (2008).
17. E. Piskounova *et al.*, *Cell* **147**, 1066 (2011).
18. F. Jotereau, F. Heuze, V. Salomon-Vie, H. Gascan, *J. Immunol.* **138**, 1026 (1987).
19. S. Ranganath *et al.*, *J. Immunol.* **161**, 3822 (1998).
20. B. P. Lewis, C. B. Burge, D. P. Bartel, *Cell* **120**, 15 (2005).
21. A. Krek *et al.*, *Nat. Genet.* **37**, 495 (2005).
22. T. L. Carvalho, T. Mota-Santos, A. Cumano, J. Demengeot, P. Vieira, *J. Exp. Med.* **194**, 1141 (2001).
23. J. B. Carey, C. S. Moffatt-Blue, L. C. Watson, A. L. Gavin, A. J. Feeney, *J. Exp. Med.* **205**, 2043 (2008).
24. W. Haas, P. Pereira, S. Tonegawa, *Annu. Rev. Immunol.* **11**, 637 (1993).
25. K. Grigoriadou, L. Boucontet, P. Pereira, *J. Immunol.* **171**, 2413 (2003).
26. Y. J. Lee *et al.*, *J. Exp. Med.* **207**, 237 (2010).
27. K. Benlagha, T. Kyin, A. Beavis, L. Teyton, A. Bendelac, *Science* **296**, 553 (2002).
28. L. Gapin, J. L. Matsuda, C. D. Surh, M. Kronenberg, *Nat. Immunol.* **2**, 971 (2001).
29. A. Bendelac *et al.*, *Science* **268**, 863 (1995).
30. E. S. Alonzo, D. B. Sant'Angelo, *Curr. Opin. Immunol.* **23**, 220 (2011).
31. M. A. Weinreich, O. A. Odumade, S. C. Jameson, K. A. Hogquist, *Nat. Immunol.* **11**, 709 (2010).
32. M. Verykokakis, M. D. Boos, A. Bendelac, B. L. Kee, *Immunity* **33**, 203 (2010).
33. D. Lai *et al.*, *J. Exp. Med.* **208**, 1093 (2011).
34. M. A. Weinreich *et al.*, *Immunity* **31**, 122 (2009).
35. F. Tajima, T. Deguchi, J. H. Laver, H. Zeng, M. Ogawa, *Blood* **97**, 2618 (2001).
36. T. D. Randall, I. L. Weissman, *Blood* **89**, 3596 (1997).
37. V. I. Rebel *et al.*, *Exp. Hematol.* **24**, 638 (1996).
38. S. J. Morrison, H. D. Hemmati, A. M. Wandycz, I. L. Weissman, *Proc. Natl. Acad. Sci. U.S.A.* **92**, 10302 (1995).
39. C. T. Jordan, J. P. McKearn, I. R. Lemischka, *Cell* **61**, 953 (1990).
40. T. Ito, F. Tajima, M. Ogawa, *Exp. Hematol.* **28**, 1269 (2000).
41. M. J. Kiel *et al.*, *Cell* **121**, 1109 (2005).
42. J. Lacombe *et al.*, *Blood* **115**, 792 (2010).
43. K. Kataoka *et al.*, *J. Exp. Med.* **208**, 2403 (2011).
44. K. Ikeda, P. J. Mason, M. Bessler, *Blood* **117**, 5860 (2011).
45. C. Mayr, M. T. Hemann, D. P. Bartel, *Science* **315**, 1576 (2007).
46. A. Polesskaya *et al.*, *Genes Dev.* **21**, 1125 (2007).
47. M. J. Kiel, T. Iwashita, O. H. Yilmaz, S. J. Morrison, *Dev. Biol.* **283**, 29 (2005).
48. J. A. Brown, V. A. Boussiotis, *Clin. Immunol.* **127**, 286 (2008).
49. K. M. Haas, J. C. Poe, D. A. Steeber, T. F. Tedder, *Immunity* **23**, 7 (2005).
50. P. J. Rauch *et al.*, *Science* **335**, 597 (2012).
51. C. Belles *et al.*, *J. Immunol.* **156**, 4280 (1996).
52. D. I. Godfrey, M. Kronenberg, *J. Clin. Invest.* **114**, 1379 (2004).

Acknowledgments: We thank W. E. Paul for his generous support and advice throughout; T. Bender, J. Daniel, B. J. Fowlkes, R. Germain, M. Lenardo, W. E. Paul, and M. Schlissel for critical reading of this manuscript and constructive suggestions; K. Laky and B. J. Fowlkes for valuable advice and antibodies; NIH Tetramer Core Facility for reagents; M. Holt for NKT cell discussions; P. Burr for sequencing; J. Edwards and C. Eigsti for cell sorting; M. Foster for animal care; R. Zahr for technical support; and N. Bartonicek (EMBL-EBI, Hinxton, UK) for providing the RefSeq 3′UTR library for Sylamer analysis. We gratefully acknowledge the high-performance computational capabilities of the Biowulf Linux cluster at the NIH (http://biowulf.nih.gov) and NIAID Office of Cyber Infrastructure and Computational Biology High-Performance Computing cluster required for massively parallel sequencing analyses. The data reported in this paper are tabulated in the main text and in the Supporting Online Material. The RNA-Seq and NanoString data are available in the Gene Expression Omnibus (GEO) database (www.ncbi.nlm.nih.gov/geo) under the accession nos. GSE34854, GSE35081, and GSE35107. The materials and reagents used in the paper are available under a Materials Transfer Agreement. We apologize that we could not cite all the relevant references because of space limitations. The Integrative Immunobiology Unit is supported by the Intramural Research Program of the NIAID, NIH. The authors declare no competing financial interests.

Supporting Online Material

www.sciencemag.org/cgi/content/full/science.1216557/DC1
Materials and Methods
Figs. S1 to S13
Tables S1 and S2
References (*53*–*59*)

14 November 2011; accepted 1 February 2012
Published online 16 February 2012;
10.1126/science.1216557

Designing Responsive Buckled Surfaces by Halftone Gel Lithography

Jungwook Kim,[1] James A. Hanna,[2] Myunghwan Byun,[1] Christian D. Santangelo,[2]* Ryan C. Hayward[1]*

Self-actuating materials capable of transforming between three-dimensional shapes have applications in areas as diverse as biomedicine, robotics, and tunable micro-optics. We introduce a method of photopatterning polymer films that yields temperature-responsive gel sheets that can transform between a flat state and a prescribed three-dimensional shape. Our approach is based on poly(*N*-isopropylacrylamide) copolymers containing pendent benzophenone units that allow cross-linking to be tuned by irradiation dose. We describe a simple method of halftone gel lithography using only two photomasks, wherein highly cross-linked dots embedded in a lightly cross-linked matrix provide access to nearly continuous, and fully two-dimensional, patterns of swelling. This method is used to fabricate surfaces with constant Gaussian curvature (spherical caps, saddles, and cones) or zero mean curvature (Enneper's surfaces), as well as more complex and nearly closed shapes.

Soft materials are ideal for designing structures that reversibly change shape in response to stimuli. Techniques for fabricating and actuating responsive structures include swelling of patterned gels (*1*–*4*) and electroactive polymers (*5*), light-induced switching of liquid-crystal elastomers (*6*–*8*), actuation of dielectric elastomers on rigid frames (*9*), recovery of shape-memory polymers (*10*), and growth of muscle cells on compliant polymeric supports (*11*). An approach with great potential for the design of complex actuating structures is the buckling of thin sheets into three-dimensional (3D) shapes induced by spatially nonuniform growth, a common motif in biological morphogenesis (*12*–*16*). Because bending is less costly than compression for thin sheets, the nonuniform stresses developed as a result of patterned growth are relieved by out-of-plane deformation. Nevertheless, fundamental questions remain to be answered before this principle can be used as a practical means to form precise 3D structures. Chief among these is our incomplete understanding of how in-plane stresses translate to 3D shapes. Although nonuniform swelling is connected geometrically to Gaussian curvature (*17*), bending elasticity typically still plays an important role in determining the final structure (*18*, *19*). Surprisingly, some swelling patterns that should provide constant negative Gaussian curvature lead to wrinkling, even though they are not geometrically required to do so (*17*). In addition, swelling patterns exist for which in-plane stresses cannot be completely relieved by buckling; in such cases, the resulting shapes remain largely unexplored.

Efforts to understand shaping driven by nonuniform growth and to translate these principles into practical strategies for controlling the shapes of thin sheets were inspired nearly a decade ago by studies of the buckling of torn plastic sheets (*20*). More recently, Sharon and co-workers (*17*) developed a method wherein temporal control over the composition of a monomer solution introduced into a Hele-Shaw cell was used to write patterns in the shrinkage of a thermally responsive gel. Though an elegant step toward the design of materials with structures defined by patterned growth, this approach is limited to profiles that vary in only one direction, fundamentally restricting the 3D configurations that can be accessed. Thus, the need for strategies to print truly arbitrary patterns of expansion or contraction in synthetic materials has remained a central challenge for the field (*21*).

Here, we describe a solution to this challenge through an approach we call "halftone gel lithography," based on a simple two-mask lithographic patterning of photo-cross-linkable copolymer films. Even though the halftone swelling patterns yield in-plane stresses that cannot be eliminated entirely, we find that sufficiently thick sheets smooth out these sharp transitions and yield predictable 3D shapes. This method enables the prescription of effectively smooth swelling profiles on thin sheets with arbitrary 2D geometries, thereby providing access to complex 3D structures. This work opens the door not only to addressing fundamental questions surrounding growth-induced shaping of thin sheets but also to practical fabrication of responsive gel microdevices based on the principles of nonuniform growth.

Our method relies on a temperature-responsive *N*-isopropylacrylamide (NIPAm) copolymer containing photo-cross-linkable benzophenone (*22*) acrylamide (BPAm) units (Fig. 1A). Acrylic acid (AAc) comonomers are included to increase hydrophilicity, and rhodamine B methacrylate (RhBMA) facilitates imaging by fluorescence microscopy. Cross-linking is achieved by exposure of solution-cast copolymer films (with dry thicknesses $h \approx 7$ to 17 μm) to ultraviolet (UV) light (~360 nm), which activates the benzophenone units to form covalent cross-links between polymer chains. The key to spatially patterned swelling is that the conversion of BPAm to cross-links, and therefore the swelling of the material, can be tuned through the dose of UV. We characterize the material in terms of the equilibrium areal swelling ratio Ω, defined as the ratio of the area of a homogeneous film in the fully swelled state in aqueous solution (1 mM NaCl, 1 mM phosphate buffer; pH 7.2) to the area in the dry, as-cross-linked state. As shown in fig. S1, a small dose of UV light (0.2 J/cm^2) is sufficient to gel the polymer film and gives rise to the highest achievable swelling ratio of $\Omega_{high} = 8.2$ at 22°C, whereas maximum conversion of BPAm at a much larger dose (13.9 J/cm^2) leads to materials with substantially reduced swelling, $\Omega_{low} = 2.3$ at 22°C.

This material system provides considerable flexibility for generating swelling patterns on thin elastic sheets. Using traditional photomasks with high contrast between opaque and nearly transparent regions, a series of n different masks aligned in succession allows any region of the sheet to receive one of 2^n distinct irradiation doses. In some cases, simple patterns consisting of only a few discrete levels of swelling may be adequate to achieve the desired control of shape; however, this scenario is poorly understood compared to that of plates with smoothly varying metrics. The use of a large number of masks would allow for fine gradations in swelling, presumably allowing smooth metrics to be approximated, with the drawback that an increased number of mask alignment steps makes the process more difficult and less robust. Alternatively, true "grayscale" lithographic techniques could be employed to provide nearly continuous variations in light intensity through masked or maskless exposures, but these methods require complex lithographic processes or mask fabrication steps (*23*, *24*).

Instead, we focus on a simple approach inspired by the ubiquitous printing method of halftoning, wherein continuous variations in tone are simulated using only a few colors of ink. The process of halftone gel lithography is illustrated in Fig. 1, B to G. An initial photomask is used to define the overall shape of the object by providing a small dose of UV light that sets the swelling of the material to Ω_{high}. A second mask is used to define a pattern of circular dots of diameter d that are extensively cross-linked to restrict their swelling to Ω_{low}. We use a hexagonal lattice of dots with a lattice spacing a that is held constant on any given sheet, while d is varied in space, thus allowing nearly continuous changes in swelling to be printed in 2D. Whereas traditional halftone printing takes advantage of the

[1]Polymer Science and Engineering, University of Massachusetts, Amherst, MA 01003, USA. [2]Department of Physics, University of Massachusetts, Amherst, MA 01003, USA.

*To whom correspondence should be addressed. E-mail: csantang@physics.umass.edu (C.D.S.); rhayward@mail.pse.umass.edu (R.C.H.)

limited resolution of the human eye to provide the illusion of a homogeneous tone from closely spaced dots, our approach relies on the elasticity of the thin polymer sheet to locally smooth out the sharp contrast between the highly cross-linked dots and lightly cross-linked matrix, thereby yielding an intermediate degree of swelling.

To calibrate the method, we first explore the swelling of disks with dots of uniform diameter. As indicated in Fig. 1H, these disks show globally homogeneous swelling by an amount Ω that can be continuously tuned between the two extremes Ω_{low} and Ω_{high} by changing the area fraction of low-swelling regions, defined for $d \leq a$ as

$$\phi_{low} = \frac{\pi}{2\sqrt{3}}\left(\frac{d}{a}\right)^2 \quad (1)$$

Given that Ω is largely insensitive to ϕ_{low} beyond the point when neighboring dots begin to touch—that is, at $\phi_{low} \geq 0.91$—for simplicity we restrict dot sizes to $d \leq a$ without appreciably restricting the accessible range of swelling.

A simple model to describe swelling comes from considering the two gel regions as lumped 1D elements in parallel [see the supporting online material (SOM) for details], yielding the prediction

$$\frac{\phi_{low} + \alpha(1-\phi_{low})}{\Omega^{1/2}} = \frac{\phi_{low}}{\Omega_{low}^{1/2}} + \frac{\alpha(1-\phi_{low})}{\Omega_{high}^{1/2}} \quad (2)$$

where α is the ratio of the elastic moduli in the two material regions. Although this model captures the essential qualitative physics of mutually constrained swelling, it is too simple to yield quantitative agreement with material properties; thus, in practice α is treated as a fitting parameter. As shown in Fig. 1H, a value of $\alpha = 0.56$ provides a good fit to the observed swelling of halftoned composite gels. As expected based on the well-known temperature sensitivity of NIPAm copolymers, at each value of ϕ_{low} the composite disks deswell with increasing temperature, as shown in Fig. 1I. However, since the lightly cross-linked regions show more pronounced deswelling, the values of swelling converge to a narrow range between 1 and 2 at 45° to 50°C.

Whereas the composite disks described in Fig. 1 behave as homogeneous materials on length scales longer than the lattice dimension, the compressive stresses present in the lightly cross-linked matrix may cause local buckling when the disks are made sufficiently thin. To prevent this, we expect that the length scale of the lattice should not be much larger than h. Indeed, when we vary the dot size and spacing at constant $\phi_{low} = 0.4$, we find a critical lattice spacing, $a_c = (7.9 \pm 0.8)h$, below which the sheets remain flat and above which the high-swelling regions form buckled ridges spanning neighboring dots (Fig. 1J). Although the prefactor relating a_c and h will depend somewhat on ϕ_{low}, for the remainder of the discussion we will keep $a \leq 4h$, which is sufficient to avoid local buckling in all cases.

Having established that halftoning provides access to nearly continuous variations in swelling for disks with homogeneous dot sizes, we next consider the printing of spatially varying, axisymmetric, patterns of growth corresponding to target shapes with constant Gaussian curvature K, as shown in Fig. 2, A to D. Following Sharon and co-workers (*17*, *18*, *21*), we refer to $\Omega(\mathbf{r})$ as the "target metric" encoding the local equilibrium distances between points on the surface. A sheet of vanishing thickness should adopt the isometric embedding of this target metric with the lowest bending energy (*18*), provided that such an embedding exists. Written in terms of the coordinates on the flat, unswelled gel sheet, the target curvature at a material point $\mathbf{r}$ is set by the swelling factor $\Omega(\mathbf{r})$ according to Gauss's *theorema egregium*, $K = -\nabla^2 \ln\Omega/(2\Omega)$ (*25*). Thus, where r represents the radial position in a cylindrical coordinate system and c, R, and β are constants, swelling factors of the form

$$\Omega(r) = c\left(\frac{r}{R}\right)^{\beta} \quad (3)$$

should yield $K = 0$, whereas those of the form

$$\Omega(r) = \frac{c}{[1 + (r/R)^2]^2} \quad (4)$$

should yield constant $K = 4/(cR^2)$. Figure 2F shows four example metrics: a piece of a saddle surface with $K = -16.8$ mm^{-2}, a cone with an excess angle (*26*) specified by a swelling power-law exponent $\beta = 1$, a spherical cap with $K = 5.7$ mm^{-2}, and a cone with a deficit angle specified by $\beta = -0.4$. The corresponding patterns of dots were computed by evaluating the value

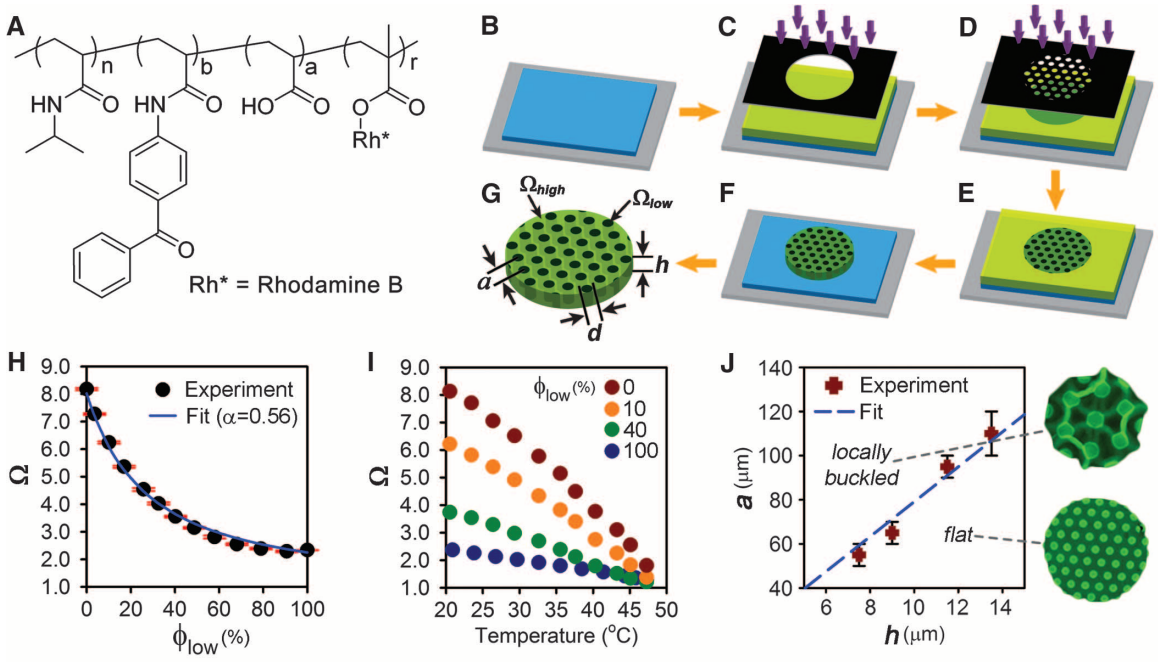

Fig. 1. Halftone gel lithography and characterization of composite disks. (**A**) Chemical structure of the photo-cross-linkable and temperature-responsive NIPAm copolymer. (**B** to **G**) A schematic illustration of halftone gel lithography. (B) On a silicon wafer coated with a sacrificial layer, (C) the copolymer film (thickness h = 7 to 17 μm) is solution-cast and exposed to a small dose of UV light through the first photomask and subsequently (D) a large dose through the second photomask. (E) The patterned film is (F) developed to remove uncross-linked material and (G) immersed in aqueous solution to release it from the substrate and induce swelling. (**H**) The areal expansion ratio Ω of composite disks at 22°C is plotted against the area fraction of dots ϕ_{low}. Experimental data (black solid circles) are fitted with Eq. 2 (blue line). The error bars denote standard deviations for six independent measurements. (**I**) The temperature dependence of Ω of the composite disks is shown for four different values of ϕ_{low}. (**J**) Below a thickness-dependent critical lattice spacing a_c, disks remain flat, whereas above a_c they undergo local buckling between neighboring dots. The value of a_c is plotted for a range of film thicknesses (symbols), along with a least squares fit of a linear relationship with zero intercept (dashed line).

of $\Omega(r)$ at each lattice point according to Eqs. 3 and 4, determining the corresponding value of ϕ_{low} from the fit of Eq. 2 to the data in Fig. 1H, and finally setting the size of the dot at that lattice point according to Eq. 1. Because the power-law metrics in Eq. 3 diverge or vanish at the origin, it is necessary to cut out a small region around the center of each of the two cones.

The shapes adopted by the corresponding gel sheets (Fig. 2, A to D) are measured by laser scanning confocal fluorescence microscopy (LSCM) and analyzed as described in the SOM. Each of the four surfaces shows only small deviations about an average Gaussian curvature, with the exception of the regions near the free edges, where our analysis yields artifactual curvatures (due to the finite thickness of the gel sheets, the surface meshing procedure used yields additional points on the edges that do not accurately reflect the 2D geometries of the sheets). After excluding regions of the surface within $2h$ of the edges to avoid these artifacts, we find the average Gaussian curvatures of the spherical cap and saddle to be 6.2 mm^{-2} and –20.6 mm^{-2}, respectively, with nearly axisymmetric distributions of curvature (fig. S2A). Both values are in reasonable agreement with the target values, although the tendency of disks with uniform dot sizes to show slight curvatures (with radii of 2 mm) suggests the presence of slight through-thickness variations in swelling (see SOM for details) that may contribute to the observed deviations from the programmed curvature. Interestingly, we do not observe a boundary layer with negative Gaussian curvature around the edge of the spherical cap as has been reported for truly smooth metrics (*17*, *18*), possibly reflecting the influence of the through-thickness variations in swelling. For both cones, the average Gaussian curvatures, excluding regions at the free edges, are close to zero. Further, Fig. 2E shows a plot of the deficit angle δ measured for five different cone metrics with power law exponents $-1 \le \beta < 0$, which agrees closely with the programmed value $\delta = -\pi\beta$.

We next consider metrics of the form

$$\Omega(r) = c[1 + (r/R)^{2(n-1)}]^2 \qquad (5)$$

corresponding to Enneper's minimal surfaces with n nodes. These surfaces all have zero mean curvature and so are expected to minimize the elastic energy for these metrics at vanishing thickness (*18*). Although Eq. 5 is axisymmetric, Enneper's surfaces spontaneously break axial symmetry by forming n wrinkles. In Fig. 2, G to J, we demonstrate patterned surfaces with n = 3 to 6, each of which reproduces the targeted number of wrinkles. As shown in the maps of curvature in Fig. 2 (and azimuthally averaged plots in fig. S2B), each surface has small mean curvature and negative Gaussian curvature that matches closely with the target profile. For a given film thickness, increasing n eventually leads to a saturation in the number of wrinkles, because the bending energy arising from Gaussian curvature increases with n (for the films with $h \approx 7$ μm in Fig. 4, a metric with $n = 8$ yielded only six wrinkles). However, given the subtle differences between the metrics plotted in Fig. 2F, the ability to accurately reproduce the programmed number of wrinkles for n = 3 to 6 is a strong testament to the fidelity of the metrics patterned by this technique.

The true power of our approach lies in the fabrication of nonaxisymmetric swelling patterns. As a simple demonstration, we first consider the problem of how to form a sphere through growth. For the axisymmetric metric described in Eq. 4, the maximum value of r/R to which this metric can be experimentally patterned is restricted by the accessible range of swelling. In our case, this range is $\Omega_{high}/\Omega_{low} \approx 3.7$, limiting the maximum portion of a sphere that can be obtained to slightly less than half. Although further improvements in the material system are likely to increase the available range, the axisymmetric metric is inherently an inefficient way to form a sphere, because as one seeks to go beyond a hemisphere and toward a closed shape, the required swelling contrast diverges rapidly. Given access to 2D metrics, however, a number of well-established conformal mappings of the sphere onto flat surfaces are known from the field of map projections. For example, the Peirce quincuncial projection (*27*) maps a sphere of radius R onto a square using the metric

$$\Omega(x,y) = 2\frac{\left|dn\left(\frac{x+iy}{R}\middle|\frac{1}{\sqrt{2}}\right)sn\left(\frac{x+iy}{R}\middle|\frac{1}{\sqrt{2}}\right)\right|^2}{\left[1+\left|cn\left(\frac{x+iy}{R}\middle|\frac{1}{\sqrt{2}}\right)\right|^2\right]^2} \qquad (6)$$

where sn, cn, and dn are Jacobi elliptic functions, and x and y are the components of $\mathbf{r}$. This metric still has four cusp-like singularities where $\Omega(\mathbf{r}) = 0$; however, one of its useful properties as a map projection is that only a small portion

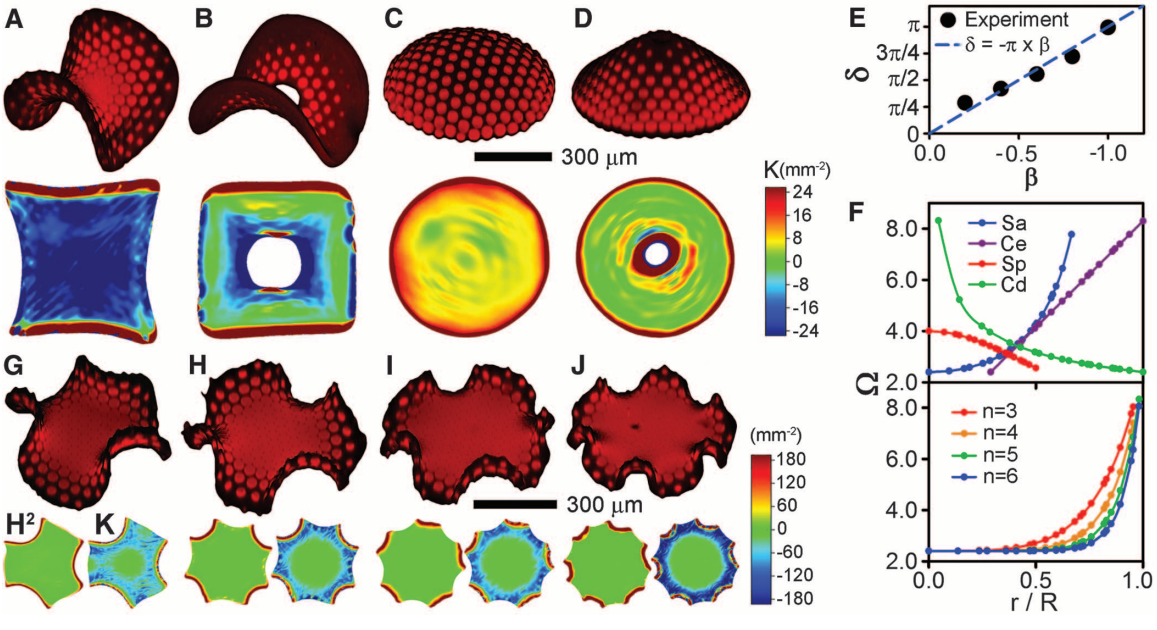

Fig. 2. Halftoned disks with axisymmetric metrics. Patterned sheets programmed to generate (**A**) a piece of saddle surface (Sa), (**B**) a cone with an excess angle (Ce), (**C**) a spherical cap (Sp), and (**D**) a cone with a deficit angle (Cd). (Top) 3D reconstructed images of swollen hydrogel sheets and (bottom) top-view surface plots of Gaussian curvature. Initial thicknesses and disk diameters are 9 and 390 μm, respectively, although the apparent thickness of sheets is enlarged due to the resolution of the LSCM. (**E**) Measured values of deficit angle δ for cones with five different exponents β (see Eq. 3) (black solid circles) and the programmed values (blue dashed line). (**F**) Swelling factors for the target metrics as a function of normalized radial position on the unswelled disks r/R, with points plotted at values corresponding to lattice points to indicate the resolution with which Ω is patterned. (**G** to **J**) Patterned sheets programmed to generate Enneper's minimal surfaces with n = (G) 3, (H) 4, (I) 5, and (J) 6 wrinkles upon swelling as dictated by Eq. 5. 3D reconstructed images (top) and top-view surface plots of squared mean curvature H^2 and Gaussian curvature K (bottom). Initial thicknesses and disk diameters are 7 and 390 μm, respectively.

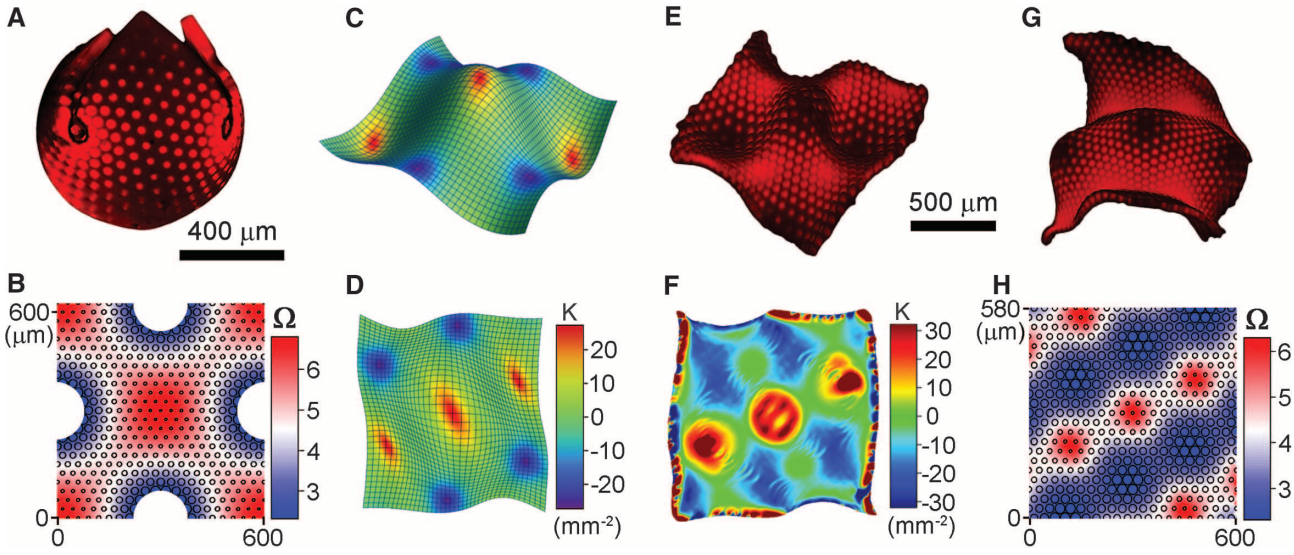

Fig. 3. Nonaxisymmetric swelling patterns. (**A**) A 3D reconstructed image of the nearly closed spherical shape formed by the metric of Eq. 6 and shown in (**B**); the sizes and positions of open circles correspond to those of the low-swelling dots. Before swelling, the patterned gel sheet was 9 μm thick, with lateral dimensions of 600 by 620 μm. (**C**) The target height profile of the corrugated surface, also shown in (**D**) top view. The grid represents the coordinate lines of the conformal coordinate system. (**E**) 3D reconstructed image and (**F**) Gaussian curvature of the sheet swollen into a shape similar to the target surface. (**G**) 3D reconstructed image of the shape adopted when each of the three regions of positive curvature along the center diagonal buckle in the same direction. (**H**) The swelling pattern used to generate sheets in (E) to (G). The sizes and positions of open circles correspond to those of the low-swelling dots. Before swelling, the patterned gel sheets were 9 μm thick and had lateral dimensions of 600 by 580 μm.

of the area of the sphere requires large distortions. Thus, we can approximate the metric by excising the small regions of the square where Ω falls below the experimentally accessible range, as shown in Fig. 3B. The resulting swelled shape (Fig. 3A) does indeed approximate that of a sphere (see fig. S3 for plots of surface curvatures) with four small regions removed, although the four corners of the square do not quite close. The reason for the latter behavior remains under investigation but may arise from the excised singularities and/or the finite bending energy of the sheet. Nonetheless, the contrast between the nearly closed shape achieved in Fig. 3A and the limited spherical caps that may be obtained for the same material system with an axisymmetric metric highlights the importance of 2D patterning, even for generating axisymmetric shapes.

Beyond fabricating simple shapes with constant target Gaussian curvature, our approach opens the door to shapes of arbitrary complexity. Although numerous fundamental questions and practical challenges remain to establishing the necessary design rules, we take a first step toward the construction of shapes whose swelling factors are not known a priori by considering a corrugated surface (Fig. 3C) described by the height function $H(x,y) = H_0 [\cos(2\pi x/L) + \cos(\pi x/L + \sqrt{3}\pi y/L)]$, where $2L$ is the width of the sheet. We choose H_0 = 60 μm and L = 300 μm. Determining an appropriate swelling factor is equivalent to finding a conformal coordinate system on the surface (as described in the SOM) and yields the swelling function shown in Fig. 3H. This example highlights some of the remaining challenges in designing arbitrary 3D shapes, because sheets patterned according to Fig. 3H often fail to form the desired shape upon swelling. The three local maxima in growth, lying along the line cutting diagonally through the center of the sheet, each represent regions of positive target Gaussian curvature; however, each may achieve its desired local curvature by buckling either upward or downward. Indeed, rather than buckling in the manner described by $H(x,y)$, these local maxima in swelling may instead all buckle in the same direction, as shown in Fig. 3G (again, possibly reflecting a preference for buckling in one direction due to slight through-thickness variations in swelling). However, in some cases, the sheets do swell into the corrugated conformation shown in Fig. 3E, which is very similar to the programmed surface $H(x,y)$, as can also be seen by comparing the targeted (Fig. 3D) and measured (Fig. 3F) Gaussian curvatures. The use of a glass micropipette to hold the patterned sheet against the substrate during swelling (upon cooling from 40° to 22°C) tends to constrain the sheet to swell into the corrugated shape, and initially misfolded sheets can also be "snapped through" into the desired configuration by application of force to the center-most region of positive curvature. Thus, we conclude that such surfaces with complex swelling patterns may in general form multiple different shapes that are locally metastable and that additional constraints may therefore be required to ensure that a specific shape is chosen.

Finally, we demonstrate the responsiveness of the patterned sheets to changes in temperature using another nonaxisymmetric metric that combines that for an Enneper's surface with four

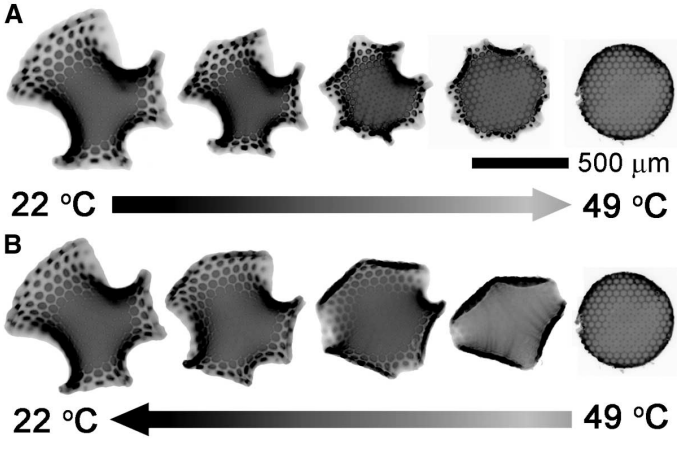

Fig. 4. Thermal actuation of patterned sheets. (**A**) When the temperature of the aqueous medium is increased, the hybrid Enneper's surface deswells and recovers its flat shape by 49°C. (**B**) Upon lowering the temperature to 22°C, the disk swells back to the initial hybrid shape through a different pathway. Initial thickness and disk diameter are 7 and 390 μm, respectively.

nodes along $0 < \theta < \pi$ with that for an Enneper's surface with two nodes along $\pi < \theta < 2\pi$. Remarkably, despite the sharp changes in the metric at $\theta = 0$ and π, the sheet does adopt the desired hybrid shape when swelled at room temperature, as shown in Fig. 4 (and as a movie in the SOM). As temperature is increased, Ω_{high} and Ω_{low} both decrease, but also converge, causing the buckled disc to first decrease in size and eventually flatten by 49°C. A subsequent decrease in temperature to 22°C causes the disc to regain its initial shape, although the progression of intermediate shapes is not the same. A more detailed study of the pathways and kinetics of swelling and deswelling is an interesting subject for future study.

In conclusion, we have demonstrated a simple method for halftone lithography of photo-cross-linkable copolymers that permits fabrication of stimulus-responsive gel sheets with micrometer-scale thicknesses and 2D patterned swelling. As long as the dots used to define the halftone pattern are smaller than several times the film thickness, the material behaves as a homogeneous elastic composite on length scales larger than the dot pattern. By patterning spatial variations in dot size, the degree of swelling of the composite gel sheets can be tuned effectively continuously across a wide range using only two high-contrast photomasks. This method provides access not only to simple radially symmetric metrics that yield shapes with nearly constant Gaussian curvature or almost zero mean curvature but also to truly 2D patterns of swelling. Thus, it represents a powerful method for fabricating stimuli-responsive gel micro-devices and studying fundamental questions about how 3D shapes are formed through differential growth in 2D.

References and Notes

1. Z. B. Hu, X. M. Zhang, Y. Li, *Science* **269**, 525 (1995).
2. J. R. Howse *et al.*, *Nano Lett.* **6**, 73 (2006).
3. B. Kaehr, J. B. Shear, *Proc. Natl. Acad. Sci. U.S.A.* **105**, 8850 (2008).
4. G. H. Kwon *et al.*, *Small* **4**, 2148 (2008).
5. E. W. H. Jager, E. Smela, O. Inganäs, *Science* **290**, 1540 (2000).
6. T. Ikeda, M. Nakano, Y. Yu, O. Tsutsumi, A. Kanazawa, *Adv. Mater. (Deerfield Beach Fla.)* **15**, 201 (2003).
7. M. Camacho-Lopez, H. Finkelmann, P. Palffy-Muhoray, M. Shelley, *Nat. Mater.* **3**, 307 (2004).
8. T. J. White *et al.*, *Soft Matter* **4**, 1796 (2008).
9. G. Kofod, W. Wirges, M. Paajanen, S. Bauer, *Appl. Phys. Lett.* **90**, 081916 (2007).
10. A. Lendlein, H. Jiang, O. Jünger, R. Langer, *Nature* **434**, 879 (2005).
11. A. W. Feinberg *et al.*, *Science* **317**, 1366 (2007).
12. P. B. Green, *Int. J. Plant Sci.* **153**, (S3), S59 (1992).
13. U. Nath, B. C. W. Crawford, R. Carpenter, E. Coen, *Science* **299**, 1404 (2003).
14. E. Sharon, M. Marder, H. L. Swinney, *Am. Sci.* **92**, 254 (2004).
15. J. Dervaux, M. Ben Amar, *Phys. Rev. Lett.* **101**, 068101 (2008).
16. H. Liang, L. Mahadevan, *Proc. Natl. Acad. Sci. U.S.A.* **108**, 5516 (2011).
17. Y. Klein, E. Efrati, E. Sharon, *Science* **315**, 1116 (2007).
18. E. Efrati, E. Sharon, R. Kupferman, *Phys. Rev. E Stat. Nonlin. Soft Matter Phys.* **80**, 016602 (2009).
19. M. A. Dias, J. A. Hanna, C. D. Santangelo, *Phys. Rev. E Stat. Nonlin. Soft Matter Phys.* **84**, 036603 (2011).
20. E. Sharon, B. Roman, M. Marder, G.-S. Shin, H. L. Swinney, *Nature* **419**, 579 (2002).
21. E. Sharon, E. Efrati, *Soft Matter* **6**, 5693 (2010).
22. R. Toomey, D. Freidank, J. Rühe, *Macromolecules* **37**, 882 (2004).
23. Z. Cui, J. Du, Y. Gu, *Proc. SPIE* **4984**, 111 (2003).
24. L. Erdmann, A. Deparnay, G. Maschke, M. Längle, R. Brunner, *J. Microlith. Microfab.* **4**, 041601 (2005).
25. M. do Carmo, *Differential Geometry of Curves and Surfaces* (Prentice Hall, New York, 1976).
26. M. M. Müller, M. B. Amar, J. Guven, *Phys. Rev. Lett.* **101**, 156104 (2008).
27. C. S. Peirce, *Am. J. Math.* **2**, 394 (1879).

Acknowledgments: We acknowledge stimulating discussions with M. M. Müller and E. Sharon at the Aspen Center for Physics, where part of this work was done. This research was funded by the Army Research Office through W911NF-11-1-0080 and the National Science Foundation through DMR-0846582, and made use of facilities supported by the NSF Materials Research Science and Engineering Center at the University of Massachusetts (DMR-0747756) and NSF grant BBS-8714235.

Supporting Online Material

www.sciencemag.org/cgi/content/full/335/6073/1201/DC1
Materials and Methods
SOM Text
Figs. S1 to S3
Movie S1
References (*28*–*34*)

14 October 2011; accepted 5 January 2012
10.1126/science.1215309

Coking- and Sintering-Resistant Palladium Catalysts Achieved Through Atomic Layer Deposition

Junling Lu,[1] Baosong Fu,[2] Mayfair C. Kung,[3] Guomin Xiao,[2] Jeffrey W. Elam,[1] Harold H. Kung,[3] Peter C. Stair[4,5]*

We showed that alumina (Al_2O_3) overcoating of supported metal nanoparticles (NPs) effectively reduced deactivation by coking and sintering in high-temperature applications of heterogeneous catalysts. We overcoated palladium NPs with 45 layers of alumina through an atomic layer deposition (ALD) process that alternated exposures of the catalysts to trimethylaluminum and water at 200°C. When these catalysts were used for 1 hour in oxidative dehydrogenation of ethane to ethylene at 650°C, they were found by thermogravimetric analysis to contain less than 6% of the coke formed on the uncoated catalysts. Scanning transmission electron microscopy showed no visible morphology changes after reaction at 675°C for 28 hours. The yield of ethylene was improved on all ALD Al_2O_3 overcoated Pd catalysts.

The two main routes to the deactivation of catalysts consisting of metal nanoparticles (NPs) adsorbed on metal oxide supports are coking (the blocking of the metal surface by the accumulation of carbon on the metal) and sintering (the formation of larger metal particles, which lowers overall surface area and activity). Catalyst deactivation is costly, because catalysts must be regenerated or replaced and because processes are shut down while these steps are taken (*1*). Efforts to solve these two problems have typically focused on one or the other individually, although they often occur simultaneously.

Coke formation (or carbon deposition) during hydrocarbon reactions (*2*–*4*) is often addressed by passivating the active metal with traces of sulfur, triphenylphosphites, tin, bismuth, *et al.* (*5*–*10*); formation of an alloy (*5*, *9*–*12*); or accelerated coke removal through gasification (*9*, *13*). The sintering of metal NPs at high temperatures, particularly above the Tammann temperature (half of the bulk melting point in degrees kelvin), has been prevented in a few cases through steric stabilization by an overlayer of inorganic oxide such as mesoporous silica (*14*, *15*), tin oxide (*16*), zirconia (*17*), or ceria (*18*). In these examples, oxide shells, tens of nanometers thick, are formed around the metal NPs by chemical vapor deposition, dendrimer encapsulation, or grafting. The shell thickness is often poorly controlled, which leads to a decrease in catalytic activity from mass transfer resistance associated with shells that are thicker than desired. None of the above methods has achieved simultaneous inhibition of coking and sintering of supported metal catalysts, while maintaining high catalytic activity in high-temperature applications.

We report that Al_2O_3 overcoats, with a thickness near 8 nm, on supported Pd catalysts can effectively inhibit coke formation and greatly improve the thermal stability of Pd at temperatures

[1]Energy Systems Division, Argonne National Laboratory, Argonne, IL 60439, USA. [2]School of Chemistry and Chemical Engineering, Southeast University, Nanjing, 211189, China. [3]Department of Chemical and Biological Engineering, Northwestern University, Evanston, IL 60208–3120, USA. [4]Department of Chemistry, Northwestern University, Evanston, IL 60208, USA. [5]Chemical Science and Engineering Division, Argonne National Laboratory, Argonne, IL 60439, USA.

*To whom correspondence should be addressed. E-mail: pstair@northwestern.edu

in excess of its Tammann temperature. The Al_2O_3 overcoats were synthesized with precise thickness control by means of atomic layer deposition (ALD) (*19*), a self-limiting growth process for depositing highly conformal thin films on surfaces regardless of whether the materials are flat or possess high-aspect-ratio features, high surface area, or high porosity (*20*–*22*). Surface area measurements [nitrogen isotherm or Brunauer-Emmett-Teller (BET) measurements] and CO chemisorption indicate that the overcoated Pd NPs become accessible to reagent gases through the development of microporosity inside the overcoating layer after high-temperature treatments. When tested for the catalytic oxidative dehydrogenation of ethane (ODHE), which has a documented susceptibility to heavy coke formation at high oxygen conversions (*23*, *24*), the overcoating greatly reduced catalyst deactivation by coking and sintering at high temperatures. In addition, the ethylene yield was increased by more than a factor of 10.

The ALD Al_2O_3 overcoating was carried out in a viscous flow reactor by alternately exposing the sample to cycles of trimethylaluminum and water at 200°C (*19*, *25*). Overcoats with 45 cycles were applied to a conventional Pd/Al_2O_3 catalyst with a particle size of 2.8 ± 0.52 nm ($45Al/Pd/Al_2O_3$), synthesized by wet impregnation onto γ-Al_2O_3. The overcoat thickness was 7.7 ± 0.4 nm, according to high-resolution transmission electron microscope measurements [figs. S1 and S2 (*19*)]. The Pd loadings before and after overcoating, as determined by inductively coupled plasma atomic emission spectroscopy, were 1.88 and 1.03%, respectively.

ODHE was conducted using a feed stream containing ethane and oxygen at a ratio of 3:1. The activities of the catalyst with and without ALD Al_2O_3 overcoating were compared by using the same weight of metal in the reactor. The reaction tests were conducted in a quartz tube reactor, with the void space packed with fine quartz chips to suppress homogeneous gas-phase reactions. The catalyst, diluted with 1 g of fine quartz chips, was heated in a stream of 10% oxygen in helium at a ramp rate of 2°C/min to 700°C and held at that temperature for 120 min before the ODHE reaction test. The flow rates of ethane, oxygen, and helium were 9, 3, and 38 standard cubic centimeters per minute (sccm), respectively (*19*).

At 675°C, the initial ethane and oxygen conversions were 55 and 100%, respectively, for the uncoated Pd/Al_2O_3 sample after being stabilized for 10 min. This catalyst demonstrated a very poor performance (Fig. 1); the major products were CO and CO_2, at a yield of 12 and 6%, respectively, whereas the yield of the desired product, ethylene, was only 1.9%. All product yields quickly decreased to zero in less than 30 min when the reactor was completely plugged by coke and the reaction stopped, consistent with previous reports (*23*, *24*).

The Pd sample overcoated with 45 cycles of ALD Al_2O_3 demonstrated some decrease in activity: Ethane and oxygen conversions were 37 and 99% at a steady state, respectively. However, this catalyst showed dramatic improvements in performance, with an increased yield of ethylene and stable activity for ~1700 min [Fig. 1 and fig. S3 (*19*)]. The yield of ethylene, which was initially 12% and then gradually increased to a steady state of 23% after about 500 min, is competitive with the best catalysts for ODHE reported (*26*–*29*). The yields of undesired products—CO, CO_2, and CH_4—were suppressed and were stable at 5.1, 3.9, and 0.9%, respectively. The increased yield of CO relative to CO_2 most likely results from the reverse water gas shift (WGS) reaction and from CO_2- and H_2O-facilitated dehydrogenation in this oxygen-depleted environment (*26*, *30*).

We quantified the reduced coke formation by the ALD Al_2O_3 overcoat using in situ thermogravimetric analysis under reaction conditions with a flow of ethane (10.5 sccm), oxygen (3.5 sccm), and helium (66.5 sccm) over the catalyst at 650°C. For the uncoated Pd/Al_2O_3 sample, 11.83 mg of coke was formed on 20 mg of sample after 60 min of reaction. For $45Al/Pd/Al_2O_3$, the deposited coke was reduced by 94% to only 0.40 mg [fig. S4 (*19*)]. Inhibition of coke formation on $45Al/Pd/Al_2O_3$ as compared with the

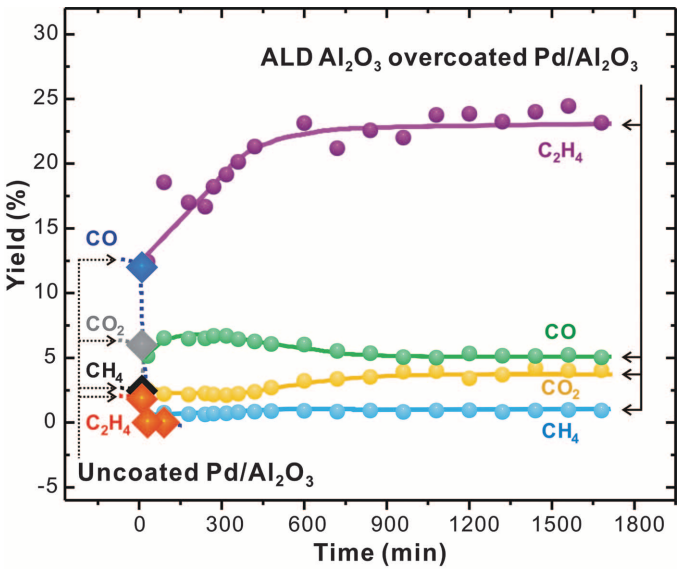

Fig. 1. Products yield on the Pd/Al_2O_3 samples with and without ALD Al_2O_3 overcoat during ODHE reaction as a function of reaction time under identical reaction conditions. Diamonds with a dashed line, product yields on the uncoated Pd/Al_2O_3 sample; circles with solid lines, product yields on the $45Al/Pd/Al_2O_3$ sample.

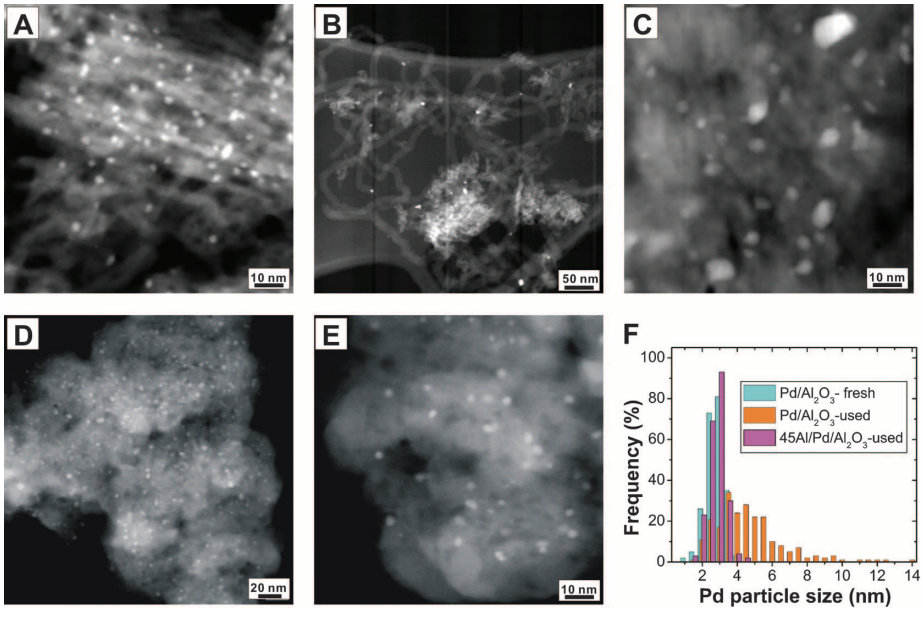

Fig. 2. STEM images of fresh and used samples after ODHE reaction testing. (**A**) The fresh Pd/Al_2O_3 sample. (**B** and **C**) The used Pd/Al_2O_3 sample at 675°C for 30 min at low (B) and high (C) magnification. (**D** and **E**) The used $45Al/Pd/Al_2O_3$ sample at 675°C for ~1700 min at low (D) and high (E) magnification. (**F**) Pd particle size distributions of these three samples.

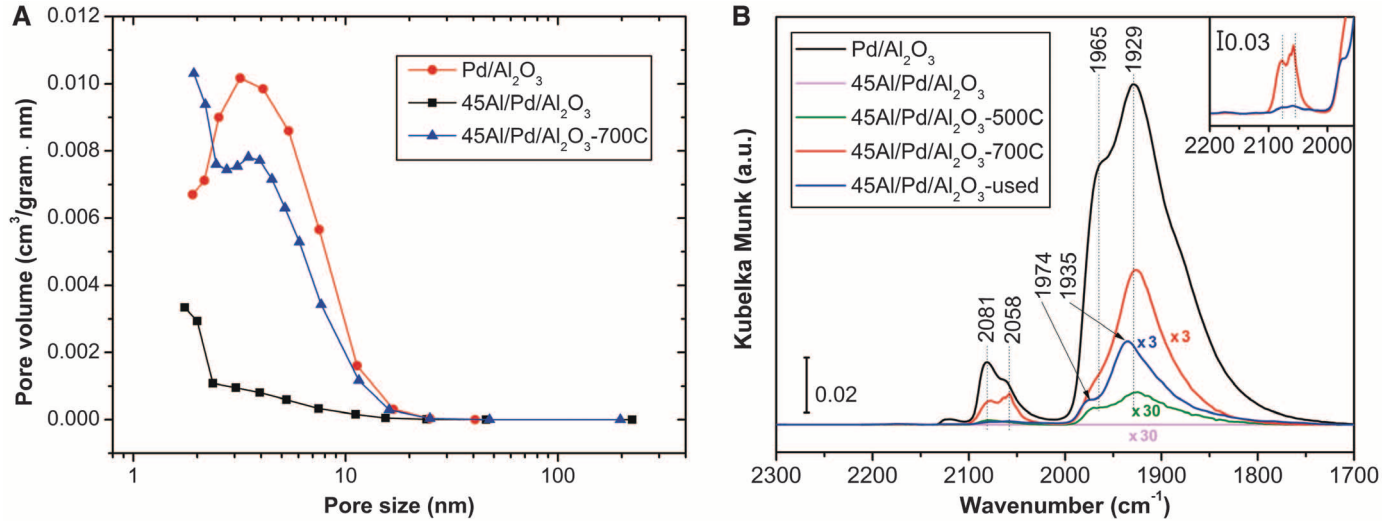

Fig. 3. Structural characterization of ALD Al_2O_3 overcoats and accessibility of embedded Pd NPs after high-temperature treatments. (**A**) Pore size distribution calculated from the adsorption branch of BET isotherms: the uncoated Pd/Al_2O_3, fresh $45Al/Pd/Al_2O_3$, and $45Al/Pd/Al_2O_3$-700C samples. (**B**) IR spectra of CO chemisorption on the Pd samples with and without ALD Al_2O_3 overcoats at the CO saturation coverage: the uncoated Pd/Al_2O_3, fresh $45Al/Pd/Al_2O_3$, $45Al/Pd/Al_2O_3$-500C, $45Al/Pd/Al_2O_3$-700C, and $45Al/Pd/Al_2O_3$-used samples. IR absorbance is in arbitrary Kubelka-Munk units. The inset is the higher–wave number region for the $45Al/Pd/Al_2O_3$-700C and $45Al/Pd/Al_2O_3$-used samples, showing the near-absence of edge and corner sites after reaction.

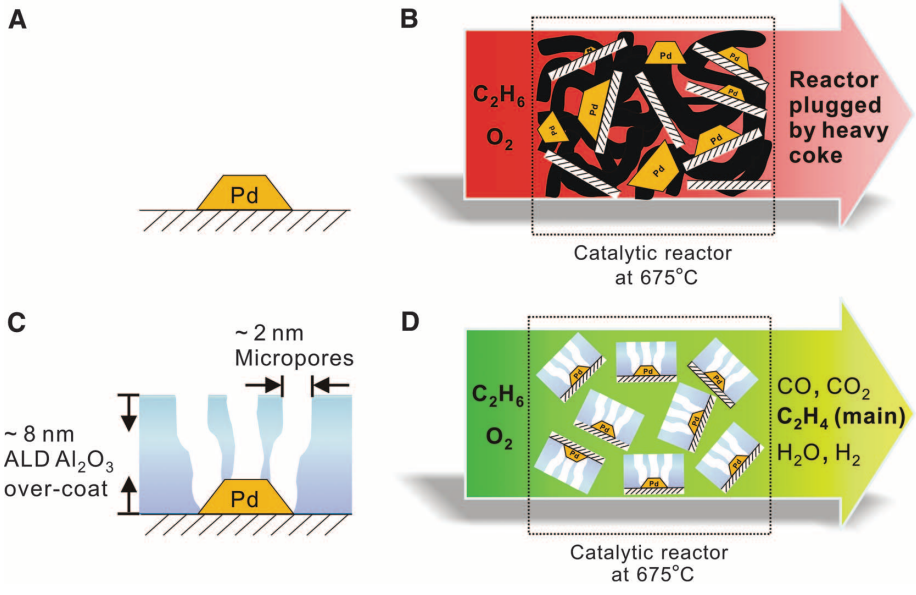

Fig. 4. A schematic model of Pd/Al_2O_3 catalysts with and without ALD Al_2O_3 overcoat during ODHE reaction at 675°C. (**A**) The uncoated Pd/Al_2O_3 catalyst. (**B**) The uncoated Pd/Al_2O_3 catalyst during ODHE reaction, in which filamentous carbon (thick black lines) plugged the reactor and there was substantial sintering and leaching of Pd NPs from the support (barred white lines). (**C**) The Pd catalyst with an ~8-nm ALD Al_2O_3 overcoat, which contained ~2-nm micropores after activation. (**D**) The ALD Al_2O_3–overcoated Pd/Al_2O_3 catalyst during ODHE reaction, on which the microporous Al_2O_3 overcoat trapped and stabilized the Pd NPs, inhibiting Pd NP leaching and coke formation, while greatly enhancing ethylene formation.

uncoated catalyst explains the maintenance of high activity at 675°C in Fig. 1.

The effect of overcoating on the thermal stability of Pd particles was determined from particle size measurements in fresh and used catalysts, using scanning TEM [(STEM), with a JEOL JEM-2100F microscope]. For the used uncoated Pd/Al_2O_3 catalyst, a large amount of filamentous carbon was observed, consistent with coke formation during the ODHE reaction (Fig. 2B). Leaching of Pd NPs from the Al_2O_3 support driven by filamentous carbon growth was also observed (Fig. 2B) (*2*–*4*). After only 30 min of reaction at 675°C, the Pd NPs also became substantially larger, with a much broader particle size distribution due to sintering (4.6 ± 1.92 nm, Fig. 2, B, C, and F). However, the Pd particle size on the $45Al/Pd/Al_2O_3$-used catalyst (2.8 ± 0.46 nm, Fig. 2, D to F) was essentially unchanged after ~1700 min of reaction at 675°C. We determined that 45 cycles of ALD Al_2O_3 were required to stabilize Pd NPs under these high-temperature reaction conditions, because some sintering was observed after reaction on a catalyst coated with only 30 cycles of ALD Al_2O_3 [figs. S9 to S11 (*19*)].

The porosity of the ALD Al_2O_3 overcoats after high-temperature pretreatment was determined by nitrogen BET measurements (with an ASAP 2020 analyzer, Micromeritics). In order to measure the changes in surface area and pore size distribution, the quantity of adsorbed nitrogen and the surface area were normalized based on the weight of the starting catalyst, Pd/Al_2O_3. The BET surface area decreased from 253 to 30 m^2/gram on the freshly coated material [figs. S5 and S6 (*19*)]. Calcining at 700°C for 120 min in 10% oxygen in helium, followed by reduction in 5% hydrogen in helium at 300°C for 30 min ($45Al/Pd/Al_2O_3$-700C), restored the BET surface area to 213 m^2/gram [fig. S7 (*19*)]. Figure 3A shows that the initial, uncoated Pd/Al_2O_3 catalyst was mesoporous, with an average pore size of 6.6 nm. After 45 cycles of ALD Al_2O_3 overcoating, the mesopores disappeared, revealing the dramatic BET surface area decrease. This result is not surprising, because the thickness of the ALD Al_2O_3 overcoat was sufficient to fill the mesopores. After high-temperature treatment, 6.6-nm mesopores reappeared, and new, ~2-nm pores were formed (Fig. 3A). The pores formed as a result of structural changes in the amorphous Al_2O_3 overcoating layer caused by dehydration (*31*), the removal of carbon residues

resulting from the ALD process, and dewetting of the Al_2O_3 overcoats from the surface of the Pd NPs. The latter may be the result of the large lattice mismatch between palladium and alumina. These pores made it possible for the embedded Pd NPs to be accessible to reagents, while the overcoat imparted high thermal stability.

To further determine the accessibility of the Pd NPs embedded under the ~8-nm-thick ALD Al_2O_3 overcoat, we measured diffuse reflectance infrared (IR) spectra using CO as a probe molecule, because there is extensive information about CO chemisorption on Pd NPs (*19*, *32*). As shown in Fig. 3B, the fresh Pd/Al_2O_3 sample without an Al_2O_3 overcoat exhibited two strong peaks at 1929 and 1965 cm^{-1} and two weaker peaks at 2058 and 2081 cm^{-1}. These peaks can be assigned to μ_2-bridge-bonded CO on (111) facets, μ_2-bridge-bonded CO on step and facet edges, linear CO on step and facet edges, and linear CO on the Pd corner atoms of Pd NPs, respectively (*25*, *32*). After 45 cycles of ALD Al_2O_3 were applied, all of the CO chemisorption peaks disappeared, which is consistent with complete covering of the Pd NPs. However, after calcination at 500°C for 120 min in 10% oxygen in helium and then reduction in 5% hydrogen in helium at 300°C for 30 min ($45Al/Pd/Al_2O_3$-500C), a low-intensity chemisorbed CO peak was detected. The restored chemisorbed CO peak became more pronounced when the calcination temperature was increased to 700°C, followed by the same reduction procedure ($45Al/Pd/Al_2O_3$-700C). These results clearly indicated that the ALD Al_2O_3 overcoats became porous after high-temperature treatments, restoring gas accessibility to the Pd NPs, which is consistent with the BET measurements. On the used sample ($45Al/Pd/Al_2O_3$-used), the bridge-bonded CO IR feature is very similar to that of the $45Al/Pd/Al_2O_3$-700C sample, except for a slight decrease in intensity and a small blue shift due to CO-CO lateral interactions. In comparison to uncoated Pd NPs, the features associated with CO bonded to edges and corners on the coated samples had substantially lower intensity than the feature due to CO on facet planes, which indicates that the Al_2O_3 overcoating preferentially decorated the low-coordinated Pd sites, such as steps and edges on both the 700°C activated and used samples.

Figure 4 shows a schematic model of Pd/Al_2O_3 catalysts with and without an ALD Al_2O_3 overcoat during ODHE reaction at 675°C. For the uncoated Pd/Al_2O_3 catalyst, substantial deactivation of Pd was due to heavy coking by filamentous carbon and Pd particle sintering, with leaching of Pd from the Al_2O_3 support surface (Fig. 4, A and B). For the ALD Al_2O_3–overcoated Pd/Al_2O_3 catalyst, the ALD Al_2O_3 overcoat preferentially blocks the low-coordinated Pd surface sites that favor C-C bond scission and hydrogen stripping to produce C1 fragments that lead to coke, CH_4, CO, and CO_2 while favoring the formation of ethylene on the facets (*12*, *33*). The role of C1 species in coking is supported by the observation that when the hydrocarbon reagent was methane, coke was formed on the alumina-overcoated Pd catalysts, but not when either ethane or propane was the reagent [figs. S15 and S16 and table S1 (*19*)]. The identification of low-coordinated Pd surface sites as the centers for coke formation is consistent with Nørskov *et al*., who observed that carbon nanofibers developed initially at step edges on nickel surfaces (*34*). They also found that restructuring of atomic step edges on the nickel surface, a process that involves surface diffusion of both carbon and nickel atoms, facilitated fiber growth. Because Ostwald ripening also proceeds via the release of low-coordinated surface metal atoms, the edge and corner atoms play a central role in both sintering and coking (*34*). Therefore, exceptional resistance to sintering and coking in high-temperature catalytic reactions appears to be achieved because the edge and corner atoms are selectively blocked and stabilized by alumina overcoats. Meanwhile, a lower selectivity to ethylene on alumina-coated catalysts with a smaller particle size is expected and was observed [table S2 (*19*)], because the terraces are a smaller portion of the surface on the smaller particles.

Additional contributions to coke inhibition that are consistent with the model of Fig. 4 cannot be ruled out. (i) The Al_2O_3 overcoat divides the Pd NPs' surface into ensembles of Pd atoms that are too small to support coke formation. This follows a model proposed by Sachtler *et al*., in which hydrogenolysis reactions require large ensembles, whereas the adsorption of modifiers (sulfur, gold, tin, and carbon) breaks up the periodicity of the surface to prevent coke formation (*10*). (ii) The size of the pore channels in the alumina overcoat inhibits carbon filament formation, because the typical filament diameter is much larger (~17 nm) than the pore diameter in the Al_2O_3 overcoat (Figs. 2B and 3A). (iii) The concentrations of reagents, including reactants and products, are limited within the microporous channels at the Pd NPs, so that bimolecular reactions (including radical chains) that are necessary to form coke are inhibited.

Finally, in order to determine the contribution to ethylene selectivity from nonoxidative DHE, the reaction in the absence of oxygen was examined on another 45-cycle ALD Al_2O_3–coated Pd sample under otherwise identical conditions. The yield of ethylene was only 4.6% at the ethane conversion of 7.0% [fig. S17 (*19*)]. Ethylene formed through the direct DHE reaction pathway contributed only a minor amount to the dramatic increase in ethylene yield observed for the ODHE reaction. Most likely, CO_2- and H_2O-facilitated dehydrogenation play an important role toward the end of the catalyst bed, where oxygen has been consumed (*19*, *26*, *30*).

References and Notes

1. R. J. Farrauto, C. H. Bartholomew, *Fundamentals of Industrial Catalytic Processes* (Blackie, London, 1997).
2. J. Barbier, *Appl. Catal.* **23**, 225 (1986).
3. J. A. Moulijn, A. E. van Diepen, F. Kapteijn, *Appl. Catal. A Gen.* **212**, 3 (2001).
4. E. E. Wolf, F. Alfani, *Catal. Rev.* **24**, 329 (1982).
5. J. R. Rostrup-Nielsen, I. Alstrup, *Catal. Today* **53**, 311 (1999).
6. K. K. Ghosh, D. Kunzru, *Ind. Eng. Chem. Res.* **27**, 559 (1988).
7. D. T. Wickham, J. Engel, M. E. Karpuk, U.S. Patent 6,482,311 B1 (2002).
8. J. Radnik *et al*., *Angew. Chem. Int. Ed.* **44**, 6771 (2005).
9. D. L. Trimm, *Catal. Today* **49**, 3 (1999).
10. P. Biloen, J. N. Helle, H. Verbeek, F. M. Dautzenberg, W. M. H. Sachtler, *J. Catal.* **63**, 112 (1980).
11. N. Macleod, J. R. Fryer, D. Stirling, G. Webb, *Catal. Today* **46**, 37 (1998).
12. A. K. Rovik, S. K. Klitgaard, S. Dahl, C. H. Christensen, I. Chorkendorff, *Appl. Catal. A Gen.* **358**, 269 (2009).
13. T. Horiuchi *et al*., *Appl. Catal. A Gen.* **144**, 111 (1996).
14. S. H. Joo *et al*., *Nat. Mater.* **8**, 126 (2009).
15. M. Seipenbusch, A. Binder, *J. Phys. Chem. C* **113**, 20606 (2009).
16. K. Yu, Z. C. Wu, Q. R. Zhao, B. X. Li, Y. Xie, *J. Phys. Chem. C* **112**, 2244 (2008).
17. P. M. Arnal, M. Comotti, F. Schuth, *Angew. Chem. Int. Ed.* **45**, 8224 (2006).
18. M. Cargnello *et al*., *Dalton Trans.* **39**, 2122 (2010).
19. Materials, methods, and supporting data are available on *Science* Online.
20. S. M. George, *Chem. Rev.* **110**, 111 (2010).
21. R. L. Puurunen, *J. Appl. Phys.* **97**, 121301 (2005).
22. B. S. Lim, A. Rahtu, R. G. Gordon, *Nat. Mater.* **2**, 749 (2003).
23. M. Huff, L. D. Schmidt, *J. Phys. Chem.* **97**, 11815 (1993).
24. S. S. Bharadwaj, L. D. Schmidt, *J. Catal.* **155**, 403 (1995).
25. H. Feng, J. L. Lu, P. C. Stair, J. W. Elam, *Catal. Lett.* **141**, 512 (2011).
26. F. Cavani, N. Ballarini, A. Cericola, *Catal. Today* **127**, 113 (2007).
27. P. Concepcion *et al*., *Catal. Today* **96**, 179 (2004).
28. Z. S. Chao, E. Ruckenstein, *J. Catal.* **222**, 17 (2004).
29. K. D. Chen, A. T. Bell, E. Iglesia, *J. Phys. Chem. B* **104**, 1292 (2000).
30. K. Nakagawa *et al*., *Catal. Today* **84**, 149 (2003).
31. J. D. Ferguson, A. W. Weimer, S. M. George, *Thin Solid Films* **371**, 95 (2000).
32. T. Lear *et al*., *J. Chem. Phys.* **123**, 174706 (2005).
33. Z. P. Liu, P. Hu, *J. Am. Chem. Soc.* **125**, 1958 (2003).
34. S. Helveg *et al*., *Nature* **427**, 426 (2004).

Acknowledgments: The work was financially supported by The Dow Chemical Company under the Dow Methane Challenge Award and by the U.S. Department of Energy, Office of Basic Energy Sciences, Hydrogen Fuel Initiative, Chemical Sciences, under contract DE-AC-02-06CH11357. Applications for U.S. and international patents with the title "Metal Catlayst Composition" have been filed. All data and images are available in the body of the paper or as supporting online material. We thank J. T. Miller for providing the Pd/Al_2O_3 sample, F. A. Rabuffetti and K. R. Poeppelmeier for technical assistance on TGA measurements, M. M. Schwartz and C. L. Marshall for technical assistance on BET measurements, F. H. Ribeiro and F. Sollberger for particle dispersion measurements, and N. M. Schweitzer and D. Barton for helpful discussions. B.F. acknowledges financial support in part by the China Scholarship Council.

Supporting Online Material

www.sciencemag.org/cgi/content/full/335/6073/1205/DC1
Materials and Methods
Figs. S1 to S17
Tables S1 and S2
References (*35*–*41*)

19 August 2011; accepted 2 February 2012
10.1126/science.1212906

Isolated Metal Atom Geometries as a Strategy for Selective Heterogeneous Hydrogenations

Georgios Kyriakou,[1] Matthew B. Boucher,[2] April D. Jewell,[1] Emily A. Lewis,[1] Timothy J. Lawton,[1] Ashleigh E. Baber,[1] Heather L. Tierney,[1] Maria Flytzani-Stephanopoulos,[2] E. Charles H. Sykes[1]*

Facile dissociation of reactants and weak binding of intermediates are key requirements for efficient and selective catalysis. However, these two variables are intimately linked in a way that does not generally allow the optimization of both properties simultaneously. By using desorption measurements in combination with high-resolution scanning tunneling microscopy, we show that individual, isolated Pd atoms in a Cu surface substantially lower the energy barrier to both hydrogen uptake on and subsequent desorption from the Cu metal surface. This facile hydrogen dissociation at Pd atom sites and weak binding to Cu allow for very selective hydrogenation of styrene and acetylene as compared with pure Cu or Pd metal alone.

Typical heterogeneous catalysts for hydrogenation reactions often contain noble metals and alloys based on platinum, palladium, rhodium, and ruthenium. Although these metals are active at modest temperature and pressure for a variety of heterogeneous hydrogenations, including alkenes and alkynes, they are not always selective toward the desired product and are expensive. Given that molecular hydrogen (H_2) dissociation is often the rate-limiting step, one strategy is to engineer the minimal catalytic ensemble that will activate H_2 but not the other reactants. Along these lines, several studies have shown that individual atoms of Pt, Pd, or Au in charged or ionic states supported on oxides can efficiently catalyze a number of important reactions (*1*–*4*). Our recent work provides evidence that, in the Pt catalyzed water-gas shift reaction, it is not the metal nanoparticle as such but an ionic species stabilized on the surface of the oxide support that functions as the active site for catalytic turnover (*3*).

In a different but related thrust, we are interested in how the reactivity of a catalytically active metal is altered when it is atomically dispersed in the surface layer of a more inert host metal. Such an approach, if successful, would offer a means to both temper the reactivity of a very active element and to design catalysts with very small amounts of the precious metal. Besenbacher *et al*. showed that the opposite strategy can be effective in reducing the reactivity of a metal by adding small amounts of Au to a Ni surface to prevent coking of the Ni and improve steam-reforming performance (*5*). In a series of low-temperature scanning tunneling microscopy (LT-STM) and density functional theory (DFT) studies, we investigated the formation of a class of bimetallic alloy systems, which we term single-atom alloys (SAAs), and their interaction with H_2 (*6*–*8*). Two key characteristics of SAAs are (i) the more active of the two components (in our case Pd) is present in the surface of the host metal at very low concentrations [~0.01 monolayer (ML)] and (ii) atoms of the more active component (Pd) are thermodynamically more stable when surrounded by the host metal such that no dimers or trimers are present at low coverage. Theory predicts in a simple homogeneous surface slab that Pd:Cu ratios up to 1:2 yield individual, isolated Pd atoms that are more stable when surrounded by Cu as compared with Pd dimers or trimers (*6*).

This effect is depicted in the STM image in Fig. 1 for a 0.01 ML Pd in Cu (111) [Pd/Cu(111)] alloy surface (*9*). Detailed investigation of the alloying process reveals that, depending on the substrate temperature upon Pd deposition, alloying occurs mainly in either the topmost layer (~350 K) or in the subsurface layers at a higher sample temperature (~500 K) (*6*–*8*, *10*). The evaporated Pd adatoms adsorb on the substrate and diffuse over the terraces in a random walk fashion until they are trapped at the nearest ascending step edge where place exchange and alloying into the copper surface layer takes place. DFT calculations by Sholl and co-workers (*7*) reveal that, despite the relatively low barrier of Pd to traverse step edges, it binds very strongly to ascending step edges, and we find experimentally that it remains there during subsequent reaction.

The Pd/Cu SAA surface displays a rather uncommon energetic landscape for the dissociation and chemisorption of hydrogen. Unlike Pd, the pristine Cu(111) surface is inert toward the dissociation of unactivated H_2 in ultrahigh vacuum (UHV) because of the dissociation barrier on the order of 0.4 eV (*11*). Critically, we find that a small quantity of Pd atoms in the Cu surface makes the SAA active toward the uptake of H_2, which can dissociate on the Pd monoatomic entities and then spill over onto the bare Cu(111) terraces. Chopra *et al*. recently reported a related effect involving Ti_2Al_2 complexes in a Ti-doped Al(111) surface that efficiently activated H_2 (*12*). Also, Wittstock *et al*. suggested that, in the case of the oxidative coupling of methanol, the activity of nanoporous Au, prepared by dealloying of AuAg alloys, may be rationalized either by a local change of the d-band structure or by dissociation of oxygen on Ag followed by spillover onto the Au (*13*). LT-STM (5 K) enabled us to directly visualize individual hydrogen adatoms (H_a) on the Cu(111) surface that spilled over from Pd atom sites in a 0.01 ML Pd/Cu(111) surface after exposure to ~10 Langmuirs (L, 10^{-6} torr·s) of H_2 at 80 K (Fig. 1C). Hydrogen atoms appear as depressions in the STM images because of the lower electron tunneling probability through the H-metal complex as compared with the bare metal at energies near the Fermi level (typically <0.1 eV) (*14*, *15*).

Temperature-programmed desorption (TPD) measurements of H_2 desorption from Pd/Cu were acquired after exposing two different Pd coverages (Fig. 2A, 0.01 ML Pd, and Fig. 2B, 0.1 ML Pd) to H_2 at 85 K. In both cases, the alloys were prepared by depositing Pd on Cu(111) at a sample temperature of 380 K for appropriate time intervals in order to generate surfaces with different densities of Pd atoms substituted into the surface layer. Desorption of H_2 from the 0.01 ML Pd/Cu(111) alloy surface (Fig. 2A) occurred in a

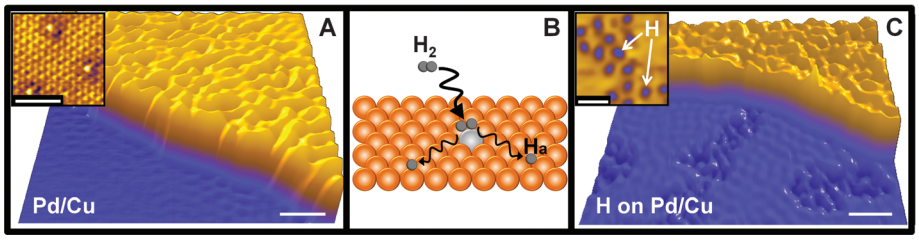

Fig. 1. STM images showing atomically dispersed Pd atoms in a Cu(111) surface and hydrogen atoms that have dissociated and spilled over onto the Cu surface. (**A**) Pd alloys into the Cu(111) surface preferentially above the step edges as evidenced by the rumpled appearance of the upper terrace (scale bar indicates 5 nm). (Inset) Atomic resolution of the Pd/Cu alloy on the upper terrace showing individual, isolated Pd atoms in the surface layer appearing as protrusions (scale bar, 2 nm). (**B**) Schematic showing H_2 dissociation and spillover at individual, isolated Pd atom sites in the Cu surface layer. (**C**) Islands of H atoms imaged after hydrogen uptake appear as depressed regions on the clean Cu(111) lower terrace (scale bar, 5 nm). (Inset) High-resolution image of individual hydrogen atoms on Cu(111) (scale bar, 2 nm). Images recorded at 5 K.

[1]Department of Chemistry, Tufts University, 62 Talbot Avenue, Medford, MA 02155, USA. [2]Department of Chemical and Biological Engineering, Tufts University, 4 Colby Street, Medford, MA 02144, USA.

*To whom correspondence should be addressed. E-mail: charles.sykes@tufts.edu

single state that initially shifted to lower temperatures upon increasing the H_a coverage, as expected for a second-order desorption process. A 200-L H_2 exposure yielded a surface H_a coverage of 0.2 ML. The peak maximum (210 K) was much lower than that expected for H_2 desorption from Cu(111) (310 K) (*16*) or Pd(111) (320 K) (*17*). This effect demonstrates that individual, isolated Pd atoms both assist adsorption and spillover of H_a onto Cu(111) by acting as the dissociation site for H_2 and, as would be expected from microscopic reversibility, serve as low-barrier exit routes for H_2 during the desorption process. In comparison, desorption of H_2 from Cu(111) occurs at ~310 K because of a large recombination barrier and from Pd(111) at ~320 K because of strong binding. Theoretical modeling has indicated that at higher Pd:Cu ratios two-atom Pd ensembles are best for activating H_2 (*18*), but our data in the very low coverage regime reveal that Pd monomers in the Cu surface are sufficient to induce the low-temperature hydrogen activation and desorption observed here.

Increasing the surface concentration of Pd to 0.1 ML yielded an even lower H_2 desorption maximum (175 K) compared with that of the 0.01 ML Pd/Cu(111) surface for the same nominal H_2 exposure; the amount of H_2 desorbing from the surface (~0.4 ML) increased by a factor of 2 for the same 200-L exposure. The increase of the H_a surface coverage coupled with the even lower desorption temperature suggests that increasing the number of Pd monoatomic entities in the surface effectively increases the number of entrance and exit routes of hydrogen on and off the Cu(111) surface. Surface strain also serves to lower the H_2 desorption temperature, because the addition of larger Pd atoms (diameter d_{Pd} = 0.275 nm) to a smaller Cu(111) lattice (d_{Cu} = 0.256 nm) imparts compressive strain in the surface. This weakens the binding of H to the Pd atoms from which they desorb, resulting in a lower desorption temperature (*19*). Further increases of the Pd coverage to 1 ML (Fig. 2C) resulted in broad desorption features that saturated after small H_2 doses with an H_a coverage ~0.7 ML. These desorption profiles are consistent with a rather heterogeneous surface of energetically different adsorption sites ranging from Pd monoatomic entities to 2-ML-high Pd islands, which shifted the desorption feature to higher temperatures, as expected for desorption of H_2 from Pd(111) or high Pd content Pd/Cu alloys (*17*, *18*).

The potential energy diagram shown in Fig. 3 illustrates the vastly different energetics of the interaction of hydrogen with Pd(111), Cu(111), and Pd/Cu SAAs. Energies and activation barriers are taken from (*6*, *20*). The Pd(111) and Cu(111) surfaces display a difference in the dissociative adsorption of hydrogen. Although H_2 dissociation on Pd(111) is not activated (activation energy $E_a \approx 0$ eV), on Cu(111) it is hampered by a rather large activation barrier of 0.4 eV. Conversely, the binding energy of H_a on Cu(111) is about 0.2 eV, which is much weaker than that on Pd(111) (0.6 eV) (*6*, *20*). The weak binding of H_a on, and activated desorption of H_2 from Cu versus the strong binding of H_a on, and nonactivated desorption of H_2 from Pd lead to almost identical H_2 desorption temperatures from both surfaces (310 to 320 K). The situation, however, is drastically different on Pd/Cu SAA surfaces.

Our TPD data revealed that single Pd atoms in the Cu(111) surface lowered the activation barrier to H_2 dissociation and bound H_a weakly enough to allow it to spill over onto the Cu surface. The net effect is a surface that can easily activate H_2 dissociation (as evidenced by efficient uptake at 85 K) but also bind it weakly. A similar type of behavior has been theoretically predicted for a related class of surface alloys termed near-surface alloys (NSAs) (*20*, *21*). NSAs involve a single layer of one metal either supported on or sandwiched between layers of a different host metal. Such NSAs have been shown to form even when bulk alloys are not thermodynamically stable. It is predicted that, in addition to binding reactants more weakly than the corresponding pure metals, NSAs can also dissociate reactants more readily. The important catalytic properties of NSAs have been demonstrated with both model single-crystal alloy surfaces and nanoparticle catalysts (*22*–*24*). For example, a single Ni layer on Pt(111) exhibits increased activity in the reforming of oxygenates as compared with Pt(111), a subsurface Ni ML, or a thick Ni layer on Pt(111) (*23*). RuPt core-shell nanoparticles also display enhanced reactivity in the preferential oxidation of CO in the presence of H_2 feed as compared with traditional PtRu nanoalloys, monometallic mixtures of nanoparticles, and pure Pt particles (*24*). By contrast, our SAAs are not layer-on-layer like the NSAs but use an extremely low surface concentration of the active metal in the surface layer, thus allowing the host surface to preserve its original properties. In the present case, the Cu(111) host surface, which is in overwhelming excess (99:1), binds H_a weakly.

Inspired by this vastly different energetic landscape for hydrogen adsorption and desorption, we investigated the capacity of Pd/Cu SAAs to perform low-temperature, selective catalytic hydrogenations by using two probe molecules: styrene and acetylene. Styrene serves as a model alkene in UHV studies (*25*) because it can bond strongly to metals through π interactions. The heterogeneously catalyzed hydrogenation of trace acetylene to ethene is of major industrial importance, and the adsorption of acetylene has also been extensively studied on both Cu(111) and Pd(111) by various techniques (*26*, *27*). Figure 4A shows representative data acquired from a 0.01 ML Pd/Cu(111) SAA after adsorbing 0.2 ML of H_a followed by 0.5 ML of styrene. The sole hydrogenation product of the reaction of styrene with H_a was ethylbenzene, which desorbed at 260 K with a 13% conversion and >95% selectivity based on the detection limit of our mass spectrometer. Unreacted styrene also desorbed during the

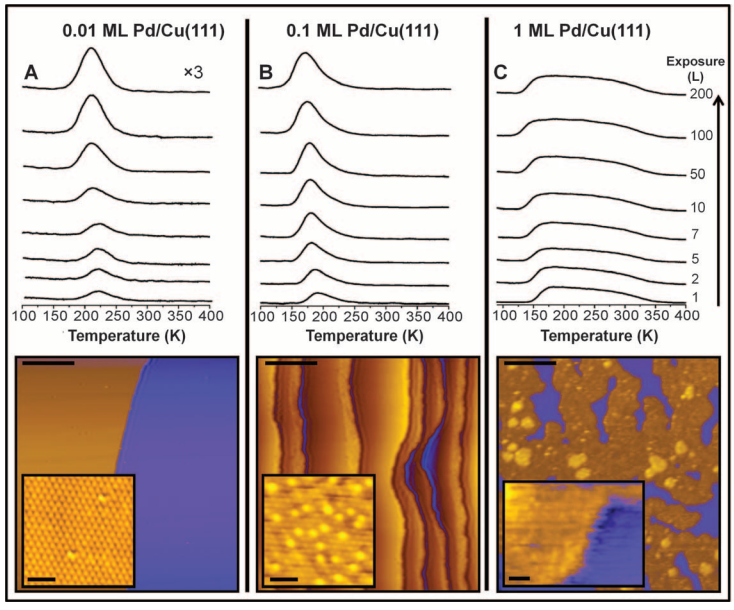

Fig. 2. TPD of H_2 as a function of Pd coverage and corresponding STM images of Pd/Cu(111) surface alloys. (**A**) H_2 uptake on 0.01 ML Pd/Cu(111); STM image of 0.01 ML Pd/Cu(111) showing that the low Pd coverage leaves the Cu(111) surface mostly unaffected. (Inset) High-resolution image of a region above a step edge where individual Pd surface atoms reside. (**B**) H_2 uptake on 0.1 ML Pd/Cu(111); STM image of 0.1 ML Pd/Cu(111). The step edges appear scalloped because of the formation of a denser substitutional alloy on their upper terrace. (Inset) High-resolution image in the vicinity of the step edge where the Pd/Cu(111) surface alloy consisting predominantly of Pd monomers can be seen. (**C**) H_2 uptake on 1 ML Pd/Cu(111); STM image of 1 ML Pd/Cu(111) showing the onset of 2 ML high Pd island formation before completion of the first layer. (Inset) Image of the Pd island and Cu(111) interface. The scale bars in all full-size STM images are 20 nm, and the scale bars of the insets are 3 nm.

temperature-programmed reaction (TPR) sweep, with all desorption features being essentially identical to what is expected for styrene adsorption on clean Cu(111) (figs. S1 and S3). This reveals that the very small amount of Pd in the Cu(111) surface (1:99) does not alter the adsorption properties of the molecule. The absence of any high-temperature H_2 desorption features indicates that there is essentially no decomposition of styrene on the 0.01 ML Pd/Cu(111) surface. In other words, the single Pd atoms have converted the otherwise entirely inactive Cu(111) surface into an effective and very selective hydrogenation catalyst by providing both a low-energy entrance route for H_a and many Cu sites where it is weakly bound.

The Pd/Cu SAA also catalyzed the hydrogenation of acetylene to ethene with high selectivity. Earlier work by Lambert and co-workers (*27*) has shown that desorption of acetylene from the clean Cu(111) surface produces ethene (8% conversion) through decomposition and self-hydrogenation of acetylene at ~330 K, as well as small quantities of coupling products (mainly benzene desorbing at ~320 K). Figure 4B and fig. S4 show representative TPR spectra for the hydrogenation of acetylene on a 0.01 ML Pd/Cu(111) SAA after adsorbing 0.2 ML of H_a and 0.5 ML of acetylene. Hydrogenation of acetylene proceeded via two distinct pathways. The high-temperature (330 K) pathway is similar to the TPR of acetylene from Cu(111) in the absence of any preadsorbed Pd or H_a (fig. S1), and we assigned this pathway to the decomposition and self-hydrogenation of acetylene at high temperatures on Cu(111) (*27*). The conversion of acetylene in the high-temperature pathway is estimated to be 14% (ethene, 4%; surface carbon, 8%; and benzene, 2%). The low-temperature ethene formation pathway, in which acetylene reacts with preadsorbed H_a on Cu(111), corresponds to 3% conversion of the initially adsorbed acetylene with >95% selectivity based on the detection limit of our mass spectrometer.

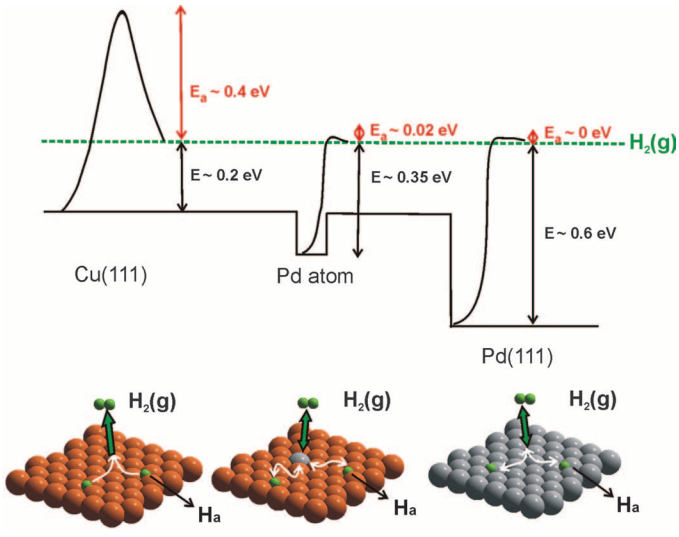

Fig. 3. Potential energy diagram depicting the mode of action of a Pd SAA surface compared with those of pure Cu(111) and Pd(111). Dissociative adsorption of H_2 on Cu(111) (orange) is a highly activated process. On Pd(111) (gray), H_2 dissociation is practically barrierless, but the adsorbed atoms are bound strongly. In the case of an isolated Pd atom, the dissociation barrier is low, hydrogen is weakly bound, and it can spill over onto the Cu(111) surface.

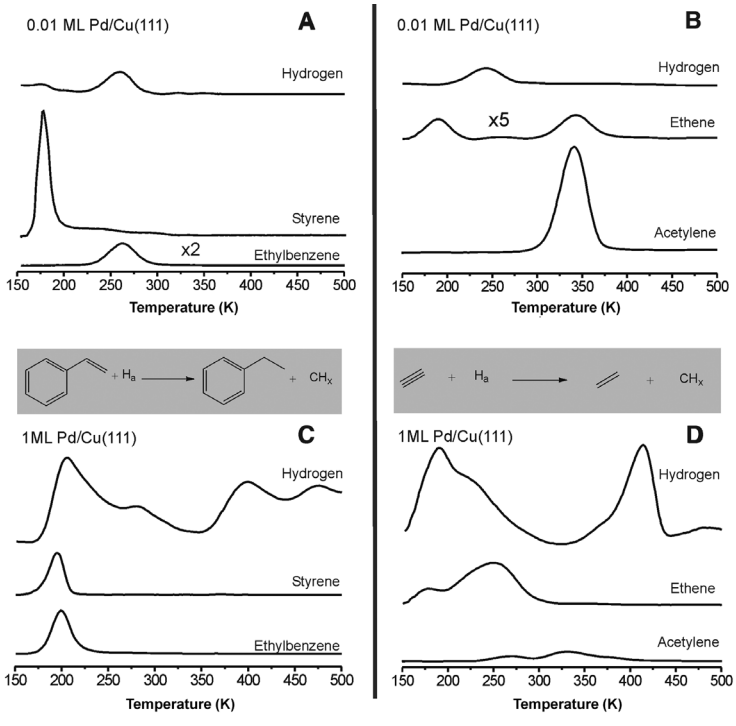

Fig. 4. Representative TPR data showing the increase in selectivity obtained by atomically dispersing Pd atoms in Cu versus the extensive decomposition of the reactants on a 1-ML Pd layer. (**A**) Styrene hydrogenation on 0.01-ML Pd/Cu(111) alloy. (**B**) Acetylene hydrogenation on 0.01-ML Pd/Cu(111) alloy surface. (**C**) Styrene hydrogenation on 1-ML Pd/Cu(111) alloy. (**D**) Acetylene hydrogenation on 1-ML Pd/Cu(111). In all cases, near-saturation H_a was deposited at 85 K followed by 0.5 ML of the hydrocarbon at 150 K.

In marked contrast to the selective hydrogenation chemistry on SAAs, the hydrogenation of styrene and acetylene on 1 ML Pd/Cu(111) (Fig. 4, C and D) was accompanied by an extensive decomposition of both molecular species and dramatically lower hydrogenation selectivity. As the STM image in Fig. 2C illustrates, higher Pd coverages resulted in the formation of large Pd islands. These islands exhibited the common tendency of Pd, which has not been preconditioned with C, to decompose organic molecules and form adsorbed CH_x fragments on the surface that evolve H_2 at a higher temperature, resulting in considerably lower selectivities (*28*). The TPR measurements shown in Fig. 4C indicate that the overall conversion of styrene to ethylbenzene and surface carbon is 80% with the selectivity toward ethylbenzene being 38%. In other words, ~50% of the initially adsorbed reactant decomposed on the surface. A similar picture was observed in the case of acetylene hydrogenation on 1 ML Pd/Cu(111) (Fig. 4D); 60% of the initially dosed acetylene decomposed to form surface carbon with no coupling products observed. The overall conversion of acetylene was 90%, whereas the selectivity toward ethene was 33%.

Our results demonstrate that very small quantities of individual, isolated catalytically active metal atoms can substantially influence the catalytic properties of less reactive metals. Minority Pd atoms (1%) in a Cu surface activate hydrogen, which then populates bare Cu areas (99%) where it is weakly bound and effective for hydrogenation, yielding a bifunctional surface with different regions facilitating different steps in the reaction. From a practical application standpoint, the small amounts of precious metal required to produce SAAs generates a very attractive alternative to most traditional bimetallic catalysts. Recent advances in catalyst synthesis mean that synergistic effects, whereby different components of the catalyst have a particular function in the overall reaction mechanism, are indeed possible with practical dispersed catalysts (*29*). Implementation of the SAA approach to the design of real catalysts requires consideration of the effect of higher reaction temperature, which may cause the minority active element to segregate into the bulk of the

more inert host and hence a loss in activity. However, there are now many experimental and theoretical examples of metal alloys under realistic conditions in which the more active element is stabilized at the surface by adsorbates (*21*, *30*–*32*). This adsorbate-induced reverse segregation effect is understood in terms of the adsorbate binding more strongly to the element, which would normally segregate to the bulk and result in a reversal of the surface segregation behavior (*21*). In the case of the Cu/Pd system, the stabilization resulting from segregation of Cu to the surface is small (0.02 eV) (*31*) compared with the ~0.4-eV increase in binding of H to Pd versus Cu (*6*, *20*). The fact that Pd segregation to the Cu surface has been observed experimentally in Pd/Cu catalysts under realistic hydrogenation operating conditions bodes well for the utility of this atomic geometry in real catalysts (*32*).

References and Notes

1. S. Abbet *et al.*, *J. Am. Chem. Soc.* **122**, 3453 (2000).
2. J. C. Fierro-Gonzalez, V. A. Bhirud, B. C. Gates, *Chem. Commun.* **42**, 5275 (2005).
3. Y. Zhai *et al.*, *Science* **329**, 1633 (2010).
4. J. M. Thomas, Z. Saghi, P. L. Gai, *Top. Catal.* **54**, 588 (2011).
5. F. Besenbacher *et al.*, *Science* **279**, 1913 (1998).
6. H. L. Tierney, A. E. Baber, J. R. Kitchin, E. C. H. Sykes, *Phys. Rev. Lett.* **103**, 246102 (2009).
7. D. O. Bellisario *et al.*, *J. Phys. Chem. C* **113**, 12863 (2009).
8. H. L. Tierney, A. E. Baber, E. C. H. Sykes, *J. Phys. Chem. C* **113**, 7246 (2009).
9. Methods and additional data are available as supporting material on *Science* Online.
10. A. Bach Aaen, E. Lægsgaard, A. V. Ruban, I. Stensgaard, *Surf. Sci.* **408**, 43 (1998).
11. T. Kammler, J. Küppers, *J. Chem. Phys.* **111**, 8115 (1999).
12. I. S. Chopra, S. Chaudhuri, J. F. Veyan, Y. J. Chabal, *Nat. Mater.* **10**, 884 (2011).
13. A. Wittstock, V. Zielasek, J. Biener, C. M. Friend, M. Bäumer, *Science* **327**, 319 (2010).
14. L. J. Lauhon, W. Ho, *Phys. Rev. Lett.* **85**, 4566 (2000).
15. T. Mitsui, M. K. Rose, E. Fomin, D. F. Ogletree, M. Salmeron, *Nature* **422**, 705 (2003).
16. G. Anger, A. Winkler, K. D. Rendulic, *Surf. Sci.* **220**, 1 (1989).
17. G. E. Gdowski, T. E. Felter, R. H. Stulen, *Surf. Sci.* **181**, L147 (1987).
18. C. Sousa, V. Bertin, F. Illas, *J. Phys. Chem. B* **105**, 1817 (2001).
19. A. Roudgar, A. Groß, *Surf. Sci.* **597**, 42 (2005).
20. J. Greeley, M. Mavrikakis, *J. Phys. Chem. B* **109**, 3460 (2005).
21. J. Greeley, M. Mavrikakis, *Nat. Mater.* **3**, 810 (2004).
22. J. Knudsen *et al.*, *J. Am. Chem. Soc.* **129**, 6485 (2007).
23. O. Skoplyak, M. A. Barteau, J. G. Chen, *J. Phys. Chem. B* **110**, 1686 (2006).
24. S. Alayoglu, A. U. Nilekar, M. Mavrikakis, B. Eichhorn, *Nat. Mater.* **7**, 333 (2008).
25. J. T. Roberts, R. J. Madix, *J. Am. Chem. Soc.* **110**, 8540 (1988).
26. W. T. Tysoe, G. L. Nyberg, R. M. Lambert, *Chem. Commun.* **11**, 623 (1983).
27. G. Kyriakou, J. Kim, M. S. Tikhov, N. Macleod, R. M. Lambert, *J. Phys. Chem. B* **109**, 10952 (2005).
28. B. Brandt *et al.*, *J. Phys. Chem. C* **112**, 11408 (2008).
29. H.-L. Jiang, Q. Xu, *J. Mater. Chem.* **21**, 13705 (2011).
30. F. Tao *et al.*, *Science* **322**, 932 (2008).
31. D. Priyadarshini *et al.*, *J. Phys. Chem. C* **115**, 10155 (2011).
32. J. A. Anderson, M. Fernández-García, G. L. Haller, *J. Catal.* **164**, 477 (1996).

Acknowledgments: We thank the U.S. Department of Energy (FG02-10ER16170) for financial support, NSF (CBET 0828666) for partial support (M.B.B.) and for a Graduate Research Fellowship (A.D.J.), the Department of Education for a Graduate Assistance in Areas of National Need fellowship (E.A.L.), and Tufts University for a Tufts Collaborates Seed Grant (E.C.H.S., M.F.-S., and G.K.).

Supporting Online Material

www.sciencemag.org/cgi/content/full/335/6073/1209/DC1
Materials and Methods
SOM Text
Figs. S1 to S4
References (*33*–*37*)

27 October 2011; accepted 30 January 2012
10.1126/science.1215864

An Impactor Origin for Lunar Magnetic Anomalies

Mark A. Wieczorek,[1]* Benjamin P. Weiss,[2] Sarah T. Stewart[3]

The Moon possesses strong magnetic anomalies that are enigmatic given the weak magnetism of lunar rocks. We show that the most prominent grouping of anomalies can be explained by highly magnetic extralunar materials from the projectile that formed the largest and oldest impact crater on the Moon: the South Pole–Aitken basin. The distribution of projectile materials from a model oblique impact coincides with the distribution of magnetic anomalies surrounding this basin, and the magnetic properties of these materials can account for the intensity of the observed anomalies if they were magnetized in a core dynamo field. Distal ejecta from this event can explain the origin of isolated magnetic anomalies far from this basin.

Beginning with the Apollo era, spacecraft observations have shown that portions of the lunar crust are strongly magnetized (*1*–*4*), yet their origin has remained unresolved. The lithologies of the source rocks for these anomalies are unknown, their time of magnetization acquisition is poorly constrained, and it is unclear whether the magnetization process was thermoremanent or shock-related (*5*, *6*). As a result, the origin of the magnetizing fields is a matter of debate, with possibilities including a core dynamo, transient fields generated during impacts, and the amplification of ambient fields by impact-generated plasmas (*7*–*13*).

A key difficulty is that most lunar magnetic anomalies have not been recognized to correlate with known geologic structures. A few impact basins possess central magnetic anomalies (*12*, *14*, *15*), but these anomalies are typically weak and are not representative of the most intense anomalies, most of which are located on the far side of the Moon (Fig. 1). Impact basin ejecta deposits are statistically somewhat more magnetic than other geologic units, but the magnetic signatures of the ejecta from any given basin are quite variable (*16*). A few prominent anomalies on the far side of the Moon are located near the antipodes of four young impact basins (*2*, *3*), suggestive of an exotic impact origin (*17*), but many strong anomalies are not associated with basin antipodes, and most basins do not possess antipodal anomalies.

It is also difficult to reconcile the strengths of these anomalies with the magnetic properties of known endogenous lunar materials. This is because lunar materials are very weakly magnetic relative to terrestrial materials: The saturation remanent magnetizations of mare basalts and pristine highlands rocks are weaker than those of mid-ocean ridge basalt by two to four or more orders of magnitude (*18*, *19*). To demonstrate this, we calculated the thickness of magnetized materials required to generate a representative 10-nT anomaly at an altitude of 30 km as a function of the magnetizing field strength and rock thermoremanence susceptibility (ratio of thermoremanence to the magnetizing field) (Fig. 2). The thermoremanence susceptibility correlates with both the abundance of magnetic carriers in the rock and the rock's saturation remanent magnetization (supporting online material), and lunar paleomagnetic studies imply ancient field strengths between ~1 and 120 μT (*5*, *20*, *21*). We find that even the highest postulated paleofield strengths would require extremely thick deposits of unidirectionally magnetized materials to account for the lunar magnetic anomalies. For example, more than 100 km of pristine feldspathic highland rocks would be required, but these thicknesses are greater than the thickness of the entire lunar crust. More than 10 km of mare basalts would be required, but this far exceeds the thickness of most maria (*11*). Even the relatively highly magnetic mafic impact melts, most of which are thought to be derived from the Imbrium impact event (*22*), would require thicknesses of at least several kilometers, but none of the magnetic anomalies show the topographic expressions that might be expected for such locally thick ejecta deposits.

However, there is a major geologic structure that correlates with some of the largest lunar magnetic anomalies and that has received little consideration previously. The far-side hemisphere of the Moon hosts the largest known unequivocal

[1]Institut de Physique du Globe de Paris, Université Paris Diderot, 94100 Saint-Maur des Fossés, France. [2]Department of Earth, Atmospheric, and Planetary Sciences, Massachusetts Institute of Technology, Cambridge, MA 02139, USA. [3]Department of Earth and Planetary Sciences, Harvard University, Cambridge, MA 02138, USA.

*To whom correspondence should be addressed. E-mail: wieczor@ipgp.fr

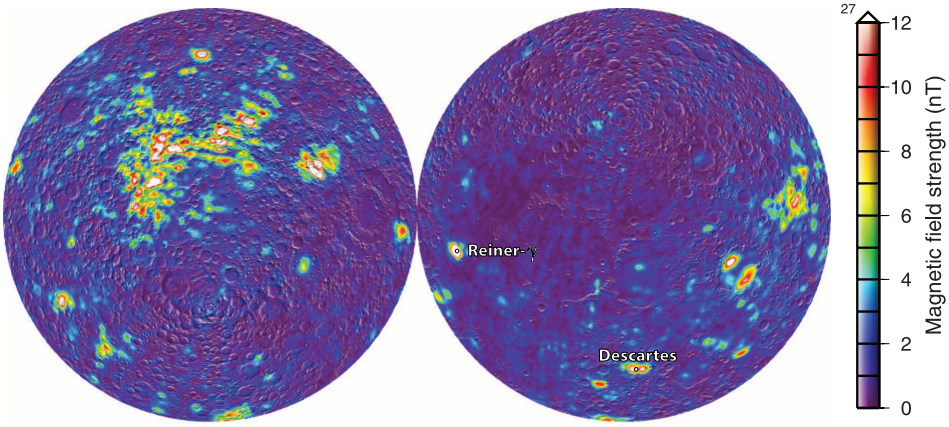

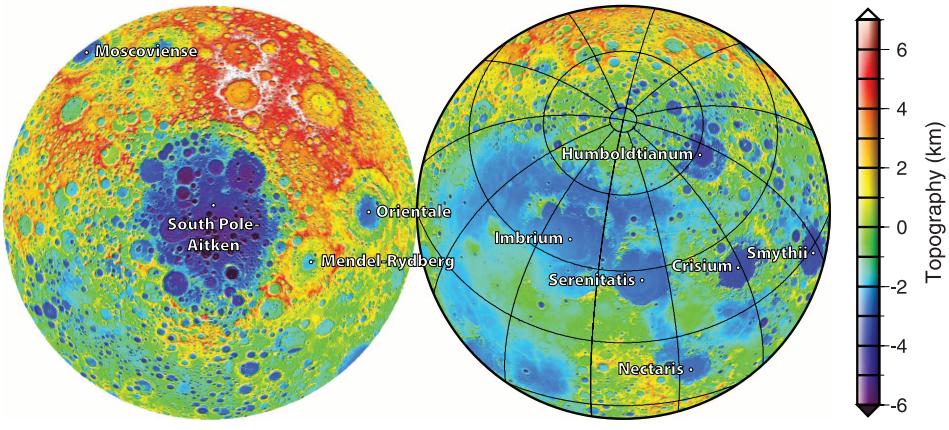

Fig. 1. Magnetic field strength and topography centered over the South Pole–Aitken basin (left) and opposite hemisphere of the Moon (right). Upper panel: Total magnetic field strength from the sequential Lunar Prospector model of (*4*) evaluated 30 km above the surface. Lower panel: Topography from Lunar Reconnaissance Orbiter laser altimeter data (*34*). Ellipses elongated in the north-south direction denote the inner basin floor and outer structural rim of the South Pole–Aitken basin (*23*), and the connecting lines join the respective semiminor and semimajor axes. All images show half of the lunar surface and are displayed in a Lambert azimuthal equal-area projection overlain by a shaded relief map derived from the surface topography.

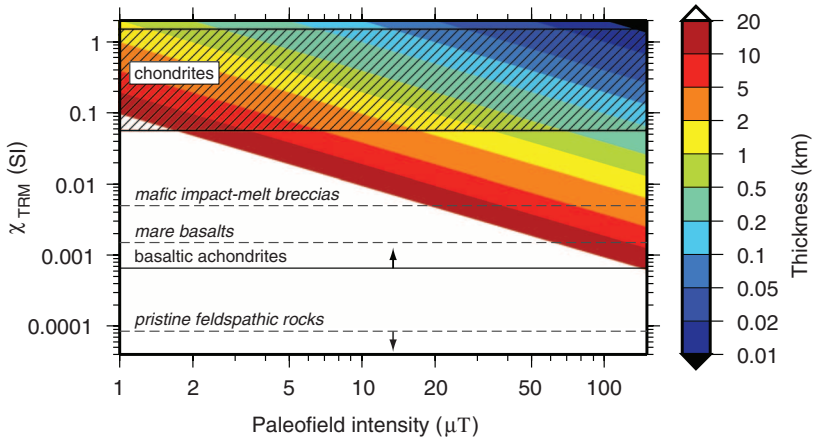

Fig. 2. Thickness of magnetic materials required to generate a 10-nT anomaly 30 km above the lunar surface. Thermoremanent magnetizations acquired in a dipolar field were determined for each thermoremanence susceptibility, χ_{TRM} (in SI units), and surface paleofield intensity within a representative disk 60 km in diameter at 30° latitude. The maximum magnetic field strength scales linearly with disk thickness, and the disk thicknesses would differ by a factor of ~2 for anomalies located at the poles and equator, or for disk diameters of 35 and 200 km. Representative thermoremanence susceptibilities of lunar (dashed) and meteoritic (solid) materials are denoted by horizontal lines (data from tables S2 and S3).

impact structure in the solar system: the South Pole–Aitken basin (Fig. 1). With a mean diameter of ~2200 km, this basin is elongated in the north-south direction and was likely formed by an oblique impact, with the projectile coming from either the north or south (*23*). The most prominent grouping of lunar magnetic anomalies coincides with the northern rim of this basin, precisely where one would expect projectile materials to have been deposited if the impact direction was from the south.

We propose that materials from the South Pole–Aitken impactor are the source materials for many of the largest lunar magnetic anomalies. With high concentrations of metallic iron and other magnetic minerals, typical projectile materials are on average about two orders of magnitude more magnetic than endogenous lunar crustal materials (Fig. 2). If the projectile was similar to a chondritic meteorite, and if these materials were magnetized by cooling in a steady core dynamo field, integrated thicknesses of only a few hundred meters would be required to account for the strength of the lunar anomalies. If the projectile was instead differentiated, the projectile core materials would have been even more magnetic than undifferentiated chondritic meteorites.

Projectile materials should be incorporated into impact deposits in abundances sufficient to substantially change the magnetic properties of these rocks. Terrestrial impact melts are known to contain materials from the impactor ranging from less than 1 weight percent (wt%) up to several wt% (*24*, *25*). The mafic impact melts sampled during the Apollo missions are thought to have formed during one or more basin-forming impact events (primarily Imbrium) and contain ~1 to 2 wt% macroscopic metallic iron that was derived from the core of a differentiated planetesimal (*22*, *26*). Given the enormous size of the South Pole–Aitken basin, the projectile that formed this basin would have been ~10 times as massive as that which formed the next largest lunar basin, and comparable in mass to all other basin-forming projectiles combined. Numerical simulations show that most of the projectile would accrete to the Moon in a molten or partially molten state for an average impact angle and velocity (*27*).

We assessed the hypothesis that projectile materials from the South Pole–Aitken impact event are responsible for the majority of lunar magnetic anomalies by tracking the fate of projectile materials in a suite of impact simulations. Our simulations used a three-dimensional Eulerian shock physics code with self-gravity and multiphase equations of state for crustal, mantle, and core materials (supporting online material). The rheologies of the target and projectile materials were dependent on pressure, temperature, and strain rate (*28*). The model Moon possessed a silicate crust 50 km thick, with a forsterite mantle and a small iron core, whereas the projectile was treated as being either homogeneous in composition or differentiated with a silicate mantle and iron core. Simulations were run for more than 1 hour after the impact, which allowed most of the ejecta to re-impact the Moon.

As a representative case, a 45° oblique impact at 15 km s^{-1} of a differentiated projectile 200 km in diameter completely excavated the crust of the Moon over an area ~1200 km in diameter and formed a thick impact melt pool in the basin interior (Fig. 3). The resulting ring of crustal thickening is similar in size to the topographic rim of the South Pole–Aitken basin, although it is not elliptical. Differences in crater shape and crustal structure between the model and observations may result from gravitational and viscous modification processes that are not accounted for in the simulations, or from the relatively low spatial resolution used to model the lunar crust. In the simulation, most of the projectile silicate mantle was vaporized and lost to space, and only ~1% of these materials were retained in the proximal ejecta. The retained projectile mantle materials were deposited downrange and exterior to the basin's excavation cavity, and possessed integrated thicknesses close to 100 m extending about one crater diameter from the basin rim. Only a negligible fraction of the projectile core was vaporized, and almost 80% of these materials were retained on the surface of the Moon. The retained projectile core materials were deposited primarily near the downrange basin rim with thicknesses up to a few kilometers.

We calculated the magnetic signature of the projectile deposits by assuming that they acquired a thermoremanence by cooling in the presence of a global dipolar field (supporting online material), although transient fields and shock remanence acquisition are also possible (*8*). The projectile mantle was modeled using the magnetic properties of basaltic achondrites, which have thermoremanence susceptibilities less than those of chondritic materials by about three orders of magnitude (Fig. 1). The magnetic properties of projectile core materials are not well known (*29*) and will depend primarily on how the projectile metal is mixed with silicate materials in the impact process (which will determine the grain sizes, shapes, and magnetostatic interactions between the metal particles). As a very conservative estimate, we used a thermoremanent susceptibility of 0.5 SI units for the core materials, which is representative of the ordinary and enstatite chondrites. Given that these chondritic materials contain only a few tens of wt% metallic iron, the true thermoremanent susceptibility of projectile core materials is probably several times our chosen value.

If the dipole field strength on the surface of the Moon was just 5 μT when this basin formed [at the low end of most paleofield estimates (*5*)], the projectile core materials would give rise to several magnetic anomalies with intensities of more than 10 nT at 30 km altitude (Fig. 3). Both the intensities and the spatial distribution of these magnetic anomalies are similar to those observed adjacent to the South Pole–Aitken basin. Although most of the strong anomalies are located near the downrange rim of the impact basin, a few strong anomalies are found exterior to the basin rim as well.

We have investigated the sensitivity of these results by testing impact angles of 30°, 45°, and 60° from vertical; impact velocities of 10, 15, and 30 km s^{-1}; and impactor diameters of 150, 200,

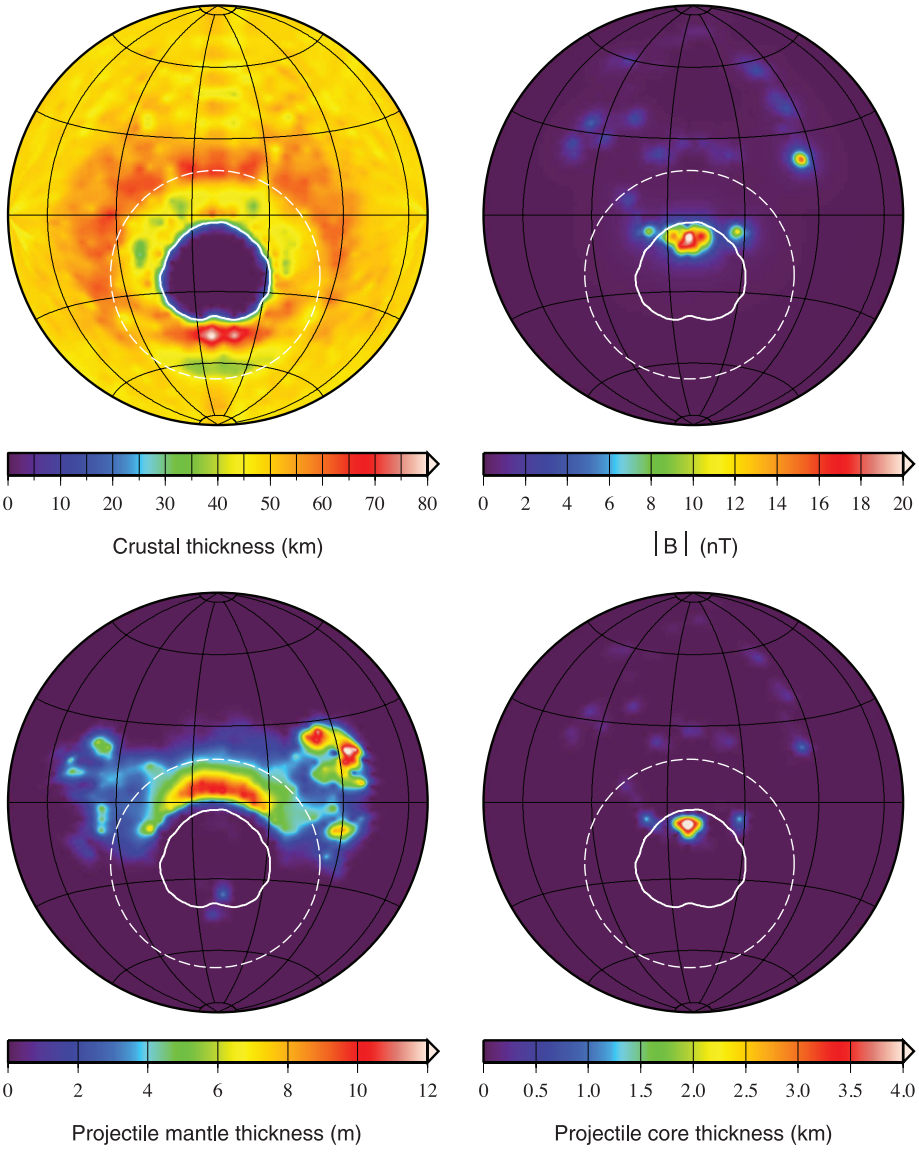

Fig. 3. Crustal thickness (top left), predicted magnetic field strength |*B*| (top right), integrated thickness of projectile mantle materials (bottom left), and integrated thickness of projectile core materials (bottom right) for a representative impact event sufficient to form the South Pole–Aitken basin. This oblique impact simulation used a differentiated projectile 200 km in diameter with a core 110 km in diameter. The impact direction was from south to north, the impact velocity was 15 km s^{-1}, and the impact angle from vertical was 45°. The projectile component delivered to the Moon acquired a thermoremanent magnetization in a dipolar field with a surface field strength of 5 μT. All images show half of the lunar surface and are displayed in a Lambert azimuthal equal-area projection. The solid white contour denotes where the crustal thickness has been reduced by a factor of 2 and is an approximate boundary for the extent of the deep melt sheet; the dashed outer ellipse is an approximation of the location of the final basin rim.

and 260 km (figs. S1 to S4). The overall distribution and thickness of proximal ejecta materials differed by a factor of ~3, depending on resolution, which is small in comparison to the uncertainty in the magnetic paleofield strength. For impact angles of 30° from vertical, the projectile core materials were deposited in the central portion of the basin, where they can sink through the melt sheet. For impact angles of 60° from vertical, a larger fraction of the projectile escaped the Moon's gravity, and the projectile core materials were deposited exterior to the basin rim. For homogeneous projectiles (figs. S5 to S8), the projectile materials were deposited farther downrange than for a similar impact of a differentiated projectile. If the projectile materials had the magnetic properties of average chondritic meteorites, dipole field strengths of 100 μT would generate magnetic anomalies that are similar to those observed on the Moon. Larger impact velocities favor projectile vaporization, leading to weaker magnetic anomalies. Although both differentiated and undifferentiated projectiles can account for the distribution and intensities of lunar magnetic anomalies, differentiated projectiles with impact angles of 45° most easily account for the strong anomalies that are located near the rim of the South Pole–Aitken basin. In our simulations, some projectile materials were deposited far from the basin rim, and this distal ejecta could potentially explain the existence of strong isolated anomalies on the lunar nearside, such as Reiner-γ and Descartes (Fig. 1).

Large impact events were common in the early evolution of the solar system, and these would certainly have accreted important quantities of highly magnetic materials to the crusts of all the terrestrial planets and moons. A giant northern lowlands–forming oblique impact on Mars (*30*, *31*) could help to explain the existence of strong crustal magnetic anomalies in the southern highlands of Mars that are otherwise difficult to understand (*32*, *33*). Similar magnetic anomalies might be expected to surround the Caloris basin on Mercury. Impact basin–associated magnetic anomalies should scale with the amount of retained projectile materials, and hence with basin size. Being exogenic in origin, planetary magnetic anomalies could be used to search for ancient meteoritic materials.

References and Notes

1. P. Dyal, C. W. Parkin, W. D. Daily, *Rev. Geophys. Space Phys.* **12**, 568 (1974).
2. L. Hood *et al.*, *J. Geophys. Res.* **106**, 27825 (2001).
3. D. L. Mitchell *et al.*, *Icarus* **194**, 401 (2008).
4. M. E. Purucker, J. B. Nicholas, *J. Geophys. Res.* **115**, E12007 (2010).
5. M. Fuller, S. M. Cisowski, in *Geomagnetism*, J. A. Jacobs, Ed. (Academic Press, London, 1987), vol. 2, pp. 307–455.
6. J. Gattacceca *et al.*, *Earth Planet. Sci. Lett.* **299**, 42 (2010).
7. W. D. Daily, P. Dyal, *Phys. Earth Planet. Inter.* **20**, 255 (1979).
8. L. L. Hood, Z. Huang, *J. Geophys. Res.* **96**, 9837 (1991).
9. D. Crawford, P. Schultz, *Int. J. Impact Eng.* **23**, 169 (1999).
10. D. R. Stegman, A. M. Jellinek, S. A. Zatman, J. R. Baumgardner, M. A. Richards, *Nature* **421**, 143 (2003).
11. M. A. Wieczorek *et al.*, *Rev. Mineral. Geochem.* **60**, 221 (2006).
12. M. Le Bars, M. A. Wieczorek, Ö. Karatekin, D. Cébron, M. Laneuville, *Nature* **479**, 215 (2011).
13. C. A. Dwyer, D. J. Stevenson, F. Nimmo, *Nature* **479**, 212 (2011).
14. L. Hood, *Icarus* **211**, 1109 (2011).
15. J. Halekas, R. Lin, D. Mitchell, *Meteorit. Planet. Sci.* **38**, 565 (2003).
16. J. Halekas *et al.*, *J. Geophys. Res.* **106**, 27841 (2001).
17. L. Hood, N. Artemieva, *Icarus* **193**, 485 (2008).
18. D. Wang, R. Van der Voo, D. R. Peacor, *Geosphere* **1**, 138 (2005).
19. P. Rochette, J. Gattacceca, A. V. Ivanov, M. A. Nazarov, N. S. Bezaeva, *Earth Planet. Sci. Lett.* **292**, 383 (2010).
20. I. Garrick-Bethell, B. P. Weiss, D. L. Shuster, J. Buz, *Science* **323**, 356 (2009).
21. E. K. Shea *et al.*, *Science* **335**, 453 (2012).
22. R. L. Korotev, *J. Geophys. Res.* **105**, 4317 (2000).
23. I. Garrick-Bethell, M. T. Zuber, *Icarus* **204**, 399 (2009).
24. R. Tagle, L. Hecht, *Meteorit. Planet. Sci.* **41**, 1721 (2006).
25. R. Tagle, R. T. Schmitt, J. Erzinger, *Geochim. Cosmochim. Acta* **73**, 4891 (2009).
26. R. L. Korotev, *J. Geophys. Res.* **92**, E491 (1987).
27. E. Pierazzo, H. J. Melosh, *Meteorit. Planet. Sci.* **35**, 117 (2000).
28. L. E. Senft, S. Stewart, *Earth Planet. Sci. Lett.* **287**, 471 (2009).
29. A. Brecher, L. Albright, *J. Geomag. Geoelectr.* **29**, 379 (1977).
30. J. C. Andrews-Hanna, M. T. Zuber, W. B. Banerdt, *Nature* **453**, 1212 (2008).
31. M. M. Marinova, O. Aharonson, E. Asphaug, *Nature* **453**, 1216 (2008).
32. J. E. P. Connerney *et al.*, *Geophys. Res. Lett.* **28**, 4015 (2001).
33. D. J. Dunlop, J. Arkani-Hamed, *J. Geophys. Res.* **110**, E12S04 (2005).
34. D. E. Smith *et al.*, *Geophys. Res. Lett.* **37**, L18204 (2010).

Acknowledgments: Supported by CNRS, the MIT-France Seed Funds program, the NASA Lunar Science Institute, and the NASA Lunar Advanced Science and Exploration Research Program. The cratering calculations were run on the Odyssey cluster supported by the FAS Science Division Research Computing Group at Harvard University. We thank B. Carbone for administrative help. All author modifications of the CTH code (available by licensing from Sandia National Laboratory) are available upon request.

Supporting Online Material

www.sciencemag.org/cgi/content/full/335/6073/1212/DC1
SOM Text
Figs. S1 to S8
Tables S1 to S4
References (*35*–*86*)

3 October 2011; accepted 30 January 2012
10.1126/science.1214773

Reconstruction of *Microraptor* and the Evolution of Iridescent Plumage

Quanguo Li,[1] Ke-Qin Gao,[2] Qingjin Meng,[1] Julia A. Clarke,[3] Matthew D. Shawkey,[4]* Liliana D'Alba,[4] Rui Pei,[5] Mick Ellison,[5] Mark A. Norell,[5] Jakob Vinther[3,6]

Iridescent feather colors involved in displays of many extant birds are produced by nanoscale arrays of melanin-containing organelles (melanosomes). Data relevant to the evolution of these colors and the properties of melanosomes involved in their generation have been limited. A data set sampling variables of extant avian melanosomes reveals that those forming most iridescent arrays are distinctly narrow. Quantitative comparison of these data with melanosome imprints densely sampled from a previously unknown specimen of the Early Cretaceous feathered *Microraptor* predicts that its plumage was predominantly iridescent. The capacity for simple iridescent arrays is thus minimally inferred in paravian dinosaurs. This finding and estimation of *Microraptor* feathering consistent with an ornamental function for the tail suggest a centrality for signaling in early evolution of plumage and feather color.

Feather colors in extant birds (Aves) are generated from pigments and a variety of nanostructural architectures (*1*, *2*). Iridescent colors, an integral part of the avian plumage color gamut involved in signaling and display, are produced through coherent light scattering by laminar or crystal-like arrays generated by layers of materials with different refractive indices—namely, keratin, melanin, and sometimes air—in feather barbules (*1*, *2*). Melanosomes can be arranged in single or multiple layers (*1*, *2*), and recent work shows that even slight organization of melanosomes can produce weakly iridescent (glossy) colors (*3*). Iridescent nanostructures are diverse and have evolved independently numerous times in extant birds (*4*), but whether they are exclusively avian innovations or appear earlier in dinosaur evolution has been unknown.

Thus far, fossil evidence of iridescent plumage has been limited to a 47-million-year-old isolated avian feather from Germany (Grube Messel) (*5*). This feather preserved in fine nanostructural detail the organization typical of many iridescent avian melanosome arrays. Such pristine preservation is rare, however, and so far unknown in

[1]Beijing Museum of Natural History, 126 Tianqiao South Street, Beijing 100050, People's Republic of China. [2]School of Earth and Space Sciences, Peking University, Beijing 100871, People's Republic of China. [3]Department of Geological Sciences, University of Texas at Austin, 1 University Station C1100, Austin, TX 78712, USA. [4]Department of Biology and Integrated Bioscience Program, University of Akron, Akron, OH 44325–3908, USA. [5]Department of Paleontology, American Museum of Natural History, 79th Street at Central Park West, New York, NY 10024, USA. [6]Department of Geology and Geophysics, Yale University, New Haven, CT 06520–8109, USA.

*To whom correspondence should be addressed. E-mail: shawkey@uakron.edu

the 150- to 120-million-year-old fossils from China that have proven critical for investigating the relative timing of innovations in coloration and plumage evolution in dinosaurs (*6*, *7*). Methods to investigate the presence of iridescent arrays in these and similarly preserved fossils have not been developed.

We investigated the relations between melanosome properties and iridescent arrays in Aves prompted by the melanosome characteristics and plumage preserved in a previously unknown fossil feathered dinosaur specimen (BMNHC PH881, Beijing Museum of Natural History; Fig. 1 and figs. S3 to S5) referred to as *Microraptor* (*8*). *Microraptor* has consistently been recovered as part of Paraves, a clade that includes troodontid, dromaeosaurid, and avialan theropod dinosaurs (*9*–*11*). The articulated specimen was recovered near Lamadong (Jianchang County, western Liaoning Province) and displays previously reported characteristics of this "four-winged" dinosaur [e.g., (*9*)], including asymmetrically vaned hind limb feathers that are about 80% of the length of the asymmetrically vaned primary wing feathers (Fig. 1 and fig. S4), as well as previously unknown plumage data. Feathers in BMNHC PH881 are particularly well preserved on the right forelimb, left hindlimb, and the tail as dark imprints (Fig. 1). No lighter and darker banding, spangles, or patches (*6*, *7*, *12*) were observed. Initial sampling of these feathers revealed apparent sheetlike, end-to-end orientation of elongate melanosomes (Fig. 2F) similar to the subtle organization resulting in glossy black avian feathers (*3*).

To investigate melanosome characteristics in avian iridescent arrays, we sampled melanosome morphology from a phylogenetically diverse set of iridescent feathers from extant birds (*7*, *8*, *12*) (table S4). Although some iridescent feathers contain highly divergent morphologies (e.g., hollow and flattened melanosomes in iridescent hummingbird feathers) that would be readily recognizable in the fossil record, most [13 out of 19 array types in (*2*)] contain rods similar to those in matte feathers. We focused on the latter in our sampling. These samples and denser sets from matte black, brown, and gray extant bird feathers were added to our existing database [(*7*, *12*), new $n = 168$]. Relative to those from black feathers, melanosomes from iridescent feathers were found to be significantly longer (~1160 versus 1000 nm) and narrower (~211 versus 279 nm), providing higher aspect ratios (~5.4 versus 3.5; Figs. 2 and 3). Quadratic discriminant analysis (*8*), a standard method that allows classification of unknown samples from data on known samples, of these data predicted color of extant bird feathers with 82% accuracy (Fig. 2B and tables S1 and S2), showing that iridescent colors could reliably be detected. Samples of the 47-million-year-old fossil feather previously inferred as iridescent on the basis of nanoscale melanosome organization (*5*) were also classified as iridescent with an 86% probability (Fig. 2B).

To then assess the colors and color patterns of the specimen, we took 26 samples of ~1 mm by 1 mm from throughout the feathered areas. All but six revealed numerous dense assemblages of melanosome imprints (*8*). Morphological measurements from melanosome imprints were acquired and analyzed in the same manner as the modern feathers (*8*). Melanosomes from BMNHC PH881 are within the range of extant melanosome dimensions and are predicted as either iridescent or black (Fig. 2 and table S2) with 58 to 100% probabilities. Six samples lacked melanosomes but had no associated light banding of the type correlated with low melanosome density in previous specimens (*6*, *7*, *12*). They were covered instead by an amorphous organic matrix (fig. S1), suggesting the absence of visible melanosomes may be preservational and not representative of melanosome absence and white (or other pigmentary) coloration.

Evidence of a sheetlike, end-to-end orientation of melanosomes (Fig. 2F) was present in 10 samples from BMNHC PH881. Thickness of the keratin cortex overlaying the melanosomes in barbules determines the color (e.g., black-blue sheen) of many glossy black iridescent feathers (*3*), but the lack of preserved keratin prevented the assignment to a particular iridescent hue. Copresence of other pigment types like carotenoids

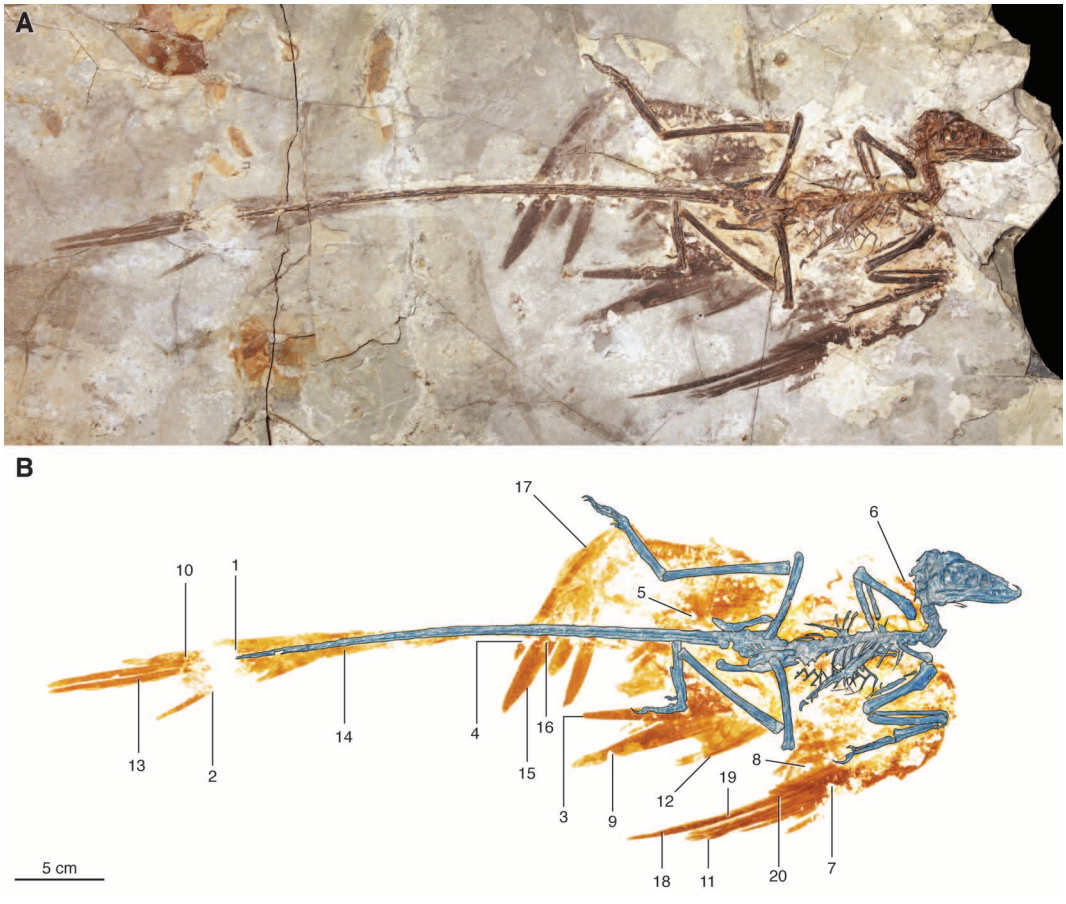

Fig. 1. *Microraptor* specimen BMNHC PH881. (**A**) Photographic image and (**B**) color-coded image (blue-gray, bone; orange, feathers). Numbers in (B) indicate location of samples used in assessment of preserved melanosomes and reference table S2.

in *Microraptor* cannot be excluded but would be masked by the dense melanin deposition. These data allow a conservative reconstruction of *Microraptor* as black with a glossy, weakly iridescent sheen (Fig. 4). Interpretations of *Microraptor* as nocturnal based on scleral ring morphology (*13*) contrast with its dark glossy plumage, a trait not found in extant nocturnal birds (*14*).

Generation of iridescent color by simple arrays of elongate, high–aspect ratio melanosomes, shared by extant birds and *Microraptor*, may be part of the color repertoire of a Middle Jurassic paravian ancestor. However, given known homoplasy in Aves and the phylogenetic lability of iridescence in particular (*4*, *15*), multiple origins of iridescence in early Paraves must be considered. Indeed, a sufficiently high density of elongate melanosomes may trigger physical processes that lead to self-assembly into iridescent nanostructures during barbule development (*16*), suggesting that iridescence could evolve easily relative to other complex traits. Hypotheses concerning the function of iridescent colors have centered on intraspecific communication (*17*). Many are used in courtship displays (*17*, *18*), and studies have shown that female birds prefer males with brighter iridescent color (*19*) and that its expression is condition-dependent (*20*, *21*), a key prediction of honest advertisement models of sexual selection (*22*). Indeed, although it has only recently been studied as a distinctive color type, several extant bird species are sexually dimorphic in glossy color (*23*). Other functions like

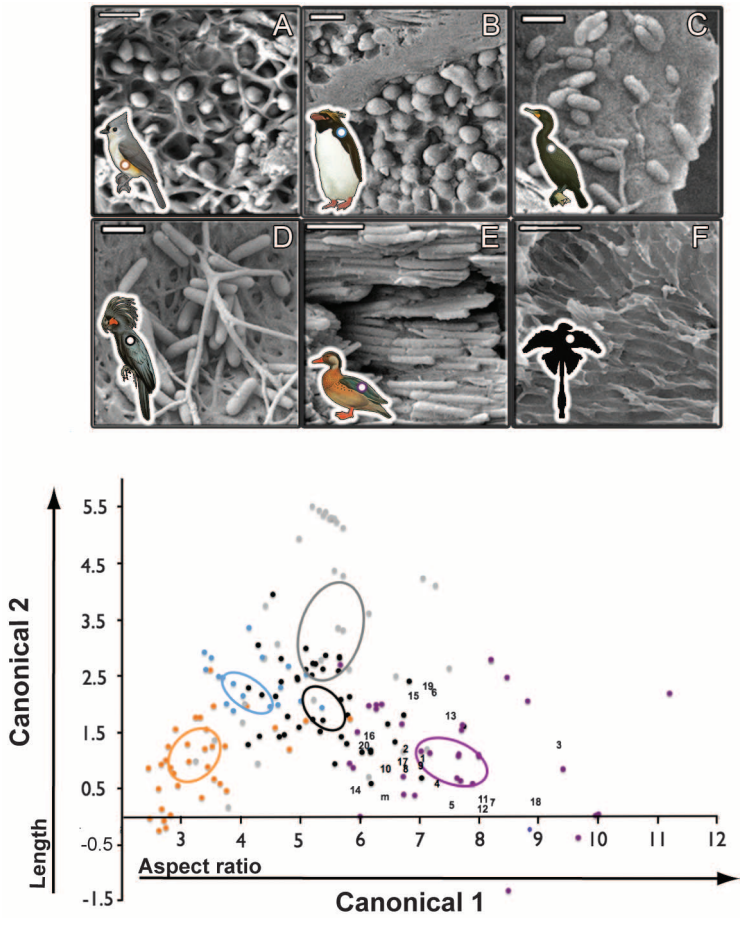

Fig. 2. Scanning electron micrograph images of representative melanosome samples from (**A**) brown, (**B**) "penguin-type" brown-black [a distinct melanosome morphology; see (*12*)], (**C**) gray, (**D**) black, (**E**) iridescent extant avian feathers, and (**F**) BMNHC PH881. Insets of the sampled species are from (*14*): tufted titmouse, *Baeolophus bicolor*; macaroni penguin, *Eudyptes chrysolophus*; double-crested cormorant, *Phalacrocorax auritus*; palm cockatoo, *Probosciger aterrimus*; Brazil duck, *Amazonetta brasiliensis*; dot illustrates approximate location of sampling. (**Bottom**) Quadratic discriminant analysis of measured melanosome properties (*8*) in 168 samples of black, brown, gray, extant penguin brown-black (blue), iridescent (purple), and BMNHC PH881 feathers. Numbers refer to BMNHC PH881 samples (Fig. 2 and table S2), and m refers to a Grube Messel feather with iridescent nanostructure (*5*). For simplicity, only the first two axes (explaining 88% of the variance; see SOM) are shown. Circles indicate 95% confidence limits of means.

	BLACK	BROWN	GRAY	PENGUINS	IRIDESCENT	FOSSIL	ANOVA F^* D.F.= 5,182
Ratio	3.7 ± 0.1^{b}	1.8 ± 0.1^{c}	3.3 ± 0.2^{b}	2.4 ± 0.2^{c}	5.7 ± 0.2^{a}	5.6 ± 0.2^{a}	**67.2**
Long axis (nm)	1002.3 $\pm 22.5^{c}$	497.5 $\pm 31.1^{d}$	1248.8 $\pm 76.7^{a}$	920.4 $\pm 28.4^{a}$	1142.6 $\pm 46.9^{a,b}$	1060.1 $\pm 34.2^{b,c}$	**34.5**
Short axis (nm)	279.9 $\pm 8.7^{b}$	281.6 $\pm 13.7^{b}$	402.5 $\pm 29.6^{a}$	421.1 $\pm 20.7^{a}$	208.6 $\pm 8.5^{c}$	195.5 $\pm 7.9^{c}$	**25.6**

Fig. 3. Melanosome characteristics of extant feather samples and BMNHC PH881. Means ± 1 SE and one-way analysis of variance (ANOVA) of the measurements taken from melanosomes in feathers of extant bird species and BMNHC PH881. Values in the same row not sharing the same letter in superscript are significantly ($P < 0.05$) different from one another (Student's *t* test). Melanosomes in column labeled "Penguins" are sampled from crown Sphenisciformes (Spheniscidae), which have a morphology (~low aspect ratio, large size) distinct from other birds (*12*).

Fig. 4. Reconstruction of the Early Cretaceous paravian dinosaur, *Microraptor*: Inferred color has its basis in analysis of BMNHC PH881, whereas assessment of plumage also incorporated data from digital overlays of the plumage in eight previously published specimens (*8*).

camouflage, interspecific signaling, and feather strengthening through melanosome alignment have been proposed but are largely untested (*16*). Although we cannot assign a definitive function to iridescence in *Microraptor*, a role in signaling aligns with data on the plumage of BMNHC PH881.

BMNHC PH881 has a complete set of distal tail feathers preserved (Fig. 1 and fig. S5). The longest tail feathers in *Microraptor* are a midline pair that form the most posterior part of the fan (Figs. 1 and 4 and figs. S5 and S6). Previously interpreted as a relatively broad, teardrop-shaped surface (*9*, *24*) or as paired, laterally expanded rectangular winglike surfaces (*25*) with an important contribution to lift and stability (*24*, *25*), the fan surface area (e.g., linked to lift production) is appreciably narrower. This reconstruction is consistent with evidence from two other specimens with well-preserved tail feathering (*8*) (fig. S6). Although reassessment here of *Microraptor* feathering based on BMNHC PH881 and eight previously published specimens (Fig. 4) (*8*) will provide a basis for further model-based estimation of potential aerodynamic implications, the graduated tail shape with a pair of long, midline feathers may be consistent with an ornamental or signaling function (*26*).

Paired single, or several, sets of elongate streamerlike tail feathers are seen in basal birds, including all known Enantiornithes and *Confuciusornis*, and have been interpreted as sexual ornaments (*27*, *28*). A similar elongate streamer morphology (*29*) as well as patterned tails with stripes and spangles (*7*) are now known in several nonavialan maniraptorans. Tail feathering may have commonly functioned as an ornament in coelurosaurs despite considerable modification in bony tail form and presumably function. The long bony tail in Paraves is inherited from nonflying ancestors (*30*). It has been ascribed utility in basal paravian maneuvering, lift generation, and landing, but it is also lost early in the evolution of birds. Tail-feather fanning musculature or novel functional linkage with the forelimb has been inferred only later in bird evolution in short-tailed taxa (*27*, *30*). Although tail structure and locomotor role shifted substantially, a signaling function may have been maintained. Iridescent color and the plumage in BMNHC PH881, with other recent findings (*6*, *7*, *27*, *29*), suggest that feather ornaments were diverse and that multiple cues may have been copresent (*31*). Sexual selection [e.g., as honest signals (*21*), arbitrary ornaments, or congener recognition (*32*, *33*)] may be expected to interplay importantly with selection for aerodynamic attributes early in the evolution of birds.

References and Notes

1. R. O. Prum, in *Bird Coloration, Vol. 1, Mechanisms and Measurements*, G. E. Hill, K. J. McGraw, Eds. (Harvard Univ. Press, Boston, 2006), pp. 295–353.
2. H. Durrer, in *Biology of the Integument 2: Vertebrates*, M. Bereiter-Hahn. A. G. Matolsky, K. S. Richards, Eds. (Springer-Verlag, Berlin, 1986), pp. 239–247.
3. R. Maia, L. D'Alba, M. D. Shawkey, *Proc. Biol. Sci.* **278**, 1973 (2011).
4. M. C. Stoddard, R. O. Prum, *Behav. Ecol.* **22**, 1042 (2011).
5. J. Vinther, D. E. G. Briggs, J. Clarke, G. Mayr, R. O. Prum, *Biol. Lett.* **6**, 128 (2010).
6. F. C. Zhang *et al.*, *Nature* **463**, 1075 (2010).
7. Q. Li *et al.*, *Science* **327**, 1369 (2010); 10.1126/science.1186290.
8. Materials and methods are available as supporting material on *Science* Online.
9. X. Xu *et al.*, *Nature* **421**, 335 (2003).
10. X. Xu, H. You, K. Du, F. Han, *Nature* **475**, 465 (2011).
11. A. H. Turner, D. Pol, J. A. Clarke, G. M. Erickson, M. A. Norell, *Science* **317**, 1378 (2007).
12. J. A. Clarke *et al.*, *Science* **330**, 954 (2010); 10.1126/science.1193604.
13. L. Schmitz, R. Motani, *Science* **332**, 705 (2011).
14. J. Del Hoyo *et al.*, Eds., *Handbook of the Birds of the World* (Lynx Editions, Barcelona, 1992–2011).
15. M. D. Shawkey, M. E. Hauber, L. K. Estep, G. E. Hill, *J. R. Soc. Interface* **3**, 777 (2006).
16. R. Maia, R. H. F. Macedo, M. D. Shawkey, *J. R. Soc. Interface*, published online 24 August 2011 (10.1098/rsif.2011.0456).
17. S. M. Doucet, M. G. Meadows, *J. R. Soc. Interface* **6** (suppl. 2), S115 (2009).
18. E. Scholes, *Auk* **123**, 967 (2006).
19. A. T. D. Bennett, I. C. Cuthill, J. C. Partridge, K. Lunau, *Proc. Natl. Acad. Sci. U.S.A.* **94**, 8618 (1997).
20. K. J. McGraw, E. A. Mackillop, J. Dale, M. E. Hauber, *J. Exp. Biol.* **205**, 3747 (2002).
21. S. M. Doucet, *Condor* **104**, 30 (2002).
22. M. A. Andersson, *Sexual Selection* (Princeton Univ. Press, Princeton, NJ, 1994).
23. M. B. Toomey *et al.*, *Behav. Ecol. Sociobiol.* **64**, 1047 (2010).
24. S. Chatterjee, R. J. Templin, *Proc. Natl. Acad. Sci. U.S.A.* **104**, 1576 (2007).
25. D. E. Alexander, E. Gong, L. D. Martin, D. A. Burnham, A. R. Falk, *Proc. Natl. Acad. Sci. U.S.A.* **107**, 2972 (2010).
26. A. L. R. Thomas, *Bioscience* **47**, 215 (1997).
27. J. A. Clarke, Z. Zhou, F. Zhang, *J. Anat.* **208**, 287 (2006).
28. L. M. Chiappe, J. Marugán-Lobón, S. Ji, Z. Zhou, *Biol. Lett.* **4**, 719 (2008).
29. F. C. Zhang, Z. H. Zhou, X. Xu, X. L. Wang, C. Sullivan, *Nature* **455**, 1105 (2008).
30. S. M. Gatesy, K. P. Dial, *Evolution* **50**, 2037 (1996).
31. A. P. Møller, A. Pomiankowski, *Behav. Ecol. Sociobiol.* **32**, 167 (1992).
32. R. O. Prum, *Evolution* **64**, 3085 (2010).
33. R. A. Fisher, *The Genetical Theory of Natural Selection* (Dover, New York, 1958).

Acknowledgments: The research was funded by NSF EAR 0938199, Air Force Office of Scientific Research FA9550-09-1-0159, National Natural Science Foundation of

China 40532008, Beijing Municipal Bureau of Human Resources, Beijing Academy of Science and Technology (BJAST) Innovation Team Fund, University of Texas at Austin, and the American Museum of Natural History. The Copenhagen Museum of Natural History (J. Fjeldsaa) and the Yale University Peabody Museum (R. O. Prum and K. Zyskowski) provided extant feather samples. The fossil specimen is accessioned to the Beijing Museum of Natural History (BMNHC). Data are presented in the supporting online material.

Supporting Online Material

www.sciencemag.org/cgi/content/full/335/6073/1215/DC1
Materials and Methods
Figs. S1 to S9
Tables S1 to S3
References (*34*–*52*)
Database S1

9 September 2011; accepted 9 February 2012
10.1126/science.1213780

Intensifying Weathering and Land Use in Iron Age Central Africa

Germain Bayon,* Bernard Dennielou, Joël Etoubleau, Emmanuel Ponzevera, Samuel Toucanne, Sylvain Bermell

About 3000 years ago, a major vegetation change occurred in Central Africa, when rainforest trees were abruptly replaced by savannas. Up to this point, the consensus of the scientific community has been that the forest disturbance was caused by climate change. We show here that chemical weathering in Central Africa, reconstructed from geochemical analyses of a marine sediment core, intensified abruptly at the same period, departing substantially from the long-term weathering fluctuations related to the Late Quaternary climate. Evidence that this weathering event was also contemporaneous with the migration of Bantu-speaking farmers across Central Africa suggests that human land-use intensification at that time had already made a major impact on the rainforest.

A major vegetation change occurred in Central Africa during the third millennium before the present (B.P.), when mature evergreen trees were abruptly replaced by savannas and secondary grasslands (*1*–*4*). The consensus is that the forest disturbance was caused by a regional climate change (*1*–*4*). However, this episode of forest clearance occurred contemporaneously with the migration of Bantu-speaking peoples from near the modern-day Nigeria-Cameroon border (*5*–*9*). The so-called Bantu expansion led to the diffusion of agriculture and iron-smelting technology across Central Africa, with potential impacts on the environment (*10*). Whether the Bantu farmers played an active role in the Central African deforestation event remains an open question.

To provide further constraints on this issue, we used a marine sediment record recovered off the mouth of the Congo River to reconstruct the late Quaternary history of chemical weathering in Central Africa (Fig. 1). This core (KZAI-01; 05°42′S, 11°14′E), collected at a water depth of 914 m, provides a continuous record of the Congo River sediment discharge for roughly the past 40,000 years [see supporting online material (SOM)]. Although changes in chemical weathering intensity on continents are driven primarily by natural factors—such as physical weathering rates, vegetation, rainfall, and temperature (*11*, *12*)—intensive land use and accelerated soil denudation by increasing the surface area of minerals and rocks exposed to weathering can also dramatically lead to much higher rates of chemical alteration (*13*). The degree of chemical weathering of fine-grained sediments can be inferred from the ratio of aluminum to potassium (Al/K). Potassium is highly mobile during chemical weathering and typically depleted in soils, whereas aluminum is one of the most immobile elements, being incorporated into secondary clay minerals such as kaolinite (see SOM text). High Al/K ratios in Congo fan sediments are therefore considered to be indicative of periods of intense chemical weathering in the Congo basin (*14*). Because downcore variations of the bulk chemical composition can also reflect changes in the sediment source, we measured neodymium (Nd) and hafnium (Hf) isotopic ratios to discriminate between both weathering and provenance signals in our sediment record. The Nd isotopic signature of terrigenous sediments is retained during continental weathering and subsequent transport, thereby providing direct information on the geographical provenance of sediment (*15*). Hafnium isotopes exhibit globally similar behavior but are also prone to substantial fractionation during chemical weathering, because incongruent dissolution of silicate rocks leads to products of erosion having very distinctive but systematic Hf isotopic signatures (see SOM text) (*16*, *17*).

In this study, we quantitatively determined the bulk sedimentary major element composition of KZAI-01 at a 5-cm sampling interval (Fig. 2), corresponding to a temporal resolution of ~100 to 400 years. The age model for KZAI-01 is based on accelerator mass spectrometry (AMS) radiocarbon measurements of mixed marine carbonate fractions and tuning to a well-dated nearby sediment record from the Gulf of Guinea (GeoB6518-1; see location in Fig. 1). We also obtained additional age constraints from ^{14}C-AMS dating of bulk sediment organic carbon (Fig. 2). Figure 3A shows that the Nd isotopic composition of sediments deposited at site KZAI-01 (average $\varepsilon_{Nd} \sim -15.9 \pm 0.6$) is almost constant and very similar to that reported for present-day riverine particulates from the Congo basin (*18*). This indicates that the source of material delivered to the ocean by the Congo River has remained unchanged during the Late Quaternary. In contrast, Hf isotopes display significant downcore variations (from $\varepsilon_{Hf} \sim -6.8$ to -13.9), which correlate well with the Al/K depth profile (Fig. 3, A and B). Because grain size is homogeneous in this core, with medians ranging from 4 to 6 μm (*17*), the large range of ε_{Hf} values cannot be explained by changes in the relative proportions of mineral phases with distinct Hf isotope signatures. Therefore, these data show that downcore fluctuations of both ε_{Hf} and Al/K ratios at site KZAI-01 reflect variations in chemical weathering intensity within the Congo River drainage basin, rather than changes in sediment provenance and/or grain size.

Comparison of our proxy data with organic geochemical and molecular records from core GeoB6518-1 suggests that much of the weathering signal at site KZAI-01 is driven by continental precipitation. From ~20,000 to 3500 years ago, our weathering record exhibits strong correlation with the precipitation signal from core GeoB6518-1, inferred from the deuterium composition of plant waxes (Fig. 3C) (*19*, *20*). This observation suggests that chemical alteration in the Congo basin has responded quickly to regional climatic changes, at least for the time scales being considered here. The trends toward wetter conditions that are visible in the GeoB6518-1 deuterium record, between ~18 to 13 and ~12 to 9 ky B.P., coincide well with marked periods of intensifying chemical weathering. Similarly, the progressive onset of dryer conditions since ~6 ky B.P., which marks the end of the African Humid Period, is accompanied by lower weathering rates. Reduced weathering rates also occurred during the Younger Dryas, between ~12.8 and 11.5 ky B.P., a period characterized by lower precipitation levels in Central Africa (*19*). In comparison, the evolution of mean annual temperatures in Central Africa has been very gradual since the last deglaciation, rising smoothly from ~21° to 25°C (*21*). Most likely, this suggests that temperature only played a minor role in controlling past chemical weathering variations in the Congo basin during the Late Quaternary.

Institut Français de Recherche pour l'Exploitation de la Mer (IFREMER), Unité de Recherche Géosciences Marines, F-29280 Plouzané, France.

*To whom correspondence should be addressed. E-mail: gbayon@ifremer.fr

From ~3500 years B.P., an abrupt trend toward higher Al/K and Hf isotope values indicates rapidly intensifying chemical weathering. The weathering peak, centered at ~2500 years B.P., is characterized by the highest Al/K and ε_{Hf} values measured throughout core KZAI-01, indicating that global weathering rates in the Congo basin during that period were higher than at any other time in the past 40,000 years. After ~2000 years B.P., chemical weathering intensity values decreased slightly but still remained at much higher levels than before 3000 years B.P. The weathering episode occurred contemporaneously with the major vegetation change in Central Africa during the third millennium B.P., illustrated in Fig. 3E by the sudden increase in the abundance of herbaceous pollen taxa (*Gramineae*) at Lake Barombi Mbo (see location in Fig. 1) (*3*). This event is well documented in numerous palynological and sedimentological records (*1*–*4*), from the equatorial Atlantic coastal area to the eastern border of the Congo basin, near the Great Lakes region of Africa (Fig. 1). At many sites, proxy records for past vegetation patterns indicate a major loss of primary forest between ~3000 and 2200 calendar years B.P. and its replacement by savannas and other pioneer formations. To some extent, this large-scale deforestation event shaped the African rain forest into its present-day vegetation patterns (*1*, *2*). The cause usually invoked for the forest disturbance is a global shift toward seasonally dryer conditions in Central Africa (*1*, *4*). This hypothesis is in agreement with the Late Holocene rainfall signals for tropical regions, which indicate reduced precipitation levels from ~4000 years B.P. (*1*, *19*). At that time, one would expect the weathering signal at site KZAI-01 to follow the same way it evolved during the past 40 ky when continental climate became dryer; i.e., toward lower intensity levels (lower Al/K ratios). Instead, evidence that chemical alteration strongly intensified during the third millennium B.P., thus departing from the long-term weathering fluctuations related to the Late Quaternary climate, suggests that this weathering event was not triggered by natural climatic factors.

We are confident that this pulse of intense chemical weathering does not reflect reworking of sediments on the shelf, due to sea-level rise, for example, or denudation of strongly weathered ancient soils from the Congo basin. At the time of deposition, the global mean sea level in the oceans had already been close to modern values for several millennia at least (*22*). In addition, the calibrated ages for bulk organic matter samples in this part of core KZAI-01, which include a substantial continental organic fraction (*23*), agree well with those inferred from our age model (determined from radiocarbon dating of marine carbonate material) (see table S3). Importantly, this suggests that the suspended particles transported by the Congo River during that period were mainly derived from relatively young soils rather than from older tropical soils. Taken together, these observations clearly show that

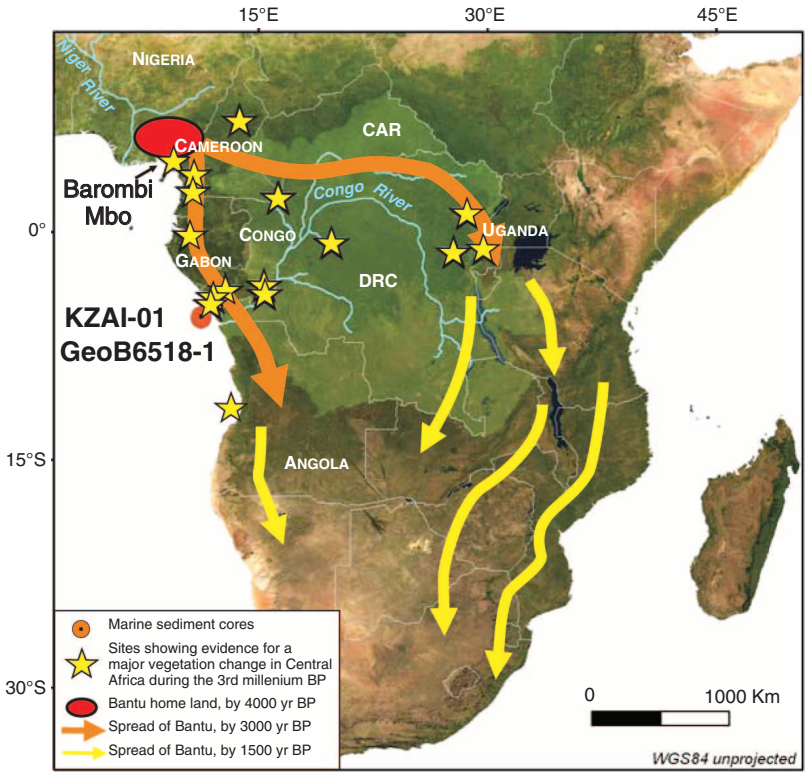

Fig. 1. African satellite map showing the location of the studied core (KZAI-01). A major vegetation change was reported at a number of sites in Central Africa between ~3000 and 2000 years ago (yellow stars) (fig. S1), with evidence for a substantial loss of primary forest and expansion of savannas and other pioneer formations. This deforestation event was contemporaneous with the migration of Bantu-speaking agriculturalists originating from the Nigeria-Cameroon area. During the third millennium B.P., Bantu farmers spread both southward (across Atlantic equatorial Africa) and eastward (through the Congo watershed), reaching Angola and the Great Lakes region by ~2500 years B.P., respectively (thick orange arrows). Thin yellow arrows represent subsequent migration waves toward southern Africa. CAR, Central African Republic; DRC, Democratic Republic of the Congo.

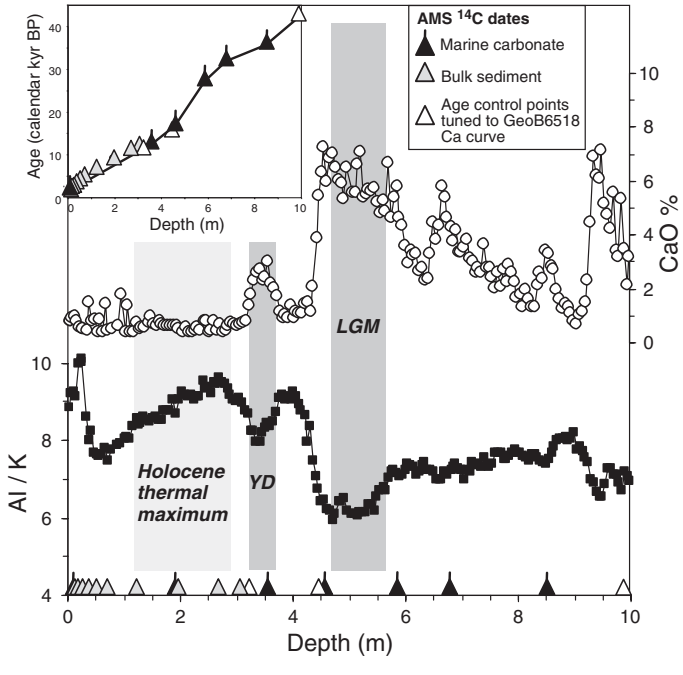

Fig. 2. CaO concentrations (weight percent) and Al/K ratios versus core depth (m) in core KZAI-01. The triangles indicate the position of AMS ^{14}C dates for mixed marine carbonate fraction (black) and bulk organic matter (gray), as well as the age control points tuned to the well-dated nearby core GeoB6518-1 (white). The upper-left inset shows the depth versus calendar age plot for KZAI-01. LGM, Last Glacial Maximum; YD, Younger Dryas; kyr, thousand years.

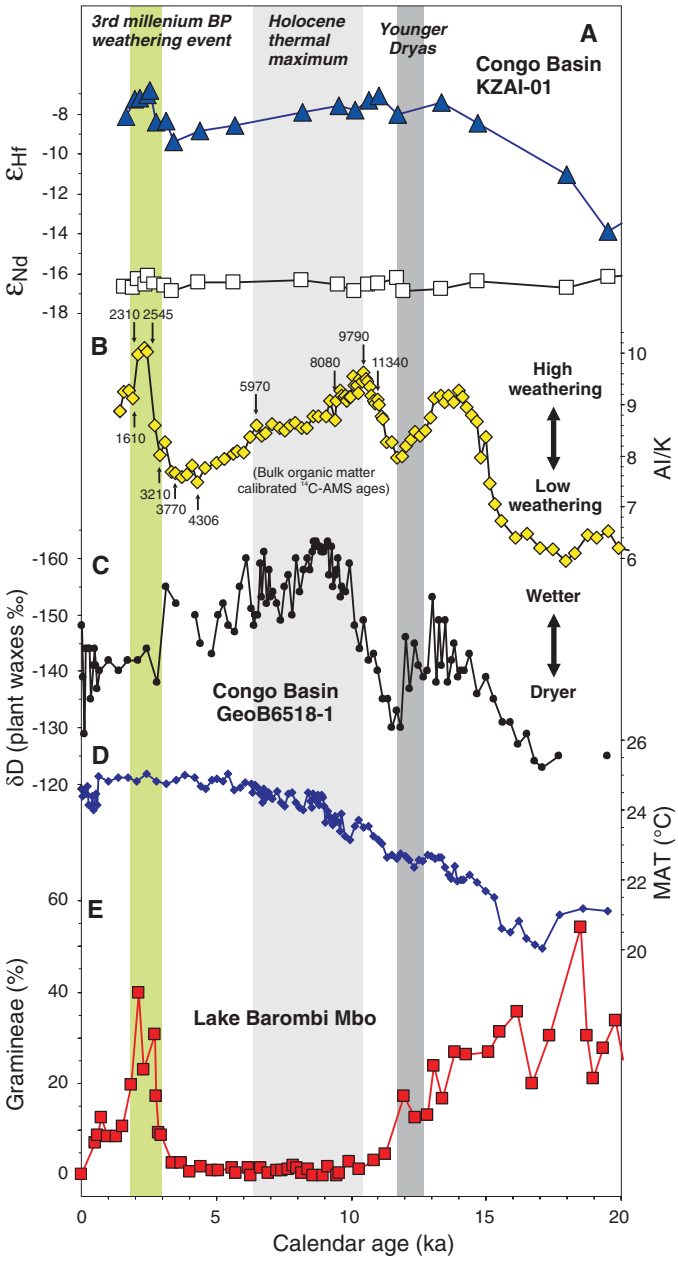

Fig. 3. Proxy records for source provenance and chemical weathering intensity in core KZAI-01 and comparison with paleoclimatic and paleovegetation records. (**A**) Neodymium and hafnium isotopic composition in core KZAI-01 (expressed as ε_{Nd} and ε_{Hf}, respectively), as proxies for sediment provenance and chemical weathering intensity. (**B**) The Al/K record from core KZAI-01 indicating variations of chemical weathering intensity in Central Africa. (**C**) Plant-wax δD values (per mil) in core GeoB6518-1, as an index of precipitation changes in Central Africa (*19*). (**D**) The annual mean annual temperature (MAT) record of the Congo basin in core GeoB6518-1, based on biomarkers (*21*). (**E**) Abundance of pollen from herbaceous plants (mainly *Gramineae*) at the Lake Barombi Mbo (Cameroon), reflecting the relative presence of savannas versus forests in western equatorial Africa (*3*). ka, thousand years ago.

the anomalously high Al/K values in the upper part of core KZAI-01 correspond to a true contemporaneous signal of chemical weathering from the Congo basin.

In fact, recent archaeological surveys showed that the deforestation event in the third millennium B.P. coincided with the large-scale settlement of Bantu-speaking farmers in subequatorial Africa (*4*, *10*, *24*). The first Bantu speakers were cultivators in the eastern Nigeria and western Cameroon area, who began to spread eastward and southward ~4000 years ago (*5*–*9*). From the third millennium B.P., a major expansion wave was associated with the introduction of agriculture into the central African rainforest (*5*, *10*, *24*). This period coincides with marked increases in the abundance of oil palm pollen at numerous sites across West and Central Africa, interpreted as evidence for intensifying plant cultivation (*25*). In this region, numerous archeological sites containing ceramics, domesticated crop remains, oil palm nuts, and stone tools were dated between ~3000 and 2000 years ago (*24*, *26*–*29*). At that time, the cultivation of savanna crops, such as pearl millet and yams, was made possible by the onset of seasonality alternance between wet and dry seasons (*4*, *24*). The discoveries of several iron-working furnaces and smelted iron artifacts in Cameroon, Gabon, the Central African Republic, and Congo, dating from the same period or even older, also indicated that the Bantu farmers were carrying the technology for iron metallurgy (*29*–*33*).

One hypothesis to link the rainforest crisis to intensifying human activities in Central Africa during the third millennium B.P. has been to propose that the deforestation event created favorable conditions for the settlement of Bantu farmers across Central Africa, through opening of savanna corridors (*4*, *34*). Alternatively, the introduction of novel agricultural practices and iron-smelting technology may also have led to intensive land clearance for shifting cultivation and charcoal production, thus being partly responsible for the major vegetation change ~2500 years ago (*10*). Because land use, anthropogenic deforestation, and agriculture would have increased rates of soil erosion and, as a consequence, chemical weathering, intensifying human activities in subequatorial Africa hence represent a plausible explanation for the weathering episode in the third millennium B.P. Based on our results, it is difficult to assess the degree to which human land use and/or climate change played a role during this Late Holocene deforestation event. However, evidence from our proxy record that chemical weathering rates at that time were unprecedented during the past 40,000 years clearly suggests that the environmental impact of the human population in the central African rainforest was already extensive ~2500 years ago, at least greater than that induced by the Late Quaternary climatic oscillations.

References and Notes

1. A. Vincens *et al.*, *J. Biogeogr.* **26**, 879 (1999).
2. J. A. Maley, *IDS Bull.* **33**, 13 (2002).
3. J. Maley, P. Brenac, *Rev. Palaeobot. Palynol.* **99**, 157 (1998).
4. A. Ngomanda, K. Neumann, A. Schweizer, J. Maley, *Quat. Res.* **71**, 307 (2009).
5. J. Diamond, P. Bellwood, *Science* **300**, 597 (2003).
6. T. N. Huffman, *Annu. Rev. Anthropol.* **11**, 133 (1982).
7. D. W. Phillipson, *African Archaeology* (Cambridge Univ. Press, Cambridge, 1993).
8. J. Vansina, *J. Afr. Hist.* **25**, 129 (1984).
9. C. J. Holden, *Proc. R. Soc. London Ser. B Biol. Sci.* **269**, 793 (2002).
10. K. J. Willis, L. Gillson, T. M. Brncic, *Science* **304**, 402 (2004).
11. A. F. White, A. E. Blum, *Geochim. Cosmochim. Acta* **59**, 1729 (1995).
12. J. Gaillardet, B. Dupré, P. Louvat, C. J. Allègre, *Chem. Geol.* **159**, 3 (1999).
13. P. A. Raymond, J. J. Cole, *Science* **301**, 88 (2003).
14. R. R. Schneider, B. Price, P. J. Müller, D. Kroon, I. Alexander, *Paleoceanography* **12**, 463 (1997).
15. S. L. Goldstein, R. K. O'Nions, P. J. Hamilton, *Earth Planet. Sci. Lett.* **70**, 221 (1984).
16. G. Bayon *et al.*, *Geology* **34**, 433 (2006).
17. G. Bayon *et al.*, *Earth Planet. Sci. Lett.* **277**, 318 (2009).
18. C. J. Allègre, B. Dupré, P. Négrel, J. Gaillardet, *Chem. Geol.* **131**, 93 (1996).
19. E. Schefuß, S. Schouten, R. R. Schneider, *Nature* **437**, 1003 (2005).
20. Hydrogen isotope abundances (δD, in per mil relative to Vienna standard mean ocean water) in terrestrial plant waxes are controlled by the precipitation-evaporation balance and humidity levels in tropical areas, therefore reflecting predominantly continental rainfall fluctuations (*19*).
21. J. W. H. Weijers, E. Schefuß, S. Schouten, J. S. Sinninghe Damsté, *Science* **315**, 1701 (2007).
22. K. Fleming *et al.*, *Earth Planet. Sci. Lett.* **163**, 327 (1998).
23. J. W. H. Weijers, S. Schouten, E. Schefuß, R. R. Schneider, J. S. Sinninghe Damsté, *Geochim. Cosmochim. Acta* **73**, 119 (2009).
24. K. Neumann *et al.*, *Quat. Int.* **249**, 53 (2012).
25. M. A. Sowunmi, *Veg. Hist. Archaeobot.* **8**, 199 (1999).

26. B. Clist, *Afr. Archaeol. Rev.* **7**, 59 (1989).
27. J. Denbow, *Afr. Archaeol. Rev.* **8**, 139 (1990).
28. C. M. Mbida, W. Van Neer, H. Doutrelepont, L. Vrydaghs, *J. Archaeol. Sci.* **27**, 151 (2000).
29. A. A. Ndong, *L'Anthropologie* **106**, 135 (2002).
30. M. K. H. Eggert, in *The Archaeology of Africa; Food, Metals and Towns*, T. Shaw, P. Sinclair, B. Andah, A. Okpoko, Eds. (Routledge, London, 1993), pp. 289–329.
31. R. Oslisly, in *The Growth of Farming Communities in Africa from the Equator Southwards*, vols. 29-30, J. E. G. Sutton, Ed. (Azania, Nairobi, Kenya, 1994), pp. 324–331.
32. E. Zangato, A. F. C. Holl, *J. Afr. Archaeol.* **8**, 7 (2010).
33. D. Schwartz, H. de Foresta, R. Deschamps, R. Lanfranchi, *C. R. Acad. Sci. Paris Ser. 2* **310**, 1293 (1990).
34. D. Schwartz, *Bull. Soc. Geol. Fr.* **163**, 353 (1992).

Acknowledgments: This work was sponsored by the French National Research Agency (ANR), via the ECO-MIST project (2010 JCJC 609 01). Core KZAI-01 was collected during the Zaiango project funded by IFREMER and TOTAL (chief scientist: B. Savoye). We thank F. Jansen for providing five radiocarbon dates and giving access to the x-ray fluorescence core-scanner data set for core GeoB6518; J. Maley for stimulating discussion, sharing bibliographic resources, and providing Lake Barombi Mbo pollen data; Y. Germain for help in the laboratory; and W. F. Ruddiman, N. C. Chu, and five anonymous referees for their constructive comments on the manuscript. The data reported in this paper are listed in the SOM.

Supporting Online Material

www.sciencemag.org/cgi/content/full/science.1215400/DC1
Materials and Methods
SOM Text
Fig. S1
Tables S1 to S3
References (*35*–*67*)

17 October 2011; accepted 2 February 2012
Published online 9 February 2012;
10.1126/science.1215400

A Bruce Effect in Wild Geladas

Eila K. Roberts,[1] Amy Lu,[1,2] Thore J. Bergman,[1,3] Jacinta C. Beehner[1,4]*

Female rodents are known to terminate pregnancies after exposure to unfamiliar males ("Bruce effect"). Although laboratory support abounds, direct evidence for a Bruce effect under natural conditions is lacking. Here, we report a strong Bruce effect in a wild primate, the gelada (*Theropithecus gelada*). Female geladas terminate 80% of pregnancies in the weeks after a dominant male is replaced. Further, data on interbirth intervals suggest that pregnancy termination offers fitness benefits for females whose offspring would otherwise be susceptible to infanticide. Taken together, data support the hypothesis that the Bruce effect can be an adaptive strategy for females.

More than half a century ago, biologist Hilda Margaret Bruce demonstrated that recently pregnant female mice (*Mus musculus*) terminate pregnancies after exposure to unfamiliar males ("Bruce effect") (*1*–*3*). Since these initial experiments, the Bruce effect has been experimentally confirmed across a multitude of rodent taxa [and domestic horses (*4*)] under exclusively captive conditions [(*5*, *6*); reviewed in (*7*)]. However, despite the bounty of support for the Bruce effect in the laboratory, it remains unknown whether it occurs under natural conditions. At least two experimental studies conducted on wild rodents failed to find a Bruce effect (*8*, *9*), and all other reports of male-induced pregnancy termination from wild populations have been based on indirect evidence [i.e., a drop in the birthrate: rodents (*10*), lions (*11*), wild horses (*12*)] or anecdotal evidence [i.e., direct observations of several aborted fetuses after the arrival of new males in Hanuman langurs (*13*, *14*), hamadryas baboons (*15*), yellow baboons (*16*), and geladas (*17*)]. The most comprehensive study to demonstrate a Bruce effect in a noncaptive setting was conducted on wild (feral) horses relying on visual observations of pregnancy and estrus to ascertain fetal loss (*12*). This conspicuous dearth of direct support has led some to propose that the Bruce effect is nothing more than a laboratory artifact with no functional explanation (*18*, *19*).

Certainly, the Bruce effect has been a conundrum to biologists since its discovery, as many [including Darwin (*20*)] have pondered the evolutionary reasons that a female would terminate a pregnancy. The leading adaptive hypothesis is that it evolved as a countertactic for females whose offspring would be susceptible to infanticide after the arrival of a new male (*21*, *22*). Under certain conditions, it may be less costly for a female to terminate a pregnancy than to waste investment on otherwise "doomed" offspring. However, no captive or wild studies have demonstrated a fitness advantage for females that terminate pregnancies in response to novel males.

Here, we use 5 years of demographic and hormone data to test for a Bruce effect in a wild primate population with a high risk of infanticide—the gelada (*Theropithecus gelada*). Anecdotal accounts on abortions after male replacements (*17*, *23*) prompted us to investigate whether female geladas exhibit a Bruce effect and, if so, whether such an effect is adaptive.

Geladas are terrestrial, Old World monkeys that live in polygynous, matrilineal, one-male units ("groups") comprising one dominant male and 1 to 12 females (*24*). Reproductive success for dominant males is contingent upon maintaining reproductive control over the group. Threats to dominant males come from bachelor males residing in all-male groups. Once a dominant male is ousted and replaced by a bachelor, the bachelor male gains reproductive access to all of the group's females and often kills any dependent offspring sired by his predecessor (*17*, *23*). As nonseasonal breeders with prolonged interbirth intervals (*23*) and high paternity certainty (*25*), gelada males presumably employ infanticide as an adaptive strategy. It causes (previously) lactating females to resume cycling almost immediately, thus accelerating the next conception by the infanticidal male (*23*). After male replacements, 43.8% of infants are lost to suspected infanticide by males (*23*). Given this high frequency of infanticide after male replacements, a Bruce effect could be adaptive for pregnant females if it minimizes the interbirth interval between successful offspring.

To test for a Bruce effect, we collected demographic and behavioral data from a wild population of geladas living in the Simien Mountains National Park in Ethiopia. Our study population comprised 110 females across 21 groups over a 5-year period (January 2006 to June 2011). First, we used demographic data to examine the pattern of births relative to male replacements ($N = 28$ replacements). Specifically, we examined the number of births during the 6 months after a male replacement for each group. Assuming a 183-day gestation (±4.8 days; $N = 16$ females), any infants born during this period would presumably have been sired by the predecessor (i.e., candidates for a Bruce effect). To control for seasonality in male replacements and/or births, we paired each group that experienced a male replacement ("replacement group") with a comparable group that did not experience one ("control group"). We selected control groups that: (i) had not experienced

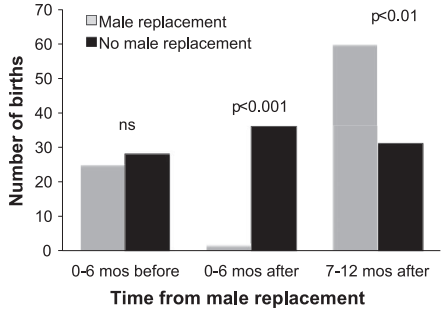

Fig. 1. Number of births for groups with and without male replacements. Sum of births from groups with a male replacement (light gray) as compared with a similar-sized group at the same time that did not experience a male replacement (black). Paired groups were compared (Wilcoxon signed-ranks test) 0 to 6 months before male replacement, 0 to 6 months after male replacement, and 7 to 12 months after male replacement.

[1]Department of Psychology, University of Michigan, Ann Arbor, MI 48109, USA. [2]New York Consortium of Evolutionary Primatology, New York, NY 10016, USA. [3]Department of Ecology and Evolutionary Biology, University of Michigan, Ann Arbor, MI 48109, USA. [4]Department of Anthropology, University of Michigan, Ann Arbor, MI 48109, USA.

*To whom correspondence should be addressed. E-mail: jbeehner@umich.edu

a male replacement during the previous year, (ii) had not already been used as a control group, and (iii) had a nearly equivalent (±2) number of females as replacement groups. When more than one choice was available ($N = 4$ cases), we conservatively chose the control group with fewer females. We then compared the number of births for replacement (28 male replacements, 140 females) and control groups (0 male replacements, 136 females) across the same period of time.

Consistent with a Bruce effect, replacement groups exhibited a pattern strikingly different from that of control groups (Fig. 1). During the 6 months before male replacements, paired groups exhibited no difference in the number of births (Wilcoxon signed-ranks test: $Z = -0.43$; $P = 0.67$). However, during the 6 months after male replacements, replacement groups exhibited significantly fewer births than control groups (Wilcoxon signed-ranks test: $Z = -3.56$; $P < 0.001$). Indeed, only two infants sired by the predecessor were born after male replacements (compared with 36 infants born in control groups). During the 7 to 12 months after male replacements, replacement groups exhibited a twofold increase in births compared with control groups (Wilcoxon signed-ranks test: $Z = -2.65$; $P < 0.01$).

Although these data are compelling, they provide only indirect evidence for a Bruce effect. To directly determine whether this reduction in births was due to pregnancy termination, we used fecal hormone data collected from specific females. Daily or weekly hormone sampling from all 110 females was not feasible. Therefore, we sampled females at different frequencies (daily, weekly, or monthly) based on their likelihood of being (or getting) pregnant during the study (Table 1). Steroid hormones (i.e., estradiol metabolites) were extracted from feces in the field, preserved using a solid-phase extraction cartridge, stored at subzero temperatures until analysis, and assayed for 17β-estradiol (E2) using a radioimmunoassay kit produced by MP Biomedicals [see supporting online material (SOM) for details].

We used estrogen metabolite profiles to identify all pregnancies, including those that did not result in a live birth ("pregnancy failures"). To do this, we used samples from females with daily sampling to establish normative fecal estrogen (fE) levels for the nonperiovulatory period (mean fE = 4.98 ± 0.69 ng/g; $N = 7$) and the periovulatory period (mean fE = 21.45 ± 4.95 ng/g; $N = 7$). We then assigned pregnancy based on a steady rise in fE above periovulatory levels (*26*). For females without daily hormone samples, a pregnancy was assigned if two fE values across more than 5 days were above periovulatory levels. A pregnancy failure was assigned if no live birth resulted from a hormonally determined pregnancy. One pregnant female (and her group)

Table 1. Fecal hormone sample schedule and collection rates.

	Groups	Females	Fecal samples*	Sample rate
High coverage	5	10	331	1 sample/1.9 days
Mid coverage	14	62	670	1 sample/7.6 days
Low coverage	18	88	1000	1 sample/29.2 days
Total	20†	106†	2001	

*Number of females in each category does not include all females in the group. High-coverage females were selected based on probability of being or becoming pregnant. †Groups and females are represented by more than one "coverage" schedule; therefore, the total number of groups and females does not add up to the sum of each category.

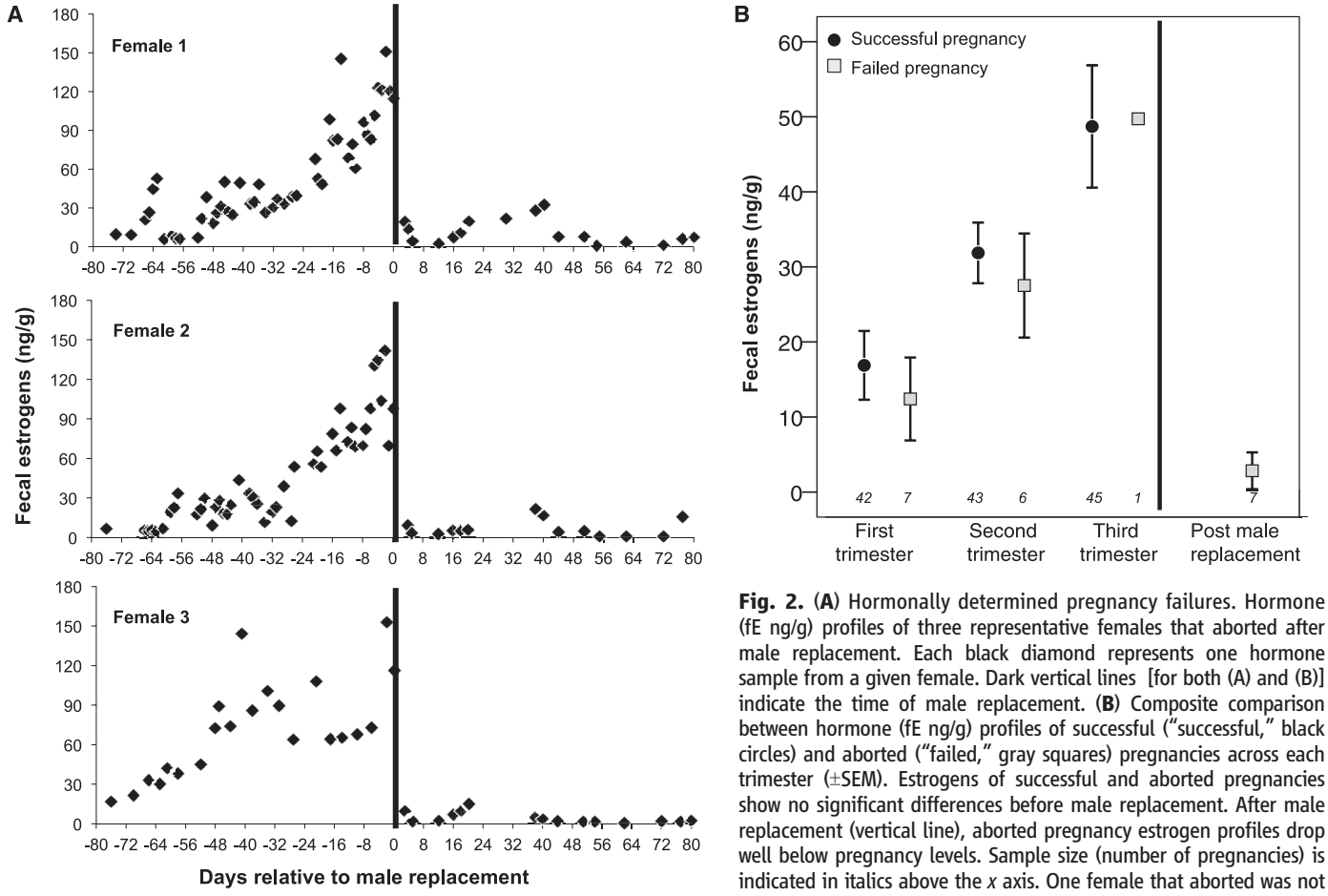

Fig. 2. (**A**) Hormonally determined pregnancy failures. Hormone (fE ng/g) profiles of three representative females that aborted after male replacement. Each black diamond represents one hormone sample from a given female. Dark vertical lines [for both (A) and (B)] indicate the time of male replacement. (**B**) Composite comparison between hormone (fE ng/g) profiles of successful ("successful," black circles) and aborted ("failed," gray squares) pregnancies across each trimester (±SEM). Estrogens of successful and aborted pregnancies show no significant differences before male replacement. After male replacement (vertical line), aborted pregnancy estrogen profiles drop well below pregnancy levels. Sample size (number of pregnancies) is indicated in italics above the *x* axis. One female that aborted was not included in the figure because we were unable to obtain a hormone sample from her immediately after male replacement; she is known to have aborted because she expelled a poorly developed fetus (*23*) the day after a male replacement.

disappeared for 3 weeks around the expected time of birth and reappeared with no infant. We do not know if she aborted or lost the infant shortly after birth. Because this case was not associated with a male replacement, we conservatively included it as the only pregnancy failure in the background rate. After identifying all pregnancy failures, we then examined the timing of failures relative to male replacements ($N = 9$ replacements, for this subset of data) to determine whether the rate of failure during the month after male replacements was higher than the background rate.

The hormone data unambiguously confirm that females terminated pregnancies after male replacements (Fig. 2, A and B). Of 60 hormonally determined pregnancies, only nine ended in pregnancy failure, with eight of these occurring during the 2 weeks after a male replacement (range 3 to 13 days after replacement). These eight failures occurred in eight different females across five male replacements. Ten of these hormonally determined pregnancies spanned a male replacement. Of these 10 pregnancies, 8 ended in failure during the 2 weeks after a male replacement. The pregnancy failure rate after male replacements (80%, or 8 failures in 10 pregnancies) was significantly higher than the background rate (2%, or 1 failure in 50 pregnancies; binomial test: $P < 0.001$). In one male replacement, the new male cleaved off a "daughter" group from a "parent" group (i.e., a group fission). The pregnancy failure after the fission occurred in the parent group (still led by the presumed sire), not the daughter group. Therefore, it is unclear whether this case represents a Bruce effect (i.e., male-induced) or just a pregnancy failure. Results do not change if we place this failure in the background category (binomial test: $P < 0.001$).

To establish the timing of pregnancy failures, we used fE values to estimate the day of conception. Fecal estrogen data from successful pregnancies indicated that pregnancy fE is indistinguishable from nonpregnant fE until the third week of pregnancy for this species ($N = 11$ pregnancies with weekly sampling), a result also found for another closely related species (*26*). Therefore, for all pregnancy failures, we assigned conception as 21 days before the initial fE rise above periovulatory levels. Based on these estimates, at the time of abortion, one female was in the first trimester (gestation day 54), six females were in the second trimester (gestation days 76 to 116), and one female was in the third trimester (gestation day 151), suggesting that a Bruce effect in geladas may be possible at any stage of gestation (table S2). In only two cases did we observe the aborted fetus (table S1). For the other six cases (particularly late second- and third-trimester pregnancy terminations), we speculate that the fetus was expelled and lost during the night on the sleeping cliffs.

An analysis of interbirth intervals (IBIs) indicates that a Bruce effect may have fitness benefits for gelada females (Fig. 3). Note that all IBIs calculated below refer to the time period between a surviving infant and the subsequent infant. Outside the context of male replacements, the mean IBI for this population was 2.37 years (±0.51 SD; $N = 37$ IBIs). After male replacements, the mean IBI for females that aborted was 2.65 years (±0.54 SD; $N = 6$ IBIs), a nonsignificant difference from the population mean (Mann-Whitney test: $Z = -1.21$; $P = 0.23$). By contrast, females that lost their infants to infanticide had an IBI of 3.62 years (±0.82 SD; $N = 3$). To increase the sample size for statistical comparisons, we added IBIs from females that lost their infants due to other causes (i.e., predation or illness: IBI = 3.81 ± 0.44 years; $N = 2$), resulting in a mean IBI of 3.70 years (±0.63 SD; $N = 5$). This IBI after the death of an infant is significantly longer than the population mean (Mann-Whitney test: $Z = -3.24$; $P = 0.001$) (Fig. 3) or the IBI after abortions (Mann-Whitney test: $Z = -2.19$; $P = 0.028$) (Fig. 3). Correcting for the odds of infanticide (43.8%), the average IBI for females that do not abort is 2.95 years—still higher than either the population mean or the IBI after abortion. Further, because male tenure as the dominant male in a group [~3 years (*23*)] is longer than the mean IBI for this population, females that time conceptions with male replacements are likely to be weaning (or have weaned) those infants by the time the next male replacement occurs.

What might the proximate mechanism be for a Bruce effect in geladas? In rodents, the presence of strange males can trigger a Bruce effect through pheromonally induced gonadotropin release in the female, causing decreased prolactin secretion (*3*, *27*, *28*). Additionally or alternatively, a Bruce effect could also be triggered by heightened levels of physiological stress associated with new males [e.g., increased levels of aggression (*16*) or elevated infanticide risk] or other stressful situations [e.g., elevated predation risk (*29*)]. The latter mechanism would suggest that a Bruce effect is part of a more general female strategy to curtail investment in offspring that may not survive. At present, because abortions occurred almost immediately after male replacements, our hormonal and behavioral data were not sufficiently fine-grained across these critical few days to test a stress mechanism.

Taken together, the demographic and hormonal data suggest that the Bruce effect is not only a frequent counterstrategy to infanticide employed by pregnant geladas (used by 80% of pregnant females after male replacements) but also an advantageous one. Under conditions where infant survival is minimal due to susceptibility to infanticide, natural selection should favor females that retain the ability to terminate pregnancies before a hefty investment in gestation and lactation. Pregnancy termination by females (in particular, a Bruce effect) may be a facultative response that allows females to maximize their reproductive output in a rapidly changing social [or physical (*30*)] environment.

It is unclear how widespread the Bruce effect may be across mammals. First, data are scarce. Demonstrating a Bruce effect in a wild population requires frequent hormone sampling from females both before and after an unpredictable event (i.e., a male replacement). The effect may therefore be difficult to detect and possibly more widespread than we realize.

Second, a Bruce effect may not constitute an adaptive countertactic to infanticide for all female mammals. As previously reported (*6*), only species characterized by polygyny or monogamy, high paternity certainty, and high infanticidal risk should be prime candidates for a Bruce effect. However, equally important, a female's subsequent offspring must be less susceptible to infanticide than her current one. In other words, a female should only exhibit a Bruce effect if there is some certainty that her next offspring will be spared the same fate. The reproductive suppression model (*31*) suggests that, when future reproductive conditions are likely to be better than present ones, females should suppress reproduction; and when future conditions are unlikely to improve, females should continue with current reproduction regardless of cost. In geladas, male tenure as the dominant male (~3 years) is roughly equivalent to the IBI (2.62 years). Therefore, females that immediately conceive with an incoming male have a high probability that the new sire will remain dominant until the offspring is weaned. Species without such assurance should not exhibit a Bruce effect. For example, chacma baboons (*Papio ursinus*)—also characterized by polygyny, high paternity certainty, and high infanticide rates—have a much shorter male tenure [~6 months (*32*)] than IBI [~2 years (*33*)]. Under such circumstances, females that conceive with a dominant male have a very low probability that the sire will remain dominant through weaning (indeed, a chacma female is likely to see three to four different males across her 2-year lactational

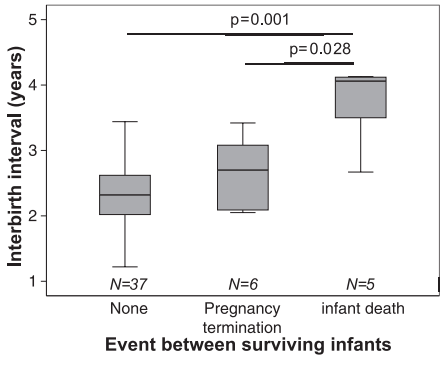

Fig. 3. Boxplot of interbirth intervals between successfully weaned infants (whiskers represent highest and lowest values). Interbirth intervals (in years) for females experiencing different events between infants. None: two successive infants; pregnancy termination: an abortion between surviving infants; infant death: an infant death between surviving infants. Sample size (number of interbirth intervals) is indicated in italics above the *x* axis.

amenorrhea). When prospects for future offspring survival are no better than those for the current offspring, a Bruce effect is not an effective strategy. Investigating whether the reproductive suppression model explains the distribution of a Bruce effect across mammals must await further data from natural populations.

References and Notes

1. H. M. Bruce, *Nature* **184**, 105 (1959).
2. H. M. Bruce, *J. Reprod. Fertil.* **1**, 96 (1960).
3. A. S. Parkes, H. M. Bruce, *Science* **134**, 1049 (1961).
4. L. Bartos, J. Bartosova, J. Pluhacek, J. Sindelarova, *Behav. Ecol. Sociobiol.* **65**, 1567 (2011).
5. S. D. Becker, J. L. Hurst, *Proc. R. Soc. Lond. B Biol. Sci.* **276**, 1723 (2009).
6. N. Pillay, A. A. Kinahan, *Behaviour* **146**, 139 (2009).
7. J. B. Labov, *Am. Nat.* **118**, 361 (1981).
8. H. M. de la Maza, J. O. Wolff, A. Lindsey, *Behav. Ecol. Sociobiol.* **45**, 107 (1999).
9. S. J. Mahady, J. O. Wolff, *Behav. Ecol. Sociobiol.* **52**, 31 (2002).
10. F. F. Mallory, F. V. Clulow, *Can. J. Zool.* **55**, 1 (1977).
11. B. C. R. Bertram, *J. Zool.* **177**, 463 (1975).
12. J. Berger, *Nature* **303**, 59 (1983).
13. G. Agoramoorthy, S. M. Mohnot, *Hum. Evol.* **3**, 279 (1988).
14. G. Agoramoorthy, S. M. Mohnot, V. Sommer, A. Srivastava, *Hum. Evol.* **3**, 297 (1988).
15. F. Colmenares, M. Gomendio, *Folia Primatol. (Basel)* **50**, 157 (1988).
16. M. E. Pereira, *Am. J. Primatol.* **4**, 93 (1983).
17. U. Mori, R. I. M. Dunbar, *Z. Tierpsychol.* **67**, 215 (1985).
18. F. H. Bronson, A. Coquelin, Eds., *The Modulation of Reproduction by Priming Pheromones in House Mice: Speculations on Adaptive Function* (Plenum Press, New York, 1980), pp. 243–265.
19. J. O. Wolff, *Bioscience* **53**, 421 (2003).
20. C. Darwin, *The Descent of Man, and Selection in Relation to Sex* (Murray, London, 1971).
21. P. L. Schwagmeyer, *Am. Nat.* **114**, 932 (1979).
22. S. B. Hrdy, *Ethol. Sociobiol.* **1**, 13 (1979).
23. J. C. Beehner, T. J. Bergman, *Am. J. Primatol.* **70**, 1152 (2008).
24. R. I. M. Dunbar, *Reproductive Decisions: An Economic Analysis of Gelada Baboon Social Strategies* (Princeton University Press, Princeton, 1984).
25. T. J. Bergman, N. Snyder-Mackler, S. C. Alberts, *Am. J. Phys. Anthropol.* **144**, 88 (2011).
26. J. C. Beehner, N. Nguyen, E. O. Wango, S. C. Alberts, J. Altmann, *Horm. Behav.* **49**, 688 (2006).
27. C. J. Dominic, *J. Reprod. Fertil.* **11**, 415 (1966).
28. S. R. Milligan, *J. Reprod. Fertil.* **46**, 97 (1976).
29. S. D. Becker, J. L. Hurst, in *Chemical Signals in Vertebrates*, J. L. Hurst, Ed. (Springer, New York, 2008), vol. 11, pp. 141–150.
30. J. C. Beehner, D. A. Onderdonk, S. C. Alberts, J. Altmann, *Behav. Ecol.* **17**, 741 (2006).
31. S. K. Wasser, D. P. Barash, *Q. Rev. Biol.* **58**, 513 (1983).
32. W. J. Hamilton III, J. B. Bulger, *Behav. Ecol. Sociobiol.* **26**, 357 (1990).
33. D. L. Cheney *et al.*, *Int. J. Primatol.* **25**, 401 (2004).

Acknowledgments: Supported by the Wildlife Conservation Society (SSF grant 67250), the National Geographic Society (grant 8100-06), the Leakey Foundation, the National Science Foundation (grants BCS-0715179 and BCS-0824592), and the University of Michigan. Thanks to the Ethiopian Wildlife Conservation Authority, the wardens and staff of the Simien Mountains National Park, and the participants of the University of Michigan Gelada Research project, particularly A. Le Roux, N. Snyder-Mackler, D. Pappano, C. Wilton, J. Jarvey, S. Liberman, A. Spencer, V. Wilson, N. Sands, M. Zakalik, H. Gelaye, E. Jejaw, and A. Fanta for help in the field and T. Parr for help in the laboratory. All protocols were noninvasive and were approved in Ethiopia (Ethiopian Wildlife Conservation Authority) and the United States (University of Michigan University Committee on Use and Care of Animals, protocols 09554 and 0001011). The authors declare no competing financial interests. All authors contributed extensively to the work presented in this paper. Data available in the SOM.

Supporting Online Material

www.sciencemag.org/cgi/content/full/science.1213600/DC1
Materials and Methods
Table S1
Data Files 1 to 3
References (*34*)

6 September 2011; accepted 26 January 2012
Published online 23 February 2012;
10.1126/science.1213600

Molecular Determinants of Scouting Behavior in Honey Bees

Zhengzheng S. Liang,[1] Trang Nguyen,[2] Heather R. Mattila,[3] Sandra L. Rodriguez-Zas,[1,4] Thomas D. Seeley,[5] Gene E. Robinson[1,2,6]*

Little is known about the molecular basis of differences in behavior among individuals. Here we report consistent novelty-seeking behavior, across different contexts, among honey bees in their tendency to scout for food sources and nest sites, and we reveal some of the molecular underpinnings of this behavior relative to foragers that do not scout. Food scouts showed extensive differences in brain gene expression relative to other foragers, including differences related to catecholamine, glutamate, and γ-aminobutyric acid signaling. Octopamine and glutamate treatments increased the likelihood of scouting, whereas dopamine antagonist treatment decreased it. These findings demonstrate intriguing similarities in human and insect novelty seeking and suggest that this trait, which presumably evolved independently in these two lineages, may be subserved by conserved molecular components.

An important challenge in behavioral biology is to elucidate the molecular basis of individual differences in behavior. Scouting behavior in the honey bee, *Apis mellifera*, provides an excellent opportunity to explore this issue for two reasons. First, there are striking individual differences in this behavior—some bees act as scouts and others never do so. Second, scouting is performed in two distinct contexts: scouting for new food sources or new nest sites, which suggests an underlying tendency to seek something new. Novelty-seeking behavior has been studied in vertebrates, including humans (*1*, *2*), but not in insects.

Food scouts, who make up 5 to 25% of a colony's foraging force, search independently for new food sources and continue to do so even when plentiful sources have been found (*3*–*5*). Non-scouts do not search for novel food sources and instead rely on information from scouts (communicated via "dance language") to guide their foraging. By constantly discovering new flower patches, food scouts help ensure a high influx of food to their colony, despite the ephemeral nature of each patch (*5*).

Nest scouts make up <5% of the population of a swarm, which is a fragment of a colony that has left its natal nest to start a new colony. Nest scouts search independently for potential nesting cavities and collectively choose the best one, whereas non-scout swarm members rely on information from scouts to guide them to their new home (*6*). Nest scouting also is a crucial behavior; a colony's survival depends on its nest scouts finding suitably protective living quarters.

To determine the consistency of novelty seeking in individual bees across the two behavioral contexts, we determined whether nest scouts are prone to also act as food scouts. We identified and marked nest scouts in both artificial and natural swarms (*6*). We then identified food scouts with the standard "hive-moving" assay (*5*, *7*), after installing each swarm in a beehive and moving it at night (when bees don't forage) to a new location outside the bees' original home range. This assay identifies food scouts as the first bees to return to their hive in the morning; under these circumstances, each successful forager must have located a food source on her own. There was a robust tendency of nest scouts to seek novel resources across different contexts, but it did not translate into every nest scout showing food-scouting behavior. In nine trials involving eight different colonies over 2 years, nest scouts were on average 3.4 times more likely to become food scouts than were bees that did not search for nest sites during swarming (Fig. 1A). These results demonstrate that some bees show consistent novelty seeking across diverse behavioral contexts.

To explore the molecular basis of novelty seeking in bees, we developed a behavioral assay for food scouts (Fig. 1B) that tests novelty

[1]Neuroscience Program, University of Illinois at Urbana–Champaign, Urbana, IL, USA. [2]Institute of Genomic Biology, University of Illinois at Urbana–Champaign, Urbana, IL, USA. [3]Department of Biological Sciences, Wellesley College, Wellesley, MA, USA. [4]Department of Animal Sciences, University of Illinois at Urbana–Champaign, Urbana, IL, USA. [5]Department of Neurobiology and Behavior, Cornell University, Ithaca, NY, USA. [6]Department of Entomology, University of Illinois at Urbana–Champaign, Urbana, IL, USA.

*To whom correspondence should be addressed. E-mail: generobi@illinois.edu

seeking more strongly than did previous scout assays (*3*, *5*, *7*). A large screened outdoor enclosure provided experimental control of food sources under otherwise naturalistic conditions. Foragers from a glass-walled observation hive were trained to a training feeder that initially was the only food source available to them. After 2 to 3 days of training, a novel feeder with different visual and odor cues was placed at another location in the enclosure. The foraging bees thus had two possible food sources, familiar and novel; some bees discovered the novel feeder and switched to it. This procedure was repeated on several consecutive days, and each time the novel feeder was given new visual and odor cues and placed in a new location. Only bees that switched to two or more different novel feeders, after being seen at least once at the training feeder, were collected as scouts. These rigorous criteria minimized the possibility of identifying scouts on the basis of an accidental discovery of a novel feeder. The proportion of scout bees identified with this assay (31.2, ± 9.7% SD, n = 182 bees, six trials) is roughly consistent with what has been observed under more natural conditions (*3*–*5*), suggesting that accidental discoveries of novel feeders were not a major source of error. Bees that met our criteria for identifying food scouts were collected to compare their brain gene expression with that of control non-scouts (foragers that were never observed to switch to a novel feeder).

Whole-genome microarray analysis revealed a large neurogenomic signature for scouting behavior in the bee brain. Sixteen percent (1219 out of 7539) of the transcripts on the microarray showed significant (false discovery rate <0.05) differences in mRNA abundance between scouts and non-scouts (table S3, A and B, and table S4). Among the differentially expressed genes were several related to catecholamine, glutamate, and γ-aminobutyric acid (GABA) signaling, which are involved in regulating novelty seeking and reward in vertebrates (*1*, *2*, *8*). For example, the down-regulation of a dopamine receptor gene in honey bee scouts parallels results for a similar gene in individual mammals that are prone to novelty seeking (*9*). These signaling systems also are implicated in personality differences between humans that are related to novelty seeking (*10*, *11*).

Quantitative reverse-transcriptase polymerase chain reaction analysis confirmed the microrarray results for five genes related to catecholamine, glutamate, and GABA signaling (Fig. 2A and fig. S1, A and B): D1-type dopamine receptor *DopR1*, glutamate transporters *Eaat-2* and *Vglut*, AMPA-type glutamate receptor *Glu-RI*, and GABA transporter *Gat-a*. Three additional catecholamine receptor genes also were differentially expressed but were undetected in microarray analysis: *DopR2* (D1-type) (*12*), *Octβ2R* (β-adrenergic type octopamine receptor), and *OctR1* (α-adrenergic type) (*13*) (fig. S1B and tables S1 and S2).

Linear discriminant analysis (LDA) showed a strong separation between scouts and non-scouts based on the expression values for 10 neural signaling genes related to catecholamine, glutamate, and GABA signaling (Fig. 2B). In addition, we used these 10 genes to show that scouts identified with either the new feeder–discovery assay or the hive-moving assay showed strong similarities in brain gene expression to each other (fig. S2).

The association between scouting and catecholamine, glutamate, and GABA signaling pathways could reflect effects of this behavior on brain gene expression or effects of individual differences in these pathways on scouting, or both. We used the transcriptomic results as the basis for designing experiments to test causal relationships, hypothesizing that neurochemical treatment would influence scouting behavior. We tested this hypothesis with the hive-moving assay, because it results in rapid identification of numerous scouts. We collected non-scouts and provided them with a chronic (25 to 30 hours) oral neurochemical treatment (as specified in the next paragraph) in cages (20 bees per cage) in their hive before moving it overnight to a location outside the colony's original home range.

Behavioral observations the following morning (14 hours after stopping the treatment) revealed that glutamate [monosodium glutamate (MSG)] caused a significant increase in scouting (Fig. 3A), whereas the vesicular glutamate transport blocker Chicago Sky Blue significantly attenuated the MSG effects (Fig. 3B). Octopamine caused a weaker, but still significant, increase in scouting (Fig. 3A). These results are consistent with predictions based on microarray analysis. In contrast, dopamine antagonists caused a significant decrease in scouting (Fig. 3C), which was contrary to microarray-based prediction. Effects were not seen in all trials (figs. S3 to S5), suggesting that factors such as food availability, colony conditions, worker genotype, or other unknown variables also affect the probability of becoming a scout. The treatments did

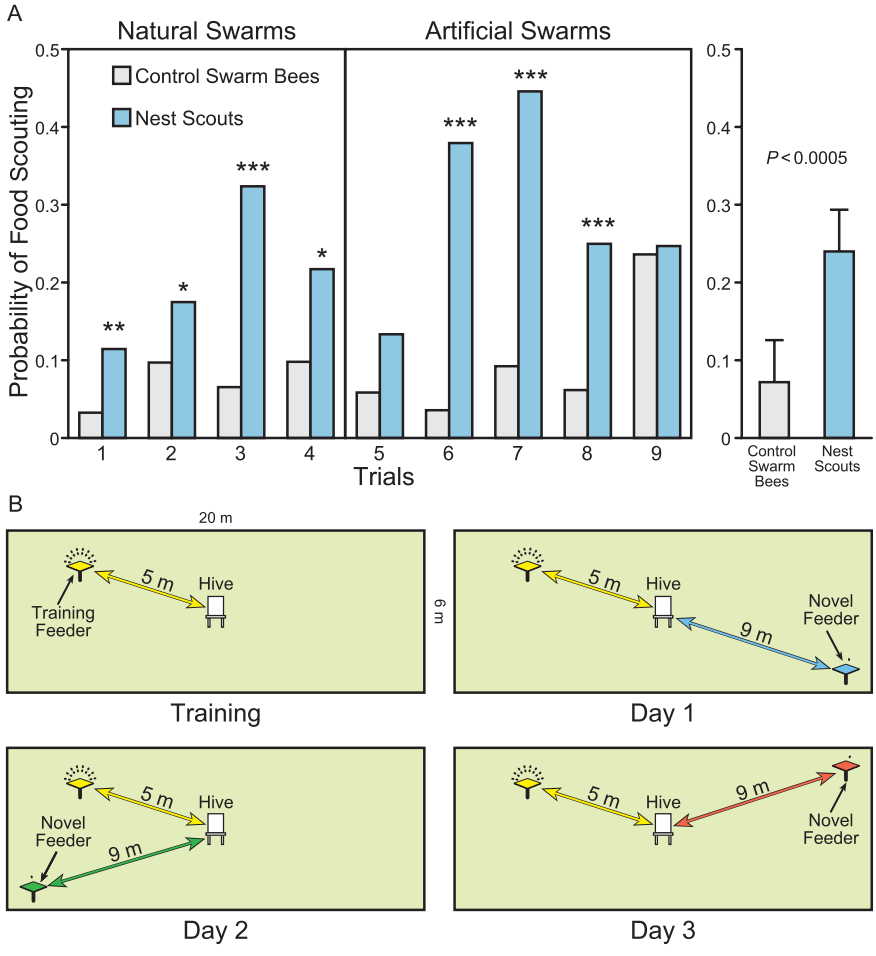

Fig. 1. (**A**) Consistent novelty-seeking behavior across different contexts. Nest scouts were significantly more likely to later act as food scouts than were non-scout swarm members. The graph shows the probabilities of food scouting for nine trials: four natural swarms and five artificial swarms, with eight different colonies (Fisher's exact test, 2-tailed test; *P < 0.05, **P < 0.01, ***P < 0.001), and the overall mean probabilities [least-square means and standard errors; mixed-model analysis of variance (ANOVA), 2-tailed test]. (**B**) Feeder-discovery assay for identifying food scouts. Additional details are in the text and supporting online material.

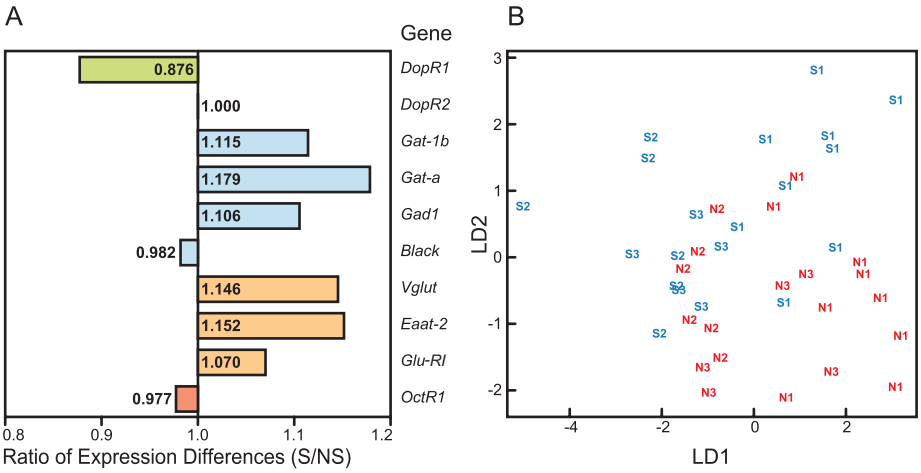

Fig. 2. Transcriptomic analyses of individual differences in novelty-seeking between food scouts (S) and non-scouts (NS) (n = 20 bees per group). (**A**) Selected microarray results highlight differences in brain expression for 10 dopamine, octopamine, glutamate, or GABA signaling genes related to novelty seeking, motivation, and reward in vertebrates. *DopR2* and *OctR1* did not show significant differences in expression (in the latter case, probably because of very low expression levels). GABA transporter 1A gene (*Gat-a*) expression was one of the best correlates of scouting behavior (permutation t test, P < 0.05). (**B**) Results of LDA for genes shown in (A) demonstrate clear separation between most scouts and non-scouts based on differences in brain gene expression (standardized expression values: mean = 0, SD = 1). This plot of LD1 versus LD2 accounted for 82% of the variation in brain gene expression across scouts and non-scouts (n = 20 bees per group). S1, S2, S3 and N1, N2, N3: scouts and non-scouts, respectively, from three different colonies.

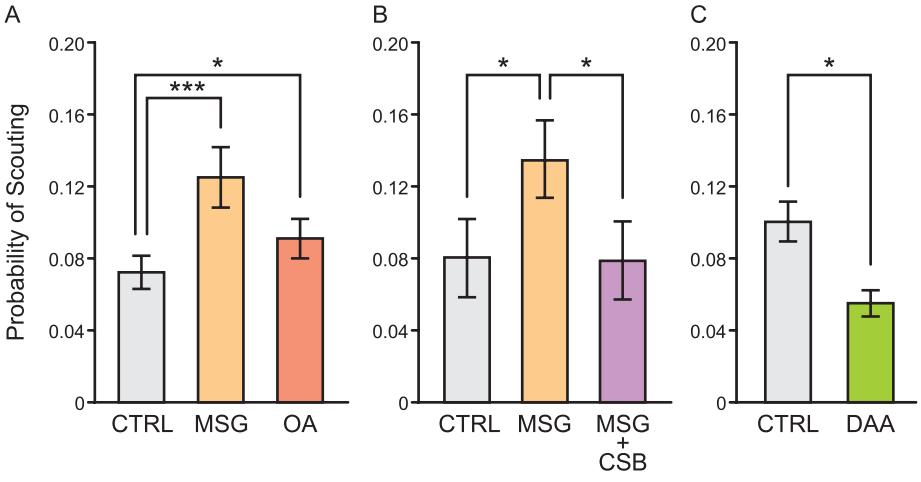

Fig. 3. Glutamate or octopamine treatment increased the probability of scouting, whereas dopamine antagonist treatment decreased it (*P < 0.05, ***P < 0.0001). (**A**) Oral administration of MSG to non-scouts in sugar syrup (20 mg/ml) caused a significant effect in 7 out of 12 trials (with 11 colonies) over 2 years, an overall 73% increase in scouting probability as compared to sucrose-fed–only control bees (P < 0.0001, mixed-model ANOVA, 2-tailed test). Octopamine (OA) treatment (4 mg/ml) caused a significant effect in 3 out of 10 trials (in nine colonies) over 2 years, an overall 37% increase in scouting probability (P < 0.05). Statistical tests were performed on square root–transformed data; the graph represents the untransformed mean ± SE of 12 trials for MSG (with 11 colonies) and 10 trials for octopamine (with 9 colonies); results of individual trials are shown in figs. S3 and S4. (**B**) The glutamate vesicular transporter blocker Chicago Sky Blue (CSB) (4 mg/ml) blocked the effect of MSG on scouting (P < 0.05, least-square mean ± SE for four previously MSG-responsive colonies; results of individual trials are shown in fig. S3). (**C**) Non-scout foragers treated with dopamine antagonists (DAA) (either the D1-receptor antagonist SCH-23390, the "pan-receptor" antagonist Flupenthixol, or both) showed an overall 44% decrease in scouting probability in seven trials over three colonies (P < 0.05, the graph represents least-square mean ± estimated error; mixed-model ANOVA, 2-tailed test; results of individual trials are shown in fig. S5). The probability of scouting was calculated from the proportion of foragers in each treatment group that exhibited scouting behavior, based on a precise count of foragers when releasing them from treatment cages.

not cause excess mortality (table S6), aberrant locomotion, hyperactivity, or a general increase in foraging activity (fig. S6), and they were dose-dependent (fig. S7), which suggests that there were specific treatment effects on scouting behavior. GABA or a GABA receptor agonist (TACA) did not affect the probability of scouting (fig. S8), so the role of this neurotransmitter in bee scouting remains unclear.

Multiple neurotransmitter systems appear to be involved in the regulation of scouting in honey bees, but it is not known how they interact at the circuit level. Glutamatergic and dopaminergic neurons are both found in the vertical lobes of the mushroom bodies, a part of the insect brain involved in reward learning (*14*, *15*). *DopR1* and *Eaat-2* gene expression is colocalized to the same type of interneurons that provide sensory input into these lobes (*16*, *17*). These findings, together with our own, suggest the vertical lobes of the mushroom bodies as one possible neuroanatomical locus for novelty-seeking behavior in honey bees, although other brain regions are probably involved as well.

Our results demonstrate intriguing parallels between honey bees and humans in novelty-seeking behavior. Although the molecular mechanisms that produce this behavioral variation are similar, it is unknown whether both species inherited them from a common ancestor or evolved them independently. Given the phylogenetic separation of bees and humans, we believe it is likely that these mechanisms represent part of a basic tool kit that has been used repeatedly in the evolution of behavior. Further support for this view comes from the finding that individual differences in food-searching behavior in nematodes (*Caenorhabditis elegans*) are caused, in part, by noncoding polymorphisms in *tyramine receptor 3*, which encodes a receptor for a catecholamine closely related to octopamine and dopamine (*18*).

It is common to look to animal models to generate insights that may be applicable to human behavior. Our findings highlight the potential of the converse—using insights from human research to further elucidate the molecular basis of animal behavior. Animal studies, informed by inferences from human research, might in turn help identify evolutionarily conserved molecular mechanisms underlying consistent differences in various behaviors among humans, thus helping us better understand how and why these behavioral differences exist.

References and Notes

1. M. T. Bardo, R. L. Donohew, N. G. Harrington, *Behav. Brain Res.* **77**, 23 (1996).
2. A. D. Fidler *et al.*, *Proc. Biol. Sci.* **274**, 1685 (2007).
3. T. zu Oettingen-Spielberg, *Z. Vgl. Physiol.* **31**, 454 (1949).
4. M. Lindauer, *Z. Vgl. Physiol.* **34**, 299 (1952).
5. T. D. Seeley, *Behav. Ecol. Sociobiol.* **12**, 253 (1983).
6. T. D. Seeley, *Honeybee Democracy* (Princeton Univ. Press, Princeton, NJ, 2010).

7. C. Dreller, *Behav. Ecol. Sociobiol.* **43**, 191 (1998).
8. J. B. Becker, R. L. Meisel, *Handbook of Neurochemistry and Molecular Neurobiology: Behavioral Neurochemistry, Neuroendocrinology and Molecular Neurobiology* (Springer, New York, 2007).
9. D. Viggiano, D. Vallone, H. Welzl, A. G. Sadile, *Behav. Genet.* **32**, 315 (2002).
10. R. P. Ebstein *et al.*, *Nat. Genet.* **12**, 78 (1996).
11. J. Benjamin *et al.*, *Nat. Genet.* **12**, 81 (1996).
12. J. A. Mustard *et al.*, *Brain Res. Mol. Brain Res.* **113**, 67 (2003).
13. P. D. Evans, B. Maqueira, *Invert. Neurosci.* **5**, 111 (2005).
14. F. W. Schürmann, K. Elekes, M. Geffard, *Cell Tissue Res.* **256**, 399 (1989).
15. G. Bicker, S. Schäfer, O. P. Ottersen, J. Storm-Mathisen, *J. Neurosci.* **8**, 2108 (1988).
16. R. Kucharski, E. E. Ball, D. C. Hayward, R. Maleszka, *Gene* **242**, 399 (2000).
17. P. T. Kurshan, I. S. Hamilton, J. A. Mustard, A. R. Mercer, *J. Comp. Neurol.* **466**, 91 (2003).
18. A. Bendesky, M. Tsunozaki, M. V. Rockman, L. Kruglyak, C. I. Bargmann, *Nature* **472**, 313 (2011).

Acknowledgments: Special thanks to M. K. Carr-Markell and J. Recchia-Rife for extensive help in the field. We also thank the following: C. Nye and K. Pruiett (bee management); A. Brockmann, P. Date, J. Dotterer, L. Felley, M. Girard, S. Kantarovich, H. S. Pollock, and M. Wray (field assistance); T. Newman (molecular studies); S. Aref and A. Toth (statistics); E. Hadley (graphics); and A. M. Bell, D. F. Clayton, R. C. Fuller, J. S. Rhodes, C. W. Whitfield, and members of the Robinson laboratory (review of the manuscript). Supported by NSF Frontiers in Biological Research grant EF 0425852 (B. L. Schatz, PI, BeeSpace Project); NIH Director's Pioneer Award 1DP1OD006416 (G.E.R); and the Illinois Sociogenomics Initiative (G.E.R). Microarray data meet Minimum Information About Microarray Experiment (MIAME) standards and are available at ArrayExpress (www.ebi.ac.uk/arrayexpress, #E-MTAB-491). Z.S.L. and G.E.R. conceived the project, designed the experiments and wrote the paper; Z.S.L. performed sample collection, molecular and field experiments, and analyses; T.N. and S.L.R.-Z. performed microarray experiments and statistical analyses, respectively; and H.R.M. and T.D.S. contributed to protocol development and sample collection and co-wrote the paper.

Supporting Online Material

www.sciencemag.org/cgi/content/full/335/6073/1225/DC1
Materials and Methods
SOM Text
Figs. S1 to S8
Tables S1 to S6
References

14 September 2011; accepted 1 February 2012
10.1126/science.1213962

Atomic View of a Toxic Amyloid Small Oligomer

Arthur Laganowsky,[1]* Cong Liu,[1] Michael R. Sawaya,[1] Julian P. Whitelegge,[2] Jiyong Park,[1] Minglei Zhao,[1] Anna Pensalfini,[3] Angela B. Soriaga,[1] Meytal Landau,[1] Poh K. Teng,[1] Duilio Cascio,[1] Charles Glabe,[3] David Eisenberg[1]†

Amyloid diseases, including Alzheimer's, Parkinson's, and the prion conditions, are each associated with a particular protein in fibrillar form. These amyloid fibrils were long suspected to be the disease agents, but evidence suggests that smaller, often transient and polymorphic oligomers are the toxic entities. Here, we identify a segment of the amyloid-forming protein αB crystallin, which forms an oligomeric complex exhibiting properties of other amyloid oligomers: β-sheet–rich structure, cytotoxicity, and recognition by an oligomer-specific antibody. The x-ray–derived atomic structure of the oligomer reveals a cylindrical barrel, formed from six antiparallel protein strands, that we term a cylindrin. The cylindrin structure is compatible with a sequence segment from the β-amyloid protein of Alzheimer's disease. Cylindrins offer models for the hitherto elusive structures of amyloid oligomers.

Studies from many laboratories have suggested that the molecular agents in amyloid-related conditions are not the associated protein fibrils that have long been taken as the defining feature of these disorders but instead are lower molecular weight entities, often termed small amyloid oligomers (*1*–*7*). These oligomers are not generally stable aggregates; they appear as transient species during the conversion of their monomeric precursors to more massive, stable fibrils, and sometimes they appear as an ensemble of sizes and shapes. This polymorphic and time-dependent nature of small amyloid oligomers has made it difficult to pin down their assembly pathways, their stoichiometries, their atomic-level structures, their relationship to fibrils, and their pathological actions (*1*, *8*–*10*). What has emerged is a consensus, minimal definition of small amyloid oligomers: They are noncovalent assemblies of several identical chains of proteins also known to form amyloid fibrils; the oligomers exhibit greater cytotoxicity than either the monomer or fibrils formed from the same protein; in many cases, the oligomer is recognized by a "conformational" antibody (A11) that binds oligomers but not fibrils, regardless of the sequence of the constituent protein (*5*). This suggests that oligomers display common conformation features that differ from those of fibrils (*11*).

In seeking to better define small amyloid oligomers, we chose to work with αB crystallin (ABC). This protein is a chaperone (*12*–*14*) that forms amyloid fibrils (*15*), but the fibrils form more slowly than those of the β-amyloid peptide (Aβ) or islet amyloid polypeptide (IAPP), so that the oligomeric state may be trapped before the onset of fibrillization. We have identified a segment of ABC that forms a relatively stable small oligomer, which satisfies the definition of a small amyloid oligomer given in the preceding paragraph.

We identified the oligomer-forming segment of ABC by inspection of its three-dimensional (3D) structure (*16*) and by applying the RosettaProfile algorithm to its sequence. This algorithm identifies sequence segments that form the steric-zipper spines of amyloid fibrils (*17*, *18*). We noted that two segments of high amyloidogenic propensity, with sequences KVKVLG and GDVIEV (where D indicates Asp; E, Glu; G, Gly; I, Ile; K, Lys; and V, Val), share the same Gly residue 95 at the C terminus of the first segment and the N terminus of the second; moreover, the entire 11-residue segment KVKVLGDVIEV forms a hairpin loop in the 3D structure of ABC (Fig. 1A), with Gly at its center. As predicted, the second six-residue segment GDVIEV, termed G6V (Table 1 defines the structures described in this report), forms fibrils and microcrystals (fig. S1). The microcrystals enabled us to determine the atomic structure of G6V (fig. S2), which proved to be a standard class 2 steric zipper (*19*), essentially an amyloid-like protofilament.

The hairpin segment KVKVLGDVIEV (termed K11V) formed both amyloid fibrils and oligomers. Upon shaking at elevated temperature, K11V forms fibrils similar to those of the parent protein (ABC) from which the segment is derived (*15*) and similar to those of a tandem repeat of $K11V^{V2L}$ (K11V-TR, see below) (Fig. 1B; fig. S1, B and C; and table S1). The fibrils range from 20 to 100 nm in diameter as viewed by electron microscopy (fig. S1). X-ray diffraction of dried fibrils displayed rings at 4.8 and 12 Å resolutions, consistent with the signature cross-β pattern of amyloid fibrils (fig. S1C). The amyloid fibrils of K11V-TR bind the specific amyloid dye congo red, producing apple-green bifringerance under polarized light (fig. S1D), and are immunoreactive with the fibril-specific, conformation-dependent antibody OC (Fig. 1E) (*20*). Together these results prove that the segments G6V, K11V, and K11V-TR are all capable of converting to the amyloid state (*21*, *22*), as is their parent protein, ABC.

Under physiological conditions, the segments K11V, K11V-TR, and a sequence variant with Leu replacing Val at position 2 ($K11V^{V2L}$) all form stable small oligomers intermediate in size

[1]Department of Biological Chemistry and Department of Chemistry and Biochemistry, University of California Los Angeles (UCLA), Howard Hughes Medical Institute (HHMI), UCLA-DOE Institute for Genomics and Proteomics, Los Angeles, CA 90095, USA. [2]The Neuropsychiatric Institute (NPI)–Semel Institute for Neuroscience and Human Behavior, UCLA, Los Angeles, CA 90024, USA. [3]Department of Molecular Biology and Biochemistry, University of California, Irvine, CA 92697, USA.

*Present address: Department of Chemistry, Chemistry Research Laboratory, University of Oxford, Oxford, UK.
†To whom correspondence should be addressed. E-mail: david@mbi.ucla.edu

between monomer and fiber. For each sequence, we determined the number of molecules in the oligomers by size-exclusion high-performance liquid chromatography (SEC-HPLC) and native mass spectrometry experiments. Purified recombinant K11V^{V2L} and K11V-TR, a tandem repeat of K11V^{V2L}, eluted as oligomeric complexes by SEC (Fig. 1C). For example, the K11V-TR complex was estimated to be ~8 kD in mass, corresponding roughly to three tandem segment chains. As an additional check on the stoichiometry of the tandem repeat K11V-TR oligomer, we subjected peak fractions to native nanoelectrospray mass spectrometry. Mass spectra showed abundant ions of K11V-TR oligomers with masses corresponding to three peptide chains (Fig. 1D and fig. S3). Furthermore, we were able to isolate ions of the K11V-TR oligomer and perform collision-induced dissociation (CID) of this trimeric peptide complex into monomeric units of mass equal to that of the K11V-TR peptide (fig. S4). Similar experiments show that K11V and K11V^{V2L} form hexameric oligomers (Table 1 and fig. S3). Thus, native mass spectrometry is consistent with SEC-HPLC in suggesting a stoichiometry of a K11V oligomer of six chains and a K11V-TR oligomer of three tandem chains. These results are consistent with crystallography and energetic considerations (see below).

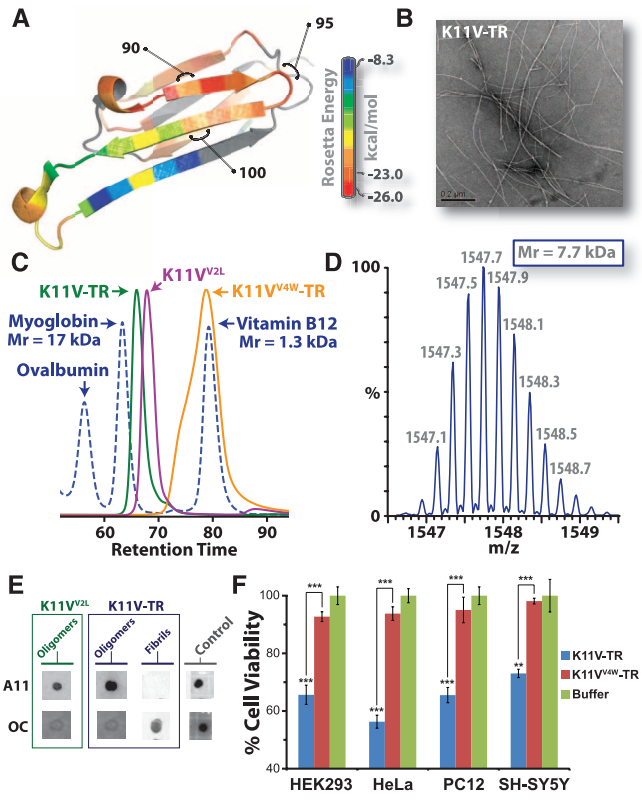

Fig. 1. The cylindrins derived from ABC, an amyloid-forming protein, exhibit the properties of oligomeric state, immunoreactivity, and cytotoxicity commonly ascribed to small amyloid oligomers. (**A**) Ribbon diagram of a single subunit of ABC (*16*), colored by propensity to form amyloid, with red being the highest and blue the lowest propensity. The segment from residue 90 to 100, termed K11V, forms the cylindrin. (**B**) Representative electron micrograph of amyloid fibrils formed by K11V-TR. (**C**) Overlaid size-exclusion chromatograms showing protein standards (blue dashed curve) and cylindrin segments. K11V^{V2L} (purple curve; 1.2 kD per chain) and K11V-TR (green curve; 2.5 kD per chain) cylindrin segments migrate as oligomeric complexes. A mutant form of K11V-TR that disrupts oligomer formation of the cylindrin peptide, K11V^{V4W}-TR (orange curve; 2.7 kD per chain), migrates as a dimeric or monomeric species. (**D**) Native nanoelectrospray mass spectrum of K11V-TR peak fractions from SEC-HPLC reveals trimeric tandem-repeat cylindrin oligomers, confirming that the oligomeric complexes coincide in mass with the crystallized cylindrins. Expansion of the most abundant ion series of a +5 charge state corresponding to a molecular mass of three K11V-TR chains, coinciding with the crystallographic trimeric oligomer with a mass accuracy of 3.93 parts per million (ppm), is shown, with mass/charge (*m/z*) labels. (**E**) Immunodot blot analysis of solutions of K11V^{V2L} and K11V-TR oligomers and K11V-TR fibrils with prefibrillar oligomer-specific, polyclonal antibody A11 (*5*); and a mixture of fibril-specific monoclonal antibodies, OC (*11*). Solutions of cylindrin-forming segments are recognized by A11 but not by the OC antibody. In contrast, K11V-TR fibrils are recognized only by the OC antibody. Positive controls are shown to the right (*5*). (**F**) Cylindrin K11V-TR is toxic to four mammalian cell lines. Cell viability levels return to nearly 100% when we tested the control variant K11V^{V4W}-TR. All samples were at a final concentration of 100 μM. Results represent mean ± SEM. Student's *t* test ($N = 4$): $^{**}P < 0.01$; $^{***}P < 0.001$.

These ABC K11V oligomers exhibit molecular properties in common with amyloid oligomers from other disease-related proteins. We probed blots of the recombinant segments with the polyclonal A11, amyloid-oligomer–specific conformational antibody (*5*). Both single and tandem repeat segments are recognized by the A11 antibody (Fig. 1E and fig. S1E). By using a cell viability assay on mammalian cells, we observed oligomers to be toxic, displaying dose-response effects similar to those of Aβ involved in Alzheimer's disease (*2*, *23*, *24*) (Fig. 1F and fig. S5). To test whether membrane disruption is responsible for this toxicity, as suggested for human islet amyloid polypeptide (hIAPP) (*25*, *26*), we performed liposome dye release experiments. The hIAPP peptide diminished liposome integrity leading to dye release, but the K11V-TR did not exhibit this trend (fig. S6). In contrast to oligomeric solutions, no toxicity was observed for the fibrils of G6V. Thus, ABC segments in oligomeric form are cytotoxic but suggest a more complicated mechanism of toxicity than membrane disruption.

Table 1. Structures and stoichiometries of amyloid-related oligomers discussed in this report, derived from ABC. Peptide segment amino acid sequences are provided in table S1. A dash entry indicates sample was not tested or unknown. MS, native mass spectrometry.

Protein/peptide segment (residue numbers)	Structure	PDB ID	Oligomer size by			Immunoreactivity	Toxicity
			Crystallography	SEC	MS		
ABC truncated (68–162)	Network of dimers linked by domain swapping	3L1G	2 to indefinitely large	2–4*	2–6 and 10–24*	–	No†
K11V	Cylindrin	3SGO	6	–	6‡	–	–
K11V^{V2L}	Cylindrin V2L variant	3SGP	6	6	6‡	A11	Yes
K11V-TR	Cylindrin tandem repeat V2L variant	3SGR	3	3	3‡	A11	Yes
K11V^{V4W}-TR	Cylindrin tandem repeat V2L/V4W variant	–	–	1–2	–	No§	No
G6V	Fibril steric zipper	3SGS	Indefinitely large	–	–	No	No

*Data refer to truncated ABC (*16*). †Data refer to full-length ABC (*50*). ‡Data shown in fig S3. §Very weak binding. Data shown in fig. S1E.

We next determined the crystal structures of various ABC K11V oligomers. A screen produced x-ray–grade crystals of K11V, but structure determination by molecular replacement with fiberlike probes failed, suggesting that the ABC segment oligomers possess a previously unobserved type of amyloid structure. Turning to the single-wavelength anomalous dispersion method for phase determination, we synthesized K11V derivatives with Br substitutions at position 2 or 8 of the K11V sequence, K11V-Br2 and K11V-Br8, with the leucine-resembling nonnatural amino acid (2-bromoallyl)-glycine. Both derivatives crystallized and led to structure determinations (table S2) at 1.4 Å resolution. Molecular replacement based on these structures led to the closely related structures of K11V itself as well as K11V-TR and $K11V^{V2L}$.

The structure of K11V, the amyloid-related oligomer, is a six-stranded antiparallel barrel of cylindrical shape, consistent in mass with our solution studies, that we term a cylindrin. The cylindrin (Fig. 2) is distinctly different in structure from either the native structure of ABC (Fig. 1A) or from its G6V segment (fig. S2), a dual β-sheet steric zipper. It is also distinct from other structures currently in the Protein Data Bank (PDB) (SOM text) but resembles several previously proposed β-barrel models (*27*–*31*). Each strand of the cylindrin is bonded to one neighboring strand by a strong interface and to a second by a weak interface. The strong interface (between purple and green chains, Fig. 2, B and C) is formed by 12 hydrogen bonds and splays outward at the ends. The weak interface is formed by eight hydrogen bonds: four from the main chain, two mediated through side-chain interactions, and two through a water bridge (Fig. 2C). The axial channel of the cylindrin is closed by the hydrophobic interactions of two inward-pointing sets of three valine side chains and is devoid of water (Fig. 2C). The surface area buried (A_b) per residue in the strand-packing interface of the cylindrin is 87 $Å^2$, smaller than the 131 $Å^2$ value for the strand-to-strand interface of the steric zipper of GNNQQNY (N, Asn; Q, Gln; and Y, Tyr) (*32*). Similarly the cylindrin-packing interface has a shape complementarity (*Sc*) value of 0.75, somewhat smaller than the value of 0.80 for the GNNQQNY interface (table S3). Thus, the cylindrin structure has features in common with a steric zipper in being formed from hydrogen-bonded β strands and having a dry interior, but it is cylindrical rather than nearly flat and is probably less stable, as suggested by the lower A_b and *Sc* values.

To provide adequate cylindrin material for biochemical and toxicological studies, we generated a synthetic gene to express in bacteria a tandem repeat, K11V-TR, of the well-diffracting $K11V^{V2L}$ segment, covalently linked through a double glycine linker and containing an additional N-terminal glycine (fig. S7 and table S1). This K11V-TR peptide reduces the complexity of the cylindrin assembly process from six to three chains (Fig. 2, D and E). We were able to determine the K11V-TR crystal structure, even though the glycine linkers produce some disorder in the crystals (table S2). Other than the glycine linkers and the Val-to-Leu replacement, the cylindrical bodies of the six-stranded K11V and the three double-stranded K11V-TR oligomers are essentially identical. Energetic considerations suggest that the cylindrin should be stable in solution: The surface area buried per interchain interface of K11V-TR is 841 $Å^2$, nearly as much as for the foldon trimerization domain, 1092 $Å^2$ (PDB 1RFO), and cylindrin forms twice as many hydrogen bonds

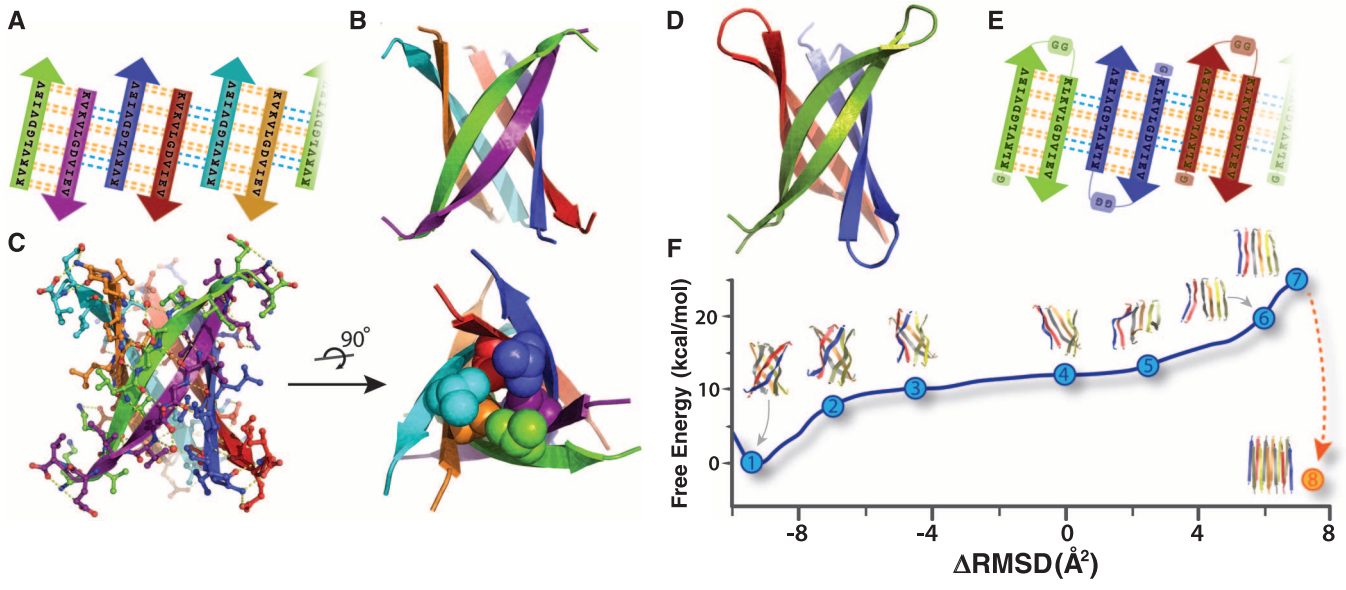

Fig. 2. Crystal structures of cylindrins and computed free energy change of the simulated structural transition from cylindrin to a fibril. Each colored β strand (arrow) is composed of 11 amino acid residues from ABC of sequence KVKVLGDVIEV (K11V). (**A**) Schematic of unrolled cylindrin (outside view), illustrating strand-to-strand registration. Hydrogen bonds between the main chains of neighboring strands are shown by yellow dashed lines; hydrogen bonds mediated by water bridges or side chains are shown by blue dashed lines. (**B**) Ribbon representation of the cylindrin crystal structure. Pairs of strands form antiparallel dimers, which assemble around a threefold axis down the barrel axis of the cylindrin. The height of the cylindrin is 22 Å. The inner dimension of the cylindrin, around the waist from Cα to Cα, is 12 Å, and at the splayed ends the diameter is 22 Å. (**C**) The cylindrin with side chains shown as atoms and hydrogen bonds in yellow. Twelve backbone hydrogen bonds stabilize the strong interface between tightly twisted antiparallel strands (e.g., between green and purple chains). The weaker interface between the pairs of tightly twisted strands is formed by four main-chain hydrogen bonds, with an additional two hydrogen bonds coming from a water bridge and two hydrogen bonds from side-chain interactions (e.g., between purple and blue chains). The dry interior of the cylinder is closed by triplets of Val residues, shown as spheres, at the top and bottom. (**D**) Crystal structure of K11V-TR formed by three chains of 25 residues each. (**E**) Schematic of unrolled K11V-TR cylindrin (outside view). Similar hydrogen-bonding patterns are formed as in (A). (**F**) The computed Gibbs free energy at 300 K for a cylindrin forced to a fibril. The reaction coordinate measures the difference in root mean square deviation (ΔRMSD) from the two end points: the cylindrin and the in-register antiparallel β sheet (IAB). The cylindrin set the free energy minimum (point 1). The transition was initiated by disrupting the weak interface (points 2 and 3). As the cylindrin unrolls, the weak interface requires complete dissociation of backbone hydrogen bonds (points 4 and 5), whereas the strong interfaces maintains hydrogen bonding (point 6). The IAB has a higher free energy than the cylindrin (point 7), and when two IABs associate and interdigitate to form a steric zipper (point 8) the free energy drops to 5.2 kcal/mol per peptide lower than the cylindrin (table S4).

between neighboring chains as does the foldon domain.

For a negative control of cylindrin structure and properties, we generated a variant form of the tandem segment, K11V^{V4W}-TR in which the V4W substitution occurs in both repeats (table S1). This substitution was predicted on the basis of the K11V crystal structure to disrupt oligomer formation through steric clash of core, buried residues. This variant peptide eluted in the mass range of a dimeric or monomeric species by SEC-HPLC and displayed reduced cell toxicity (Fig. 1F and fig. S5).

To compare cylindrins to fibers, we define a cylindrin as a toxic, amyloid-related, oligomeric, cylindrically shaped β barrel formed from antiparallel, extended protein strands and having the cylinder filled with packed side chains. A cylindrin resembles a steric zipper in having a packed interior but differs from a steric zipper in an important respect, which may illuminate the reaction pathway from oligomers to fibrils. When unrolled into a β sheet, each antiparallel pair of strands in the cylindrin sheet (Fig. 2A) is out of register with neighboring pairs by six residues (shear number is six) (fig. S8) (*33*). In contrast, the β strands in full amyloid fibers (*22*, *34*, *35*) and short steric zippers (*19*) are in register. This means that a cylindrin unrolled into a sheet would not be an in-register structure, ready to bond with an identical sheet to form the steric zipper spine of an amyloid fiber. The transition from cylindrin to steric zipper involves breaking of hydrogen bonds and re-registration of the strands into an in-register structure, as we have simulated by targeted molecular dynamics, followed by free energy perturbation in explicit solvent (Fig. 2F and SOM text). We chose the end target as an antiparallel sheet, on the basis of Fourier transform infrared (FTIR) experiments (SOM text). These calculations suggest that the transition from cylindrin to an antiparallel fiberlike structure involves crossing a high free energy, implying that fibers may nucleate from monomers without passing through cylindrin-like oligomeric states (*36*–*38*); that is, cylindrin is likely to be off pathway to fiber formation.

An important question is whether the ABC cylindrin is a possible model for amyloid oligomers formed by well-studied toxic proteins, such as Aβ and hIAPP. There is evidence that amyloid oligomers share common structural features. For example, studies have suggested oligomers are β-sheet rich (*38*–*40*), and several toxic oligomers are recognized by the A11 conformational antibody (*41*), which also recognizes the cylindrin. A11 also recognizes α-hemolysin, a soluble β-barrel protein (*42*). Thus, the cylindrin structure may represent the common structural core of amyloid oligomers (SOM text). To investigate this possibility, we used the Rosetta-Profile method (*18*) to ask whether other toxic sequences, or segments of them, are compatible with the cylindrin structure. We found that the C-terminal segment of Aβ is reasonably compatible with the cylindrin structure and, with a two-residue registration shift between pairs of antiparallel strands, a very good fit with the cylindrin structure is obtained (fig. S11). This finding in itself does not imply that this is the structure of the Aβ toxic species, but it is in agreement with the observation of hexamers of Aβ oligomers by native mass spectrometry analysis (*43*).

The ABC cylindrin may represent one of many possible assemblies of cylindrin-like structures. The number of strands or shear number may vary. For example, Aβ oligomers have been described ranging in size from dimers and tetramers to hexamers and dodecamers (*43*–*45*). Those with larger numbers of strands could have open central channels as modeled by others (*46*, *47*), whereas cylindrins having smaller numbers of strands would have dry interfaces similar to crystallographically (*48*, *49*) and computationally (*44*) derived models. Parallel assemblies could also form cylindrin-like structures, such as those previously modeled (*27*, *46*). In fact, strong evidence for the extreme polymorphism of amyloid oligomers suggests that cylindrin-like assemblies could exist in a variety of structures with a variety of properties, including varying stabilities and toxicities (*39*, *44*).

References and Notes

1. B. Caughey, P. T. Lansbury Jr., *Annu. Rev. Neurosci.* **26**, 267 (2003).
2. W. F. Xue *et al.*, *J. Biol. Chem.* **284**, 34272 (2009).
3. R. Kodali, R. Wetzel, *Curr. Opin. Struct. Biol.* **17**, 48 (2007).
4. M. D. Kirkitadze, G. Bitan, D. B. Teplow, *J. Neurosci. Res.* **69**, 567 (2002).
5. R. Kayed *et al.*, *Science* **300**, 486 (2003).
6. G. Bitan, E. A. Fradinger, S. M. Spring, D. B. Teplow, *Amyloid* **12**, 88 (2005).
7. C. G. Glabe, *J. Biol. Chem.* **283**, 29639 (2008).
8. F. Chiti, C. M. Dobson, *Annu. Rev. Biochem.* **75**, 333 (2006).
9. F. Chiti, C. M. Dobson, *Nat. Chem. Biol.* **5**, 15 (2009).
10. J. C. Rochet, P. T. Lansbury Jr., *Curr. Opin. Struct. Biol.* **10**, 60 (2000).
11. R. Kayed *et al.*, *Mol. Neurodegener.* **2**, 18 (2007).
12. J. Horwitz, *Proc. Natl. Acad. Sci. U.S.A.* **89**, 10449 (1992).
13. S. Jehle *et al.*, *Proc. Natl. Acad. Sci. U.S.A.* **108**, 6409 (2011).
14. H. Ecroyd, J. A. Carver, *Cell. Mol. Life Sci.* **66**, 62 (2009).
15. S. Meehan *et al.*, *J. Mol. Biol.* **372**, 470 (2007).
16. A. Laganowsky *et al.*, *Protein Sci.* **19**, 1031 (2010).
17. M. J. Thompson *et al.*, *Proc. Natl. Acad. Sci. U.S.A.* **103**, 4074 (2006).
18. L. Goldschmidt, P. K. Teng, R. Riek, D. Eisenberg, *Proc. Natl. Acad. Sci. U.S.A.* **107**, 3487 (2010).
19. M. R. Sawaya *et al.*, *Nature* **447**, 453 (2007).
20. F. Sarsoza *et al.*, *Acta Neuropathol.* **118**, 505 (2009).
21. A. V. Kajava, U. Baxa, A. C. Steven, *FASEB J.* **24**, 1311 (2010).
22. J. Greenwald, R. Riek, *Structure* **18**, 1244 (2010).
23. B. M. Austen *et al.*, *Biochemistry* **47**, 1984 (2008).
24. P. Picone *et al.*, *Biophys. J.* **96**, 4200 (2009).
25. M. F. Engel *et al.*, *Proc. Natl. Acad. Sci. U.S.A.* **105**, 6033 (2008).
26. L. Khemtémourian, M. F. Engel, R. M. Liskamp, J. W. Höppener, J. A. Killian, *Biochim. Biophys. Acta* **1798**, 1805 (2010).
27. P. M. Pryciak, J. D. Conway, F. A. Eiserling, D. Eisenberg, in *Protein Structure, Folding, and Design*, D. L. Oxender, Ed. (Alan R. Liss, New York, 1986), vol. 39, pp. 243–246.
28. F. R. Salemme, D. W. Weatherford, *J. Mol. Biol.* **146**, 119 (1981).
29. F. R. Salemme, D. W. Weatherford, *J. Mol. Biol.* **146**, 101 (1981).
30. Y. Shafrir, S. Durell, N. Arispe, H. R. Guy, *Proteins* **78**, 3473 (2010).
31. J. D. Conway, thesis, UCLA (1986).
32. R. Nelson *et al.*, *Nature* **435**, 773 (2005).
33. A. G. Murzin, A. M. Lesk, C. Chothia, *J. Mol. Biol.* **236**, 1369 (1994).
34. T. L. Benzinger *et al.*, *Proc. Natl. Acad. Sci. U.S.A.* **95**, 13407 (1998).
35. R. Tycko, *Annu. Rev. Phys. Chem.* **62**, 279 (2011).
36. N. B. Last, E. Rhoades, A. D. Miranker, *Proc. Natl. Acad. Sci. U.S.A.* **108**, 9460 (2011).
37. J. W. Wu *et al.*, *J. Biol. Chem.* **285**, 6071 (2010).
38. K. Kar, M. Jayaraman, B. Sahoo, R. Kodali, R. Wetzel, *Nat. Struct. Mol. Biol.* **18**, 328 (2011).
39. S. Chimon *et al.*, *Nat. Struct. Mol. Biol.* **14**, 1157 (2007).
40. K. Ono, M. M. Condron, D. B. Teplow, *Proc. Natl. Acad. Sci. U.S.A.* **106**, 14745 (2009).
41. J. L. Tomic, A. Pensalfini, E. Head, C. G. Glabe, *Neurobiol. Dis.* **35**, 352 (2009).
42. Y. Yoshiike, R. Kayed, S. C. Milton, A. Takashima, C. G. Glabe, *Neuromolecular Med.* **9**, 270 (2007).
43. S. L. Bernstein *et al.*, *Nat. Chem.* **1**, 326 (2009).
44. M. Ahmed *et al.*, *Nat. Struct. Mol. Biol.* **17**, 561 (2010).
45. G. Bitan, S. S. Vollers, D. B. Teplow, *J. Biol. Chem.* **278**, 34882 (2003).
46. H. Jang *et al.*, *J. Mol. Biol.* **404**, 917 (2010).
47. H. A. Lashuel, D. Hartley, B. M. Petre, T. Walz, P. T. Lansbury Jr., *Nature* **418**, 291 (2002).
48. C. Liu *et al.*, *J. Am. Chem. Soc.* **133**, 6736 (2011).
49. V. A. Streltsov, J. N. Varghese, C. L. Masters, S. D. Nuttall, *J. Neurosci.* **31**, 1419 (2011).
50. F. C. Dehle, H. Ecroyd, I. F. Musgrave, J. A. Carver, *Cell Stress Chaperones* **15**, 1013 (2010).

Acknowledgments: We thank L. Goldschmidt for the 3D profile scan of ABC; J.-P. Colletier, D. Anderson, G. Fujii, J. Stroud, H. Chang, S. Sievers, J. Weissman, J. L. P. Benesch, G. Hochberg, and C. V. Robinson for useful discussion; J. Navarro at the UCLA Crystallization Facility; A. Berk and D. Guo for help with tissue culture experiments; and C. Ralston at the Advanced Light Source (ALS) 8.2.2 and K. Rajashankar and beamline staff at Argonne Photon Source (APS), Northeastern Collaborative Access Team beamlines 24-ID-E/C, for data collection. The last is supported by award RR-15301 from the National Center for Research Resources of the NIH. Use of the Advanced Photon Source, an Office of Science User Facility operated for the U.S. Department of Energy (DOE) Office of Science by Argonne National Laboratory, was supported by the U.S. DOE under contract no. DE-AC02-06CH11357. We thank the NIH Chemistry Biology Interface Training program (award 5T32GM008496) sponsorship for A.L., UCLA Dissertation Year fellowships awarded to A.L. and M.Z., NSF award MCB-0445429, NIH award 1R01-AG029430, award NIH-016570 from Alzheimer's Disease Research at UCLA, and HHMI for support. Atomic coordinates and structure factors have been deposited in the PDB with the following accession codes: K11V (3SGO), K11V-Br2 (3SGM), K11V-Br8 (3SGN), K11V^{V2L} (3SGP), K11V-TR (3SGR), and GDVIEV (3SGS). A11 is available under a uniform biological material transfer agreement with the University of California, Irvine. UCLA has filed a provisional patent on cylindrin as the possible generic etiologic agent of amyloid diseases.

Supporting Online Material

www.sciencemag.org/cgi/content/full/335/6073/1228/DC1
Materials and Methods
SOM Text
Figs. S1 to S11
Tables S1 to S4
References (*51*–*82*)

25 August 2011; accepted 5 January 2012
10.1126/science.1213151

Triggering a Cell Shape Change by Exploiting Preexisting Actomyosin Contractions

Minna Roh-Johnson,[1]* Gidi Shemer,[1]* Christopher D. Higgins,[1] Joseph H. McClellan,[1] Adam D. Werts,[1] U. Serdar Tulu,[2] Liang Gao,[3] Eric Betzig,[3] Daniel P. Kiehart,[2] Bob Goldstein[1]†

Apical constriction changes cell shapes, driving critical morphogenetic events, including gastrulation in diverse organisms and neural tube closure in vertebrates. Apical constriction is thought to be triggered by contraction of apical actomyosin networks. We found that apical actomyosin contractions began before cell shape changes in both *Caenorhabitis elegans* and *Drosophila*. In *C. elegans*, actomyosin networks were initially dynamic, contracting and generating cortical tension without substantial shrinking of apical surfaces. Apical cell-cell contact zones and actomyosin only later moved increasingly in concert, with no detectable change in actomyosin dynamics or cortical tension. Thus, apical constriction appears to be triggered not by a change in cortical tension, but by dynamic linking of apical cell-cell contact zones to an already contractile apical cortex.

During development, dramatic rearrangements of cells and epithelia play key roles in shaping animals (*1*–*4*). Many rearrangements are driven by apical constriction, including neural tube closure (*4*), failure of which is a common human birth defect (*5*). Apical constriction is generally driven by contraction of apical actomyosin networks (*4*). However, it is not well understood how the stresses and tensions generated by actomyosin networks produce cell shape changes in developing organisms (*6*).

To address this issue, we examined cortical actomyosin dynamics during *Caenorhabitis elegans* gastrulation. In *C. elegans*, two endodermal precursor cells (Ea and Ep) internalize through apical constriction (*7*–*9*). Transgenic green fluorescent protein (GFP) myosin II–containing particles formed in each cell's apical cortex, enriched in Ea/p similarly to endogenous myosin (*9*). The ability to resolve large numbers of particles made it possible to track the detailed dynamics of ac-

[1]Department of Biology, University of North Carolina at Chapel Hill, Chapel Hill, NC 27599, USA. [2]Department of Biology, Duke University, Durham, NC 27708, USA. [3]Janelia Farm Research Campus, Howard Hughes Medical Institute, Ashburn, VA 20147, USA.

*These authors contributed equally to this work.
†To whom correspondence should be addressed. E-mail bobg@unc.edu

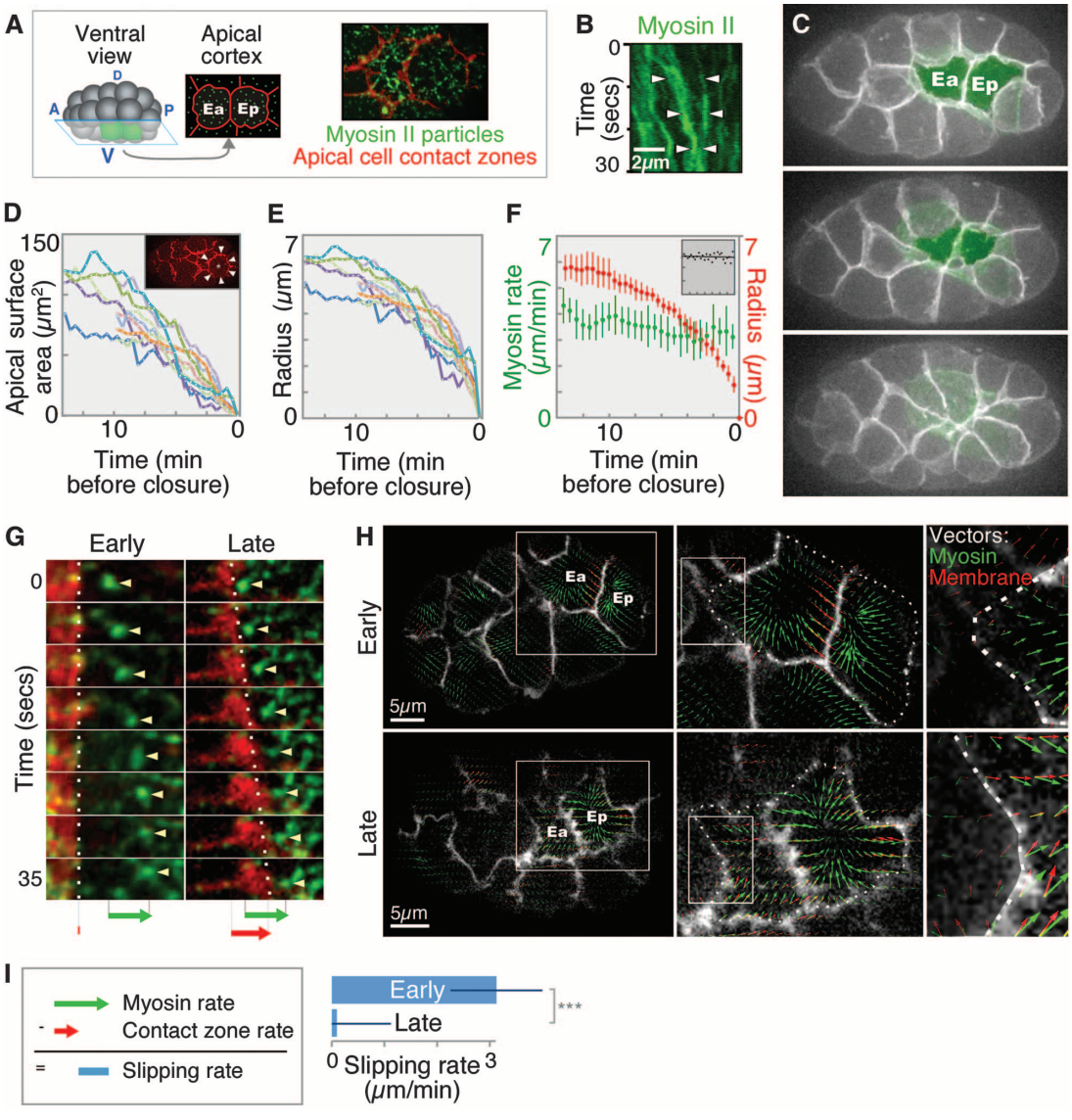

Fig. 1. Actomyosin contraction precedes the rapid shrinking of the apical surface. (**A**) Diagram of imaging method. (**B**) NMY-2::GFP coalescence (white arrowheads) in apical cortex of Ea/p cell. (**C**) Shrinking of apical surfaces during gastrulation (projections of 10 1-μm *z* planes, with Ea/p false-colored). (**D**) Ea/p cell apical surface areas over 575 or 825 s (five embryos each) before closure of the apical surface. (Inset) Apical cell–cell contact zones (arrowheads) on Ep (asterisk). (**E**) Average radius of apical surfaces derived from area measurements. (**F**) Mean and 95% CI of radius and myosin particle rate over time. (Inset) Myosin directionality (net distance over total distance, vertical scale 0 to 1) over time (time scale: same as larger graph). (**G**) Movements of individual myosin particles (arrowheads) near contact zones (white dotted lines) in early or late stages of closure. Arrows at bottom indicate relative distances traveled by each. (**H**) PIV, three magnifications. Boxes indicate enlarged areas. Left to right are whole embryo at plane of Ea/p apical cortex, Ea/p cells (outlined by dotted line), and part of Ea at border with another cell. (**I**) Slipping rate calculated from individual particles and contact zones ($P < 0.001$, Student's *t* test).

tomyosin networks (Fig. 1A, fig. S1, and movie S1). Neighboring myosin particles moved short distances toward each other into multiple coalescence points, with most particles moving centripetally (toward the center of the apical cell surface) and with new particles forming near apical cell boundaries (Fig. 1B and fig. S2). These particles appear to be components of contracting actomyosin networks because F-actin coalesced similarly (fig. S2) and myosin particles near the center of each coalescence moved at a slower speed than did those further away (fig. S3), as seen in other contracting actomyosin networks (*10*). Particle tracking and fluorescence recovery after photobleaching (FRAP) experiments suggested that the networks were continuously remodeled by exchange of myosin molecules on and off particles, as expected (fig. S3).

To investigate how apical actomyosin networks shrink apical cell surfaces, we tracked the outlines of these surfaces, the apical cell-cell contact zones, quantitatively (Fig. 1, C and D). Apical areas shrunk gradually or not at all at first (Fig. 1, D to F) (*11*) and then accelerated. We predicted that actomyosin contraction would also begin gradually and accelerate in concert with the contact zones (Fig. 1E). Instead, myosin particles moved centripetally quite rapidly throughout this period [3.19 ± 0.14 μm/min, mean ± 95% confidence interval (CI)] (Fig. 1F), at first with little or no accompanying contact zone movement. Myosin particles near contact zones at first streamed away from the contact zones, which were in many

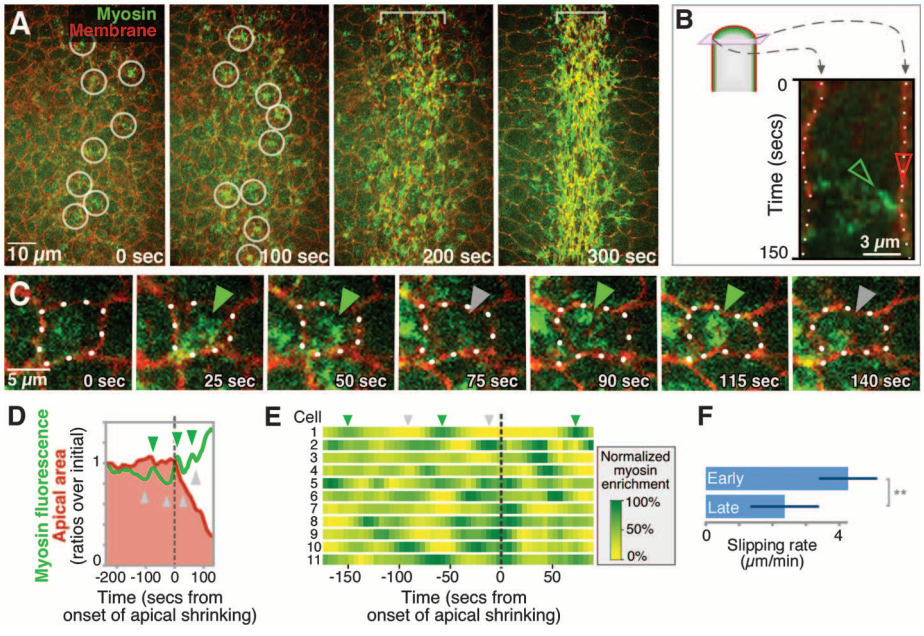

Fig. 2. Periodic actomyosin coalescence occurs before apical cell profiles shrink in *Drosophila* gastrulation. (**A**) *Drosophila* ventral furrow formation. Circles mark apical myosin enrichment seen before apical cell profiles began to shrink. (**B**) Kymograph of a cell (diagrammed) showing myosin (green) movement toward a stationary cell-cell boundary (red) before apical shrinking began. (**C**) Myosin coalesced (green arrowheads) and dissipated (gray arrowheads) before apical cell profiles began to shrink. This is shown quantitatively from one cell in (**D**) and from 11 cells chosen at random in (**E**). Heatmaps in (E) show local maxima of apical myosin levels (three-timepoint running averages of myosin level at each timepoint minus the average of 10 timepoints before and after, normalized to maximum and minimum). Green and gray arrowheads mark one case as in (C). Cell 3 is a rare example in which peaks were not seen before apical shrinking began. (**F**) Slipping rate, defined as in Fig. 1I, early (before apical shrinking, n = 33 cells, 3 embryos) and late (during apical shrinking, n = 27 cells, 3 embryos), P < 0.01 (Student's t test).

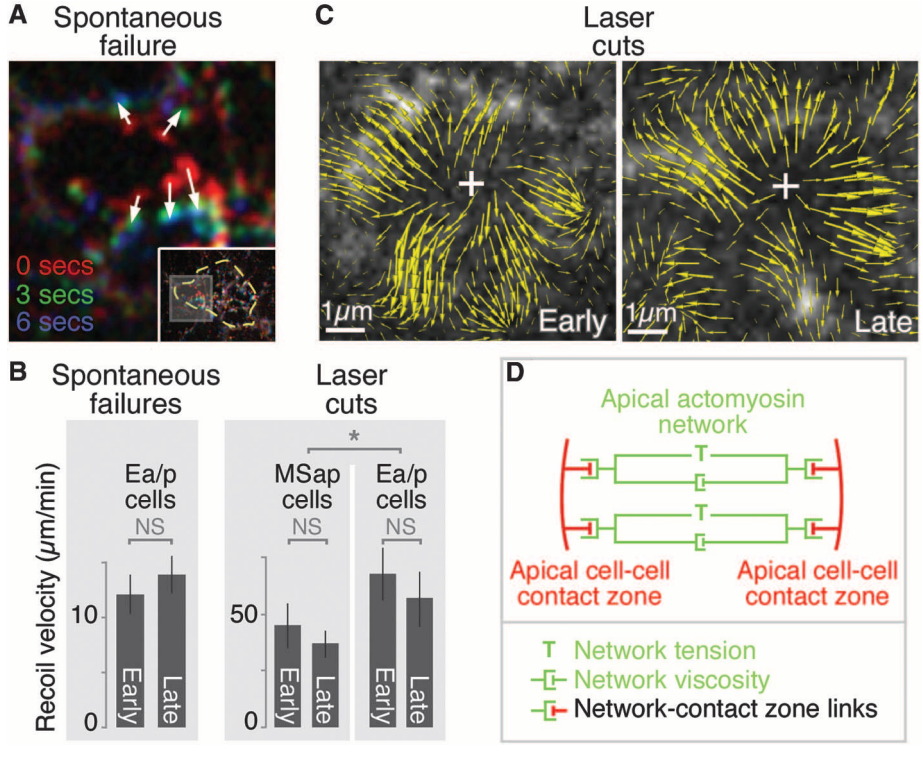

Fig. 3. Cortical tension associated with apical constricton is established early and changes little as apical shrinking accelerates in *C. elegans*. (**A**) A spontaneous failure, with three timepoints overlain in three colors. (Inset) Entire Ea/p cell apical cortex outlined with enlarged region indicated. Arrows mark individual myosin particles springing apart. (**B**) Similar data from Ea/p cortical laser cuts done in early or late stages by means of PIV as in Fig. 1H. (**C**) Initial recoil speeds of myosin particles after spontaneous failures at early (n = 13 myosin particles within 1 μm of center of recoil, six embryos) and late (20 particles, seven embryos) stages, or after laser cuts (48 particles within 4 μm of cut site, seven embryos per stage). Exponential decay T1/2 was 2.20 s in early stages, n = 12 particles; 2.38 s in late stages, n = 20 particles. (**D**) Working model of forces acting on contact zones (red) and within Ea/p apical actomyosin networks (green, with multiple, interconnected network elements represented as two elements here for simplicity). Results suggest that cortical tension (T) and network stiffness or viscous drag (green dashpots) within Ea/p change little from early to late stages.

cases almost stationary, suggesting that the actomyosin network and contact zones were only weakly mechanically connected at this stage (we refer to actomyosin contractions without contact zone movement as uncoupled movements) (Fig. 1G and movies S2 and S3). Later, contact zones appeared to move almost in unison with many of the myosin particles (referred to as coupled movements) (Fig. 1G and movie S4), suggesting that the myosin and contact zones may have become mechanically connected. Contact zones were never seen to overtake myosin particles in the Ea/p cortex (movies S2 to S5), suggesting that neighboring cells were not simply migrating over Ea/p cells.

Our observations were not entirely consistent with a simple pattern of uncoupled movements early and coupled movements later (fig. S4); instead, some variation existed at each stage. Tracking movements by means of particle image velocimetry (PIV) demonstrated that in general, the myosin particles and contact zones moved increasingly in unison as time progressed (Fig. 1H). We confirmed this result by measuring the rates of individually tracked myosin particles and nearby contact zones, defining the difference between these two rates as a slipping rate (Fig. 1I). Actomyosin contractions appeared to drive contact zone movements with ~25% efficiency in early stages, increasing to ~81% efficiency near the end of Ea/p internalization, based on comparison of measurements from cells with a computer simulation (fig. S5 and movie S6). Labeling cell surfaces with quantum dots or a plasma membrane marker demonstrated that cell surfaces moved in concert with underlying actomyosin network contractions—there may be strong frictional force or drag force between the actomyosin network and the overlying plasma membrane (fig. S6). Thus, slipping between actomyosin and membrane occurred specifically at apical cell contact zones, and the relationship between cytoskeletal dynamics and cell shape change during apical constriction is more dynamic than existing models (*3*, *4*) predict.

To determine whether the phenomenon we found is conserved in other systems, we examined *Drosophila* ventral furrow cells (*11*), in which periodic actomyosin contractions cause apical cross-sectional profiles to shrink in pulses (*12*). We noticed myosin accumulations in some cells even before shrinking of apical profiles began (Fig. 2A). Myosin coalesced and moved either toward or away from stationary membranes and thus was not well connected to contact zone movements at first (Fig. 2B and movie S7). One or more rounds of myosin enrichment and dissipation occurred in most cells (89%; n = 55 cells) before apical profiles began to shrink (Fig. 2, C to E). These early actomyosin contractions occurred periodically, with a time interval of 75 ± 24 s, which is similar to that previously measured just after this stage, during apical constriction (*12*). Some of the early contractions might contribute to cell surface flattening in *Drosophila* because apical surfaces are not yet completely flattened at this stage (*13*), although many early contractions were not centripetally directed (Fig. 2B). Myosin moved at a faster rate than did nearby contact zones at first, and this difference was significantly reduced later, as also observed in *C. elegans* (Fig. 2F). Thus, the early activation of actomyosin contraction, before apical cell profiles begin to shrink, might be a conserved feature of apical constriction.

We hypothesized that a change in the apparent efficiency of actomyosin-contact zone connections suggested by our *C. elegans* results might be a secondary effect of changes in viscoelastic properties—for example, stiffening or softening of actomyosin networks in contracting cells or their neighbors. We tested this in two ways. First, we analyzed a naturally occurring phenomenon. The apical networks in Ea/p cells occasionally failed spontaneously, with centripetally moving myosin particles suddenly springing away from one another (Fig. 3A). During recoil, myosin particle movements slowed exponentially, suggesting that the apical cortex behaves as a viscoelastic network (*14*–*16*), and initial recoil speeds and their exponential decays were similar between early and late stages, suggesting little change in cortical tension or stiffness of the network over time (Fig. 3B) (*15*, *17*). Second, we cut the cortical actomyosin network using a focused ultraviolet laser beam and measured initial recoil speed as a quantitative estimate of tension in the network (*18*–*23*). The cortical network recoiled rapidly from cuts in Ea/p (Fig. 3, B and C), again with little change in initial recoil speed between early and late stages (Fig. 3B). Cutting a neighboring cell's cortex produced a recoil that also did not change significantly over time, and that was slower than in Ea/p (Fig. 3B), suggesting that network tension is lower in this cell. Thus, the large difference in the degree of coupled movement between early and late stages is accompanied by little measurable difference in the viscoelastic properties of cortical networks. These results reveal that the cortical tension associated with apical constriction (Fig. 3D) is established well before apical constriction begins and suggest that the differences between early and late stages might be explained by a change in efficiency of actomyosin–contact zone connections alone.

These results support a picture in which a continuously coalescing apical actomyosin network adds little cortical tension as it begins to move apical cell-contact zones; the tension involved in coalescing the apical actomyosin network is great compared with the small additional tension required to pull contact zones. Although this model may appear counterintuitive, it is in fact consistent with estimates of forces in other biological systems on this size scale (*19*, *24*).

Our results build a model of apical constriction in which the relevant cytoskeletal dynamics can run constitutively, transitioning to driving rapid cell shape change at a later time. We speculate that there may exist in this system a molecular clutch—a regulatable, molecular connection between actomyosin networks and contact zones, transmitting the forces generated by actomyosin contraction to the contact zones. Molecular clutches coordinate actin dynamics and adhe-

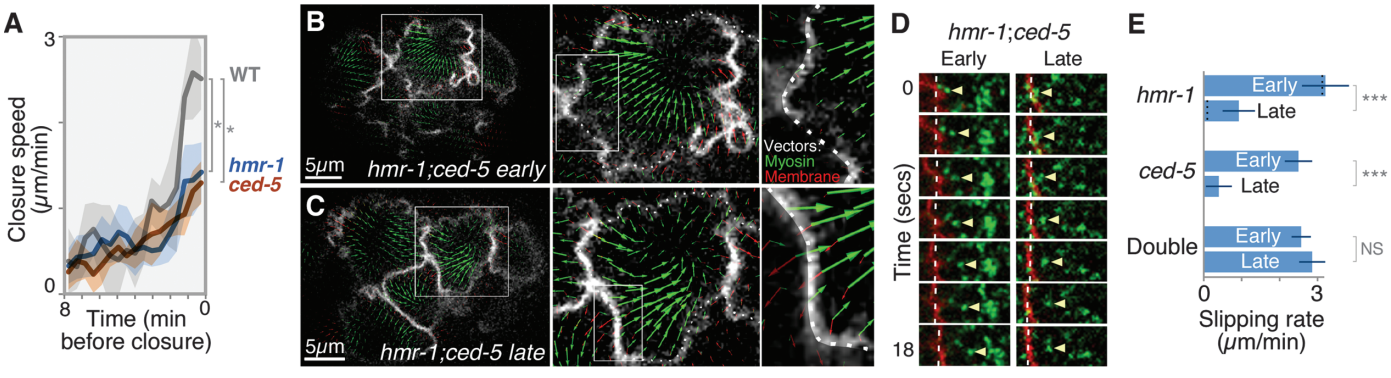

Fig. 4. Targeting classical cadherin and Rac signaling prevents coupled movements but not actomyosin contraction. (**A**) Closure speed (micrometer-per-minute decrease in average diameter) of apical cell areas in *hmr-1(RNAi)* or *ced-5(n1812)* does not reach the speed found in wild-type embryos (*P < 0.05). (**B** and **C**) PIV in *hmr-1(RNAi);ced-5(n1812)* doubles. Myosin moves centripetally with little membrane movement in the same direction at either stage. This is shown for individual particles in (**D**), with quantification as in Fig. 1I in (**E**). Black dotted lines on *hmr-1* bars in (E) mark wild type for comparison. ***P < 0.001 (Student's t test).

sion formation in migrating growth cones and cultured cells (*25*). Our results raise the possibility that there might be developmentally regulated clutches functioning in epithelial morphogenesis. Indeed, targeting a cadherin-catenin complex and a Rac pathway prevented the transition to coupled movements, genetically separating coupled movements from contractions in this system (Fig. 4 and figs. S7 to S9). Thus, cadherin-catenin complex members, Rac pathway targets, or proteins that function alongside either might contribute to a clutch. Temporal regulation of actin nucleators at contact zones could also function as a clutch, if actin polymerized in a centripetal direction from contact zones primarily at early stages. In either model, gradual engagement of a clutch would stabilize connections between a contracting actomyosin network and cell-cell boundaries. Alternatively, resistance to a slipping clutch could change over time—for example, because neighboring cells lose tension. This alternative appears unlikely because we detected no change in neighboring cell tension over time. Instead, we speculate that the degree of engagement of a molecular clutch might determine the rate of apical shrinking. As apical shrinking proceeds, this rate might be limited additionally by the rate at which apical membrane can be removed (*26*).

Recent work has highlighted a number of actomyosin-based mechanisms that drive cell shape changes in morphogenesis (*21*, *27*, *28*). Periodic contractions of actomyosin networks, flows of actomyosin, and an actomyosin-based ratchet make contributions to changing cell shapes (*12*, *23*, *29*, *30*). We found that the actomyosin contractions and cortical tension associated with a cell shape change are established even before the cell shape change begins. Thus, the immediate trigger for apical constriction is not the activation of actomyosin contractions or a change in cortical tension, suggesting a role for the dynamic connections between the actomyosin cytoskeleton and the sites of cell-cell adhesion in morphogenesis mechanisms.

References and Notes

1. P. Friedl, D. Gilmour, *Nat. Rev. Mol. Cell Biol.* **10**, 445 (2009).
2. C. J. Weijer, *J. Cell Sci.* **122**, 3215 (2009).
3. G. M. Odell, G. Oster, P. Alberch, B. Burnside, *Dev. Biol.* **85**, 446 (1981).
4. J. M. Sawyer *et al.*, *Dev. Biol.* **341**, 5 (2010).
5. A. J. Copp, N. D. Greene, *J. Pathol.* **220**, 217 (2010).
6. S. W. Grill, *Curr. Opin. Genet. Dev.* **21**, 647 (2011).
7. J. Y. Lee, B. Goldstein, *Development* **130**, 307 (2003).
8. J. Y. Lee *et al.*, *Curr. Biol.* **16**, 1986 (2006).
9. J. Nance, J. R. Priess, *Development* **129**, 387 (2002).
10. E. Munro, J. Nance, J. R. Priess, *Dev. Cell* **7**, 413 (2004).
11. Materials and methods are available as supporting material on *Science* Online
12. A. C. Martin, M. Kaschube, E. F. Wieschaus, *Nature* **457**, 495 (2009).
13. R. E. Dawes-Hoang *et al.*, *Development* **132**, 4165 (2005).
14. B. Fabry *et al.*, *Phys. Rev. Lett.* **87**, 148102 (2001).
15. M. Mayer, M. Depken, J. S. Bois, F. Jülicher, S. W. Grill, *Nature* **467**, 617 (2010).
16. F. Wottawah *et al.*, *Phys. Rev. Lett.* **94**, 098103 (2005).
17. Y. Toyama, X. G. Peralta, A. R. Wells, D. P. Kiehart, G. S. Edwards, *Science* **321**, 1683 (2008).
18. R. Fernandez-Gonzalez, S. M. Simoes, J. C. Röper, S. Eaton, J. A. Zallen, *Dev. Cell* **17**, 736 (2009).
19. M. S. Hutson *et al.*, *Science* **300**, 145 (2003).
20. D. P. Kiehart, C. G. Galbraith, K. A. Edwards, W. L. Rickoll, R. A. Montague, *J. Cell Biol.* **149**, 471 (2000).
21. A. C. Martin, M. Gelbart, R. Fernandez-Gonzalez, M. Kaschube, E. F. Wieschaus, *J. Cell Biol.* **188**, 735 (2010).
22. M. Rauzi, P. Verant, T. Lecuit, P. F. Lenne, *Nat. Cell Biol.* **10**, 1401 (2008).
23. J. Solon, A. Kaya-Copur, J. Colombelli, D. Brunner, *Cell* **137**, 1331 (2009).
24. S. W. Grill, P. Gönczy, E. H. Stelzer, A. A. Hyman, *Nature* **409**, 630 (2001).
25. T. Mitchison, M. Kirschner, *Neuron* **1**, 761 (1988).
26. J. Y. Lee, R. M. Harland, *Curr. Biol.* **20**, 253 (2010).
27. K. E. Kasza, J. A. Zallen, *Curr. Opin. Cell Biol.* **23**, 30 (2011).
28. T. Lecuit, P. F. Lenne, E. Munro, *Annu. Rev. Cell Dev. Biol.* **27**, 157 (2011).
29. L. He, X. Wang, H. L. Tang, D. J. Montell, *Nat. Cell Biol.* **12**, 1133 (2010).
30. M. Rauzi, P. F. Lenne, T. Lecuit, *Nature* **468**, 1110 (2010).

Acknowledgments: We thank K. Bloom, G. Edwards, J. Iwasa, J. Johnson, E. Munro, M. Peifer, D. Reiner, S. Rogers, and members of the Goldstein lab for comments on the manuscript; B. Eastwood and R. Taylor for help with particle image velocimetry; J. Fricks for help with statistical analysis; and A. Martin and E. Wieschaus for providing fly strains and sharing movies. This work was supported by NIH R01 GM083071 to B.G., NIH R01 GM33830 to D.P.K., and a Human Frontier Science Program postdoctoral fellowship to G.S. Data reported in this paper are presented in the main paper and in the supporting online material. U.S. patent application no. 13/160,492 concerning Bessel beam plane illumination microscopy has been filed by the Howard Hughes Medical Institute on behalf of E.B.

Supporting Online Material

www.sciencemag.org/cgi/content/full/science.1217869/DC1
Materials and Methods
Figs. S1 to S11
Table S1
References (*31*–*43*)
Movies S1 to S8

13 December 2011; accepted 27 January 2012
Published online 9 February 2012;
10.1126/science.1217869

Nucleosomes Suppress Spontaneous Mutations Base-Specifically in Eukaryotes

Xiaoshu Chen,[1,2] Zhidong Chen,[1] Han Chen,[1] Zhijian Su,[1,3] Jianfeng Yang,[1] Fangqin Lin,[1] Suhua Shi,[1] Xionglei He[1,2]*

It is unknown how the composition and structure of DNA within the cell affect spontaneous mutations. Theory suggests that in eukaryotic genomes, nucleosomal DNA undergoes fewer C→T mutations because of suppressed cytosine hydrolytic deamination relative to nucleosome-depleted DNA. Comparative genomic analyses and a mutation accumulation experiment showed that nucleosome occupancy nearly eliminated cytosine deamination, resulting in an ~50% decrease of the C→T mutation rate in nucleosomal DNA. Furthermore, the rates of G→T and A→T mutations were also about twofold suppressed by nucleosomes. On the basis of these results, we conclude that nucleosome-dependent mutation spectra affect eukaryotic genome structure and evolution and may have implications for understanding the origin of mutations in cancers and in induced pluripotent stem cells.

The mutation rates and spectra of adenine, thymine, cytosine, and guanine vary among the four bases that constitute DNA (*1*–*3*). In particular, cytosine is subject to a high rate of hydrolytic deamination, which is a major source of C→T mutations (*4*). DNA melting is a rate-limiting step for cytosine hydrolytic deamination, because only when DNA is in its single-stranded form are both the N-3 and C-4 positions of the cytosine base subject to chemical changes mediated by water (*5*). Due to ambient thermal fluctuations, a DNA double helix can spontaneously denature in local regions under normal physiological conditions within a cell, producing transient single-stranded DNA bubbles (*6*), a phenomenon called "DNA breathing." Most eukaryotic genomic DNA is packed into nucleosomes, structural units of chromatin composed of ~147 base pairs (bp) of DNA wrapped around a histone octamer and connected by ~20 to 40 bp of unwrapped linker DNA (*7*). DNA packed into nucleosomes may be more resistant to DNA breathing, and therefore subject to less cytosine deamination, than the naked DNA found in nucleosome-depleted regions (*8*).

[1]State Key Laboratory of Bio-control, College of Life Sciences, Sun Yat-sen University, Guangzhou 510275, China. [2]The Key Laboratory of Gene Engineering of Ministry of Education, College of Life Sciences, Sun Yat-sen University, Guangzhou 510275, China. [3]Gungdong Provincial Key Laboratory of Bioengineering Medicine, Jinan University, Guangzhou 510632, China.

*To whom correspondence should be addressed at 135, Xingang West, College of Life Sciences, Sun Yat-sen University, Guangzhou 510275, China. E-mail: hexiongl@mail.sysu.edu.cn

We tested whether nucleosome occupancy suppresses C→T mutations by sequencing mononucleosomal DNA from two replicates of the yeast *Saccharomyces cerevisiae* strain Y55 (fig. S1). A nucleosome occupancy score (NOS) was assigned to each nucleotide in the genome with the formula NOS = $\log_2(N/M)$, where N represents the number of times that the site was sequenced, and M is the median N of the genome (*9*). NOS represents the relative frequency within a genome that a nucleotide is covered by a nucleosome and is obtained from millions of cells, although at any given time the site is either nucleosome-occupied or not in any specific cell.

Because the substitution rate (K) is a proxy for mutation rate for functionally neutral sites, we aligned and compared the intergenic regions of three closely related yeast species: *S. cerevisiae*, *S. paradoxus*, and *S. mikatae*. Ancestral sites in *S. cerevisiae* and *S. paradoxus* were inferred by parsimony with *S. mikatae* as a designated outgroup. The rate of C→T transitions ($K_{C\to T}$) was defined as the probability that an ancestral G:C base pair has changed to an A:T base pair in an extant yeast (*9*). We observed that $K_{C\to T}$ decreased gradually with increasing NOS in *S. cerevisiae* (Fig. 1A). The $K_{C\to T}$ of sites with NOS < –3 (nucleosome-depleted regions) was 1.9 times that of sites with NOS ≥ 3 (nucleosomal regions) ($P < 10^{-16}$, two-tailed Z test). A similar result is observed when the fourfold-degenerate sites of protein-coding regions are considered (Fig. 1B and fig. S2). The pattern holds after controlling for the potential digestion bias of micrococcal nuclease that may affect the determination of nucleosome profiles (fig. S3). The $K_{C\to T}$ of fourfold-degenerate sites is higher than that of intergenic sites, suggesting stronger purifying selection on the latter, although the NOS-associated distribution of $K_{C\to T}$ is highly similar between the two site classes (ρ = 0.98, n = 8, $P < 10^{-4}$, Pearson correlation). We also sequenced the mononucleosomal DNA of *S. paradoxus* strain N17 and observed a similar reduction of $K_{C\to T}$ with increasing NOS in *S. paradoxus* (Fig. 1, C and D).

Changes in nucleosome occupancy between orthologous sites should result in corresponding changes of $K_{C\to T}$. We designated four classes for the yeast intergenic sites according to their NOS in *S. cerevisiae* (NOS_{Sc}) and *S. paradoxus* (NOS_{Sp}): Class I sites have NOS ≥ 3 in both yeasts, class II sites have $NOS_{Sc} \geq 1$ and $NOS_{Sp} \leq -1$, class III sites have $NOS_{Sc} \leq -1$ and $NOS_{Sp} \geq 1$, and class IV sites have NOS ≤ –3 in both yeasts (Fig. 1E). Because the overall substitution rate (K) of *S. cerevisiae* is ~30% higher than that of *S. paradoxus*, the $K_{C\to T}$ for the branch of *S. paradoxus* was multiplied by 1.3 to be comparable to that for the branch of *S. cerevisiae*. This normalized $K_{C\to T}$ is approximately the same between the two yeasts for either the class I sites (conserved nucleosomal regions) or the class IV sites (conserved nucleosome-depleted regions) (Fig. 1F). When nucleosome occupancy status differs between the two yeasts, as for the class II and class III sites, $K_{C\to T}$ of the species with reduced NOS is 1.5 to 1.8 times that of the species with enhanced NOS ($P < 10^{-16}$, two-tailed Z test; Fig. 1F). $K_{C\to T}$ of class III (or class II) is larger than that of class IV in *S. cerevisiae* (or *S. paradoxus*), although class IV has a smaller NOS. This is probably due to selection against C→T substitutions in class IV sites where the G+C% is as low as 25%, which might be a minimal G+C content.

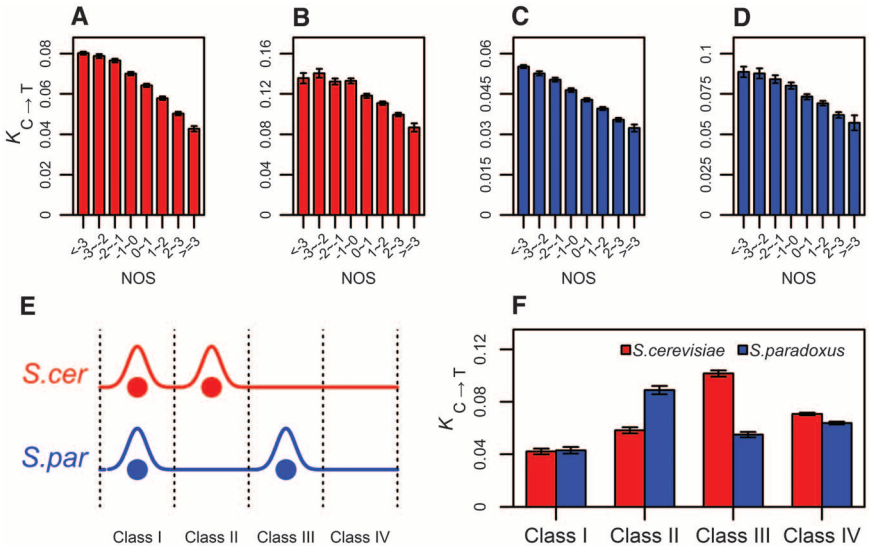

Fig. 1. The NOS-associated $K_{C\to T}$ in yeasts. (**A**) Analysis of 1.9 million intergenic sites of *S. cerevisiae*. (**B**) Analysis of 400,000 fourfold-degenerate sites of *S. cerevisiae*. (**C**) Analysis of 2.0 million intergenic sites of *S. paradoxus*. (**D**) Analysis of 400,000 fourfold-degenerate sites of *S. paradoxus*. (**E**) The four classes of sites considering NOS in both *S. cerevisiae* (*S. cer*) and *S. paradoxus* (*S. par*). (**F**) Comparisons of $K_{C\to T}$ for 35,000, 57,000, 91,000, and 546,000 sites of the class I, II, III, and IV, respectively. Errors bars represent standard error (SE).

We assessed the causal effect of nucleosomes on $K_{C\to T}$ by examining the initial nucleosome profile and tracking subsequent mutations within a cell. The yeast *UNG1* gene encodes uracil DNA glycosylase, an enzyme responsible for repairing C→U events (*10*). We deleted the *UNG1* gene from *S. cerevisiae* to boost the C→T mutation rate and measured mutations after 100 days of growth (*9*). We sequenced genomes of 81 day-100 clones and identified 162 nonredundant C→T mutations, which were compared to the nucleosome profile of the *ung1* mutant (*9*). The NOS of sites with the C→T mutation was significantly smaller than that of other G:C sites of the yeast genome ($P < 4 \times 10^{-4}$, Mann-Whitney U test). The C→T rate of nucleosome-depleted regions (NOS < –3) was 3.3 times that of regions with NOS ≥ 0 ($P < 10^{-3}$, one-tailed Z test; Fig. 2A). From this, we estimated an efficiency of nucleosome occupancy in suppressing cytosine deamination of ~70% (1 – 1/3.3). However, this number is an underestimation because we compared NOS < –3 with NOS ≥ 0, not NOS ≥ 3 (no mutation was found in the regions of NOS ≥ 3), and did not consider the nucleosome-independent rate of replication-introduced mutations (*2*). Because the vast majority of C→T mutations are due to cytosine deaminations in the *ung1* mutant, the observation of stronger effects of nucleosomes on suppressing C→T events in this mutant than in wild-type yeast is expected. Analyses of the pooled intergenic sites and silent third codon positions show a 3.2-fold difference of C→T rate between NOS < –3 and NOS ≥ 0 (P < 0.002, one-tailed Z test; Fig. 2B). These results support the hypothesis that nucleosome occupancy reduces C→T mutation rate by suppressing cytosine deamination. The reduced rate of C→T in nucleosomal DNA is not likely due to the suppression of methylcytosine (Met-C) deamination, because there is little Met-C in the yeast *S. cerevisiae* (*11*).

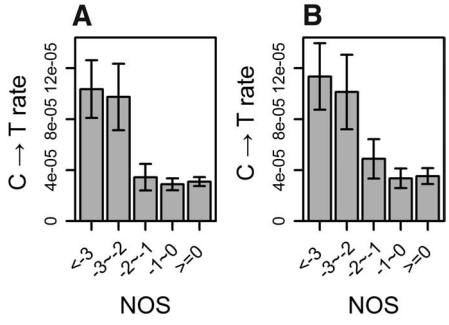

Fig. 2. Nucleosome occupancy suppresses C→T mutations. The C→T rate as a function of NOS in the *ung1* mutant for either the whole yeast genome (**A**) or the pooled intergenic sites and silent third codon positions (**B**). Errors bars represent SE.

We also examined the level of single-nucleotide polymorphisms (SNPs) (P) in the Japanese killifish medaka (*9*), with the nucleosome information from blastulae (0.5-day embryos that maintain germline character in some or all cells)

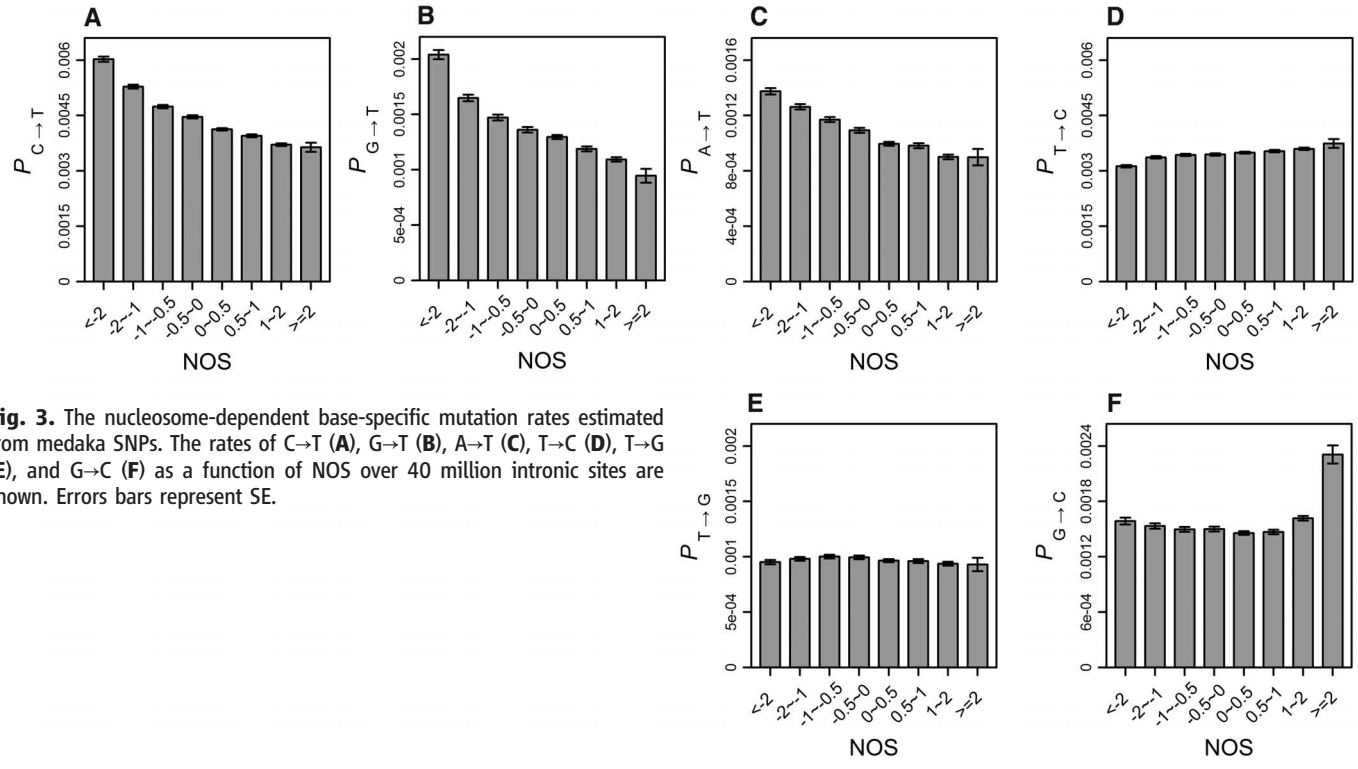

Fig. 3. The nucleosome-dependent base-specific mutation rates estimated from medaka SNPs. The rates of C→T (**A**), G→T (**B**), A→T (**C**), T→C (**D**), T→G (**E**), and G→C (**F**) as a function of NOS over 40 million intronic sites are shown. Errors bars represent SE.

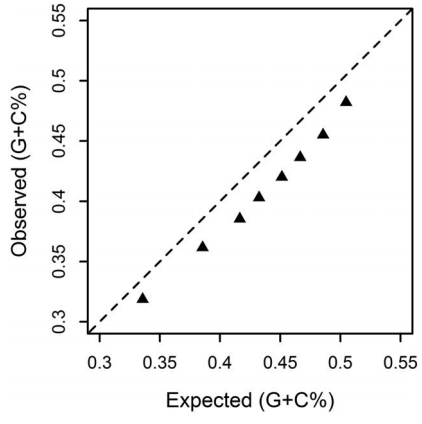

Fig. 4. NOS-associated variation of G+C% in medaka is largely explained by mutation. Each triangle represents an NOS category, and the NOS intervals (from left to right) are < −2, −2 to −1, −1 to −0.5, −0.5 to 0, 0 to 0.5, 0.5 to 1, 1 to 2, and ≥2.

generated by a previous study (*12*). We are interested in germline cells, because only mutations occurring in germline cells are of evolutionary importance in most animals. We found a similar pattern in medaka as in yeast (Fig. 3A and fig. S4); $P_{C\rightarrow T}$ decreases by ~40% from NOS < −2 to NOS ≥ 2 ($P < 10^{-16}$, two-tailed Z test; Fig. 3A). We also analyzed a nucleosome profile of the adult *Caenorhabditis elegans*, in which there is a large proportion of germline cells (*13*), and observed ~50% decrease of $K_{C\rightarrow T}$ from nucleosome-depleted regions to nucleosomal regions ($P < 10^{-16}$, two-tailed Z test; fig. S5).

It is interesting to know whether nucleosomes regulate other types of substitution mutations. Compared to between-species substitutions in yeast and nematode, both of which have a large effective population size (*14*), SNPs in medaka, which has a smaller effective population size, should be less affected by selection and thus more suitable for addressing our question. We observed a reduction of $P_{G\rightarrow T}$ and $P_{A\rightarrow T}$ with increasing NOS (Fig. 3, B and C); the $P_{G\rightarrow T}$ of nucleosome-depleted regions is 2.2 times that of nucleosomal regions ($P < 10^{-16}$, two-tailed Z-test), and the number is 1.5 for $P_{A\rightarrow T}$ ($P < 10^{-12}$, two-tailed Z test). Thus, histone octamers in eukaryotic cells appear to function like Dps, a nonspecific DNA binding protein, in *E. coli* to protect genomes from reactive oxygen species (ROS) (*15*). We observed that $P_{T\rightarrow C}$ has a 1.2-fold increase from NOS < −2 to NOS ≥ 2; $P_{T\rightarrow G}$ is essentially constant; and $P_{G\rightarrow C}$ shows no change until NOS ≥ 2 (Fig. 3, D to F). These patterns suggest that the medaka SNPs are not biased by potential selection for A+T (or against G+C) base composition in the A+T–rich nucleosome-depleted regions.

Spontaneous mutations typically arise from either DNA replication errors or DNA lesions caused by endogenous mutagens such as water and ROS (*2*). Deamination of cytosines or Met-Cs accounts for the higher rate of C→T mutation compared to T→C mutation, and the observation of a nearly equal $P_{C\rightarrow T}$ and $P_{T\rightarrow C}$ in nucleosomal regions (Fig. 3, A and D) suggests that the suppression of cytosine (or Met-C) hydrolytic deamination by nucleosomes is complete, which is consistent with the results of our yeast mutation accumulation experiment. Similarly, oxidative conversion of guanine to 8-oxoguanine may account for the higher rate of G→T mutation compared to T→G mutation, and the observation of a nearly equal rate of $P_{G\rightarrow T}$ and $P_{T\rightarrow G}$ in nucleosomal regions (Fig. 3, B and E) suggests that the protection of DNA provided by nucleosomes against oxidative mutagens is complete.

Similar studies of the *C. elegans* Bristol strain, which has two sibling lines separated by half a century and ~1000 SNPs (*16*), also showed nematode base-specific mutation rates of intronic regions as a function of NOS, with suppression of C→T, G→T, and A→T mutations by nucleosomes (fig. S6).

Although both (A+T)- and (G+C)-rich sequences are thought to disfavor nucleosome occupancy (*17*, *18*), nucleosome linkers tend to be A+T rich (*19*). We computed the expected equilibrium G+C% of each NOS category in medaka using the formula G+C% = $P_{A/T\rightarrow G/C}/(P_{G/C\rightarrow A/T} + P_{A/T\rightarrow G/C})$, where $P_{A/T\rightarrow G/C}$ and $P_{G/C\rightarrow A/T}$ stand for SNP-based rates of A/T→G/C and G/C→A/T, respectively. The expected G+C% is much lower for nucleosome-depleted DNA than for nucleosomal DNA, and on average 1.06 times that observed for all NOS categories. This suggests that weak nucleosome-independent selection may occur against G+C accumulation across the medaka genome (Fig. 4). Notably, the observed G+C% is highly correlated with the expected equilibrium G+C% ($\rho = 0.99$, $n = 8$, $P < 10^{-6}$, Pearson correlation), indicating that the nucleosome-associated variation of G+C% can be almost fully explained by mutation (Fig. 4). Thus, by adjusting mutation direction, nucleosomes serve as a G+C% modulator, accounting for most within-genome G+C%

variation and possibly the between-genome G+C% differences of eukaryotes. In addition, the nucleosome-derived within-genome G+C% variations in turn can be used to predict the nucleosome profiles (*20*).

Spontaneous mutations are not randomly distributed in a eukaryotic genome, although the underlying mechanism is poorly understood (*1*, *21*, *22*). We have revealed that nucleosomes, the most abundant eukaryotic protein-DNA complexes (*7*), likely function as a major regulator of substitution mutations in eukaryotes. Binding of proteins to DNA to suppress DNA breathing or to exclude endogenous mutagens may be how cells protect their DNA (*23*). However, DNA repair, which often works with varied efficiency between nucleosomal DNA and naked DNA (*24*), may also shape the base-specific mutation spectrum. Confounding factors such as recombination rate (*25*) and replication timing (*26*) that covary with chromatin status and affect all types of mutations cannot explain our observation, because not all mutation types show an NOS-dependent trend (Fig. 3). Regardless of the underlying mechanisms, the observed nucleosome-dependent mutation spectra have implications for understanding eukaryotic genome structure and evolution, such as the isochore structure (*27*), as well as somatic mutations in cancers and in induced pluripotent stem cells, both of which are associated with chromatin remodeling (*28*, *29*). They also suggest that conventional mutation models widely used in evolutionary analyses are oversimplified (fig. S7).

References and Notes

1. C. F. Baer, M. M. Miyamoto, D. R. Denver, *Nat. Rev. Genet.* **8**, 619 (2007).
2. H. Maki, *Annu. Rev. Genet.* **36**, 279 (2002).
3. J. W. Drake, *Annu. Rev. Genet.* **25**, 125 (1991).
4. M. Lynch *et al.*, *Proc. Natl. Acad. Sci. U.S.A.* **105**, 9272 (2008).
5. K. J. Fryxell, E. Zuckerkandl, *Mol. Biol. Evol.* **17**, 1371 (2000).
6. M. Guéron, M. Kochoyan, J. L. Leroy, *Nature* **328**, 89 (1987).
7. C. Jiang, B. F. Pugh, *Nat. Rev. Genet.* **10**, 161 (2009).
8. D. S. Gross, W. T. Garrard, *Annu. Rev. Biochem.* **57**, 159 (1988).
9. Materials and methods are available as supporting material on *Science* Online.
10. K. J. Impellizzeri, B. Anderson, P. M. Burgers, *J. Bacteriol.* **173**, 6807 (1991).
11. J. H. Proffitt, J. R. Davie, D. Swinton, S. Hattman, *Mol. Cell. Biol.* **4**, 985 (1984).
12. S. Sasaki *et al.*, *Science* **323**, 401 (2009).
13. S. Ercan, Y. Lubling, E. Segal, J. D. Lieb, *Genome Res.* **21**, 237 (2011).
14. M. Lynch, J. S. Conery, *Science* **302**, 1401 (2003).
15. A. Martinez, R. Kolter, *J. Bacteriol.* **179**, 5188 (1997).
16. K. P. Weber *et al.*, *PLoS ONE* **5**, e13922 (2010).
17. V. Iyer, K. Struhl, *EMBO J.* **14**, 2570 (1995).
18. E. Segal, J. Widom, *Curr. Opin. Struct. Biol.* **19**, 65 (2009).
19. N. Kaplan *et al.*, *Nature* **458**, 362 (2009).
20. D. Tillo, T. R. Hughes, *BMC Bioinformatics* **10**, 442 (2009).
21. N. Arnheim, P. Calabrese, *Nat. Rev. Genet.* **10**, 478 (2009).
22. K. H. Wolfe, P. M. Sharp, W. H. Li, *Nature* **337**, 283 (1989).
23. A. Sohail, C. S. Hayes, P. Divvela, P. Setlow, A. S. Bhagwat, *Biochemistry* **41**, 11325 (2002).
24. Y. Ataian, J. E. Krebs, *Biochem. Cell Biol.* **84**, 490 (2006).
25. I. V. Getun, Z. K. Wu, A. M. Khalil, P. R. Bois, *EMBO Rep.* **11**, 555 (2010).
26. C. L. Chen *et al.*, *Genome Res.* **20**, 447 (2010).
27. G. Bernardi, *Annu. Rev. Genet.* **23**, 637 (1989).
28. G. L. Dalgliesh *et al.*, *Nature* **463**, 360 (2010).
29. K. Takahashi *et al.*, *Cell* **131**, 861 (2007).

Acknowledgments: We thank J. Zhang, M. Bakewell, W. Qian, and C.-I. Wu for comments and critical reading of the manuscript. This work was supported by research grants from the National Basic Research Program of China (no. 2010CB126200), the National Natural Science Foundation of China (no. 40930212), and the Science and Technology Planning Project of Guangdong Province (no. 2009B080701090). Data are deposited in NCBI Short Read Archive (SRA040058).

Supporting Online Material

www.sciencemag.org/cgi/content/full/335/6073/1235/DC1
Materials and Methods
Figs. S1 to S10
Tables S1 to S3
References (*30*–*36*)

6 December 2011; accepted 30 January 2012
10.1126/science.1217580

Unique Processing During a Period of High Excitation/Inhibition Balance in Adult-Born Neurons

Antonia Marín-Burgin,* Lucas A. Mongiat,* M. Belén Pardi,* Alejandro F. Schinder†

The adult dentate gyrus generates new granule cells (GCs) that develop over several weeks and integrate into the preexisting network. Although adult hippocampal neurogenesis has been implicated in learning and memory, the specific role of new GCs remains unclear. We examined whether immature adult-born neurons contribute to information encoding. By combining calcium imaging and electrophysiology in acute slices, we found that weak afferent activity recruits few mature GCs while activating a substantial proportion of the immature neurons. These different activation thresholds are dictated by an enhanced excitation/inhibition balance transiently expressed in immature GCs. Immature GCs exhibit low input specificity that switches with time toward a highly specific responsiveness. Therefore, activity patterns entering the dentate gyrus can undergo differential decoding by a heterogeneous population of GCs originated at different times.

The adult hippocampus continuously generates new neurons that integrate in the dentate gyrus network and become relevant for information processing during specific learning tasks (*1*–*7*). Experimental manipulations that reduce adult neurogenesis produce impairment of hippocampus-dependent learning and behavior (*8*, *9*). Yet, the specific traits that determine the functional relevance of adult-born neurons remain unknown (*10*, *11*). Is it solely the continuous addition of new neurons to the network that is important, or are there specific functional properties only attributable to new granule cells (GCs) that are relevant to information processing?

When reaching maturity, adult-born GCs exhibit functional properties that are indistinguishable from GCs generated during development (*3*). However, while developing, immature GCs display elevated intrinsic excitability, reduced γ-aminobutyric acid (GABA)–mediated inhibition, and enhanced capacity to undergo activity-dependent synaptic potentiation (*12*–*16*). Such high intrinsic excitability would potentially allow immature GCs to be activated by entorhinal afferents in spite of their low density of glutamatergic inputs (*17*). It has thus recently been hypothesized that immature GCs might be critical to hippocampal function (*18*–*20*).

First, we investigated how immature GCs process afferent activity from entorhinal inputs and how they compare with mature GCs in the adult mouse hippocampus. We selected 4-week-old neurons because this is the earliest stage at which adult-born GCs can be reliably activated by an excitatory drive (*17*). Adult-born GCs were retrovirally labeled to express red fluorescent protein (RFP), and acute hippocampal slices were prepared 4 weeks post retroviral injection (4 WPI). Time-lapse calcium imaging was performed by using Oregon Green 1,2-bis(2-aminophenoxy)ethane-*N*,*N*,*N*′,*N*′-tetraacetic acid (BAPTA)–1 AM (OGB-1AM) to monitor the activation of immature (4 WPI, RFP^+) and mature (RFP^-) GCs in response to medial perforant path (mPP) stimulation [Fig. 1, A to D; fig. S1; and supporting online material (SOM)]. Ensemble maps representing active neuronal populations were obtained at increasing input strengths (Fig. 1E and fig. S2, A to C). The number of active immature and mature GCs increased with stronger stimuli. Each stimulus

Laboratorio de Plasticidad Neuronal, Instituto Leloir, Instituto de Investigaciones Bioquímicas de Buenos Aires–Consejo Nacional de Investigaciones Científicas y Técnicas (CONICET), Avenida Patricias Argentinas 435, 1405 Buenos Aires, Argentina.

*These authors contributed equally to this work.
†To whom correspondence should be addressed. E-mail: aschinder@leloir.org.ar

consistently activated a larger proportion of the immature GC population (Fig. 1F), suggesting that immature neurons require weaker inputs to trigger a spike.

We used electrophysiological recordings to dissect the mechanisms involved in the differential activation of immature and mature GCs. We characterized the activation profile of GCs at the single-cell level using loose patch recordings in order to detect spikes in response to mPP activation (Fig. 2, A to C). Stimuli of increasing intensity elicited spikes with increasing probability in all GCs, yet mature GCs demanded stronger inputs in order to spike. We measured the input strength required to elicit 50% spiking probability (hereafter called threshold input) (Fig. 2C and SOM). A cumulative distribution of the threshold inputs was then used to build the activation curves, which represent the fractional recruitment of the GC populations as a function of the input strength (Fig. 2D). The activation curve corresponding to mature GCs is shifted toward higher input strengths with respect to immature neurons. As an example, a stimulus that recruits ~5% of mature neurons activates ~30% of immature GCs.

These data indicate that the dentate gyrus comprises a heterogeneous population of GCs in which different subpopulations display diverse activation thresholds and support the observations obtained by using immediate early gene expression that adult-born neurons could participate in information processing in hippocampus-dependent tasks (*5*, *21*, *22*). To investigate how immature and mature GCs respond to conditions of activity that resemble those occurring during hippocampus-dependent behaviors (*23*), we measured spiking in response to 10-Hz trains delivered to the mPP. We found that immature GCs fire repeatedly during the train, whereas mature GCs fire at most a single spike (Fig. 2, F and G). Our results suggest that immature GCs might be activated during behavior by entorhinal inputs with higher probability than that of mature GCs.

The high intrinsic excitability of immature GCs is sufficient to compensate for their weak glutamatergic inputs but does not predict their lower threshold input for activation (*17*). However, mPP axons not only produce monosynaptic glutamatergic excitation of GCs, they also recruit in a feed-forward manner GABAergic inhibitory circuits, which can modulate neuronal firing in response to afferent inputs (*24*–*26*). We therefore investigated the role of inhibition in the activation of GCs. Blocking GABAergic inhibition with picrotoxin (PTX) induced a significant reduction in the input strength required to activate mature but not immature GCs (Fig. 2, C to E).

The developmental GABA switch from depolarizing to hyperpolarizing occurs in adult-born neurons (*27*). The inhibitory nature of GABAergic inputs in 4-WPI GCs was corroborated by means of perforated patch recordings and rendered hyperpolarized values of GABA reversal potential for all GCs (fig. S3). We then investigated the precise contribution of excitatory and inhibitory components that control the activation of GCs. We activated mPP axons and measured the threshold input of GCs in loose patch recordings. Subsequently, we performed whole-cell recordings in the same neurons to measure excitatory and inhibitory responses elicited at threshold input (Fig. 3A and fig. S4). Activation of mPP produced excitatory postsynaptic currents (EPSCs) and inhibitory postsynaptic currents (IPSCs), indicating that glutamatergic entorhinal axons directly activate immature and mature GCs and also recruit inhibitory interneurons that synapse into both populations. Yet, the maximal conductance of both excitatory and inhibitory responses (EPSG and IPSG) was

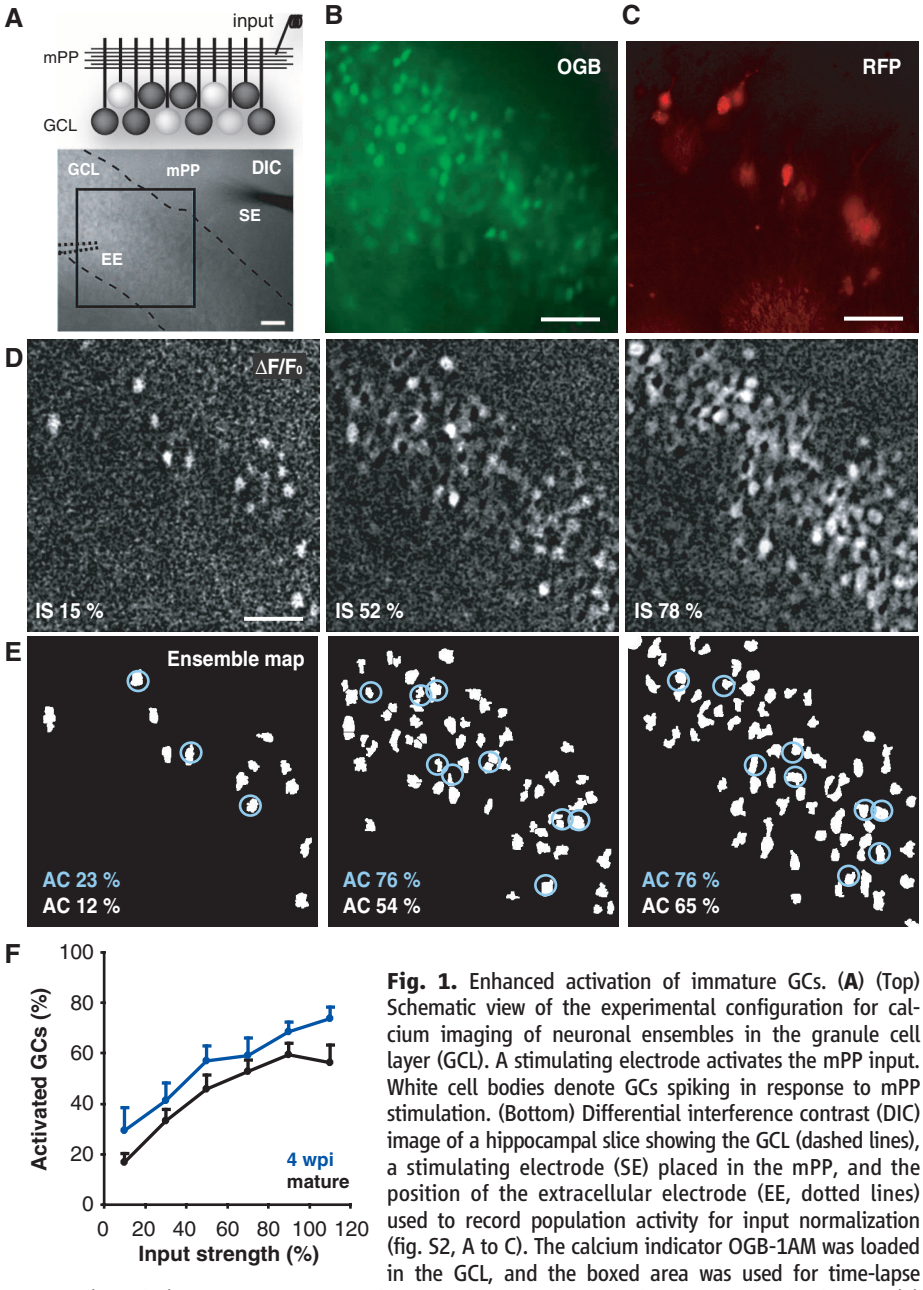

Fig. 1. Enhanced activation of immature GCs. (**A**) (Top) Schematic view of the experimental configuration for calcium imaging of neuronal ensembles in the granule cell layer (GCL). A stimulating electrode activates the mPP input. White cell bodies denote GCs spiking in response to mPP stimulation. (Bottom) Differential interference contrast (DIC) image of a hippocampal slice showing the GCL (dashed lines), a stimulating electrode (SE) placed in the mPP, and the position of the extracellular electrode (EE, dotted lines) used to record population activity for input normalization (fig. S2, A to C). The calcium indicator OGB-1AM was loaded in the GCL, and the boxed area was used for time-lapse imaging. (**B** and **C**) Larger magnification depicting the imaged area with all OGB-1AM–loaded GCs (B) and 4-WPI (RFP^+) GCs (C). (**D**) Representative experiment displaying neuronal ensembles activated at increasing input strengths [IS, assessed as percent field excitatory postsynaptic potential slope ($fEPSP_{slope}$)] (fig. S2, A to C, and SOM). Images are averages of peak $\Delta F/F_0$ of 5 trials from the same slice shown in (A) to (C). (**E**) Ensemble maps corresponding to the panels shown in (D) (fig. S1 and SOM). The percentage of active cells (ACs) is indicated for mature (RFP^-, white labels) or 4-WPI GCs (RFP^+, circled cells, blue labels). (**F**) Percentage of activated cells as a function of input strength. Immature GCs (n = 4 to 14 slices per bin) displayed higher levels of activation than those of mature GCs (n = 5 to 18 slices per bin) [$P < 0.01$, two-way analysis of variance (ANOVA)]. Data was binned every 20% input strength. Scale bars, 50 μm.

substantially larger in mature GCs (Fig. 3, A to C), maintaining a similar ratio of peak excitation/inhibition and reflecting the higher density of glutamatergic and GABAergic contacts characteristic of fully developed neurons (*3*, *14*). Four-WPI neurons displayed a significant delay in the onset of inhibition, which occurred at a time that followed spiking in those cells (Fig. 3, B and D). Thus, it is very unlikely that spike initiation in immature GCs is controlled by inhibitory circuits. We then hypothesized that the observed difference in the activation threshold relied on the excitation/inhibition balance at the precise moment of spiking. Indeed, excitation onto immature GCs (~4 nS) was about fourfold that of inhibition at the moment of spiking (~1 nS), whereas that ratio was twofold in mature GCs (~6 and ~3 nS) (Fig. 3E). To determine whether this difference was due to the slow maturation of perisomatic GABAergic synapses characteristic of newly generated GCs (*14*, *28*), we compared the strength and kinetics of direct inhibition onto 4-WPI and mature GCs. We found that direct perisomatic inhibition was slower in immature than mature GCs, whereas no differences were found for dendritic IPSCs (fig. S5). These findings indicate that the slow disynaptic inhibition kinetics observed after mPP stimulation is due to a slow IPSC rather than to a delayed recruitment of inhibitory neurons.

The observation that few active mPP terminals are sufficient to recruit immature GCs suggests that this neuronal population could respond to most inputs, acting as good integrators of afferent information. On the other hand, mature GCs that display a higher activation threshold may be recruited by specific inputs, acting as better separators (*9*, *20*). We obtained a quantitative assessment of these properties using calcium imaging to detect activation of neuronal ensembles in response to stimulation of two independent mPP inputs (Fig. 4, A to G, and fig. S6). Inputs 1 and 2 were activated separately and recruited distinct neuronal ensembles containing both immature and mature GCs, with some cells shared by both inputs. We define cells activated independently by both inputs as "good integrators." We quantified the input integration capacity as the number of GCs recruited by both inputs, normalized to the total number of cells recruited by inputs 1 and 2. The ability of a neuronal ensemble to integrate inputs increased with stimulus strength as additional mature and immature GCs were recruited by both inputs (Fig. 4H). Immature GCs exhibited higher levels of integration along the entire input range. Thus, input strengths of ~10% resulted in ~20% integration in mature neurons and ~40% integration in 4-WPI GCs. Such enhanced integration capacity was selective for immature neurons because RFP^+ neurons of 8 weeks of age [8 WPI, when functional properties are fully developed (*3*)] displayed similar input integration to RFP^- GCs. Last, the role of inhibition was assessed by means of PTX blockade of GABA-mediated signaling. PTX increased the ability of mature neurons to integrate independent inputs

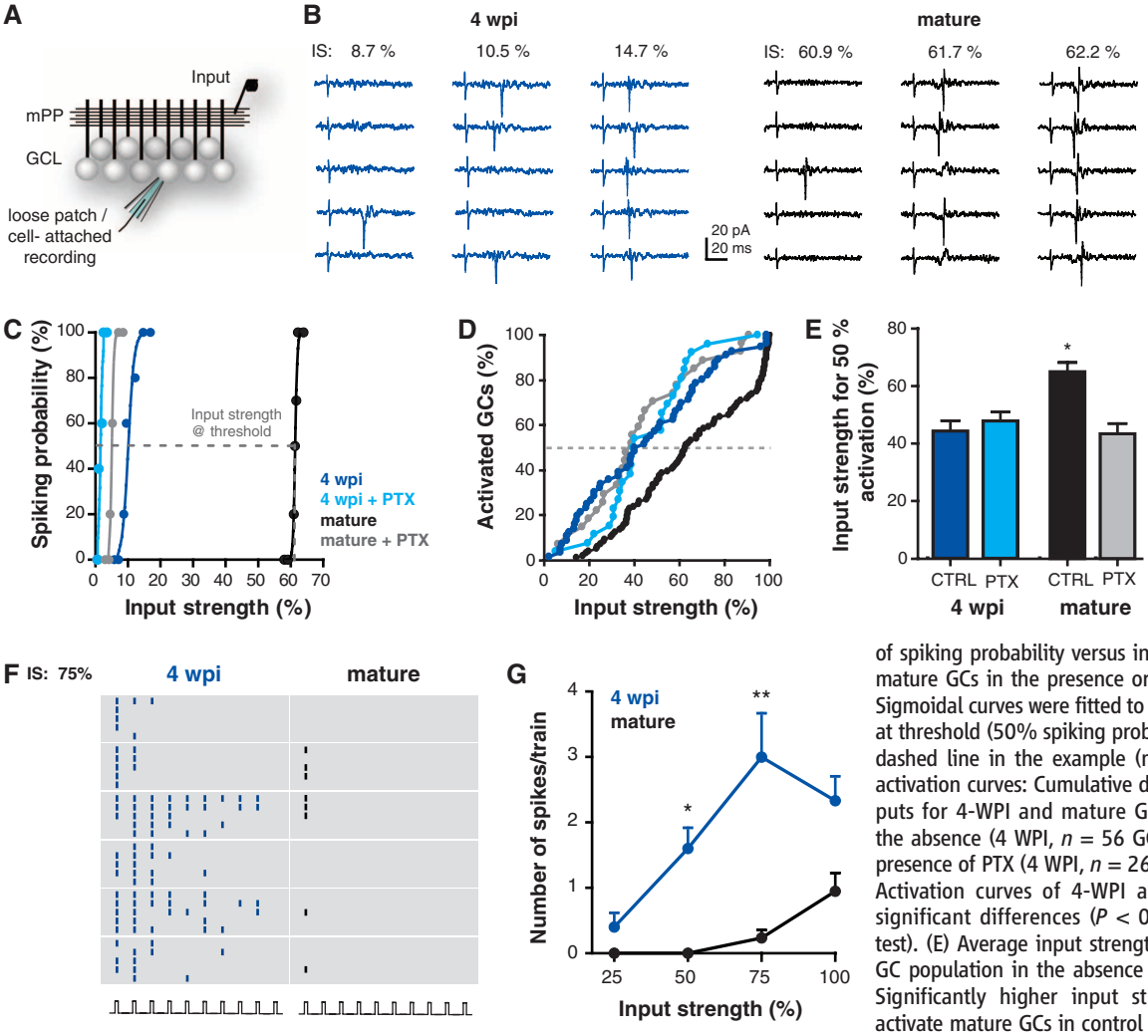

Fig. 2. Differential influence of inhibitory circuits in the activation of immature and mature GCs. (**A** to **E**) Activation of GCs evoked through stimulation of the mPP by single pulses. (A) Schematic diagram depicting the experimental configuration. A stimulating electrode (input) was placed in the mPP, and loose patch recordings were performed to measure spiking probability. (B) Example traces of a 4-WPI and a mature GC recorded at increasing input strengths (IS, normalized to the percent $fEPSP_{slope}$) (fig. S2, A to C). (C) Example curves of spiking probability versus input strength for 4-WPI and mature GCs in the presence or absence of PTX (100 μM). Sigmoidal curves were fitted to calculate the input strength at threshold (50% spiking probability), as indicated by the dashed line in the example (mature GC). (D) Population activation curves: Cumulative distributions of threshold inputs for 4-WPI and mature GC populations recorded in the absence (4 WPI, n = 56 GCs; mature, n = 96 GCs) or presence of PTX (4 WPI, n = 26 GCs; mature, n = 27 GCs). Activation curves of 4-WPI and mature GCs displayed significant differences ($P < 0.006$, Kolmogorov-Smirnov test). (E) Average input strength that recruits 50% of the GC population in the absence (CTRL) or presence of PTX. Significantly higher input strengths were required to activate mature GCs in control conditions than in all other groups (*$P < 0.001$, post-hoc Bonferroni's test after one-way ANOVA). (**F** and **G**) Activation of GCs evoked by stimulation of the mPP at 10-Hz trains. (F) Raster plot depicting spikes recorded from 4-WPI and mature GCs in response to trains (10 pulses, 10 Hz) delivered at 75% input strength (five trials per neuron). (G) Train stimulation elicits a higher number of spikes (mean ± SEM) in 4-WPI GCs than in mature GCs at increasing input strengths. *$P < 0.05$, **$P < 0.001$, after ANOVA and Bonferroni's post-hoc test (n = 7 immature GCs; n = 6 mature GCs).

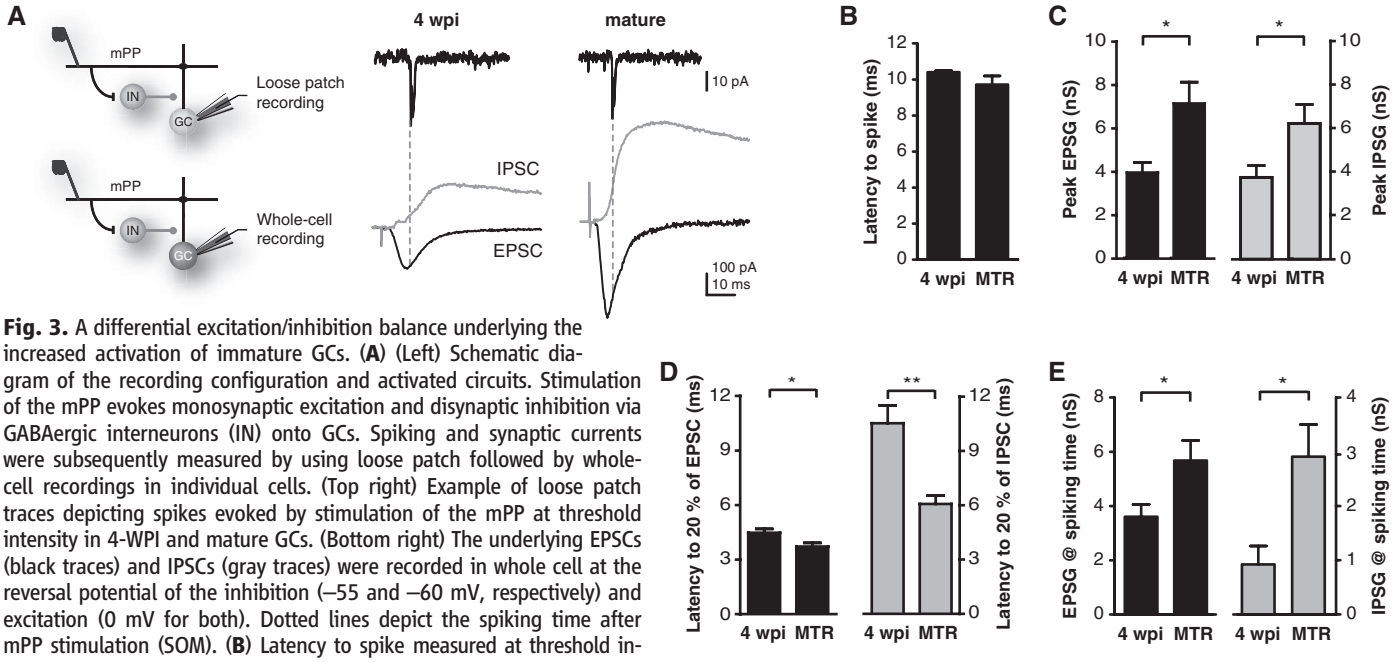

Fig. 3. A differential excitation/inhibition balance underlying the increased activation of immature GCs. (**A**) (Left) Schematic diagram of the recording configuration and activated circuits. Stimulation of the mPP evokes monosynaptic excitation and disynaptic inhibition via GABAergic interneurons (IN) onto GCs. Spiking and synaptic currents were subsequently measured by using loose patch followed by whole-cell recordings in individual cells. (Top right) Example of loose patch traces depicting spikes evoked by stimulation of the mPP at threshold intensity in 4-WPI and mature GCs. (Bottom right) The underlying EPSCs (black traces) and IPSCs (gray traces) were recorded in whole cell at the reversal potential of the inhibition (−55 and −60 mV, respectively) and excitation (0 mV for both). Dotted lines depict the spiking time after mPP stimulation (SOM). (**B**) Latency to spike measured at threshold intensity displayed similar values between 4-WPI and mature GCs. (**C**) Peak EPSG and IPSG in 4-WPI and mature GCs (*$P < 0.02$, t test). (**D**) Latency to onset for EPSCs and IPSCs show a profound delay in IPSC onset for 4-WPI neurons (*$P < 0.05$, **$P < 0.01$, t test). (**E**) EPSG and IPSG amplitudes measured at the precise time of evoked spikes (*$P < 0.05$ for EPSG and $P < 0.03$ for IPSG, t test); $n = 4$ neurons for all experiments.

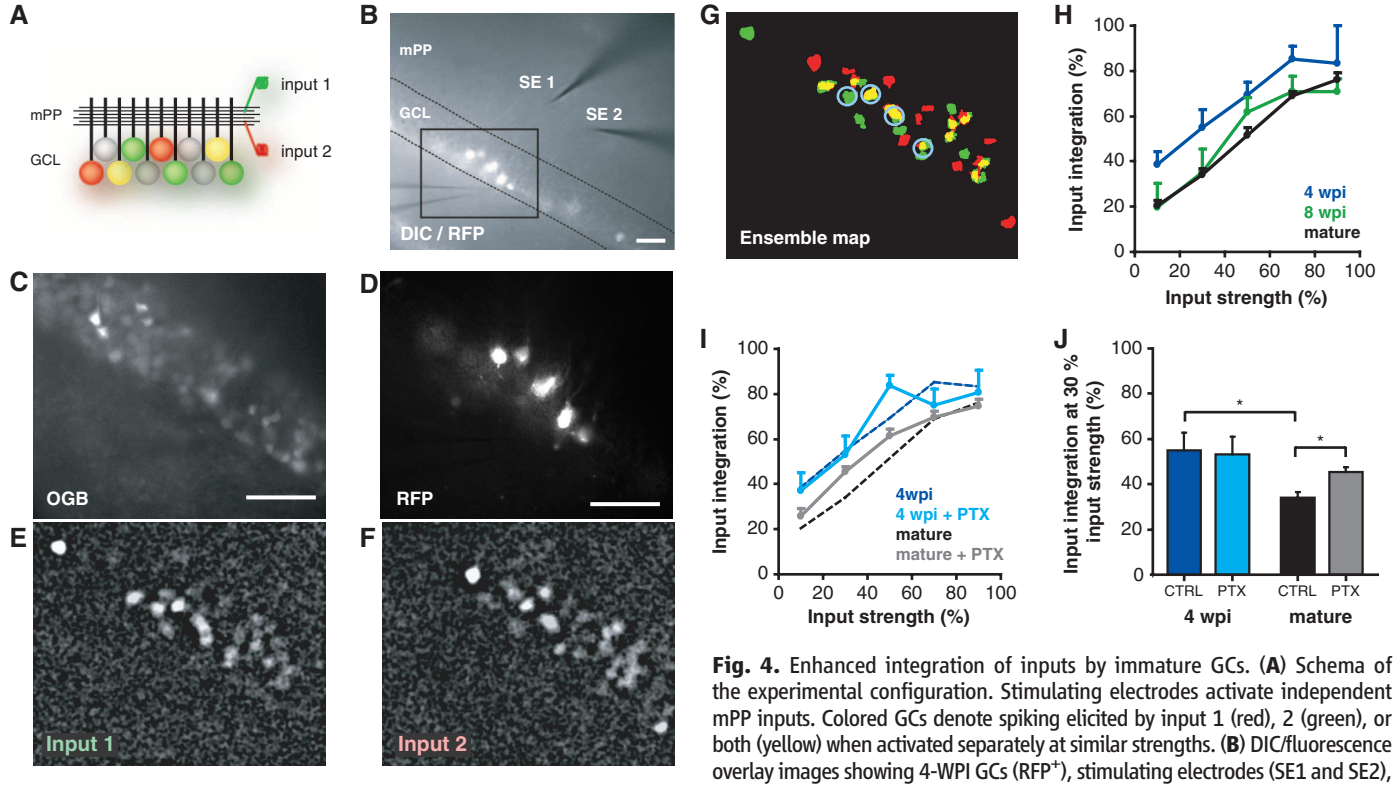

Fig. 4. Enhanced integration of inputs by immature GCs. (**A**) Schema of the experimental configuration. Stimulating electrodes activate independent mPP inputs. Colored GCs denote spiking elicited by input 1 (red), 2 (green), or both (yellow) when activated separately at similar strengths. (**B**) DIC/fluorescence overlay images showing 4-WPI GCs (RFP^+), stimulating electrodes (SE1 and SE2), the extracellular electrode used to assess input independence (fig. S6), and the boxed area used for imaging. (**C** and **D**) Imaged area depicting (C) OGB-1AM loaded cells and (D) RFP^+ GCs. (**E** to **G**) Representative experiment displaying neuronal ensembles activated by (E) input 1 and (F) 2 at similar strengths. Neurons responding to either stimulus (green, red) or both (yellow) are shown in (G) the ensemble map. Blue circles indicate active immature GCs. (**H**) Input integration of recruited ensembles, defined as the proportion of GCs responding to both inputs (activated separately) normalized to the total number of active neurons at each input strength. Input strength was assessed as percent of total activated neurons (fig. S2, D and E, and SOM). Four-WPI GCs ($n = 3$ to 16 slices per bin) displayed higher integration values than those of 8-WPI ($n = 5$ to 13 slices per bin) and mature GCs ($n = 8$ to 34 slices per bin) throughout the curves ($P < 0.01$ for both, two-way ANOVA). Data was binned in 20% intervals. (**I**) Effect of inhibition in input integration. Control curves for 4-WPI and mature GCs [dotted lines, same as in (H)] are plotted for comparison (PTX curves: $n = 3$ to 17 slices per bin, 4-WPI and $n = 11$ to 34 slices per bin, mature GCs). (**J**) Input integration at 30% strength. PTX enhanced integration in mature but not immature GCs (*$P < 0.01$, Bonferroni's test after two-way ANOVA). CTRL, control. Scale bars, 50 μm.

without altering the response of immature neuronal ensembles (Fig. 4, I and J), which is in agreement with our observation that inhibition reduces the activation of mature but not immature GCs (Fig. 2, D and E).

Our data demonstrate that immature GCs exhibit all of the features required to process information and display a low activation threshold due to an enhanced excitation/inhibition balance at the time of spike initiation. At this early developmental stage, they already release glutamate onto CA3 pyramidal cells (fig. S7). As a consequence, neuronal activity in the dentate gyrus is biased toward the immature population of principal neurons that bypass inhibitory control, whereas the activation of mature neurons is limited by inhibition (Figs. 1 and 2 and fig. S8). This is in contrast to other areas of the hippocampus and neocortex, in which inhibition exerts a global (homogeneous) control in the activity of principal cells (*25*, *29*, *30*). Hence, adult neurogenesis emerges as a mechanism that generates a distinct type of network heterogeneity. In addition, the differential control of inhibition revealed here constitutes a simple synaptic mechanism that could underlie the enhanced capacity of immature GCs to undergo activity-dependent synaptic potentiation when GABAergic inhibition is left intact (*12*, *13*, *31*). In the context of the low activation threshold described here, the increased plasticity might provide an efficient means for strengthening and reinforcing weak synaptic inputs that are repeatedly activated during a restricted time window.

The observed network heterogeneity may be crucial for the integration and separation of spatial patterns, properties that have been attributed to the dentate gyrus (*10*). Their low activation threshold and low input specificity make immature GCs appropriate substrates for pattern integration—a feature that has been proposed in computational models of adult neurogenesis (*10*, *18*, *19*, *32*). In this context, immature neurons represent a population of integrators that are broadly tuned during a transient period and may encode most features of the incoming afferent information. When becoming mature, new GCs display a high activation threshold and input specificity and will, therefore, become good pattern separators. Adult neurogenesis would then maintain the renewable cohorts of highly integrative GCs in the dentate gyrus. Last, the functional properties described here support a hypothesis in which activity reaching the dentate gyrus could undergo differential decoding through immature neuronal cohorts that are highly responsive and integrative and, in parallel, through a large population of mature GCs with sparse activity and high input specificity.

References and Notes

1. H. van Praag *et al.*, *Nature* **415**, 1030 (2002).
2. S. Jessberger, G. Kempermann, *Eur. J. Neurosci.* **18**, 2707 (2003).
3. D. A. Laplagne *et al.*, *PLoS Biol.* **4**, e409 (2006).
4. P. M. Lledo, M. Alonso, M. S. Grubb, *Nat. Rev. Neurosci.* **7**, 179 (2006).
5. V. Ramirez-Amaya, D. F. Marrone, F. H. Gage, P. F. Worley, C. A. Barnes, *J. Neurosci.* **26**, 12237 (2006).
6. C. D. Clelland *et al.*, *Science* **325**, 210 (2009).
7. C. O. Lacefield, V. Itskov, T. Reardon, R. Hen, J. A. Gordon, *Hippocampus* **22**, 106 (2012).
8. D. Dupret *et al.*, *PLoS ONE* **3**, e1959 (2008).
9. A. Sahay, D. A. Wilson, R. Hen, *Neuron* **70**, 582 (2011).
10. A. Treves, A. Tashiro, M. E. Witter, E. I. Moser, *Neuroscience* **154**, 1155 (2008).
11. G. L. Ming, H. Song, *Neuron* **70**, 687 (2011).
12. S. Wang, B. W. Scott, J. M. Wojtowicz, *J. Neurobiol.* **42**, 248 (2000).
13. J. S. Snyder, N. Kee, J. M. Wojtowicz, *J. Neurophysiol.* **85**, 2423 (2001).
14. M. S. Espósito *et al.*, *J. Neurosci.* **25**, 10074 (2005).
15. S. Ge, C. H. Yang, K. S. Hsu, G. L. Ming, H. Song, *Neuron* **54**, 559 (2007).
16. C. Schmidt-Hieber, P. Jonas, J. Bischofberger, *Nature* **429**, 184 (2004).
17. L. A. Mongiat, M. S. Espósito, G. Lombardi, A. F. Schinder, *PLoS ONE* **4**, e5320 (2009).
18. S. Becker, J. M. Wojtowicz, *Trends Cogn. Sci.* **11**, 70 (2007).
19. J. B. Aimone, J. Wiles, F. H. Gage, *Neuron* **61**, 187 (2009).
20. J. B. Aimone, W. Deng, F. H. Gage, *Neuron* **70**, 589 (2011).
21. N. Kee, C. M. Teixeira, A. H. Wang, P. W. Frankland, *Nat. Neurosci.* **10**, 355 (2007).
22. A. Tashiro, H. Makino, F. H. Gage, *J. Neurosci.* **27**, 3252 (2007).
23. J. K. Leutgeb, S. Leutgeb, M. B. Moser, E. I. Moser, *Science* **315**, 961 (2007).
24. G. Buzsàki, E. Eidelberg, *Brain Res.* **230**, 346 (1981).
25. F. Pouille, A. Marin-Burgin, H. Adesnik, B. V. Atallah, M. Scanziani, *Nat. Neurosci.* **12**, 1577 (2009).
26. L. A. Ewell, M. V. Jones, *J. Neurosci.* **30**, 12597 (2010).
27. S. Ge *et al.*, *Nature* **439**, 589 (2006).
28. S. J. Markwardt, J. I. Wadiche, L. S. Overstreet-Wadiche, *J. Neurosci.* **29**, 15063 (2009).
29. N. J. Priebe, D. Ferster, *Neuron* **57**, 482 (2008).
30. C. Poo, J. S. Isaacson, *Neuron* **62**, 850 (2009).
31. S. Ge, K. A. Sailor, G. L. Ming, H. Song, *J. Physiol.* **586**, 3759 (2008).
32. J. B. Aimone, J. Wiles, F. H. Gage, *Nat. Neurosci.* **9**, 723 (2006).

Acknowledgments: We thank M. Veggetti for technical assistance, S. Ge for the channelrhodopsin-2 viral construct, and B. Aimone, Y. Li, F. Gage, and M. Scanziani for insightful discussions. A.M.B., L.A.M., and A.F.S. are investigators of the National Research Council (CONICET). M.B.P. was supported by a CONICET fellowship. This work was supported by the Guggenheim Fellowship and by grants from the National Institutes of Health (FIRCA R03TW008607-01), the Howard Hughes Medical Institute (grant 55005963), and the Agencia Nacional de Promoción Científica y Tecnológica PICT2008 to A.F.S. and PICT2010 to A.M.B. and A.F.S.

Supporting Online Material

www.sciencemag.org/cgi/content/full/science.1214956/DC1
Materials and Methods
Figs. S1 to S8
References

7 October 2011; accepted 13 January 2012
Published online 26 January 2012;
10.1126/science.1214956

New Products

BIOLOGICAL SAMPLE STORAGE

BiOS is an automated system designed for ultralow temperature storage of sensitive biological samples. This flexible, scalable system ensures the integrity of 250,000 to more than 10 million sample tubes at temperatures down to -85˚C. All samples within the BiOS are stored in -85°C chest freezer compartments to maintain temperature stability. All internal workflows, including sample picking, are optimized to keep samples at ultralow temperatures at all times. System parts are easily accessible for service and maintenance. One- and two-dimensional barcode reading and sample tracking produce complete chain-of-custody documentation, with software tools to support 21 CFR Part 11 compliance. Multiple redundant backup systems ensure the samples stay at -85°C, even in emergencies. The BiOS can store and process multiple labware types in the same system.

Hamilton Storage Technologies
For info: 800-310-5866 | www.hamilton-storage.com

ENDOTOXIN REMOVAL

The High Capacity Endotoxin Removal Resin is designed for the cleanup of protein that is injected or transfected into cells or animals. The Pierce High Capacity Endotoxin Removal Resin combines porous cellulose beads and an FDA-approved food preservative, poly (ε-lysine), as an affinity ligand to selectively bind endotoxins. Endotoxin levels in protein samples are reduced by greater than 99% in as little as one hour using a spin cup format, and protein recovery is greater than 85%. The Pierce High Capacity Endotoxin Removal Resin peptides have a high affinity for the charged glycol-groups of an endotoxin, while the particle pores help trap endotoxins. The modified polylysine affinity ligand eliminates the toxicity concerns associated with alternative technologies that use polymixin B ligands and sodium deoxycholate buffers. The Pierce High Capacity Endotoxin Removal Resin is available in either bulk slurry packages for researchers who want to pack their own columns or convenient, single-use, spin-column formats.

Thermo Fisher Scientific
For info: 800-874-3723 | www.thermoscientific.com/pierce

AUTOMATED STAGE SYSTEM

The NZ400 NanoScan Piezo Stage System is well suited for researchers producing rapid Z sections and live cell 3-D images of specimens grown in well plates, large petri dishes, or mounted to glass slides. With the ability to create a stack of images using multiple objectives in the z-axis with nanometer precision at an amazingly high speed, the NanoScan is the perfect accessory for any 3-D imaging application. The NZ400 NanoScan Piezo Stage System offers 400 µm of travel, 2.5 nm repeatability, and closed loop control utilizing a subangstrom resolution piezo resistive sensor. Designed to mount to the Prior ProScan H117 series of high precision motorized stages, the NZ400 can also be provided as a standalone device that can be mounted onto a wide range of XY stages. Compatible with most leading imaging software packages, the NZ400 comes standard with control inputs for RS232, USB, and 0–10 V analog input.

Prior Scientific
For info: 800-877-2234 | www.prior.com

APOPTOTIC BODY DNA ANALYSIS

The D-Pop Kit simplifies the capture of DNA-containing particles from cell-free biological samples such as blood serum and plasma, urine, and eukaryotic cell culture media, and the extraction of DNA from the captured particles. Using the D-Pop Kit, apoptotic bodies and potentially other large particles are captured from biological fluids in minutes by passing them through a filter in a syringe format. The filter is then removed to a microfuge tube and the DNA is extracted from it using a rapid solid-phase extraction of DNA with non-organic reagents. The D-Pop Kit also includes control polymerase chain reaction primers for the hTERT gene to verify concentration and recovery of DNA from the sample.

Bioo Scientific
For info: 888-208-2246 | www.biooscientific.com

UV CROSSLINKER

A new high quality, inexpensive ultraviolet crosslinker makes it possible to identify and analyze trace amounts of DNA/RNA with far greater sensitivity, accuracy, and speed than with conventional analysis. The Select XLE-Series UV crosslinker covalently binds nucleic acids to membranes in less than 30 seconds—240 times faster than vacuum-oven baking. It has a unique true-ultraviolet (UV)-monitoring circuitry that safeguards valuable test results from washouts, even when the tubes age. Researchers also rely on this versatile instrument for eliminating polymerase chain reaction (PCR) contamination, nicking ethidium-bromide-stained DNA in agarose gels, gene mapping for creating cleavage-inhibiting thymine dimers, RecA mutation screening in *E. coli,* UV sterilization, and miscellaneous UV-dosage applications. The Select Series crosslinker features a "smart" user-friendly, fully programmable microprocessor, built-in "help" messages and an auto-repeat function that make its operation amazingly fast and simple. It features five 8 W tubes and is available in a choice of 254 nm, 312 nm, and 365 nm versions.

Spectronics Corporation
For info: 800-274-8888 | www.spectroline.com

Electronically submit your new product description or product literature information! Go to **www.sciencemag.org/products/newproducts.dtl** for more information.

Newly offered instrumentation, apparatus, and laboratory materials of interest to researchers in all disciplines in academic, industrial, and governmental organizations are featured in this space. Emphasis is given to purpose, chief characteristics, and availability of products and materials. Endorsement by *Science* or AAAS of any products or materials mentioned is not implied. Additional information may be obtained from the manufacturer or supplier.

POSITIONS OPEN

POSTDOCTORAL RESEARCH OPPORTUNITIES
Albert Einstein Cancer Center

Postdoctoral positions are available at the Albert Einstein Cancer Center, a major NCI-designated research institute with a broad spectrum of interdisciplinary programs and core laboratory facilities.

Research opportunities encompass: DNA repair in cells under genotoxic stress; Replication of telomeres in human embryonic stem cells; Cell fate decisions of normal- and leukemia-stem cells; Molecular evolutionary basis of HPV carcinogenesis; Selective small-molecule targeting of EBV-associated lymphomas; Cancer promotion and the liver cell cycle; The epigenetics of lung carcinogenesis; Tumor genomics of breast cancer metastasis; Glycans in cancer, immunity, development and Notch signaling; Studies on intestinal stem cell secretomes; Resistance mechanisms to targeted and anti-angiogenic drugs; Drug transporters—molecular genetics, resistance, structure-function; and PI3K pathway alterations in uterine papillary serous carcinoma.

To learn more about these projects and their faculty mentors as well as other training opportunities, go to **website: http://www.einstein.yu.edu/cancer** click on postdoctoral training.

The Albert Einstein College of Medicine is located in a residential area in close proximity to Westchester County with easy access to Manhattan. Apply through the Cancer Center webpage (as above) or write to: **Dr. Richard Seither, Albert Einstein Cancer Center, Jack and Pearl Resnick Campus, 1300 Morris Park Ave, Bronx, NY 10461.**

The Albert Einstein College of Medicine is an Equal Opportunity Employer.

POSITIVE PSYCHOLOGY POSTDOCTORAL FELLOW

The Positive Psychology Center at the University of Pennsylvania seeks an outstanding Postdoctoral Fellow to begin summer or Fall 2012, for one or more years. The fellow will analyze data and prepare publications for a large research grant on Positive Health among Army Soldiers—exploring on a large scale the influence of psychological and physical health assets on illness, health care utilization, and health care expenditure. Analyses will be conducted with large U.S. Army datasets. The fellow will work with Dr. Martin E.P. Seligman and other senior scientists. Experience with large-scale data sets using advanced statistics, as well as an understanding of the interface between mental and physical health is required. Individuals with a Ph.D. in psychology, health and human development, social epidemiology, or a related field are encouraged to apply. Applications will be reviewed on a rolling basis. The specific location (university) of this fellowship is TBD. Please send curriculum vitae, statement of interest (two pages max), and at least three references to: Libby Benson, **e-mail: lbens@psych.upenn.edu.** *The University of Pennsylvania is an Equal Opportunity/Affirmative Action Employer.*

Two **POSTDOCTORAL POSITIONS** are available at Department of Structural Biology, University of Pittsburgh School of Medicine. We are seeking self-motivated postdoctoral scientists with interpersonal and problem-solving skills. The individual will be leading multiple projects investigating virus-host cell protein interaction utilizing various biophysical techniques including, but not limited to, CD, DSC, SPR, ITC, light-scattering, Fluorescence, NMR, and X-ray crystallography. He/She will be also performing protein expression and purification in *E. coli*, insect cells and mammalian cells.

Please visit our **websites:** (1) **http://www.structbio.pitt.edu/webusers/protein** and (2) **http://www.hivppi.pitt.edu** for more detail.

Candidate must hold a Ph. D. and have a strong background in protein biochemistry and biophysics. For consideration, please send detailed curriculum vitae, cover letter, and three references to **Dr. Jinwoo Ahn, e-mail: jia12@pitt.edu.**

The University of Pittsburgh is an Affirmative Action/Equal Opportunity Employer.

POSITIONS OPEN

KOCH POSTDOCTORAL TEACHING FELLOW

The Department of Ecology and Evolutionary Biology (EEB) at Tulane University seeks to fill the inaugural Koch Postdoctoral Teaching Fellowship in Plant Ecology And Evolution, pending budgetary approval (**website: http://tulane.edu/sse/eebio/about/kochfellow.cfm**). The position is a two-year appointment, with faculty status and a start date of July 1. The department aims to recruit outstanding researchers with a Ph.D. and prior postdoctoral research experience who will merge excellence in teaching (30%), research (60%), and service (10%). Applicants are encouraged to identify a potential faculty collaborator in EEB, although those interested in independent research will be given consideration. Applicants should describe botanical courses they would be able to teach, including courses that are not in the existing curriculum and could be taught as special topics. An application (curriculum vitae, statement of research interests, and statement of teaching philosophy and interests) and three letters of recommendation focusing on both research excellence and teaching potential should be submitted electronically to the Search Committee (**e-mail: ecolevol@tulane.edu**). Please write "Koch Fellow" in the subject line. Application review will begin immediately, and the position will remain open until filled.

Tulane University is an Equal Employment Opportunity/Affirmative Action/ADA employer committed to excellence through diversity. All eligible candidates are invited to apply.

POSTDOCTORAL POSITION in Brain Targeting/Cancer Immunology

A position (two years) is available immediately in the laboratory of **Ulrich Bickel,** M.D., Department of Pharmaceutical Sciences, Texas Tech University Health Sciences Center at Amarillo. Our group focuses on blood-barrier transport mechanisms and drug delivery. The successful applicant will work on an innovative new project exploring the targeting of breast cancer metastases in brain using a novel type of monoclonal antibody (*J. Cell Physiol.* **225:**664–672; *J. Immunol.* **186:**3265–3276) funded by the DoD Breast Cancer Research Program. Candidates with background in pharmacology/pharmaceutical sciences or related areas and with hands-on experience in pharmacokinetic studies in rodents, cell culture, and histological techniques, including (confocal) fluorescence microscopy are preferred. For more information about this position and to apply, visit our **website: http://jobs.texastech.edu.** *Equal Opportunity Employer/Affirmative Action/ADA.*

Mount Sinai School of Medicine has **POSTDOCTORAL POSITIONS** available through its NCI funded training program in cancer biology. Areas of interest include: cellular signaling involving both oncogenes and tumor suppressor, regulation of gene expression including epigenetics, developmental biology, cell cycle, apoptosis, and molecular epidemiology. These positions are open to U.S. citizens or permanent residents with an M.D. or Ph.D. with experience in molecular/cellular biology. Salary will follow NIH guidelines and depend on experience. For a list of training faculty, please see **website: http://fusion.mssm.edu/training/faclist2.cfm?sec=8.**

Highly motivated candidates are encouraged to send or electronically send an application including a cover letter, a curriculum vitae, and contact information of three references to: **Postdoctoral Training in Cancer Biology, MSSM, One Gustave L. Levy Place, Box 1130, New York, NY 10029. E-mail: cancer.biology@mssm.edu.**

POSTDOCTORAL OPPORTUNITIES in computational and systems biology in the Center for Genome Dynamics at The Jackson Laboratory (**website: http://www.genomedynamics.org**). Center investigators use computation, mathematical modeling, and statistics to understand the genetics of complex traits. Requires Ph.D. (or equivalent) in quantitative field such as computer science, statistics, applied mathematics or in biological sciences with strong quantitative background. Programming experience recommended. More details at **website: http://www.jax.org/careers** (**Job ID 2311**). *The Jackson Laboratory is an Equal Opportunity Employer/Affirmative Action Employer.*

Postdoc and research **opportunities** in Brazil

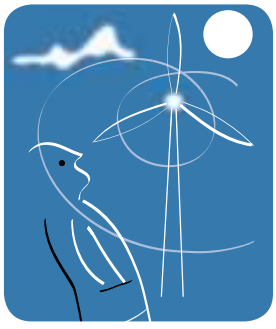
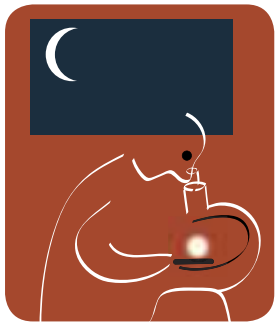
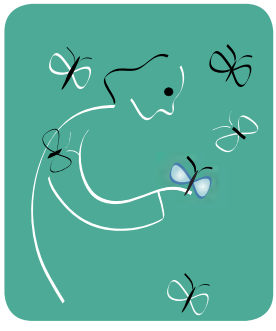
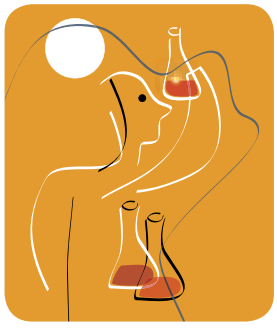
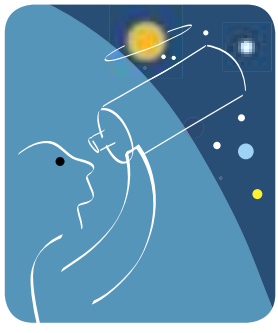
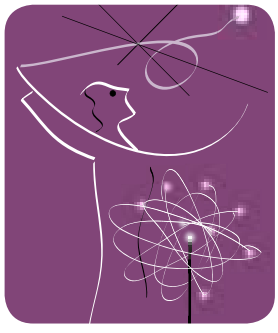

Fifty percent of all science created in Brazil is produced in the State of São Paulo. The state hosts three of the most important Latin American universities: USP, UNICAMP and UNESP. Other universities and 19 research institutes are also located in São Paulo, among them the renowned Instituto Tecnológico de Aeronáutica (ITA), Instituto Nacional de Pesquisas Espaciais (INPE) and Laboratório Nacional de Luz Síncrotron, besides most of Brazilian Industrial P&D.

The São Paulo Research Foundation (FAPESP), one of the leading Brazilian agencies dedicated to the support of research, has ongoing programs and support mechanisms to bring researchers from abroad to excellence centers in São Paulo.

The **Young Investigators Awards** is part of FAPESP's strategy to strengthen the State research institutions, favoring the creation of new research groups. See more about it at **www.fapesp.br/en/yia**

FAPESP **Post-Doctoral Scholarship** is aimed at distinguished researchers with a recent doctorate degree and a successful research track record. The fellowship enables the development of research within higher education and research institutions in São Paulo. Postdoc fellowships are available when calls for applications are issued internationally, or as individual scholarships requested on demand.

In the first case, positions are advertised at **www.fapesp.br/oportunidades** and candidates are selected through international competition. In the second, the proposal must represent an addition to a pre-existent research group and should be developed in association with faculty in higher education and research institutions in São Paulo.
More information at **www.fapesp.br/en/postdoc**

FAPESP 50 YEARS

FAPESP

www.fapesp.br/en

Postdoc Positions

The Creative Fundraiser

The Many Roles for the Postdoc in Search of Support

One of the most important skills to demonstrate in a postdoc appointment is the ability to acquire funding. Whether it is in the form of grants, fellowships, or out-right gifts, postdocs have to find ways to bring in the bucks, not only to keep their own research enterprise humming, but also to show future employers that they have experience raising money. Since most postdocs don't have a wealthy, anonymous benefactor or a venture capitalist relative who can provide unlimited reserves for their investigations, it is up to the early career scientist to get creative in finding funding. More and more postdocs (and even grad students) are demonstrating their ingenuity in where and how they seek and secure the necessary research resources. **By Alaina G. Levine**

In 2011, the National Institutes of Health (NIH) awarded a total of over $316,000 in fellowships (individual awards) and traineeships (awards made to institutions who in turn select and appoint trainees) to postdocs, according to Rod Ulane, director of the Division of Science Programs at NIH and NIH research training officer. So if you are in the biological sciences, the NIH is obviously your best and only bet for financing your early-career research, right? Wrong. While over 2,200 individuals applied for the individual awards in 2011, "the success rate for individual fellowship applicants has dropped from over 40 percent 10 years ago, to about 25 percent in 2011," explains Ulane. It is clearly one of the most competitive sources of research money, and although prestigious, it is not the only game in town. Postdocs (and graduate students preparing for their postdoc appointments) can find other sources of funding (whether they are in life sciences or not), that can support research, travel, and in some cases even wages for hiring undergraduate technicians. They just have to get creative in their fundraising approaches and start thinking beyond the most obvious and popular choices.

But first and foremost, you have to start searching for opportunities and apply for them. "Postdocs need to be aggressive about finding opportunities to write grants because the deck is often stacked against them," says **Joe Bernstein,** a postdoctoral fellow at Argonne National Laboratory, who served as the 2011 outreach committee chair for the National Postdoctoral Association. Certain agencies limit postdocs from serving as the principal investigators (PIs) on grants, so you have to do an extensive amount of research to find financing solutions that meet your unique needs and goals. But by just applying you are doing yourself and your career a huge favor, he adds, as it helps to build knowledge and skills. In addition to the almighty dollar, emerging scholars should also consider sources of support that don't directly involve money, advises Bernstein. Depending on your field, you could apply for time on specific equipment, such as a telescope or a super computer. "Millions of hours in computing time is a currency" in many research areas, such as his own field of astrophysics he says. "You are showing you can formulate a proposal for a valuable resource in competition with other people who want it, and convince the allocation committee to give you an award over other proposers," he describes. This valuable ability can absolutely "influence hiring committees."

"THE LEVERAGER"

Zeb Hogan is a world-renowned expert on megafishes—six-feet long, over 200 pound aquatic monsters that inhabit bodies of fresh water, such as rivers and lakes, all over the world. The Research Assistant Professor in the Department of Natural Resources and Environmental Science at the University of Nevada, Reno, has been funded by the National Geographic Society (NGS), in one way or another, since he was a graduate student. Now, five years out of his postdoc, he is one of only 15 NGS Fellows worldwide, and has received long-term financial support to fund expeditions to and continued>

UPCOMING FEATURES

Cancer Research: Vaccine Drug Development—March 23

Bioclusters: Eastern United States—April 6

Bioclusters: Western United States—May 4

CREDIT: (PHOTO ILLUSTRATION) *SCIENCE*; IMAGES FROM ISTOCKPHOTO.COM/PHOTOCANAL25

Where will your research lead?

Postdoctoral Program

In 2010, the Pfizer Research and Development organization launched an ambitious postdoctoral training program that encompasses its Research, Biotech, and Technology Units. We recruit highly motivated Ph.D. recipients with a demonstrable track record of scientific productivity during their graduate training and a strong interest in performing an academic-style postdoc in an industrial setting. Ideal candidates express a passion for creative research that facilitates the translation of novel biological or technological advances into innovative therapies for human diseases.

Our 2012 recruitment season is underway. Postdoctoral positions are now or will soon be available in the following areas:

ANTIBODY-PROTEIN ENGINEERING
DRUG SAFETY
INFLAMMATION & REMODELING
MUSCULOSKELETAL BIOLOGY
ONCOLOGY
PHARMACEUTICAL SCIENCES
PROTEOMICS
STEM CELLS
MEDICINAL/ORGANIC/ANALYTICAL CHEMISTRY
IMMUNOLOGY & AUTOIMMUNITY
METABOLIC DISEASES
NEUROSCIENCE
PAIN
PHARMACOKINETICS, DYNAMICS AND METABOLISM
HIGH-CONTENT CELL-BASED SCREENING
STRUCTURAL BIOLOGY

The Pfizer Research and Development organization strives to deliver innovative medicines that improve the lives of patients worldwide. Our postdoctoral program is designed to provide the research foundation that will lead to future improvements in disease therapy, while at the same time offering our trainees an exceptional career-building experience in the biomedical sciences. Our trainees perform cutting-edge research leading to publications in top-tier journals, attend high-profile scientific meetings, and interact with well-known academic labs worldwide.

You may explore and apply for specific opportunities by visiting us online at: www.pfizercareers.com.

We are proud to be an equal opportunity employer and welcome applications from people with different experiences, backgrounds and ethnic origins.

Pfizer Working together for a healthier world™

Postdoc Positions

research in endangered waterways that affect the dwindling populations of megafishes, in areas such as southeast Asia and Australia.

Hogan, 37, has received a total of five grants from the NGS, the first of which funded his graduate school research, as well as a handful of other grants from sources as varied as the Columbus Zoo and Aquarium to the International Finance Corporation (IFC). He uncovered two major tips for financing his endeavors. One is that certain grants he received while a graduate student could be extended into his postdoc appointment. While pursuing his doctoral studies at University of California, Davis, he served on a team of investigators who authored a grant proposal to the IFC to study the ecology and conservation of *Hucho taimen* (also known as Siberian salmon) in the Eg-Uur River Basin, Mongolia. The team consisted of his thesis advisor (who served on the project advisory board) as well as a professor at the University of Wisconsin, who later became his postdoc mentor. "When we wrote the proposal, two of us were grad students (myself included), one was a postdoc, one was faculty, and one was a university researcher," he explains. "Between the time that we wrote the proposal and completed the studies associated with the five-year grant, I had gone from being a grad student, to postdoc, and then finally to research faculty. In other words, the funding extended through the end of my time in grad school at UC Davis, throughout my postdoc at the University of Wisconsin, and into my first few years at the University of Nevada."

The other tactic Hogan found for successfully obtaining research funding: leveraging prior grants to obtain new ones. As a graduate student, he received support from NGS, which he was able to use as a springboard to acquire postdoc support through the NGS Conservation Trust. This grant in turn led to others, as well as special NGS honors, such as being named an NGS Young Explorer, and more recently an NGS Fellow. "Although grants from National Geographic typically only last one year, they have continued to fund my research as it has evolved," he says. "First with a smaller grant to study Mekong giant catfish, then with a larger grant to study all Mekong giants, and then finally with a multi-year grant to initiate the Megafishes Project. So, certainly, the connections and contacts that students make in grad school can extend into a postdoc and beyond."

Leveraging goes well beyond taking one grant and transforming it into another. It can also mean using your network to illuminate new or lesser-known opportunities. In particular, your PI or other research mentors can open doors to different financing solutions. "Sometimes, private foundations in particular are not used to seeing postdocs apply for grants," says **Rachel Ruhlen,** an assistant research professor at the A.T. Still Research Institute and adjunct assistant professor in the Department of Microbiology and Immunology at A.T. Still University in Kirksville, Missouri. In such a case, "you have to put together a strong team" of collaborators and mentors who will serve on the project, and having those compatriots on your side can help you land the grant, she says. Furthermore, your research partners may have access to grant information that is not well-publicized. In Ruhlen's case, she learned of a fellowship opportunity with Susan G. Komen for the Cure because her mentor served on the review panel for the foundation.

> "Sometimes, private foundations in particular are not used to seeing postdocs apply for grants... [postdocs] have to put together a strong team [of collaborators and mentors who will serve on the project]."
>
> —Rachel Ruhlen

Joe Bernstein

"THE INTERNAL FUNDRAISER"

Internal funding can mean different things to different people. It can encompass financial support from various departments within an institute, such as a home department, the vice president of research, and even the technology transfer office. It can include small grants for early-career researchers, travel support, and even publications costs.

"Don't underestimate the importance of internal funding," says Ruhlen. The 37-year-old researcher, who holds a Ph.D. in biological sciences from the University of Missouri–Columbia, completed two postdocs: one in the Department of Surgery at University of Missouri–Columbia, and the other in the Department of Pharmacy, Medicinal Chemistry, and Pharmacognosy at University of Illinois–Chicago. She started early in her quest for cash to cover her investigations. Although she was funded under two fellowships, she still needed to bring in extra support to pay for things not allowed under the fellowship, such as laboratory provisions. Internal funding filled this chasm. "I have been almost continuously on internal funding in one form or another," she says. "It rarely pays any salary dollars, but it does pay for supplies, and sometimes it will pay wages for an undergrad research assistant. It's usually a very small amount of money, less than $10,000, and only for one year. But it's a lot easier to get than external funding."

The funds may be formally distributed through request for proposals (RFPs), or informally, just by making inquiries. The latter is how Ruhlen got out of a jam in one of her postdocs. "My postdoc adviser announced he was moving to North Dakota. I couldn't uproot my family to go with him, not for a postdoc position. I had a postdoc fellowship but it only paid my salary," she says. "Where was I to get funds to do my research? I went to my department and explained the situation to them. They asked me to write up my project as if it was a grant application, and they gave me $10,000 to finish the experiments. That was enough to tide me over until I could get a real job."

Bernstein has also applied for internal grants within Argonne, through the Laboratory Directed Research and Development (LDRD) program. In this case, the discretionary money is used "to seed fund early-stage projects with a good probability of a return on investment for the Department of Energy," he explains. Projects are usually supported for up to three years.

"THE TARGETED CAMPAIGNER"

Denise Al Alam, a postdoctoral fellow at The Saban Research Institute of Children's Hospital Los Angeles, continued>

CREDITS: (FROM LEFT) PHOTO BY ART SMITH PHOTOGRAPHY; COURTESY OF ARGONNE NATIONAL LABORATORY

Postdoc Positions

discovered early on that she could apply for fellowships and grants through small, regional foundations and/or those that are focused in on very specific diseases. Originally from Lebanon, she moved to France in 2003 where she enrolled in graduate school. Shortly before earning her doctorate in immunology from the University of Reims Champagne–Ardenne, she was recruited to The Saban Research Institute to serve as a postdoctoral fellow on lung development and repair. The fellowship was funded by the American Lung Association (ALA). She later received another fellowship from the American Heart Association (AHA). "After I got to the States, I knew I would only have funding for one year," she describes. She couldn't apply for NIH or other U.S. federal government grants because of her specialized visa, so she sought out the private foundations for support.

After being awarded the fellowships from the ALA and AHA, she immediately got involved in their local chapters in Los Angeles, California. "I would go to board meetings and tell them about my research," she recalls. She also participated in public fundraising events, such as the "Fight for Air Walk" for the ALA, for which she recruited a team of people to raise money and partake in a 5 km walk to benefit the association. Al Alam recognized that by volunteering to assist with these philanthropic efforts, she not only was helping the society, but she was also promoting her research. By giving speeches to boards of directors, she was able to popularize her investigations to people of influence and high net worth. "Being in contact with these people is an advantage," she comments, because it can lead to new funding opportunities and access to hidden sources for research support. "Postdocs are very isolated. We rarely connect with people outside the lab, but I recommend we do," she continues. "Offer to help with fundraising or give a talk…It can benefit everybody—you, your team, the organization, the funding agencies," and of course, the research field itself. "We need for people to understand why we are doing this research and what it's all about."

"Offer to help with fundraising or give a talk…It can benefit everybody—you, your team, the organization, the funding agencies. We need for people to understand why we are doing this research and what it's all about."
—Denise Al Alam

Ruhlen, who received a postdoc fellowship from the Susan G. Komen for the Cure foundation, agrees that there is significant merit in volunteering to assist local chapters with fundraising efforts. "It's a fantastic idea," she says. "It will also increase your network of contacts and that's super important."

But Al Alam has not limited herself to only seeking funding from science-focused sources. As a former French resident, she can apply for grants through the French Consulate in the United States that would support collaborative research endeavors with other French scholars. For investigators who are not native to the country in which they are conducting their research, their embassy or consulate can offer surprising opportunities, she notes. "I'm Lebanese, and I'm even finding opportunities through the Lebanese government," she says, although in this case, she would have to conduct the experiments in Lebanon, which is not currently an option for her. But she has also explored funding opportunities with the Association of University Women and other groups that do not require United States citizenship of their grantees.

"THE NETWORKER"

Of all the roles a postdoc must play in order to advance as a scientist and a fundraiser, perhaps the most important is being an expert networker. Sources stress that making connections with colleagues in and out of their immediate research group, maintaining those contacts, and always striving for more associations is the key to securing financial backing of their projects. "At the end of the day it basically comes down to using contacts, collaborators, online resources, requests for proposals, advertisements, and networks to find any source of available funding," says Hogan. "While I can think of a lot of examples of postdocs funding their work (and especially grad students writing grants to then fund their postdocs), I don't see any holy grail. Stay active, keep an eye out for opportunities, and take advantage of them when they arise."

Alaina G. Levine is a science writer based in Tucson, Arizona, USA.

DOI: 10.1126/science.opms.r1200115

Featured Partictipants and Additional Resources

Featured Participants

A.T. Still Research Institute
www.atsu.edu/research

Argonne National Laboratory
www.anl.gov

National Institutes of Health
www.nih.gov

The Saban Research Institute of Children's Hospital
www.chla.org/saban

University of Nevada
www.unr.edu

Additional Resources

American Heart Association
www.heart.org

American Lung Association
www.lungusa.org

Association of University Women
www.aauw.org

Columbus Zoo and Aquarium
www.colszoo.org

French Consulate
www.consulfrance-washington.org

International Finance Corporation
www.ifc.org

National Geographic Society
www.nationalgeographic.com

Susan G. Komen for the Cure
ww5.komen.org

University of Michigan
Medical School

POSTDOCTORAL
TRAINING OPPORTUNITIES
www.med.umich.edu/postdoc

The University of Michigan Medical School is an outstanding training environment that combines world-class faculty and innovative programs of research with a rich academic tradition. For two decades Michigan has ranked among the top 10 medical schools in NIH research funding. This research effort is enhanced by 27 NIH-sponsored training programs that support Postdoctoral Scholars.

The University of Michigan recognizes the essential contributions Postdoctoral Scholars make to the University's research mission. We offer a comprehensive career development program for our Postdoctoral Scholars to help guide their choices as they prepare themselves for independent careers. We welcome inquiries from graduate students nearing completion of the Ph.D. degree regarding opportunities for postdoctoral training in the following areas:

- Alcoholism Research
- Biology of Aging
- Biology of Drug Abuse
- Cancer Biology
- Cardiovascular Research
- Cell and Molecular Dermatology
- Clinical and Basic Neuroscience
- Endocrine Dysfunction
- Endocrinology and Metabolism
- Environmental Toxicology
- Experimental Immunology
- Genome Sciences
- Hearing, Balance and Chemical Senses
- Imaging Science in Biomedicine
- Lung Disease
- Lung Immunopathology
- Medical Rehabilitation Research
- Microbial Pathogenesis
- Molecular Hematology
- Nephrology Research
- Organogenesis
- Reproductive Sciences
- Research in Gastroenterology
- Substance Abuse
- Tissue Engineering and Regeneration
- Urology Research
- Vision Research

One way to explore these programs is to attend the *Postdoc Preview* on U-M's campus on October 25-27, 2012. The *Preview* weekend will introduce outstanding upper-level graduate students in the biomedical sciences to the breadth and excitement of postdoctoral research and training at Michigan.

Apply online by August 1, 2012 at
www.med.umich.edu/postdoc/preview

The University of Michigan is an equal opportunity, affirmative action employer.

Bioinformatics and Systems Biology Core Facility Director

Systems Biology Center
Division of Intramural Research (DIR)
National Heart, Lung and Blood Institute (NHLBI)
National Institutes of Health (NIH)
Department of Health and Human Services (HHS)

We seek a Staff Scientist with expertise in **Bioinformatics and Computational Biology** to direct a newly created Bioinformatics and Systems Biology (BSB) Core Facility to serve the needs of intramural scientists in the National Heart, Lung, and Blood Institute, Bethesda, MD USA. The successful applicant will interact with scientists to optimize the design and interpretation of basic and clinical research experiments using state-of-the-art DNA-sequencing, mass spectrometry, and other techniques. He/she will supervise staff in the core, provide high level data analysis, foster interactions among scientists in NHLBI, and develop new computational solutions to specialized bioinformatics problems. State-of-the-art IT infrastructure will be provided.

The BSB Core Facility is part of an NHLBI DIR initiative in systems biology. While the core is oriented towards providing service and conducting collaborative research, the Director can devote up to 20% of his/her time to innovative and independent research in integrative computational biology. The overall mission of the DIR is to improve health through basic and clinical research, research training, and translation of discoveries to new tools to be applied directly to the field of medicine.

We seek an experienced scientist (Ph.D., M.D., or equivalent) with significant experience in large-scale data analysis, data integration, data mining, optimization techniques, algorithm design and development, and data visualization, as evidenced by citable publications. Experience with deep sequencing data and protein mass spectrometry data is highly desirable, and excellent interpersonal skills are required. Salary will be commensurate with qualifications and experience. More detailed information about the NHLBI Division of Intramural Research may be found at: **dirweb.nhlbi.nih.gov**.

Applicants should submit the following: cover letter highlighting key qualifications, current curriculum vitae with complete bibliography, names and contact information of three references, a one-page summary of the applicant's philosophy of core facility operation, and a list of three publications that provide evidence of relevant skills along with corresponding PDF copies of these publications.

The advertisement will remain open until the position is filled. PDF versions of documents sent by electronic mail are strongly preferred. Materials should be sent to Dr. Keji Zhao c/o: Katherine O'Brien, Administrative Officer, NHLBI, by email: **obrienk@nhlbi.nih.gov.**

HHS and NIH are Equal Opportunity Employers

Department of Biology Visiting Assistant/ Associate/Full Professor of Marine Biology

The Department of Biology at the University of Hawai'i at Mānoa seeks part-time professors to teach courses during the fall and/or spring semesters in a new graduate course series in Marine Biology for the 2012-2013 academic year. Highly qualified established faculty or sabbatical candidates with excellent communication skills are sought to teach lecture and lab content that includes a comprehensive survey of marine organisms, ocean and reef environments, ecological processes and current impacts on marine systems. The successful candidate(s) will work with existing Biology faculty to develop and implement these new graduate courses which are under development. Applicants must have a current faculty appointment in the life sciences with return rights to another institution, research experience in biological oceanography or marine biology and excellent teaching skills at the graduate level.

To apply, please send a single PDF document to **mblecsch@hawaii.edu** referencing position **no. 84182T**, that includes: a cover letter indicating your teaching experience, research interests and how you satisfy the minimum and desirable qualifications; a detailed curriculum vitae; three representative publications; and the names and contact information (including email address) for three professional references. Direct inquiries to **Dr. Tim Tricas (tricas@hawaii.edu)**.

POSTDOCTORAL OPPORTUNITIES

CIFAR's Junior Fellow Academy

The **Junior Fellow Academy** is an elite fellowship program for gifted early career scholars within the first three years of obtaining their Ph.D.

Junior Fellows join one of CIFAR's innovative interdisciplinary programs for two years, where they are mentored by and interact closely with some of the best researchers in Canada and around the world. Through the Junior Fellow Academy, they also become part of a community of peers, interacting regularly with Junior Fellows from all twelve programs. These experiences offer unique opportunities to build research and leadership capacity, as Junior Fellows are encouraged to think broadly and imaginatively across disciplines. The impact on a developing career path can be profound.

CIFAR Junior Fellowships are held in conjunction with a university appointment. Most Junior Fellows work as postdoctoral fellows supervised by at least one CIFAR program member. Candidates in the social sciences and humanities may hold a junior faculty position.

For more information on Fellowship eligibility, value and how to apply, please visit our website: **www.cifar.ca/JFA**.

Department of Biology Temporary Assistant Professor of Marine Biology

The Department of Biology at the University of Hawai'i at Mānoa seeks temporary part-time faculty to teach courses during the fall and/or spring semesters in a new graduate course series in Marine Biology for the 2012-2013 academic year. Highly qualified established faculty, sabbatical candidates or postdoctoral scientists are sought to teach lecture and lab content that includes a comprehensive survey of marine organisms, ocean and reef environments, ecological processes and current impacts on marine systems. The successful candidate(s) will work with existing Biology faculty to develop and implement these new graduate courses which are under development. Applicants must have a Ph.D. in biology with research experience in marine biological sciences and excellent teaching skills at the graduate level. Desirable qualifications include a minimum of one year of postdoctoral experience and an understanding of Hawaiian marine biota. For additional details see position **no. 84043T**, pending authorization to fill. at: **http://workatuh.hawaii.edu**.

To apply, please send a single PDF document to **mblecsch@hawaii.edu** that includes: a cover letter indicating your teaching experience, research interests and how you satisfy the minimum and desirable qualifications; a detailed curriculum vitae; three representative publications; and the names and contact information (including email address) for three professional references. A hard copy of the complete application package should also be mailed to **Chair, MB Temporary Professor Search Committee, Department of Biology, Rm. 2, Dean Hall, University of Hawai'i, 2450 Campus Road, Honolulu, HI 96822**. Review of applications will begin **April 6, 2012** and continue until the position is filled.

The University of Hawai'i is an Equal Opportunity/Affirmative Action Institution and encourages applications from women and minority candidates.

MINDS THAT MATTER

Los Alamos
NATIONAL LABORATORY
EST. 1943

Los Alamos National Laboratory (LANL) is a multidisciplinary research institution engaged in strategic science on behalf of national security. LANL enhances national security by ensuring the safety and reliability of the U.S. nuclear stockpile and is a center for research in a wide range of scientific disciplines, including space exploration, geophysics, renewable energy, supercomputing, medicine, and nanotechnology.

PRINCIPAL ASSOCIATE DIRECTOR

Science, Technology and Engineering

The Principal Associate Director, Science, Technology and Engineering (PADSTE) is a senior leader at Los Alamos and reports to the Laboratory Director. The role of the PADSTE is to be a steward of the Laboratory's broad scientific and engineering capabilities and to develop and implement strategies to ensure Los Alamos' preeminence as a national security science laboratory. The responsibilities include: leading five technical directorates, collaborations with universities, and the supporting science infrastructure that includes the research library, technology transfer, educational programs, and institutional computing. PADSTE is the responsible line manager of approximately 4300 scientists, engineers, post docs and students that work to support the Laboratory's three missions—assurance of the nuclear deterrent, reducing global threats, and energy security. PADSTE is directly responsible for the basic science and energy programs at Los Alamos ($270 million in FY 11), and the Laboratory Directed Research and Development program ($133 million in FY 11). Overall, the PADSTE organizations execute a budget of approximately $1.3 billion across all laboratory programs.

Minimum Job Requirements:

PADSTE is the recognized chief science officer at the laboratory, and must have a substantial and accomplished record in scientific research, especially in science or engineering related to national security. The distinguished track record should be evidenced by publications, honors and awards. The science and engineering enterprise at Los Alamos is complex; therefore the PADSTE must have a demonstrated ability to lead and manage a large mission focused organization. The PADSTE will have a record of commitment to sound business practices, safety, quality, security, environment, health, career development of scientists and engineers and diversity. As a senior laboratory leader, PADSTE will have demonstrated experience in effective decision-making and creative problem solving, and an enthusiasm to work as a member of a high performance senior leadership team. Candidates must demonstrate the ability to interact with all levels of personnel and customers, including government sponsors and industry, using excellent interpersonal, oral and written communication skills. This position requires a Q access authorization. Applicants must have the ability to obtain a Q clearance, which usually requires U.S. citizenship.

Desired Skills:

Successful experience in program development with DOE and other Federal Agencies with a science mission. Experience with interactions at the Secretarial Level. An active Q clearance is desired.

Education:

PhD in a science or engineering discipline.

Please apply online at **http://go.usa.gov/Q7L**.
(please note web address is case sensitive)

AA/EOE

UCDAVIS

Assistant Professor in Postharvest Biology and Food Safety

Research focus on postharvest plant biology with emphasis on the influence of plant biology of produce or other plant based foods upon associated microbiota, including human pathogens, research on unexplored aspects of plant/microbiota phyllosphere interactions. Develop improved handling strategies in food availability, safety, and defense. Work with academic and industrial contacts to apply knowledge of plant-microbial interactions to optimize postharvest management strategies under different environmental conditions. Identify key phenotypic or molecular traits that could improve handling strategies and food safety. Conduct mission oriented research and outreach of relevance to the California Agricultural Experiment Station; expected to operate well in multi-disciplinary teams focused on the development of practical solutions to critical issues related to food safety and postharvest handling of specialty crops grown in California and across the world, expected to contribute to teaching of core courses in the Plant Sciences undergraduate curriculum and to develop new courses in their area of expertise; teach at the graduate level within her/his area of research expertise. Advise and mentor undergraduate and graduate students, participate in departmental, college, and campus committees and interact with state, regional and national organizations as appropriate.

QUALIFICATIONS: Ph.D. or equivalent level of experience in plant physiology, plant biology, postharvest biology, plant microbial interactions or related fields.
SALARY: Commensurate with qualifications and experience.
TO APPLY: Register online at **http://recruitments.plantsciences.ucdavis.edu**. Applications accepted through **April 18, 2012**.

UC Davis is an Affirmative Action/Equal Employment Opportunity Employer and is dedicated to recruiting a diverse faculty community. We welcome all qualified applicants to apply, including women, minorities, veterans, and individuals with disabilities.

Sea Grant Maryland

Maryland Sea Grant College Program Director

The University of Maryland Center for Environmental Science and its partner institutions are seeking a dynamic and visionary director to build on Maryland Sea Grant's (MDSG) tradition of excellence to lead the organization into the future. MDSG is one of 30 regional programs, funded in part by the National Oceanic and Atmospheric Administration, that work in support of environmental stewardship and the long-term economic development and responsible use of America's coastal resources. The Director will be responsible for: (1) promoting and supporting rigorous and creative research on the Chesapeake Bay and the region's coastal marine environment, (2) synthesizing and communicating the implications of this research to stakeholders and communities that rely on these environments, (3) supporting extension education, (4) coordinating MDSG's activities with the National Sea Grant program and other regional partners and (5) directing an office of 12 staff, based in College Park, MD.

The ideal candidate will have a research background and experience of administration. Clear communication and leadership skills are essential. An earned PhD or equivalent professional qualification is preferred. The successful candidate may be eligible for a faculty appointment within the University System of Maryland. To apply, please send a curriculum vitae and a statement that provides a personal vision of Sea Grant's role in integrating research, outreach and extension education for Maryland and the region. Please include the names and contact information for three potential references. Applications should be sent to **director@cbl.umces.edu** by **April 20, 2012** to receive full consideration.

The University of Maryland Center for Environmental Science offers a competitive salary and benefits package, dependent on qualifications. UMCES is an Affirmative Action/Equal Opportunity Employer. We promote excellence through diversity and encourage women and minorities to apply.

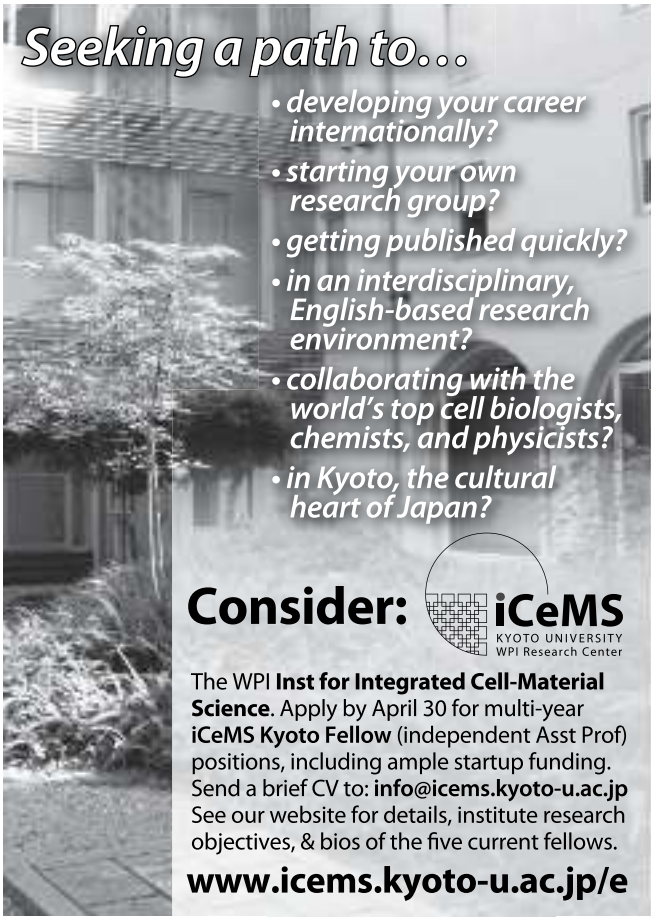

THE UNIVERSITY OF HONG KONG

Founded in 1911, The University of Hong Kong is committed to the highest international standards of excellence in teaching and research, and has been at the international forefront of academic scholarship for many years. The University has a comprehensive range of study programmes and research disciplines spread across 10 faculties and about 100 sub-divisions of studies and learning. There are over 23,400 undergraduate and postgraduate students coming from 50 countries, and more than 1,200 members of academic and academic-related staff.

Tenure-Track Assistant Professor in the Department of Chemistry (Ref.: 201200165)

Applications are invited for tenure-track appointment as Assistant Professor in the Department of Chemistry, from July 1, 2012 or as soon as possible thereafter. The post will initially be made on a three-year term with the possibility of renewal upon mutual agreement. Appointment with tenure will be considered during the second three-year contract.

Applicants should possess a Ph.D. degree in Chemistry with research interests in Materials, Energy and Environment. The appointee is expected to develop a vigorous and independent research program and excel in both undergraduate and postgraduate teaching. A suitable start-up fund for research will be provided. Information about the Department can be obtained at http://chem.hku.hk/.

A globally competitive remuneration package commensurate with the appointee's qualifications and experience will be offered. At current rates, salaries tax does not exceed 15% of gross income. The appointment will attract a contract-end gratuity and University contribution to a retirement benefits scheme, totalling up to 15% of basic salary, as well as leave, and medical benefits. Housing benefits will be provided as applicable.

Applicants should send a completed application form, together with a C.V., three letters of recommendation, a research proposal, and a teaching statement by e-mail to chemcir@hku.hk. Please indicate clearly "Ref.: 201200165" in the subject of the email. Application forms (341/1111) can be obtained at http://www.hku.hk/apptunit/form-ext.doc. Further particulars can be obtained at http://jobs.hku.hk/. **Closes April 30, 2012**.

The University thanks applicants for their interest, but advises that only shortlisted applicants will be notified of the application result.

The University is an equal opportunity employer and is committed to a No-Smoking Policy

Building on our excellence. Investing in our future.

Would you like to work at a University where great minds thrive?

FACULTY OF BIOLOGICAL SCIENCES CHAIR VACANCIES

The Faculty of Biological Sciences is one of the leading groups of life-science researchers within the UK, offering superb facilities, providing a high quality research training environment and delivering an exceptional student education. Significant investments in our infrastructure contribute to the dynamic and vibrant research environment that offers excellent opportunities for leading edge research across the breadth of Biological Sciences as well as superb cross Faculty interactions across a spectrum of disciplines. With around 2000 undergraduate students, 150 taught post graduate students and 200 research post graduate students we take pride in our teaching and we are committed to providing students with the very best student experience through research-led teaching and excellent academic support.

We wish to enhance the Faculty's academic leadership and promote growth through the appointment of four new Chairs. Applicants for these Chairs will be leading authorities in the relevant field with a strong track record in journal publications and research funding. You will have experience of winning research grants from a variety of sources and leading research teams. You will need to demonstrate the potential to develop large multi-disciplinary funded collaborations and take on leadership roles both within the Faculty and in the wider University context. With the ability to inspire students and colleagues alike, you will have a track record of integrating research with learning and teaching. All of these skills and attributes combined will enable you to deliver an excellent student experience.

Professor in Biomolecular Nuclear Magnetic Resonance (NMR)

Institute of Molecular and Cellular Biology **Reference: FBSMC0039**

The Institute of Molecular and Cellular Biology has research groups covering all the major techniques of structural biology, with highly effective links to the Schools of Chemistry and Physics and the Faculty of Medicine, under the umbrella of the Astbury Centre for Structural Molecular Biology. We seek to appoint a research leader in the field of biomolecular NMR, who will develop and sustain a research programme of international excellence in biomolecular NMR methods and their application to important questions in biology. We offer excellent facilities for NMR spectroscopy, incorporating recently upgraded 500MHz, 600MHz and 750MHz machines, contributing to an ideal environment for high profile collaborative and multi-disciplinary research.

Professor in Neuroscience

Institute of Membranes and Systems Biology **Reference: FBSMS0023**

The Institute of Membranes and Systems Biology hosts a strong group of neuroscientists covering a broad spectrum of research topics and approaches ranging from single molecule neuroscience to in vivo behavioural studies. We are a group with established strong international links with support from industry. Neuroscience research at Leeds principally consists of systems neurophysiology, ion channels, neuronal networks and neurodegeneration. From this well equipped and inspiring environment we will expect you to deliver internationally leading research and inspirational teaching.

Professor of Membrane Biology

Institute of Membranes and Systems Biology **Reference: FBSMS0024**

The Membrane Biology Research Group at Leeds plays a leading role in a wide range of research activities on membrane proteins in Europe and internationally. State-of-the-art facilities in X-ray crystallography, electron microscopy, AFM, NMR, electrophysiology, cell imaging, etc are available. In addition to international collaborations there are extensive translational research initiatives with clinicians, chemists, and physicists through our Astbury Centre for Structural Molecular Biology, and our Multidisciplinary Cardiovascular Research Centre. We seek to appoint a research leader in the field of membrane biology who will develop and sustain this internationally recognised area of our research and deliver Inspirational teaching.

Professor of Sports & Exercise Science

Institute of Membranes and Systems Biology **Reference: FBSMS0022**

We are seeking a dynamic and influential Chair in Sports and Exercise Science that will help us achieve our ambition to be one of the top five University departments in our field. Our Sports and Exercise Science research spans from molecular, cellular and computational studies of the cardiovascular system to studies of the impact of physical activity on human physiological and motor function, in health and disease. A major infrastructure development has just been completed, providing purpose built laboratory space for cardiovascular research in a prime site within the Faculty.

For further information and to apply, please visit **www.universityofleedschairs.co.uk**

POSITIVE ABOUT DISABLED PEOPLE Working for equal opportunities

UNIVERSITY OF LEEDS

REGIONAL CENTRE FOR BIOTECHNOLOGY
an institution of education, training & research

Adv.3/12

Career Opportunities in Technology Platforms in Interdisciplinary Biomedical Research

Regional Centre for Biotechnology (RCB) is an institution of education, training and research established by the Govt. of India under the auspices of UNESCO and is part of the Biotech Science Cluster (BSC) being developed by the Department of Biotechnology, Government of India, on a 200-acre site located within the NCR in Faridabad. The Centre is intended to foster innovative conceptual research and education in a wide range of biotech-related sciences.

RCB is looking for dynamic, result-oriented and dedicated aspirants to lead technology platforms in biomedical research. The candidates should have Ph.D. in any branch of Natural Sciences, Medicine or Engineering with original published work of high quality and active patents and at least 12 years of experience in interdisciplinary biomedical research using technology platforms in the fields such as proteomics/genomics, microarray, macromolecular structure characterization, high resolution microscopy, protein production, hybridoma technology etc. at Universities/Institutions/Industrial Research Laboratories including experience of guiding research at doctoral level.

It is desirable that the candidates have experience of establishing and managing relevant technology platforms for innovative research in interdisciplinary biomedical areas. A description of the RCB and its mandates and projections can be found on the website: **http://www.rcb.res.in**

The appointments will be made at senior scientific positions at different levels depending on the quantum of experience and the quality of professional achievements. Interested individuals are invited to send their curriculum vitae containing relevant details, list of publications and the names of three potential referees along with their electronic mail addressed to the Executive Director, **Regional Centre for Biotechnology, 180, Udyog Vihar, Phase-I, Gurgaon- 122016, India**. An advance electronic copy of the Curriculum Vitae may be sent to the e-mail address: **office@rcb.res.in**. The short-listed candidates will only be contacted for further discussions.

Tenure Track Position in Nutrition and Food Science The University of Missouri

The University of Missouri invites applications for a tenure track faculty position in the area of nutritional sciences and food sciences for an appointment 75% in the Department of Nutrition and Exercise Physiology and 25% in the Department of Food Science. The successful applicant will have a PhD in Nutrition or closely related discipline with postdoctoral research experience. At the assistant professor level, strong promise of obtaining and sustaining a nationally funded research program is expected. For more senior levels, an established track record of external funding is expected. The NEP department is part of three colleges, College of Human Environmental Sciences, College of Agriculture Food and Natural Resources (CAFNR), and the School of Medicine. The tenure home for this position will be in CAFNR. In the Fall of 2013 a newly renovated building will open including the MU Nutritional Center for Health (MUNCH) consisting of a research metabolic kitchen, a state of the art teaching kitchen and observational behavior lab. In addition new wet lab facilities and human research facilities will be included. MUNCH will be located near the MU Child Development Lab and researchers with an interest in obesity or childhood obesity are especially encouraged to apply. In addition excellent facilities are available in the Department of Food Science including a well-equipped sensory lab and wet labs. The successful applicant will have a research program that will utilize these facilities. It is expected the faculty will contribute to undergraduate and graduate education in the department. This search is associated with the Food for the 21st Century Nutrition for Health Group, an interdisciplinary team of researchers built on a strong tradition of interaction between physical, biological and agricultural sciences on this campus. Information about the departments can be found at the departmental links (**http://ns.missouri.edu** and **http://foodscience.missouri.edu**). Review of applications will begin immediately and will continue until the position is filled.

Successful candidates will be provided with excellent laboratory space, start-up funds, an annual operating budget of $75,000 per year for a minimum of five years and a salary commensurate with experience. Located midway between St. Louis and Kansas City, Columbia is a vibrant university town that is consistently ranked among the top small cities to live in America. To apply for this position (job posting reference **#7062**), please visit the MU website at **http://hrs.missouri.edu/find-a-job/academic/**. Please submit curriculum vitae, a narrative of research and educational interests, and the names and contact information of three references. For additional information about the position, please contact: **Deb Garrett, Business Manager, Department of Nutrition and Exercise Physiology** at **Garrettd@missouri.edu** or **573-884-1387**.

ETH

Eidgenössische Technische Hochschule Zürich
Swiss Federal Institute of Technology Zurich

Professor of Human-Environment Systems

The Department of Environmental Systems Science at ETH Zurich (www.usys.ethz.ch) invites applications for an Associate/Full Professorship in Human-Environment Systems. The Department's strategic themes include ecosystem services, resource scarcity, climate change, food security, health and environment.

The candidate should have proven expertise in analysing human-environment interactions on the global, regional and / or local scale, including human decision making. A strong quantitative focus is required, e.g. through the application of integrated modelling combining Natural and Social Sciences. A transdisciplinary approach to research (i.e. involving science-stakeholder discourse) is a plus. Candidates with outstanding scientific track records in related fields will be considered, but preference will be given to candidates with a background in Social Sciences or a multi-disciplinary background. The candidate is expected to establish a recognised research group and to integrate into research activities in related fields at ETH Zurich and within the Department. The Professorship forms part of the inter-departmental Institute for Environmental Decisions and is co-responsible for the focus Human-Environment Systems within the Master and Bachelor programme in Environmental Sciences. The new Professor will be expected to teach undergraduate level courses (German or English) and graduate level courses (English).

Please apply online at **www.facultyaffairs.ethz.ch.** Your application should include your curriculum vitae and a list of refereed publications. The letter of application should be addressed **to the President of ETH Zurich, Prof. Dr. Ralph Eichler. The closing date for applications is 15 May 2012.** ETH Zurich is an equal opportunity and affirmative action employer. In order to increase the number of women in leading academic positions, we specifically encourage women to apply. ETH Zurich is further responsive to the needs of dual career couples and qualifies as a family friendly employer.

INDIANA UNIVERSITY
BLOOMINGTON

The **School of Health, Physical Education, and Recreation (HPER)** is in the midst of transition into Indiana University School of Public Health – Bloomington. The school invites applications for **Professor and Chair** of the Department of Environmental Health.

The Chair will be instrumental in leading the department in the continuing development of research, teaching, and service activities in the department's professional disciplines. An established record in funded scientific research is essential along with the capacity to mentor junior faculty regarding tenure and promotion. The Chair is expected to secure financial resources to meet program objectives; and facilitate interaction among faculty, staff, students, and alumni. As the department continues to develop, the chair will be instrumental in recruiting and hiring additional faculty. The successful candidate will work closely with the Dean to further the School's goals and research mission.

Candidates for the position must hold a Ph.D. in Environmental Epidemiology, or Environmental Policy, or Environmental Health from an accredited school of public health or related educational institution, have several years of funded research in their discipline, a record of demonstrated scholarly achievement, an ability to collaborate across disciplines, significant administrative experience, and national/international professional engagement sufficient to warrant tenured Full Professor rank.

Salary is competitive depending upon qualifications and experience. This is a tenured 12-month academic appointment with an anticipated state date of July 1, 2012. Review of applications will begin **March 31, 2012** and continue until position is filled. Visit the department website for details on applying **http://www.envh.indiana.edu/positions.shtml**.

Indiana University is an Equal Employment Affirmative Action Employer committed to excellence through diversity.

TEXAS TECH UNIVERSITY
HEALTH SCIENCES CENTER
Paul L. Foster School of Medicine

The Center of Excellence in Infectious Disease Research at the Paul L. Foster School of Medicine, Texas Tech University Health Sciences Center, El Paso, Texas is seeking highly qualified candidates for tenure track faculty positions at the Assistant or Associate Professor level. The Center is primarily interested in investigators with research interests in infectious diseases and immunology. The position reports to the Co-Directors of the Center of Excellence for Infectious Diseases.

Minimum Qualifications:
- M.D. or Ph.D. Degree in a field related to infectious diseases or immunology,
- 3 years of postdoctoral experience, strong publication record

Experience in emerging infectious diseases and in the use of latest technologies is highly preferred. Investigators with funded grant support are particularly encouraged to apply and will be considered for the rank of Associate Professor. The selected candidate should have an interest in assisting with the development of a new Graduate School of Biomedical Sciences, a willingness to start something new and to help a new institution to grow and develop. Good communication skills and demonstrated ability to work in a collegial environment are essential.

A competitive salary, start-up package and comprehensive benefits are available. Interested candidates must apply online at **http://jobs.texastech.edu/postings/44170**; Requisition **#85288**. For further information, potential applicants may send inquiries to: **Manjunath Swamy, M.D.**, **manjunath.swamy@ttuhsc.edu** or **Premlata Shankar, M.D.**, **premlata.shankar@ttuhsc.edu**, Co-directors of the Center of Excellence for Infectious Diseases.

Texas Tech University Health Sciences Center is an Equal Opportunity/ Affirmative Action Employer.

Get a Career Plan that Works.

An exceptional career requires insightful planning and management. That's where *Science* Careers comes in. From job search to career enhancement, *Science* Careers has the tools and resources to help you achieve your goals. Get yourself on the right track today and get a real career plan that works. Visit **ScienceCareers.org**.

Science Careers

From the journal *Science* AAAS

ScienceCareers.org

Joe W. Grisham Distinguished Professorship

The Department of Pathology and Laboratory Medicine in the School of Medicine at The University of North Carolina at Chapel Hill has established a Professorship named to honor renowned physician scientist and Chair, Joe W. Grisham, MD. The Department now seeks to fill this Professorship and invites applications from established investigators who resemble Dr. Grisham in professional accomplishments and academic stature. To qualify for this tenure-track faculty position at the Professor level, candidates should have an M.D. or M.D./Ph.D. degree, training and experience in the practice of pathology, and a strong track-record of national research grant support. The candidate selected is expected to have achieved national and international standing in his/her field of expertise as reflected by an impressive record of research accomplishments as demonstrated by publications in leading peer-reviewed journals and presentations at national and international meetings. Preference will be given among equal candidates to those whose research focuses on one of the areas of Dr. Grisham's interests including cancer pathobiology, carcinogenesis, environmental pathology or hepatic pathology. All highly qualified candidates will be considered although it is preferred that they pursue research that complements and enhances the Department's existing strengths. Successful applicants will be expected to establish and maintain an extramurally funded research program, and to participate in teaching medical students, graduate students and/or residents. Some continuing involvement in the clinical program of the department would be desirable; however, the extent of clinical involvement is flexible.

The Department is a leader in research in experimental pathology, and in practice and training in pathology. Faculty members have access to Departmental based core research facilities as well as campus-wide core facilities that offer a wide range of services, including cutting-edge technologies, high-end instrumentation and technical support (**http://www.med.unc.edu/corefacilities**). More information about the Department can be found on the Department web site (**http://med.unc.edu/pathology**). The Grisham Professor will have an opportunity to join one or more of the excellent interdisciplinary Centers at UNC, such as the Lineberger Comprehensive Cancer Center. Ample relocation and start-up funds, space and infrastructure support will be provided to assure that the Grisham Professor attains his or her career goals at UNC.

Interested physician scientists should complete the online application at **jobs.unc.edu/2502516**. The online application will require an application letter, curriculum vitae, summary of career goals, and names and addresses of 5 references. Inquiries about the position can be directed to **Bill Kaufmann**, Chair of the Search Committee, at **bill_kaufmann@med.unc.edu**. For additional information about the Department, visit **http://www.med.unc.edu/pathology/**.

The University of North Carolina is an Equal Employment/ADA Employer.

Duke Kunshan University

Vice Chancellor

Duke University seeks nominations and applications for the position of founding Vice Chancellor (VC) for Duke Kunshan University. Duke Kunshan University (DKU) is a partnership of Duke University, the city of Kunshan in Jiangsu Province, China, and Wuhan University to create a world-class university that will offer a range of academic programs and conferences for students from China and throughout the world. DKU's application to the Chinese Ministry of Education is currently in review. The state-of-the-art DKU campus is now under construction on a 200 acre site within a 1,700+ acre science and technology park in Kunshan. Located in close proximity to both Shanghai and Suzhou, and connected to both by high-speed rail, the city of Kunshan is a center for business and high-tech research and manufacturing that has one of the fastest growing economies in China

The position of VC is the senior academic and administrative officer responsible for planning and delivering academic programs at DKU, and representing DKU programs in China, the US, and internationally. As the VC will be the public face of DKU's academic programs, he or she must be a scholar of international stature and an experienced academic administrator who can help lead DKU to world-class status. In accordance with the structure of joint venture universities in China, the VC will report to the DKU Chancellor and work closely with the Provost and the leadership of Duke University to fulfill the mission and attain the standards expected for DKU.

Candidates for the VC position should have a track record of internationally recognized scholarship, significant academic leadership experience at the level of Dean, Vice Provost, Vice President, or above at a major American research university, and an appreciation for and experience with the international dimensions of higher education. The full position description and additional information can be found at **www.dkuemployment.com**. Nominations and applications will be held in confidence and should be submitted promptly. Applicants should submit a CV and a statement of interest. The search committee will begin reviewing applications during the latter half of March and will continue until the position is filled. Please send information electronically (Microsoft Word or Adobe Acrobat files preferred) to:
Jennifer Boroski, Project Coordinator, Office of Global Strategy and Programs, Duke University; Jennifer.boroski@duke.edu; +1-919-613-3764

Tenure-Track Research Assistant/Associate Professor

The Department of Pathology and Laboratory Medicine at the University of North Carolina at Chapel Hill invites applications for tenure-track research faculty positions at the Assistant or Associate Professor level. Candidates must have a PhD and/or MD and a record of research accomplishments as demonstrated by publications in leading peer-reviewed journals, and a well-defined research vision. We seek individuals with interests in all areas of experimental pathology but preference will be given to those whose research complements and enhances the Department's existing strengths, e.g. in cancer, thrombosis and hemostasis, cardiovascular disease, and renal glomerular disease. Successful applicants at the Assistant Professor level will be expected to establish and maintain an extramurally funded research program. Associate level applicants are expected to have extramural funding and an established national reputation as an excellent investigator. The faculty member will be a member of the Departmental PhD Graduate Program in Molecular and Cellular Pathology and will have the opportunity to join other training programs and curricula in the School.

The Department is a leader in experimental pathology and will provide an excellent environment for research accomplishments and ample start-up funds. The School of Medicine is located on the campus of The University of North Carolina at Chapel Hill, which includes the Schools of Pharmacy and Public Health, as well as the College of Arts and Sciences. The School has many outstanding interdepartmental centers that foster interdisciplinary research. Researchers have ready access to a broad range of core facilities (**http://www.med.unc.edu/corefacilities**), many based within the Department.

Interested scientists should complete the online application at **jobs.unc.edu/2502510**. The online application will require an application letter, curriculum vitae, summary of career goals, and names and addresses of 5 references. Inquiries about the position can be directed to **Joan Taylor**, Chair of the Search Committee, at **joan_m_taylor@med.unc.edu**. For additional information about the Department, visit **http://www.med.unc.edu/pathology/**.

The University of North Carolina is an Equal Employment/ADA Employer.

POSITIONS OPEN

MOLECULAR BIOLOGIST
XEUS

XEUS in Boston, Massachusetts seeks a highly motivated, talented, and team-oriented Molecular Biologist to join a multidisciplinary team of scientists and engineers working on research, upscaling, and commercialization of our cellulosic biofuels technology. Preference will be given to applicants with experience in quantitative (RT-) PCR, fluorescence in-situ hybridization, cell transformation, molecular cloning, metabolic engineering, and assay development. The successful candidate will hold a Ph.D. in Molecular Biology or Biochemistry, with at least five years of experience postgraduation, preferably including at least two years in an industrial setting. Applicants should be able to multitask and remain flexible with changing needs, and possess good interpersonal and communication skills. Send curriculum vitae to **e-mail: recruiting@xeus.info.**

SEVERAL PERMANENT PROGRAM DIRECTORS
Division of Undergraduate Education
National Science Foundation

The National Science Foundation (NSF) is seeking qualified candidates with expertise in chemistry, engineering, or geoscience for permanent positions as Program Director in the Division of Undergraduate Education (DUE). The successful candidate will be expected to provide leadership within DUE, across NSF, and in the external scientific communities. NSF Program Directors have primary responsibility for the agency's overall mission to support innovative and merit-reviewed basic research and education that contribute to the nation's scientific strength, security, and welfare. The Division of Undergraduate Education, within the Directorate for Education and Human Resources, focuses on promoting excellence in undergraduate STEM education for all students. It supports programs that: develop educational materials and effective teaching methods reflecting the latest discoveries in the field; enhance research on learning; promote scientific literacy; and encourage connections among all educational levels.

Requirements include a Ph.D. in chemistry, engineering, or geoscience, or in disciplinary STEM education or the learning sciences as well as six or more years of experience teaching at the undergraduate level. Complete information, including quality-ranking factors, duties, and application process is available in the full position announcement at **website: http://www.usajobs.gov/GetJob/ViewDetails/309872600.** Application deadline is April 3, 2012.

NSF is an Equal Opportunity Employer.

ASSISTANT PROFESSOR in Freshwater Zoology
Columbus State University
Columbus, Georgia

The Department of Biology at Columbus State University invites applications for a tenure-track, full-time Assistant Professor in Freshwater Zoology to begin in August 2012. Research interest at organismal, population or community level is desirable, as is experience curating aquatic collections and working with government funding agencies. The candidate would be expected to maintain an active research program leading to publications. Minimum qualifications include a Doctorate in the Biological Sciences with expertise in Freshwater Zoology. Preferred qualifications: experience teaching and mentoring undergraduates; an active research program; taxonomic or systematic experience with one or more of the following organisms: crayfish, mussels and fish; and postdoctoral experience. Deadline for submission is March 16, 2012. For more information visit **website: http://hr.columbusstate.edu/jobs.asp.**

POSITIONS OPEN

ASSISTANT/ASSOCIATE PROFESSOR

The Institute of Molecular Cardiology at the University of Louisville is seeking qualified candidates to join the members of the Institute in work focusing on cell therapy for myocardial repair. Appointments will be at Assistant/Associate Professor level depending on qualifications. The successful candidate will have a track record of working with stem/progenitor cells in the cardiovascular system. He/she will join a productive, highly collegial, and multidisciplinary team of investigators supported by state-of-the-art facilities and considerable funds. Submit letter of application with curriculum vitae and statement of interest to: **Dr. Roberto Bolli, 550 South Jackson Street, ACB, Third Floor, Louisville, KY 40202.** *Affirmative Action/Equal Opportunity.*

TENURE-TRACK FACULTY POSITIONS
Physiology

The Department of Physiology at Wayne State University (WSU) School of Medicine invites applications for three tenure-track **ASSISTANT/ASSOCIATE PROFESSOR** positions. We seek motivated individuals with expertise in the areas of molecular, cellular, systems, translational physiology, and/or biophysics to strengthen and complement ongoing multidisciplinary programs in the Department (**website: http://physiology.med.wayne.edu**). Applicants with specific interest in cardiovascular research will be considered for joint appointment in the Cardiovascular Research Institute (**website: http://cvri.med.wayne.edu/index.php**).

Startup packages and salaries are highly competitive. Candidates are expected to establish active extramurally funded research programs and participate in teaching medical/graduate students. Candidates must hold Ph.D., M.D., or equivalent and apply with curriculum vitae, detailed research plan and names/contact information of three references to **e-mail: wsuphysiologyfacultysearch@med.wayne.edu.**

Review of applications will begin after April 1, 2012 and continue until positions are filled.

WSU offers 350 academic programs through 14 schools and colleges to over 31,000 students in the Detroit Midtown area. WSU School of Medicine is a state-of-the-art research environment, and is rated by the Carnegie Foundation in the top one-third of all U.S. Research Institutions. WSU was also ranked in Scientist Magazine 2009 as one of the Top 40 Best Places to Work among all U.S. Academic Institutions. *WSU is an Equal Opportunity/Affirmative Action Employer.*

CAREER OPPORTUNITY—Doctor of Optometry (O.D.) degree in 27 months for Ph.D.s in science and M.D.s. Excellent career opportunities for O.D./Ph.D.s and O.D./M.D.s in research, education, industry, and clinical practice. This unique program starts in March of each year, features small classes, and 12 months devoted to clinical care.

Contact the Admissions Office, **telephone: 800-824-5526** at **the New England College of Optometry, 424 Beacon Street, Boston, MA 02115.** Additional information at **website: http://www.neco.edu, e-mail: admissions@neco.edu.**

POSTDOCTORAL OPPORTUNITIES

POSTDOCTORAL FELLOWS

The Institute of Marine and Coastal Sciences at Rutgers University is seeking Postdoctoral Fellows in the areas of biological, chemical, geological, and physical oceanography. Prospective candidates should foster creative research avenues and interactions among existing research programs and faculty expertise. These fellowships are one-year renewable appointments. Review of applications will commence on February 15, 2012—applications will continue to be accepted after that time and reviewed on an ongoing basis. To apply, please electronically send curriculum vitae, statement of research interest, and names of three references to **Dr. Richard A. Lutz** (Director, Institute of Marine and Coastal Sciences) **e-mail: postdocsearch@marine.rutgers.edu** (please include "Postdoc" in the subject line).

Rutgers is an Equal Opportunity/Affirmative Action Employer.

POSTDOCTORAL RESEARCH FELLOW

A full-time Postdoctoral Research Fellow position is anticipated in the laboratory of **Dr. Zongbing You** in the Department of Structural & Cellular Biology, Tulane University, New Orleans, LA. This laboratory conducts research in IL-17's role in cancer. M.D. or Ph.D., experiences in cancer biology, molecular and cellular biology, and animal handling are required. The position is currently funded by NIH. Annual salary is estimated as $35,721.00 based on the local prevailing wage level and may be commensurate with experience. Applicants should send curriculum vitae to **e-mail: zyou@tulane.edu.** *Equal Opportunity/Affirmative Employer.*

HOWARD HUGHES MEDICAL INSTITUTE | JANELIA FARM RESEARCH CAMPUS

DISCOVERY AND KNOWLEDGE

Cutting-edge debate and discussion: Janelia Conferences Fall 2012

SEPTEMBER 16–19, 2012*
BioImage Informatics
[*Co-sponsored by the Max Planck Institute and held in Dresden, Germany]
Fuhui Long, Janelia Farm, HHMI
Ivo Sbalzarini, ETH Zurich
Pavel Tomancak, Max Planck Institute
Michael Unser, EPFL

SEPTEMBER 30–OCTOBER 3, 2012
Behavioral Neurogenetics of *Drosophila* Larva
Jim Truman, Janelia Farm/HHMI
Marta Zlatic, Janelia Farm/HHMI

OCTOBER 7–10, 2012
Molecular Mechanisms of Axon Degeneration
Robert Burgess, The Jackson Laboratory
Marc Freeman, HHMI/University of Massachusetts Medical School
Erika Holzbaur, University of Pennsylvania

OCTOBER 21–24, 2012
Light-Based Approaches to Neural Circuit Reconstruction
Jeff Lichtman, Harvard University
Gene Myers, Janelia Farm/HHMI
Gerry Rubin, Janelia Farm/HHMI
Stephen Smith, Stanford University School of Medicine

OCTOBER 28–31, 2012
Turning Images to Knowledge: Large-Scale 3D Image Annotation, Management, and Visualization
Erik Meijering, Erasmus MC – University Medical Center Rotterdam
Gene Myers, Janelia Farm/HHMI
Hanchuan Peng, Janelia Farm/HHMI

NOVEMBER 4–7, 2012
Fluorescent Proteins and Biological Sensors
Loren Looger, Janelia Farm/HHMI
Atsushi Miyawaki, RIKEN Brain Science Institute
Ryohei Yasuda, Duke University Medical Center
Jin Zhang, Johns Hopkins University

NOVEMBER 11–14, 2012
Neuron Types in the Hippocampal Formation: Structure, Activity, and Molecular Genetics
Giorgio Ascoli, George Mason University
Thomas Klausberger, Medical University of Vienna
Massimo Scanziani, HHMI/University of California, San Diego
Peter Somogyi, Medical Research Council

Janelia conferences are small, intense, and specialized meetings intended to encourage rapid advances and to foster collaborative interactions. There are no registration fees, and HHMI funds the local costs of the meetings, including meals and accommodations for all participants. Student scholarships are available.

APPLICATION DEADLINE IS MAY 10, 2012, 2PM ET

www.janelia.org/conferences/sci

HHMI janelia farm research campus

AAAS is here – helping scientists achieve career success.

Every month, over 400,000 students and scientists visit ScienceCareers.org in search of the information, advice, and opportunities they need to take the next step in their careers.

A complete career resource, free to the public, *Science* Careers offers a suite of tools and services developed specifically for scientists. With hundreds of career development articles, a grants and scholarships database, webinars and downloadable booklets filled with practical advice, a community forum providing real-time answers to career questions, and thousands of job listings in academia, government, and industry, *Science* Careers has helped countless individuals prepare themselves for successful careers.

As a AAAS member, your dues help AAAS make this service freely available to the scientific community. If you're not a member, join us. Together we can make a difference.

To learn more, visit **aaas.org/plusyou/sciencecareers**

AAAS + U = Δ

Be the next winner!

2011 Winner
Dr. Tiago Branco
Postdoctoral
Research Fellow
University College
London

Get recognized!
US$ 25,000 Prize

Deadline for entries:
June 15, 2012

It´s easy to apply! Learn more at:
www.eppendorf.com/prize

eppendorf & Science PRIZE FOR NEUROBIOLOGY

Eppendorf & Science Prize for Neurobiology

Kurstin Roe Photography

Congratulations to Dr. Tiago Branco on winning the 2011 Eppendorf & *Science* Prize for his studies on how dendrites discriminate temporal input sequences and apply different integration rules depending on input location. The results of Dr. Branco's research provide insight on how the brain performs computations, and suggest that even single neurons can solve complex computational tasks.

You could be the 11th winner of this award.
The annual Eppendorf & *Science* Prize for Neurobiology honors young scientists for their outstanding contributions to neurobiological research based on methods of molecular and cell biology. The winner and finalists are selected by a committee of independent scientists, chaired by *Science's* Senior Editor, Dr. Peter Stern.

To be eligible, you must be 35 years of age or younger. If you're selected as this year's winner, you will receive US$ 25,000, have your work published in *Science* and be invited to visit Eppendorf in Hamburg, Germany. Past winners and finalists have come from as far a field as China, Chile, India and New Zealand.

Yes, it can happen to you. Enter your research now!

eppendorf
In touch with life

Science
AAAS

cell sciences®

cytokine center

Browse our web site of recombinant proteins, including cytokines, growth factors, chemokines and neurotrophins. Daily shipping and competitive pricing are offered. Bulk quantities of many proteins available. Cell Sciences also carries corresponding antibodies and ELISA kits.

www.cellsciences.com

LIST OF PROTEINS

4-1BBL
4-1BB Receptor
6 Ckine
ACAD8
ACAT2
gAcrp30/Adipolean
Activin A
ACY1
ADAT1
Adiponectin
ADRP
AITRL
Akt1
Alpha-Feto Protein (AFP)
Alpha-Galactosidase A
Angiopoietin-1 (Ang-1)
Angiopoietin-2 (Ang-2)
Angiostatin K1-3
Annexin-V
apo-SAA
Apoliprotein A-1
Apoliprotein E2
Apoliprotein E3
Apoliprotein E4
APRIL
Artemin
ATF2
Aurora A
Aurora B
BAFF
BAFF Receptor
BCA-1 / BLC / CXCL13
BCMA
BD-1
BD-2
BD-3
BDNF
Bivalirudin
BMP-2
BMP-4
BMP-7
BMP-13
sBMPR-1A
Brain Natriuretic Protein
BRAK
Breast Tumor Antigen
C5a
C5L2 Peptide
C-10
C-Reactive Protein
C-Src
Calbindin D-9K
Calbindin D-28K
Calbindin D-29K
Calmodulin
Calcitonin Acetate
Carbonic Anhydrase III
Carcino-embryonic Antigen
Cardiotrophin-1
Caspase-3
Caspase-6
CD4
CD14
CD22
CD40 Ligand / TRAP
CD95 / sFas Ligand
CD105 / Endoglin
CHIPS
CNTF
Collagen
CREB
CTACK/CCL27
CTGF
CTGFL/WISP-2
CTLA-4/Fc
CXCL16
Cytokeratin 8
DEP-1
Desmopressin
Disulfide Oxidoreductase
E-selectin
ECGF
EGF
Elafin/SKALP
EMAP-II
ENA-78
Endostatin
Enteropeptidase
Eotaxin
Eotaxin-2
Eotaxin-3 (TSC)
EPHB2
EPHB4
Eptifbatide
Erk-2
Erythropoietin (EPO)
Exodus-2
Fas Ligand
Fas Receptor
FGF-1 (acidic)
FGF-2 (basic)
FGF-4
FGF-5
FGF-6
FGF-7/ KGF
FGF-8
FGF-9
FGF-10
FGF-16
FGF-17
FGF-18
FGF-19
FGF-20
sFGFR-1 (IIIc) / Fc Chimera
sFGFR-2 (IIIc) / Fc Chimera
sFGFR-3 / Fc Chimera
sFGFR-4 / Fc Chimera
sFlt-1 (native)
sFlt-1 (D3)
sFlt-1 (D4)
sFlt-1 (D5)
sFlt-1 (D7)
Flt3-Ligand
sFlt-4
sFlt-4/ Fc Chimera
Follistatin
FSH
Fractalkine/ CX3C
G-CSF
α-Galactosidase A
Galectin-1
Galectin-3
Gastrointestinal CA
GCP-2
GDF-3
GDF-9
GDF-11
GDNF
GLP-1
Glucagon
Goserelin
GM-CSF
GPBB
GROα
GROβ
GROγ
GRO/MGSA
Growth Hormone
Growth Hormone BP
GST-p21/WAF-1
HB-EGF
HCC-1
HGF
Histdyl-tRNA synthetase
Histrelin
HRG1-β1
I-309
I-TAC
IFN-α
IFN-α A
IFN-α 2a
IFN-α 2b
IFN-β
IFN-γ
IFN-Omega
IGF-I
IGF-II
proIGF-II
IGFBP-1
IGFBP-2
IGFBP-3
IGFBP-4
IGFBP-4
IGFBP-5
IGFBP-6
IGFBP-7
IL-1α
IL-1β
IL-2
IL-3
IL-4
sIL-4 Receptor
IL-5
IL-6
sIL-6 Receptor
IL-7
IL-8 (72 a.a.)
IL-8 (77 a.a.)
IL-9
IL-10
IL-11
IL-12
IL-13
IL-13 analog
IL-15
IL-16 (121 a.a.)
IL-16 (130 a.a.)
IL-17
IL-17B
IL-17D
IL-17E
IL-17F
IL-19
IL-20
IL-22
IL-31
Insulin
IP-10
JE
JNK2a1
JNK2a2
KC / CXCL1
KGF
L-asparaginase
LAG-1
LALF Peptide
LAR-PTP
LC-1
LBP
LD-78β
LDH
LEC/NCC-4
Leptin
LIGHT
LIX
LKM
LL-37
Lymphotactin
sLYVE-1
M-CSF
MCP-1 (MCAF)
MCP-2
MCP-3
MCP-4
MCP-5
MDC (67 a.a.)
MDC (69 a.a.)
MDH
MEC
Mek-1
MIA
Midkine
MIG / CXCL9
MIP-1α / CCL3
MIP-1β / CCL4
MIP-3 / CCL23
MIP-3α / CCL20
MIP-3β / CCL19
MIP-4 (PARC) / CCL18
MIP-5 / CCL15
MMP-3
MMP-7
MMP-13
Myostatin
Nanog
NAP-2
Neurturin
NFAT-1
beta-NGF
NOGGIN
NOV
NP-1
NT-1/BCSF-3
NT-3
NT-4
Ocreotide
Oncostatin M
Osteoprotegerin (OPG)
OTOR
Oxytocin
p38-α
Parathyroid Hormone
PDGF-AA
PDGF-AB
PDGF-BB
Persephin
PF-4
PIGF-1
PIGF-2
PKA α-subunit
PKC-α
PKC-γ
Pleiotrophin
PLGF-1
Polymyxin B (PMB)
PRAS40
PRL-1
PRL-2
PRL-3
Prokineticin-2
Prolactin
Protirelin
PTHrP
PTP1B
PTP-IA2
PTP-MEG2
PTP-PEST
sRANK
sRANKL
RANTES
RELM-α
RELM-β
Resistin
RPTPβ
RPTPγ
RPTPμ
SCF
SCGF-α
SCGF-β
SDF-1α
SDF-1β
Secretin
SF20
SHP-2
STAT1
c-Src
TACI
TARC
TC-PTP
TECK
TFF2
TGF-α
TGF-β1
TGF-β2
TGF-β3
Thymosin α1
sTIE-1/Fc Chimera
sTIE-2/Fc Chimera
TL-1A
TNF-α
TNF-β
sTNFR1
sTNFR2
TPO
TRAIL/Apo2L
sTRAIL R-1 (DR4)
sTRAIL R-2 (DR5)
TSH
TSLP
TWEAK
TWEAK Receptor
Urokinase
VEGF121
VEGF145
VEGF165
VEGF-C
VEGF-C I525
EG-VEGF
VEGF-E
HB-VEGF-E
sVEGFR-1
sVEGFR-2
sVEGFR-3
WISP-1
WISP-2
WISP-3
WNT-1

CELL SCIENCES INC • 480 NEPONSET STREET, BUILDING 12A, CANTON, MA 02021 • INFO@CELLSCIENCES.COM

TOLL FREE: (888) 769-1246 • TEL: (781) 828-0610 • FAX: (781) 828-0542 • WEB: WWW.CELLSCIENCES.COM

Science Mobile App Now Available for Android Phones

They say you never know when inspiration will strike. Download the *Science* mobile app for Android devices and be ready the next time you're inspired to read the latest news, research, and career advice from *Science* on your mobile phone.

To download the *Science* mobile app for Android visit **content.aaas.org/mobile**, visit the Android Market on your phone, or just scan this barcode.

Features include:

- Summaries and abstracts from *Science*, *Science Translational Medicine*, and *Science Signaling*.
- Ability to e-mail full-text links.
- The latest news from *Science*NOW.
- Career advice articles from *Science* Careers.
- Access to the *Science* weekly podcast and other multimedia.
- Content caching for reading without wi-fi access.

Science
AAAS

NEW ENGLAND BioLabs® Inc.
enabling technologies in the life sciences

Mix it up.

RE-Mix™ Restriction Enzyme Master Mixes

Restriction enzyme digests are now even easier! The same high quality restriction enzymes that you have come to trust from New England Biolabs are now available in master mix format, including enzyme, buffer and loading dye; simply add your DNA and digest.

With RE-Mix Master Mixes take advantage of:

- Simplified and shortened protocols
- Fast digestion in 15 minutes (Time-Saver qualified)
- High product quality with reproducible results

RE-Mix Master Mixes – just add your DNA and mix

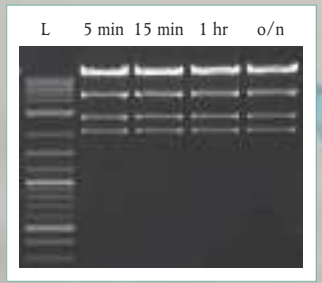

pXba DNA was digested with EcoRV-HF™ RE-Mix™ according to the recommended protocol. Lane L is the TriDye™ 2-Log DNA Ladder (NEB #N3270). The same results are obtained whether incubated for 5–15 minutes, 1 hour or overnight.

For more information, visit
www.NEBREMIX.com

GTAGC CTT
TCUTGA ATT
AGTIT G C
TTT TOUT T
GTTAC TACG

To experience the new restriction enzyme challenge from NEB, visit
www.NEBcutitout.com

Blue-footed Booby (Sula nebouxii)
© Tui De Roy

New Products

BIOLOGICAL SAMPLE STORAGE

BiOS is an automated system designed for ultralow temperature storage of sensitive biological samples. This flexible, scalable system ensures the integrity of 250,000 to more than 10 million sample tubes at temperatures down to -85˚C. All samples within the BiOS are stored in -85°C chest freezer compartments to maintain temperature stability. All internal workflows, including sample picking, are optimized to keep samples at ultralow temperatures at all times. System parts are easily accessible for service and maintenance. One- and two-dimensional barcode reading and sample tracking produce complete chain-of-custody documentation, with software tools to support 21 CFR Part 11 compliance. Multiple redundant backup systems ensure the samples stay at -85°C, even in emergencies. The BiOS can store and process multiple labware types in the same system.

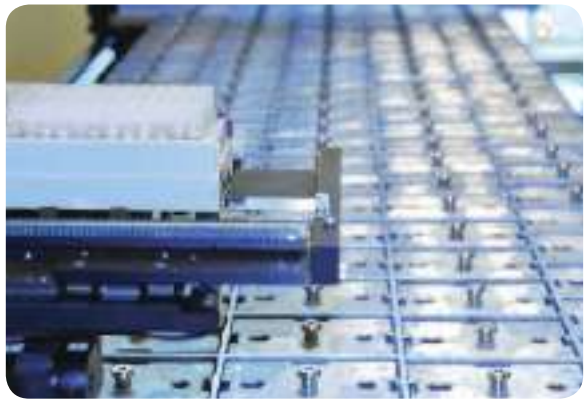

Hamilton Storage Technologies
For info: 800-310-5866 | www.hamilton-storage.com

ENDOTOXIN REMOVAL

The High Capacity Endotoxin Removal Resin is designed for the cleanup of protein that is injected or transfected into cells or animals. The Pierce High Capacity Endotoxin Removal Resin combines porous cellulose beads and an FDA-approved food preservative, poly (ε-lysine), as an affinity ligand to selectively bind endotoxins. Endotoxin levels in protein samples are reduced by greater than 99% in as little as one hour using a spin cup format, and protein recovery is greater than 85%. The Pierce High Capacity Endotoxin Removal Resin peptides have a high affinity for the charged glycol-groups of an endotoxin, while the particle pores help trap endotoxins. The modified polylysine affinity ligand eliminates the toxicity concerns associated with alternative technologies that use polymixin B ligands and sodium deoxycholate buffers. The Pierce High Capacity Endotoxin Removal Resin is available in either bulk slurry packages for researchers who want to pack their own columns or convenient, single-use, spin-column formats.

Thermo Fisher Scientific
For info: 800-874-3723 | www.thermoscientific.com/pierce

AUTOMATED STAGE SYSTEM

The NZ400 NanoScan Piezo Stage System is well suited for researchers producing rapid Z sections and live cell 3-D images of specimens grown in well plates, large petri dishes, or mounted to glass slides. With the ability to create a stack of images using multiple objectives in the z-axis with nanometer precision at an amazingly high speed, the NanoScan is the perfect accessory for any 3-D imaging application. The NZ400 NanoScan Piezo Stage System offers 400 µm of travel, 2.5 nm repeatability, and closed loop control utilizing a subangstrom resolution piezo resistive sensor. Designed to mount to the Prior ProScan H117 series of high precision motorized stages, the NZ400 can also be provided as a standalone device that can be mounted onto a wide range of XY stages. Compatible with most leading imaging software packages, the NZ400 comes standard with control inputs for RS232, USB, and 0–10 V analog input.

Prior Scientific
For info: 800-877-2234 | www.prior.com

APOPTOTIC BODY DNA ANALYSIS

The D-Pop Kit simplifies the capture of DNA-containing particles from cell-free biological samples such as blood serum and plasma, urine, and eukaryotic cell culture media, and the extraction of DNA from the captured particles. Using the D-Pop Kit, apoptotic bodies and potentially other large particles are captured from biological fluids in minutes by passing them through a filter in a syringe format. The filter is then removed to a microfuge tube and the DNA is extracted from it using a rapid solid-phase extraction of DNA with non-organic reagents. The D-Pop Kit also includes control polymerase chain reaction primers for the hTERT gene to verify concentration and recovery of DNA from the sample.

Bioo Scientific
For info: 888-208-2246 | www.biooscientific.com

UV CROSSLINKER

A new high quality, inexpensive ultraviolet crosslinker makes it possible to identify and analyze trace amounts of DNA/RNA with far greater sensitivity, accuracy, and speed than with conventional analysis. The Select XLE-Series UV crosslinker covalently binds nucleic acids to membranes in less than 30 seconds—240 times faster than vacuum-oven baking. It has a unique true-ultraviolet (UV)-monitoring circuitry that safeguards valuable test results from washouts, even when the tubes age. Researchers also rely on this versatile instrument for eliminating polymerase chain reaction (PCR) contamination, nicking ethidium-bromide-stained DNA in agarose gels, gene mapping for creating cleavage-inhibiting thymine dimers, RecA mutation screening in *E. coli,* UV sterilization, and miscellaneous UV-dosage applications. The Select Series crosslinker features a "smart" user-friendly, fully programmable microprocessor, built-in "help" messages and an auto-repeat function that make its operation amazingly fast and simple. It features five 8 W tubes and is available in a choice of 254 nm, 312 nm, and 365 nm versions.

Spectronics Corporation
For info: 800-274-8888 | www.spectroline.com

Electronically submit your new product description or product literature information! Go to **www.sciencemag.org/products/newproducts.dtl** for more information.

Newly offered instrumentation, apparatus, and laboratory materials of interest to researchers in all disciplines in academic, industrial, and governmental organizations are featured in this space. Emphasis is given to purpose, chief characteristics, and availability of products and materials. Endorsement by *Science* or AAAS of any products or materials mentioned is not implied. Additional information may be obtained from the manufacturer or supplier.

LOCATION: Jackson Park Health Club
ARTICLE: *An Electronic Second Skin*
DATE: Sep 21, 7:43am

LOCATION: University Faculty Lounge
ARTICLE: *The Visual Impact of Gossip*
DATE: Sep 21, 4:22pm

LOCATION: Gyro King
ARTICLE: *Cavemen Craved Carbs, Too*
DATE: Sep 21, 1:13pm

LOCATION: Hemlock Bar
ARTICLE: *Quantum Simulation of Frustrated Classical Magnetism in Triangular Optical Lattices*
DATE: Sep 21, 9:21pm

LOCATION: Bed
ARTICLE: *Consciousness: What, How and Why*
DATE: Sep 21, 10:56pm

A new way to look at science

The new *Science* Reader app for iPad® from AAAS puts *Science* in your hands, wherever you go. Read abstracts, career advice, and highlights from our newest journals, *Science Signaling* and *Science Translational Medicine*. Plus, AAAS members can access full text articles from *Science*. Visit iTunes App Store℠ or content.aaas.org/ipad for details.

Available on the App Store

Science
AAAS

Increasing the quality, reliability, and speed of ubiquitin-related discovery

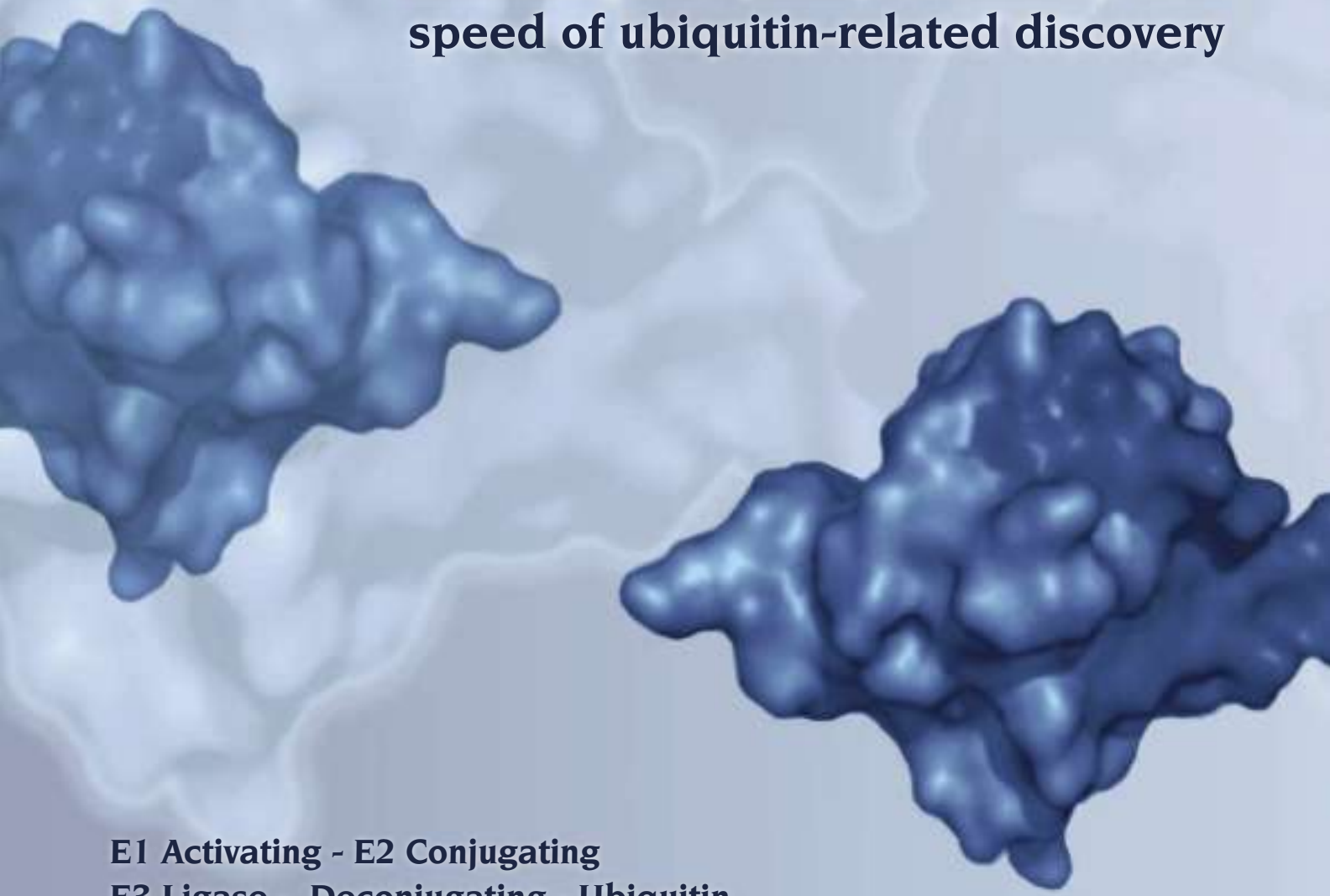

E1 Activating - E2 Conjugating
E3 Ligase - Deconjugating - Ubiquitin
SUMO - NEDD8 - ISG15 - UFM1 - Autophagy
FAT10 - Small Molecule Inhibitors - Antibodies
Kits - Substrate Proteins - Affinity Matrices

The World's Leading Producer of Ubiquitin-Related Research Products

For more information:
www.bostonbiochem.com

BostonBiochem®
An R&D Systems Company

Orders: 1.800.343.7475 | Technical Support: techserve@RnDsystems.com | Inquiries: info@bostonbiochem.com